FUNCTIONAL CHARACTERIZATION OF HUMAN CATHEPSIN F PATHOPHYSIOLOGICAL MUTATIONS

Barbara Jerič Kokelj

Doctoral Dissertation
Jožef Stefan International Postgraduate School
Ljubljana, Slovenia, May 2015

Evaluation Board:

Prof. Ddr. Boris Turk, Chairman, Jožef Stefan Institute, Jamova cesta 39, Ljubljana

Prof. Dr. Ana Plemenitaš, Member, Faculty of Medicine, Vrazov trg 2, Ljubljana

Prof. Dr. Eva Žerovnik, Member, Jožef Stefan Institute, Jamova cesta 39, Ljubljana

MEDNARODNA PODIPLOMSKA ŠOLA JOŽEFA STEFANA
JOŽEF STEFAN INTERNATIONAL POSTGRADUATE SCHOOL



Barbara Jerič Kokelj

FUNCTIONAL CHARACTERIZATION OF HUMAN CATHEPSIN F PATHOPHYSIOLOGICAL MUTATIONS

Doctoral Dissertation

FUNKCIJSKA KARAKTERIZACIJA PATOFIZIOLOŠKIH MUTACIJ ČLOVEŠKEGA KATEPSINA F

Doktorska disertacija

Supervisor: Prof. Dr. Veronika Stoka

Ljubljana, Slovenia, May 2015

Index

Abstract ..... **IX**

Povzetek ..... **X**

Abbreviations ..... **XI**

1 Introduction **1**
1.1 Protein folding, misfolding and aggregation 1
1.1.1 Principles of protein folding and quality control in the endoplasmic reticulum 1
1.1.2 ER stress and ER-associated degradation (ERAD) 3
1.1.3 Unfolded protein response (UPR) 3
1.1.4 Protein aggregation 5
1.1.5 Deposits of misfolded and aggregated proteins 6
1.1.6 Misfolded protein degradation pathways: ubiquitin-proteasome system and autophagy 10
1.1.6.1 The ubiquitin-proteasome system 10
1.1.6.2 Autophagy 11
1.2 Lysosomal storage diseases 15
1.2.1 Neuronal ceroid lipofuscinoses 15
1.2.1.1 Kufs disease 17
1.2.1.2 Cell biology of NCL 18
1.3 Cell death 21
1.3.1 Apoptosis 21
1.4 Cathepsins 24
1.4.1 Cathepsin F 28

2 Aims and Hypothesis **31**

3 Materials and Methods **33**
3.1 Materials 33
3.2 Methods 34
3.2.1 Cloning 34
3.2.2 Cell cultures and transient transfection 34
3.2.3 Cell lysates and determination of whole protein concentration 35
3.2.4 Cathepsin F deglycosylation 35
3.2.5 SDS-PAGE and Western blotting 35
3.2.6 Caspase activity 36
3.2.7 Analysis of free Ca^{2+} in the cell 36
3.2.8 Flow cytometry (FACS) 36
3.2.9 Oxidative stress 37

3.2.10 Immunocytochemistry and autofluorescence 37
3.2.11 Aggresome detection 38
3.2.12 Fluorescence confocal microscopy 39
3.2.13 Transmission electron microscopy (TEM) 39
3.2.14 RNA isolation and quantitative real time PCR (qPCR) 40
3.2.15 Statistical analysis 41

4 Results 43
4.1 Characterization of N-terminally truncated forms of human cathepsin F 43
4.1.1 N-terminally truncated forms of human cathepsin F have distinct subcellular localization to the wild type protein 43
4.1.2 Expression pattern and deglycosylation of the wild type cathepsin F and its N-terminally truncated variants 45
4.1.3 N-terminally truncated forms of human cathepsin F accumulate in aggresome-like inclusions 46
4.1.4 N-terminally truncated Δ^{19}CatF, Δ^{125}CatF and Δ^{146}CatF are p62 positive inclusions, cleared by autophagy 48
4.1.5 N-terminally truncated forms of human cathepsin F induce caspase activation 50
4.2 CLN13 mutations induce alterations in cellular homeostasis that resemble characteristics of NCL disease 51
4.2.1 Expression pattern and potential degradation pathway 51
4.2.2 Y231C, Q321R, G458A, S480L but not also S319Lfs*27 are expressed in the lysosomes 53
4.2.3 Aggregation of S319Lfs*27 mutant is not held in the endoplasmic reticulum 55
4.2.4 Terminal misfolding of the S319Lfs*27 may lead to its accumulation in the aggresomes 56
4.2.5 Evaluation of CLN13-induced changes in autophagy pathway 57
4.2.6 Expression of S319Lfs*27 induce increased accumulation of autofluorescent perinuclear material 61
4.2.7 Ultrastructural analysis by TEM 61
4.2.8 Does expression of CLN13 induce ER stress? 63
4.2.9 CLN13 mutants induced slight increase in mitochondrial superoxide and lipid peroxidation 65

5 Discussion 67
5.1 Analysis of N-terminally truncated forms of human cathepsin F in HEK293T cells 68
5.2 Characterization of CLN13 mutants in SH-SY5Y cells 72

6 Conclusions 79

7 Acknowledgements 81

8 References 83

Index of Figures 99

Index of Tables 105

Appendix..... 107

Abstract

Various truncated and mutated forms of human cathepsins have been found in physiological and pathological conditions to date. Some of the mutations or deletions may impact their trafficking and folding competences, finally resulting in enzymatically inactive proteins or toxic gain of function. Human cathepsin F (CTSF/CLN13/wtCatF) is an ubiquitously distributed lysosomal cysteine cathepsin. Its N-terminally truncated variant has been found in skeletal muscle cDNA library, whereas C-terminally truncated form and four point mutations, were found in patients with type B Kufs disease, an adult-onset neuronal ceroid lipofuscinosis.

We cloned wild type human cathepsin F (wtCatF) and its N-terminally truncated forms devoid of signal peptide only (Δ^{19}CatF), signal peptide and cystatin-like domain (Δ^{125}CatF) or the additional 20 amino acids of linker (Δ^{146}CatF) and expressed them in HEK293T cells. Our results show that N-terminal removal of only signal sequence prevents this protein from its glycosylation and usual lysosomal targeting, leading to its aggregation and accumulation in perinuclear aggresome-like inclusions. Finally, expression of N-terminally truncated forms led to the increase in caspase activity. However, induction of cell death is most probably prevented by protective autophagic sequestration and degradation of these insoluble aggregates. Thus, some crucial differences between initially described N-terminally truncated human cathepsin F and N-terminally truncated variants, expressed in HEK293T cells have been found in our study.

This study also attempted to functionally characterize CLN13 mutants found in patients with type B Kufs disease. S319Lfs*27, S480L, G458A, Y231C, Q321R and the wild type protein were cloned and expressed in SH-SY5Y neuron-like cell model. We revealed that frameshift mutation prevents the protein from lysosomal localization, leads to its aggregation and finally also accumulation in aggresome-like inclusions. Aggregates are however targeted to LAMP2-positive vesicles (most probably autolysosomes) after their autophagosomal sequestration. Immunolabelling shows that accumulation of CLN13 mutants induces swelling of LAMP2-positive vesicles, whereby accumulation of S319Lfs*27 aggregates exhibits most profound effects. In addition, we observed increased pH of the acidic organelles, which is the most plausible mechanism of the reduced autophagic flux in cells expressing CLN13 mutants. Besides, cells expressing S319Lfs*27 accumulate autofluorescent perinuclear material, increased amounts of lipids on intracellular membranes, form lamellar inclusions inside of electronically dense vesicles and infrequently display damage of mitochondria. Moreover, slight increase in mitochondrial superoxide and prominent lipid peroxidation has been found. Our results also show that CLN13 mutants are degraded by both, ubiquitin-proteasome system and autophagic pathway. Hereby we thus firstly show that CLN13 mutations induce changes in cellular homeostasis which are characteristic for neuronal ceroid lipofuscisosis disease.

Povzetek

Do danes je bilo v raznih fizioloških in patoloških razmerah najdenih veliko različnih skrajšanih in mutiranih variant človeških katepsinov. Nekatere mutacije ali delecije proteinov lahko privedejo do spremembe v njihovi lokaciji in neugodno vplivajo na njihovo zvitje, kar se lahko odraža v encimsko neaktivnih proteinih ali pridobitvi toksične funkcije. Človeški katepsin F (CTSF/CLN13/wtCatF) je splošno razširjen lizosomalni cisteinski katepsin. Njegova na N-koncu skrajšana varianta je bila izolirana iz cDNK knjižnice skeletnih mišic, pri sekvenciranju pacientov s Kufsovo boleznijo tipa B, eni od oblik nevronalne ceroidne lipofuscinoze, pa so našli tudi na C-koncu skrajšano varianto in štiri točkovne mutacije.

Klonirali smo na N-koncu skrajšane variante brez signalne sekvence (Δ^{19}CatF), brez signalne sekvence in cistatinske domene (Δ^{146}CatF) in varianto, kateri je dodatno odstranjenih še 20 amino kislin linkerja (Δ^{125}CatF), ter jih skupaj z divjim tipom (wtCatF) proteina izrazili v celični liniji HEK293T. Rezultati so pokazali, da že odsotnost samo signalne sekvence prepreči glikozilacijo proteina in njegovo lokalizacijo v lizosomih ter posledično agregacijo in nakopičenje v objedrnih, agresomom podobnih strukturah. Izražanje na N-koncu skrajšanih variant pa končno privede tudi do aktivacije kaspaz. Posledično apoptozo verjetno prepreči njihova osamitev v avtogfagosomih in razgradnja netopnih agregatov po poti avtofagije. V naši študiji smo tako pokazali mnoge razlike in razhajanja od začetnih opisov tega, na N-koncu skrajšanega proteina.

Poleg tega smo v naši študiji želeli funkcijsko okarakterizirati mutante CLN13, najdene pri pacientih s Kufsovo boleznijo tipa B. S319Lfs*27, S480L, G458A, Y231C, Q321R in divji tip proteina smo izrazili v nevronom podobnih SH-SY5Y celicah. Pokazali smo, da mutacija, pri kateri pride do premika bralnega okvirja S319Lfs*27, prepreči lizosomalno lokalizacijo tega proteina in privede do nastajanja proteinskih agregatov, ki se kopičijo v agresomom podobnih strukturah. Kljub vsemu pa agregati pripotujejo do LAMP2-pozitivnih veziklov (verjetno avtolizosomov) kot posledica avtofagije. Imuno označevanje je pokazalo, da kopičenje mutant CLN13 inducira nabrekanje LAMP2-pozitivnih veziklov, pri čemer je efekt najbolj izrazit v celicah, ki izražajo S319Lfs*27. Poleg tega smo opazili povišan pH kislih veziklov, ki je najverjetnejši razlog za opaženo zmanjšanje poteka avtofagije v celicah, ki izražajo mutante CLN13. Izkazalo se je tudi, da izražanje S319Lfs*27 sproži objedrno kopičenje avtofluorescentnega materiala, povečano nalaganje lipidov na znotrajcelične membrane, nastajanje lamelastih vključkov v elektronsko gostih veziklih, včasih pa tudi poškodbo mitohondrijev. Opazili smo še rahlo povišanje mitohondrijskega superoksida in izrazito oksidacijo lipidov znotraj celic. Z analizami smo pokazali, da se mutante CLN13 razgradijo tako po proteasomski poti kot tudi z avtofagijo. V naši študiji smo tako prvič pokazali, da mutacije CLN13 povzročijo spremembe v celični homeostazi, ki so karakteristične za skupino nevronalnih ceroidnih lipofuscinoz.

Abbreviations

Ac-DEVD.AFC	=	Ac-Asp-Glu-Val-Asp-7-amino-4-trifluoromethylcoumarin
ALIS	=	aggresome-like induced structures
ATP	=	adenosine triphosphate
BAG3	=	BAG family molecular chaperone regulator 3
		benzimidazolylcarbocyanine iodide)
BiP	=	78 kDa glucose-regulated protein
BSA	=	bovine serum albumin
CALR	=	calreticulin
cDNA	=	complementary deoxyribonucleic acid
CHOP	=	transcription factor C/EBP homologous protein
CLN13	=	ceroid lipofuscinosis neuronal protein 13
CMA	=	chaperone-mediated autophagy
CTSF	=	cathepsin F
DMEM	=	Dulbecco's Modified Eagle Medium
DMSO	=	dimethyl sulfoxide
DNA	=	deoxyribonucleic acid
DRiPs	=	defective ribosomal products
EDEM1	=	ER degradation-enhancing alpha-mannosidase-like protein1
EGFP	=	enhanced green fluorescent protein
EGTA	=	ethylene glycol tetraacetic acid
ENOX2	=	ecto-NOX disulfide-thiol exchanger 2
ER	=	endoplasmic reticulum
ERAD	=	ER-associated protein degradation
HDAC6	=	histone deacetylase 6
IPOD	=	insoluble protein deposit
JUNQ	=	juxtanuclear quality control compartment
KO	=	knockout
LAMP2	=	lysosomal-associated membrane glycoprotein 2
LC3	=	microtubule-associated protein 1 light chain 3
LSD	=	lysosomal storage disorders
M6P	=	mannose-6-phosphate
MEM	=	Eagle's Minimum Essential Medium
mRNA	=	messenger ribonucleic acid
MTOC	=	microtubule organizing center
Mw	=	molecular weight
NCL	=	neuronal ceroid lipofuscinosis
p62/SQSTM1	=	sequestosome 1
p97/VCP	=	valosin containing protein
PBS	=	Phosphate-buffered saline
PCR	=	polymerase chain reaction
PDI	=	protein disulfide isomerase
qPCR	=	quantitative real time polymerase chain reaction
ROS	=	reactive oxygen species

SD	=	standard deviation
SDS	=	sodium dodecylsulfate
SDS-PAGE	=	sodium dodecylsulfate polyacrylamide gel electrophoresis
TEM	=	transmission electron microscopy
UPR	=	unfolded protein response
UPS	=	ubiquitin-proteasome system
VIPAR	=	VPS33B interacting protein
WLL	=	white light laser

Amino acid abbreviations

Ala	A	Alanine
Arg	R	Arginine
Asn	N	Asparagine
Asp	D	Aspartic acid (Aspartate)
Cys	C	Cysteine
Gln	Q	Glutamine
Glu	E	Glutamic acid (Glutamate)
Gly	G	Glycine
His	H	Histidine
Ile	I	Isoleucine
Leu	L	Leucine
Lys	K	Lysine
Met	M	Methionine
Phe	F	Phenylalanine
Pro	P	Proline
Ser	S	Serine
Thr	T	Threonine
Trp	W	Tryptophan
Tyr	Y	Tyrosine
Val	V	Valine

1 Introduction

1.1 Protein folding, misfolding and aggregation

1.1.1 Principles of protein folding and quality control in the endoplasmic reticulum

Proteins can fold either in the cytosol or in the endoplasmic reticulum (ER). ER is the principal site for synthesis and folding of membrane proteins and proteins destined for secretory pathway. Usually, proteins that are designated to fold in the ER do not fold correctly if targeted to the cytosol and vice versa. In mammalian cells, the import of proteins into the ER starts co-translationally, before the polypeptide chain is completely synthesized (Schroder, 2008; Schroder and Kaufman, 2005). Coupled translation and translocation assures polypeptide to be released into the environment which provides it proper oxidizing conditions, high calcium concentrations and folding machinery (Rutishauser and Spiess, 2002). Soluble proteins are directed to the ER by the N-terminal signal sequence, which acts as a transfer signal that opens the aqueous pore in the Sec61p translocation complex in the ER membrane. Signal sequence then remains bound to the translocator until also the C-terminus of the protein passes through the membrane, however, it is cleaved off later on (Schroder and Kaufman, 2005; Walter and Johnson, 1994; Walter and Lingappa, 1986).

Folding of newly synthesized proteins is the crucial stage in the regulation of their biological activity, subcellular localization, trafficking and secretion. The process of folding is defined predominantly by the primary amino acid sequence and driven by the hydrophobic effect, in order to minimize the exposure of hydrophobic amino acid residues at the surface of the protein, thus achieving the lowest free Gibbs enthalpy. The most stable state of the lowest free energy is usually the native conformation of the protein (Hyttinen et al., 2014; Schroder, 2008). The number of possible conformations of the folding protein is thus limited by the burial of electrostatic interactions, such as salt bridges or hydrogen bonds in the hydrophobic core. In addition to the hydrophobic effect, catalysis of cis/trans isomerization of peptidyl-prolyl bonds governs the protein folding. Other important post-translational modifications in the ER include disulfide bond formation by protein disulfide isomerase (PDI), signal peptide cleavage and N-linked glycosylation (Alberts, 2002; Schroder, 2008). Many of the proteins are only transiently in the lumen of the ER and *en route* to other destinations, whereas some of them normally reside there. ER resident proteins contain four amino acids long C-terminal ER retention signal (KDEL) that enables them to retain in, or return to the ER. Some of these proteins function as chaperons that help other proteins to fold and assemble correctly (Alberts, 2002).

Most of the soluble and membrane-bound proteins destined for transport to the Golgi apparatus, lysosomes, plasma membrane or extracellular space are glycoproteins. Most common oligosaccharides found in glycoproteins are asparagine-linked (N-linked). However, oligosaccharides can be bound also to the side chain of serine, threonine or

hydroxylysine amino acids (named O-lined glycosylation), although this is less frequent (Alberts, 2002). N-linked glycosylation is initiated by transfer of core oligosaccharide $Glc_3Man_9GlcNAc_2$ (Glc, D-glucose; GlcNAc, 2-N-acetylamide-D-glucose; Man, D-mannose) from a lipid carrier dolichol in the ER membrane, to the side chain amide of asparagine residues in the consensus sequence Asn-X-Ser/Thr (X represents any amino acid except L-proline) in the polypeptide chain, by a set of specific glycotransferases (Aebi, 2013; Schroder, 2008). Glycosylation alters the biophysical properties of the polypeptides and affects their folding in several ways: first, glycosylation increases protein solubility due to its hydrophilic nature. Second, large hydrated volume of oligosaccharides prevents surrounding proteins from attachment and third, oligosaccharides stabilize protein conformation due to their interaction with the peptide bond. Moreover, structure of the carbohydrate indicates the folding status of the protein (Aebi, 2013; Schroder and Kaufman, 2005; Wormald and Dwek, 1999).

Exposed hydrophobic surfaces in the not-yet native polypeptide are shielded by ER chaperones like BiP (GRP78) which facilitate the translocation reaction, prevent aggregation and initiate the folding program. Glycosylation supports further recruitment of the sugar-binding lectin chaperones and other folding enzymes that catalyze folding of the polypeptides and improve folding efficiency, although most native cellular proteins probably do not interact with chaperones (Caramelo and Parodi, 2007; Noack et al., 2014). Upon addition of the oligosaccharide, terminal D-glucose residue is immediately removed by the α-glucosidase I, resulting in di-glucosylated N-glycan, which is a ligand for ER lectin malectin. Malectin has preference to bind newly synthesized polypeptides on the off-pathways of the folding program (Noack et al., 2014; Schallus et al., 2008). Subsequent removal of the second glucose by α-glucosidase II attracts calnexin or calreticulin with other associated folding enzymes (the thiol-disulphide oxidoreductase ERp57 and the peptidyl-prolyl cis/trans isomerase (PPI) CypB) (Hammond et al., 1994; Jansen et al., 2012; Noack et al., 2014). Cleavage of the remaining glucose by glucosidase II terminates association of the substrate with the folding enzymes and the polypeptide is inspected by the folding sensor UDP-glucose:glycoprotein glucosyltransferase 1 (UGGT1). Native proteins are exported to the Golgi. By contrast, non-native polypeptides are re-glycosylated by UGGT1 and thereby promoted back to calnexin and calreticulin folding system (Noack et al., 2014; Sousa et al., 1992). Cycles of glucosylation and de-glucosylation progress until the protein reaches its native conformation or is targeted for degradation. *In vitro* studies revealed that UGGT1 preferentially re-glucosylates glycoprotein in partially folded, globular conformations by recognition of exposed hydrophobic stretches. However, glycoproteins in their native conformation, random-coiled and short glycopeptides were ignored (Ellgaard and Helenius, 2003; Trombetta and Helenius, 2000).

In addition to the above mentioned Hsp70 and calnexin/calreticulin chaperone system, folded proteins may be transferred to the Hsp90 chaperone GRP94, which acts after BiP and presents unfolded substrates to calnexin/calreticulin-bound PDIs and PPIs (Ellgaard and Helenius, 2003; Schroder, 2008). In the case of quality control failure, special mechanisms can de-mannosylate and dislocate misfolded substrates across the ER membrane for proteolytic degradation (Noack et al., 2014; Schroder, 2008).

1.1.2 ER stress and ER-associated degradation (ERAD)

Misfolded proteins may occur due to the mutations, incomplete translation process resulting in defective ribosomal products (DRiPs), misfolding after translation, aberrant post-translational modifications, failed oligomerization and oxidative damage (Lamark and Johansen, 2012). It has been proposed that 30% of newly synthetized proteins are defective (Schubert et al., 2000) and about 20% of nascent polypeptides are supposed to be directed for degradation immediately, due to the improper quality (Hyttinen et al., 2014; Wickner et al., 1999). Furthermore, endoplasmic reticulum is not only organelle for production of secretory proteins, but also a major site for synthesis of sterols and phospholipids, components of all biological membranes and the main site for storage of intracellular Ca^{2+}. The majority of ER Ca^{2+} is bound to ER molecular chaperones and acts either as a survival or apoptotic signal, sensed by mitochondria (Wang and Kaufman, 2012). Perturbation of any of the physiological functions of the ER caused by accumulation of the non-native polypeptides, increased secretory demands, pathogen infection, environmental changes such as redox, ion and nutrient imbalances, defective chaperone machinery, interference of glycosylation and expression of mutated gene products, lead to the ER stress (Noack et al., 2014). Similarly, chemical stressors, such as tunicamycin or thapsigargin affect the folding of numerous glycoproteins and hence induce ER stress (Price et al., 1992).

To relieve such stress and reestablish homeostasis, cells evolved several post-translational and transcriptional responses. Prolonged retention of glycosylated proteins in the folding system of the ER activates signals for their ER-associated degradation (ERAD). As mentioned above, non-native conformations are extensively de-mannosylated by ER resident mannosidases ERManI, EDEM1, EDEM2 and EDEM3. De-mannosylated N-glycans can then recruit the ERAD lectins, which are luminal substrate recognition factors that shuttle the misfolded protein to the ER-membrane embedded adaptor proteins, coupled to the supramolecular dislocation complexes. Substrates are thus dislocated across the ER membrane, presumably through dislocons that are coupled to the membrane-embedded E3 ubiquitin ligases. Dislocons among others components comprise also PDIs and PPIs that unfold the protein to be dislocated across the ER membrane. The process of dislocation of misfolded proteins to the cytosol is regulated by the ATP-driven chaperone VCP/p97. On gaining access to the cytosol, substrates are tagged with polyubiquitin chains by E3 ligases and degraded by cytosolic 26S proteasome (Noack et al., 2014; Olzmann et al., 2013). In order to maintain cellular physiology, non-native, but also native proteins might be selected for degradation by the ERAD machinery. Interactions with misfolded proteins thus directly regulate the activity, level, localization and turnover of the ERAD components by a sort of autocrine regulatory mechanisms (known as ERAD tuning). In this case, there is no need for the transduction of signal from the ER to the nucleus for rapid adaptation (enhancement or inhibition) of the ERAD activity (Merulla et al., 2013).

1.1.3 Unfolded protein response (UPR)

Accumulation of the misfolded polypeptides in the lumen of ER trigger transcriptional responses, following signal transmission from the ER to the nucleus in the process termed unfolded protein response (UPR) (Noack et al., 2014). UPR reduces load of newly synthesized proteins into the ER through general translational arrest, degrades misfolded

proteins though ERAD and lysosome-mediated autophagic pathway, and upregulate transcription of genes coding ER folding machinery and quality control system, to maintain homeostasis in the ER or induce apoptosis, if ER stress remains immitigable (Pereira, 2013; Walter and Ron, 2011).

In mammals, UPR involves three distinct pathways, responding to the activation of three ER-resident signaling proteins, the protein kinase RNA-activated-like ER kinase (PERK), the inositol requiring enzyme 1 (IRE1α) and activating transcription factor 6 (ATF6). Unfolded proteins in the ER cause the chaperone BiP (GRP78) to dissociate from ER membrane sensors IRE1α, PERK and ATF6 and thus promote their oligomerization and activation. Further on, IRE1α and PERK are autophosphorylated. When active, IRE1α cleaves mRNA coding a UPR-specific transcription factor X-box binding protein 1 (XBP1). Spliced XBP1 mRNA is translated to the active form of the transcription factor, with a special role in regulating expression of ERAD components, lipid biosynthetic enzymes and protein quality control genes (Acosta-Alvear et al., 2007; Calfon et al., 2002; Pereira, 2013; Walter and Ron, 2011; Wang and Kaufman, 2012).

Oligomerization of PERK activates its kinase activity, resulting in phosphorylation of translation initiation factor eIF2α and reduction in protein load in the ER by suppression of general protein synthesis through indirect inactivation of eIF2 and selective increase of activating transcription factor 4 (ATF4) mRNA translation. ATF4 activates expression of several genes involved in ER function, ER stress-mediated production of reactive oxygen species and antioxidant response, ER stress-induced apoptosis and autophagy, including CHOP (transcription factor C/EBP homologous protein), GADD34 (growth arrest and DNA damage-inducible 34) and NRF2 (nuclear erythroid 2 p45-related factor 2). CHOP is a transcription factor that controls genes involved in apoptosis, GADD34 counteract PERK by dephosphorylation of eIF2α, and NRF2 induce antioxidant response genes (Han et al., 2013; Harding et al., 1999; He et al., 2001; Novoa et al., 2001; Pereira, 2013; Walter and Ron, 2011).

The transcription factor ATF6 is normally anchored in the ER membrane. However, in the ER stressed cells it traffics to the Golgi, where it is cleaved by serine and metallo-proteases S1P and S2P, respectively, to release its N-terminal cytosolic domain – ATF6(N), which translocates to the nucleus where acts as a transcription factor. When in the nucleus, ATF6(N) increases the expression of ER chaperones (BiP, PDI and GRP94), ERAD-related genes and proteins involved in organelle biogenesis. Thus, cells employ many different signaling pathways to adapt to a mild ER stress. However, if the ER stress is prolonged or too severe, disrupted proteostasis can lead to compartmentalization and autophagic degradation of parts of ER or selected substrates. Finally, if the stress is chronic and cannot be mitigated, UPR can serve as an activator of apoptotic pathway, the last line of defense to ensure survival of the multicellular organism (Haze et al., 1999; Pereira, 2013; Ron and Walter, 2007; Walter and Ron, 2011).

In addition, overload of the ER with wild type or mutant proteins or viral infection (demand for production of large amounts of viral proteins) may induce another ER stress response in the cells, termed ER overload response (EOR) (Pahl, 1999; Rutishauser and Spiess, 2002). This response is distinguished from UPR by activation of transcription factor NF-κB (Nuclear factor NF-kappa-B), leading to the activation of antiviral immune response or inflammation through expression of NF-κB target genes, many of which encode inflammatory cytokines. Hypothetically, this could explain the fact that accumulation of wild-type or mutant proteins in the ER is often accompanied by inflammation (Pahl, 1999; Rutishauser and Spiess, 2002).

1.1.4 Protein aggregation

Synthesized polypeptide chains may form diverse types of structures. Unstructured chain of new protein may fold into a monomeric or oligomeric native structure, macromolecular complex or natural protein fiber, through one or more partially folded intermediates. However, in the process of folding a protein can experience another fate, such as degradation or aggregation. Aggregation is one of the common consequences of a polypeptide chain failing to reach its functional three-dimensional structure. Protein molecules may aggregate by simple physical association with each other without any changes in primary structure or by formation of new covalent bonds. Chemical interactions between otherwise (in native state) buried hydrophobic regions on the surfaces of aberrantly folded proteins that escape all protective mechanisms and degradation pathways, give them chance to interact with each other and clump together in aggregates. Both mechanisms can occur simultaneously in a protein and can lead to a soluble or insoluble aggregates, depending on the protein and environmental conditions. The initial aggregates are usually soluble, but gradually became insoluble as they exceed certain size and solubility limits (Dobson, 2003; Stefani and Dobson, 2003; Wang, 2005).

Propensity for protein aggregation is strongly affected by primary and secondary structure, both of which are strongly influenced by environmental conditions. Generally, protein or peptide aggregation involves mostly β-sheets. Mutation of one amino acid in a peptide can strongly increase aggregation propensity, as does the changes in hydrophobicity and charge. Besides the content of the non-polar groups, the location of hydrophobic and hydrophilic residues in the sequence critically controls the aggregation. In addition, protein state is affected also with the relative thermodynamic stability of various possible conformations, kinetics of their interconversion and many other environmental factors (Dobson, 2003; Stefani and Dobson, 2003; Wang, 2005). Observations suggest that aggregation is very likely to arise from specific partially folded intermediates rather than unfolded or denatured states, even though intermediates are usually not stable and poorly populated (Fink, 1998).

Unfolded or misfolded proteins may form ordered or disordered aggregates, which might accumulate extracellularly or within several cellular compartments (Dobson, 2003; Stefani and Dobson, 2003). Amyloid fibrils, originating from prefibrilar species, are one example of ordered form of aggregate with highly organized structure and unique kinetic stability. On the other hand, inclusion bodies or amorphous deposits represent examples of disordered aggregates. Inclusion bodies are usually highly homogenous and may facilitate potential purification of aggregated proteins (Dobson, 2003; Fink, 1998). Once formed, aggregates can persist for longer periods, allowing progressive build-up of deposits in cells and tissues, leading to the various diseases, including Alzheimer's disease, Parkinson's disease, type II diabetes, spongiform encephalopathies, amyotrophic lateral sclerosis, neuronal ceroid lipofuscinoses, etc. (Stefani and Dobson, 2003). Protein aggregates usually exhibit either reduced or in many cases, no biological activity. However, there is a line of evidence showing toxic gain of function and stronger immunogenicity of aggregated protein. It is believed that prefibrilar aggregates of some proteins gain toxic functions, whereas mature fibrils are usually relatively benign (Bhatia et al., 2000; Caughey and Lansbury, 2003; Conway et al., 2000; Dobson, 2003; Jimenez et al., 2002; Sousa et al., 2001; Stefani and Dobson, 2003). The toxicity of this early aggregates is believed to result in impairment of fundamental cellular processes due to the interaction with cellular membranes, causing oxidative stress and increase in free Ca^{2+} that eventually lead to apoptotic or necrotic cell death (Stefani and Dobson, 2003). In addition, protein aggregates may inhibit the proteasomal system and induce formation of free radicals, further promoting aggregation steps. Even more, aggregated material can be

further chemically modified by a variety of cellular metabolites, including aldehydic lipid peroxidation products causing oxidation and cross-linking reactions (Grune et al., 2004).

Many studies suggest that protein aggregation is mediated by »aggregation-prone« segments in the protein sequence of protein peptide segments (Pastor et al., 2007). Increased level of aggregation-prone species may occur as a consequence of enhanced protein synthesis (elevated levels of protein concentration) or their reduced clearance, especially in the case of intrinsically unstable or natively unfolded proteins or proteins with relatively stable folding intermediates. Aggregation nucleating regions and disorder profile can be detected in the sequence of a protein utilizing various bioinformatics prediction methods (Ishida and Kinoshita, 2008; Stefani and Dobson, 2003; Thompson et al., 2006; Tsolis et al., 2013).

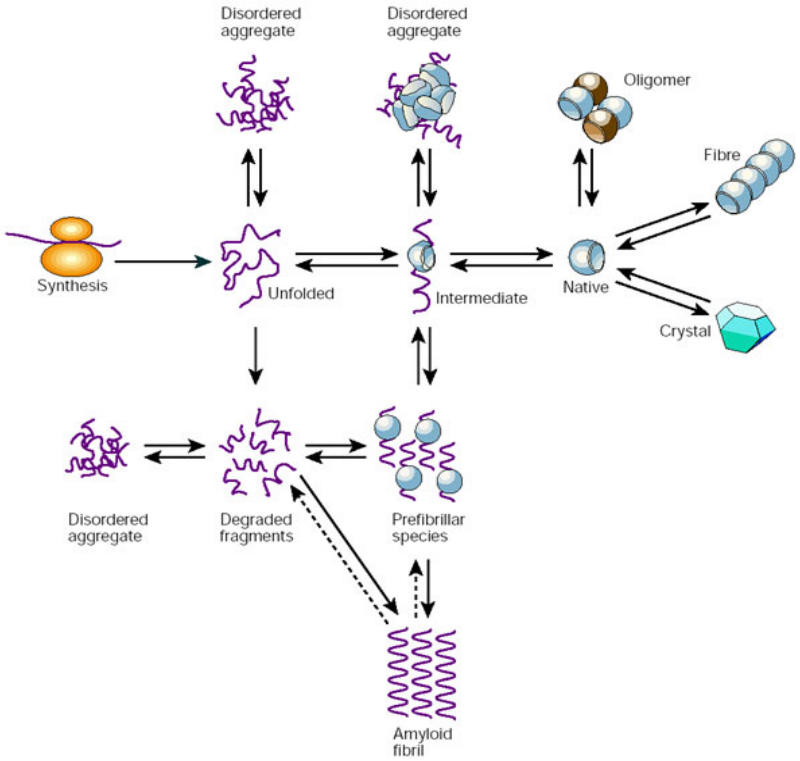

Figure 1: *Overview of the possible fates of a newly synthesized polypeptide chains.* See text for more details (Dobson, 2003).

1.1.5 Deposits of misfolded and aggregated proteins

Proteins that failed in the process of folding or oligomerization can be retained in the ER. Inside the ER, non-native proteins may accumulate in the so-called ER quality control compartment (ERQC) (Kamhi-Nesher et al., 2001). Due to their large size, aggregates are incompetent of transport and cannot diffuse freely within the ER. In addition, aggregates can serve as nuclei for aggregation of other unrelated proteins and can trap chaperones or proteases, thus leading to the disruption of normal cellular functions (Ellgaard and Helenius, 2003; Noack et al., 2014). Finally, accumulation of proteins in the ER can lead to a group of genetically based and very heterogeneous ER storage diseases (ERSDs),

arising due to the lack of the functional protein or toxic effects of misfolded/aggregated proteins. Some examples of ERSDs are: cystic fibrosis, lipid storage disorders (Gaucher's disease), Creutfeldt-Jakob disease, Parkinson's disease, amyotrophic lateral sclerosis, etc. (Roussel et al., 2013; Rutishauser and Spiess, 2002).

On the other hand, misfolded proteins may accumulate in the cytosol, or are retro-translocated from the ER to the cytosolic inclusions (Noack et al., 2014). Formation of the cellular inclusions is an organized and regulated process, conserved throughout many species (Outeiro and Lindquist, 2003). Distinct inclusions with specific characteristics, localized in different cellular compartments in yeast and mammalian cells have been found. These comprise (i) insoluble perinuclear, microtubule-dependent inclusion bodies, called aggresomes (Johnston et al., 1998; Kopito, 2000), (ii) soluble perinuclear inclusions with ERAD substrates, termed ER-associated compartments (ERACs), which are actually specialized ER subdomains, to where proteins are segregated before retro-translocation and further ubiquitin-proteasome degradation (Huyer et al., 2004; Kakoi et al., 2013; Kamhi-Nesher et al., 2001), and (iii) cytoplasmic inclusion bodies, co-localized with autophagy-related proteins (Iwata et al., 2005a).

However, Kaganovich et al. tested a small subset of aggregation prone and defect proteins under different stress conditions in yeast and mammalian cells, and discovered that quality control system arranges misfolded proteins into two distinct quality control compartments, presumably on the basis of their ubiquitination status, aggregation state and solubility (Kaganovich et al., 2008). Soluble ubiquitinated misfolded proteins have been found to accumulate first in a juxtanuclear quality control compartment (JUNQ), close to the ERAC region, which recruits proteasomes and chaperones (e.g. Hsp104). This compartment is dynamic structure that rapidly exchanges proteins with the cytosolic pool. Formation of JUNQ was closely followed by distinct cytosolic puncta and inclusions. In contrast, terminally aggregated proteins (after prolonged exposure to the stress conditions) were sequestered in a second, large perivacuolar compartment on the periphery of the cell, termed IPOD (insoluble protein deposit). At this time, juxtanuclear inclusion remained visible, but cytosolic puncta were cleared. In contrast to the JUNQ, IPOD do not exchange proteins with the cytosol and no ubiquitin signal or proteasomes could be detected within these deposit sites. On the other hand, IPOD but not JUNQ co-localized with the autophagic marker Atg8 (autophagy-related gene 8 in yeast; MAP1LC3A/LC3 in mammals) and the pre-autophagosomal structure (PAS), however, Atg8 was not required for IPOD formation. Similarly to JUNQ, IPOD contained chaperone Hsp104, which might serve to disaggregate aggregates and keep them soluble for refolding or degradation (Kaganovich et al., 2008). It should be mentioned that several studies demonstrated that yeast Hsp104 function in concert with Hsp70 and Hsp40 (Glover and Lindquist, 1998). Recently mammalian homolog of Hsp104, Hsp110 has been found too (Shorter, 2011). Despite both, JUNQ and IPOD formation depends on the polymerization of microtubules, none of them localize to microtubule organizing center (MTOC). Partitioning of misfolded proteins between IPOD and JUNQ was found to be modulated by specific interactions with cellular chaperones and (poly)ubiquitination. On the other side, ubiquitination state can determine solubility of the protein, independently of the repression of their degradation by proteasomal inhibition. Moreover, it was found that artificially induced ubiquitination can induce re-direction of IPOD substrates to the JUNQ compartment, where they could be refolded by cellular chaperone machinery (Kaganovich et al., 2008).

Insoluble misfolded or otherwise unsuccessfully refolded proteins could be targeted to another, above already mentioned juxtanuclear structures, termed aggresomes (Johnston et al., 1998). Aggresome formation is initiated by the packing of aggregated proteins into larger insoluble aggregates, which oligomerize and then multimerize into even larger

insoluble inclusions or aggregates (Grune et al., 2004; Hyttinen et al., 2014), actively transported and concentrated in the microtubule organizing center (MTOC) (Johnston et al., 1998). Formed aggresomes are usually spherical and measure about 1-3 μm in diameter (Hyttinen et al., 2014). Although ubiquitination of substrate proteins is considered to be their general feature, it could not be shown for all of the substrates found in aggresomes (Johnston et al., 2000). Nevertheless, proteasomes, molecular chaperones like Hsp70 and Hsp40 and ubiquitination enzymes are all present in the aggresomes (Hyttinen et al., 2014; Taylor et al., 2003). Enclosed by intermediate filaments such as vimentin and keratin in non-neuronal cells or neurofilaments in neurons, aggresome inclusions are stable and prevented from non-specific interactions (Hyttinen et al., 2014; Johnston et al., 1998). Another crucial component of the aggresome is the microtubule-associated deacetylase HDAC6, which has capacity to bind polyubiquitinated misfolded proteins on one side and microtubule-associated dynein motors, which transport substrate proteins to the aggresomes, on the other side (Kawaguchi et al., 2003). Additionally, HDAC6 is also important for the clearance of aggresomes via autophagy, namely for the transport of the autophagic machinery to the aggresomes. It interacts with the p62/SQSTM1 (Sequestosome-1) and enhances fusion between autophagosomes and lysosomes by actin remodeling (Iwata et al., 2005b; Lamark and Johansen, 2012). Other transporter proteins are ubiquitin-independent BAG3 (BAG family molecular chaperone regulator 3) and p97/VCP (valosin-containing protein). BAG3 interacts with CHIP (carboxy terminus of Hsp70-interacting protein) and dynein to recruit Hsp70 substrates to the aggresomes (Lamark and Johansen, 2012; Zhang and Qian, 2011). The p97/VCP is ubiquitin-associated Hsp-independent molecular chaperone, proposed to induce aggresome formation by delivery of ubiquitinated substrates to HDAC6 and likewise help in autophagosome formation (Boyault et al., 2006; Lamark and Johansen, 2012; Tresse et al., 2010). Although aggresomes were initially proposed to be a general cell response to the accumulation of aggregation-prone misfolded proteins and proteasome inhibition (Johnston et al., 1998), it has later been found that these inclusions are not obligatory products of protein misfolding *in vivo* (Beaudoin et al., 2008). Prion protein, for example, was shown to form aggresomes or dispersed aggregates in different cell lines; formation of the dispersed aggregates was insensitive to HDAC6 inhibitors and did not result in cytoskeleton rearrangements. Moreover, level of protein expression or proteasome inhibition had no effect on the formation of dispersed aggregates (Beaudoin et al., 2008).

Stress conditions including infection, inflammation, oxidative stress, transfection, ER stress and starvation may induce formation of the aggresome-like induced structures (ALIS) in the cytosol (Liu et al., 2012; Szeto et al., 2006). The same inclusions found in dendritic cells were previously termed DALIS (Lelouard et al., 2002). DALIS and ALIS have first been described as transient storage compartments of ubiquitinated, soluble proteins in aggregates, accumulating in response to LPS stimulation or puromycin treatment, respectively (Lelouard et al., 2004; Szeto et al., 2006). Although they resemble aggresomes, they do not colocalize with MTOC, as well are not surrounded by vimentin cage. ALIS accumulate ubiquitinated aggregates, nevertheless, no proteasomes were found in these structures in macrophages (Szeto et al., 2006). Colocalization of chaperones Hsp40 and Hsp90 suggests ALIS formation as a cytosolic unfolded protein response, enhancing protein refolding as well as their degradation (Liu et al., 2012). It was initially reported that inhibition of autophagy with 3-methyladenine or proteasome inhibition interrupts ALIS clearance (Szeto et al., 2006). Nevertheless, later research suggested that only lysosomal activity but not also macroautophagy is responsible for this step, despite both research groups found colocalization of ALIS with LC3B (Liu et al., 2012). Anyhow, another type of autophagy, independent of classic or alternative autophagic pathway, e.g. chaperone-mediated autophagy (CMA) or chaperone-assisted

selective autophagy (CASA) (Lamark and Johansen, 2012) could be responsible for ALIS clearance. Accumulation of ALIS is accompanied by rapid up-regulation of the p62/SQSTM1, which binds ubiquitinated aggregates with its UBA domain. Even more, results indicate that ALIS formation is actually p62-mediated. In addition, NF-κB signaling pathway was also required for p62 expression and mTOR (Mammalian target of rapamycin) activation, implying the role of the p62 and NF-κB proteins in the ALIS formation, as a response to inflammation and ER stress. Likewise the majority of metabolic pathways and responses in cells are intertwined, there is also a clear evidence of crosstalk between ALIS formation in the cytosol and UPR in the ER (Liu et al., 2012).

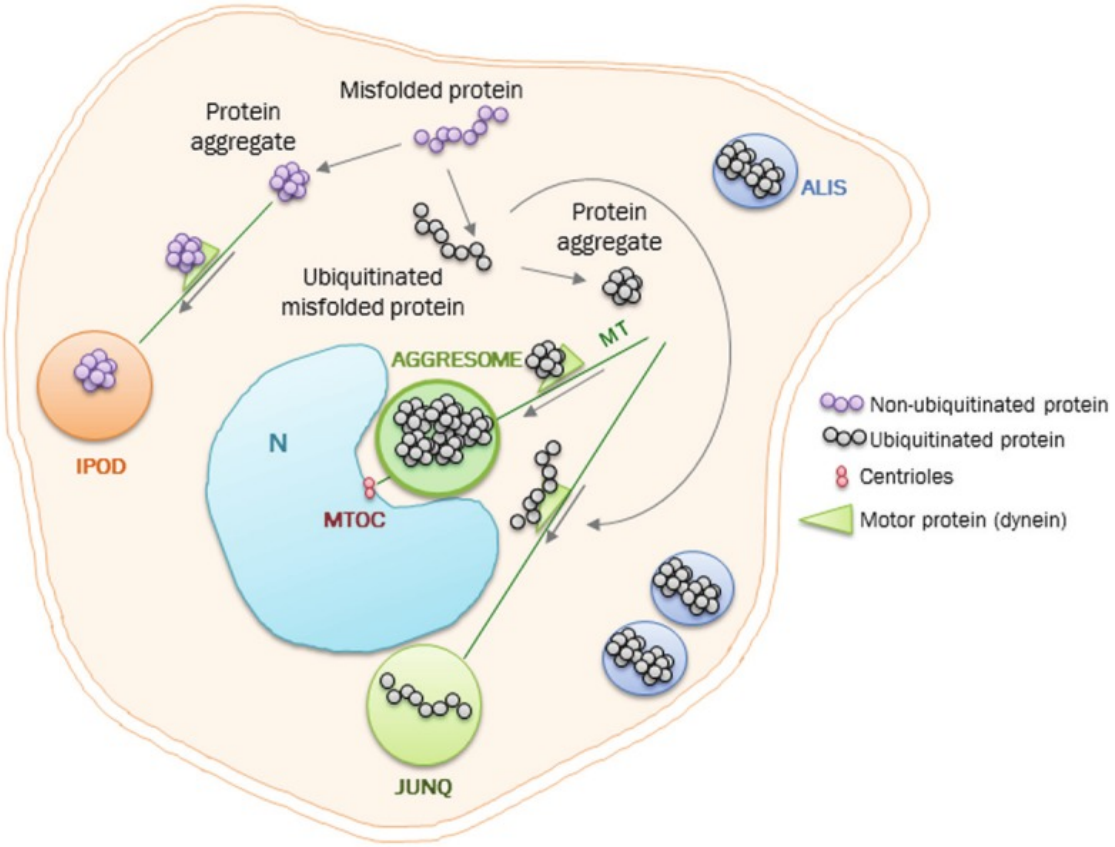

Figure 2: *Different compartments of misfolded or aggregated proteins*. Misfolded proteins may form aggregates which may be sequestered into different quality control compartments, such as JUNQ, IPOD, aggresomes or ALIS, respectively. Sequestration strategy is presumably based on their ubiquitination status, aggregation state and solubility (Takalo et al., 2013).

Accumulating evidence implies that cellular toxicity is associated with non-native soluble species, rather than large aggregates. Large soluble aggregates can thus be protective and promote cell survival. Therefore, spatial separation of aggregates may serve against proteotoxic stress and facilitate their clearance, either through ubiquitin-proteasome system, autophagic pathway or by dilution retention in mother cell during division (Arrasate et al., 2004; Kaganovich et al., 2008; Takalo et al., 2013).

1.1.6 Misfolded protein degradation pathways: ubiquitin-proteasome system and autophagy

Protein quality control is a crucial cellular process for prevention of the accumulation of potentially toxic unfolded or misfolded proteins. It is involved in the above mentioned control of the folding of newly synthesized proteins and either their refolding or degradation of non-native structures (Shang and Taylor, 2011). Therefore, if functioning appropriately and if it is not overwhelmed, quality control system may prevent from the emergence of various proteinopathies (especially neurodegenerative diseases), such as Parkinson disease, Huntington disease, Alzheimer disease, age-related macular degeneration, cystic fibrosis, lysosomal storage disease, etc. (Damme et al., 2014; Dantuma and Bott, 2014; Roussel et al., 2013; Takalo et al., 2013). Thus, cells may use two different proteolytic degradation routes: (i) Ub-proteasome system (UPS) and (ii) autophagosomal-lysosomal system (autophagy), which is responsible for the degradation of long-lived proteins and organelles (Takalo et al., 2013). There is a crosstalk between different degradation systems and loss or inhibition of one degradation pathway may result in the activation of the other pathway. Moreover, accumulating evidence suggest that the UPS and autophagic system work in a coordinated manner, rather than individually (Lilienbaum, 2013).

1.1.6.1 The ubiquitin-proteasome system

By elimination of tagged proteins UPS regulate different cellular processes, including protein degradation, cell division, signal transduction and gene expression (Kraft et al., 2010). Various forms of abnormal proteins, such as mutant, truncated, denatured and oxidized proteins are targeted for UPS-mediated degradation by covalent attachment of polyubiquitin chain. Nevertheless, most aggregated and cross-linked proteins cannot be degraded by the proteasome. Even more, proteasome activity may become inhibited by aggregates (Grune et al., 2004).

Protein ubiquitination is a multistep process, orchestrated by the three ubiquitin ligases E1, E2 and E3. First, the E1 activating enzyme activates ubiquitin by adenylation of C-terminal glycine of ubiquitin and formation of thioester bond between E1's internal cysteine residue and the activated glycine residue. In the next step, conjugating enzyme E2 transfers ubiquitin from the E1 cysteine residue to an E2 cysteine. Finally, activated ubiquitin is transferred from the E2 enzyme to the substrate recruited by the E3 ligase, either directly, or by forming an E3-ubiquitin intermediate. E3 ligase also catalyzes the formation of the isopeptide bond between the C-terminal carboxyl group of ubiquitin and amine group on the lysine residue of the substrate (Navon and Ciechanover, 2009; Shang and Taylor, 2011). Polyubiquitin chain grows through the process of binding of further ubiquitin molecules to the one of the seven lysines (K6, K11, K27, K29, K33, K48 or K63) in the previously conjugated ubiquitin. For UPS-mediated degradation, K48 is classically used. Substrates with ubiquitin molecules bound to Lys48 are recognized by the proteasome and degraded to small peptides and amino acids, whereas most of the ubiquitin molecules are recycled. Polyubiquitin chains linked to the other lysines are often implicated in differential targeting of the tagged substrates and signaling events (Hegde and Upadhya, 2011; Navon and Ciechanover, 2009). Before the substrate is recognized by the proteasome, ubiquitination can be reversed by specific deubiquitinating enzymes (DUBs), which remove ubiquitin conjugates from proteins and disassemble ubiquitin

chain. DUBs are a part of or associated with 26S proteasome, a large multisubunit proteolytic complex (Hegde and Upadhya, 2011).

26S proteasome consists of a 20S core catalytic particle (proteolytic component) and two 19S regulatory particles, attached to the both sides of cylindrically shaped 20S core. The 19S is composed of approximately 20 different proteins. This regulatory particle is responsible for the recognition, unfolding and translocation of the substrate proteins through the 20S proteasome, where they are enzymatically degraded. ATP is required for the assembly of the whole 26S complex, as well as for the unfolding, translocation and degradation process. The 20S proteasome is a barrel-shaped structure, which consists of two inner β-rings with protease activities, each made up of seven subunits, and of two outer α-rings. Specific 19S subunits recognize and unfold ubiquitin-positive substrates before their degradation. During degradation, ubiquitin moieties are removed from the proteins by DUBs and recycled (Hegde and Upadhya, 2011; Lilienbaum, 2013; Navon and Ciechanover, 2009; Takalo et al., 2013). In the canonical UPS, 26S proteasome degrades proteins in an ATP- and ubiquitin-dependent manner, although the process can be executed also in the non-canonical, ubiquitin-independent manner in some rare instances (Benaroudj et al., 2001; Shang and Taylor, 2011). Moreover, 20S proteasome also exists in a free form and is as such capable to degrade some proteins in an ATP- and ubiquitin-independent manner (Shang and Taylor, 2011; Shringarpure et al., 2001). The mechanism by which the UPS distinguishes abnormal from native proteins is still unclear, although recent studies indicate that UPS utilize some chaperones (Hsp70 and Hsp90) and their interacting proteins (CHIP) to recognize and tag abnormal proteins. If Hsp70 fails to refold a misfolded protein, Hsp70-substrate complex is recognized by the CHIP (E3 ligase), which polyubiquitinate the substrate (Su and Lau, 2009). Additionally, exposed hydrophobic regions have been proposed to provide a signal for the discrimination (Murata et al., 2001; Shang and Taylor, 2011).

Perturbations in UPS-mediated proteolysis lead to pleiotropic effects on cells, including degeneration and cell death. A decline in proteasomal activity during aging was demonstrated in the past and this inhibition seems to be much more dramatic in post mitotic cells, explaining the increased vulnerability of neurons (Grune et al., 2004; Hegde and Upadhya, 2011).

1.1.6.2 Autophagy

In contrast to K48-linked ubiquitination, K63-linked ubiquitination may target proteins for autophagy or induce cellular signaling which is not linked to proteolytic degradation (Tan et al., 2008; Wang et al., 2012). Previously published data indicate that cells utilize autophagic pathway to eliminate aggregation-prone proteins that are not degraded by ubiquitin proteasome system (Iwata et al., 2005a; Iwata et al., 2005b). Autophagy is a process in which cytoplasmic material and/organelles are transported to the lysosomes for degradation by lysosomal proteases (Damme et al., 2014). There are three major types of autophagy described in mammals: (i) macroautophagy, (ii) microautophagy and (iii) chaperone-mediated autophagy. Although they differ in the mode of substrate delivery to the lysosome, they have a common task to degrade nonfunctional cytosolic components in order to produce sources for energy production and biosynthesis. Macroautophagy delivers large substrates, such as protein aggregates, microbes and whole organelles to the double membrane-bound autophagosomes, which further fuses with endosomal and lysosomal vesicles, thus forming autolysosome. In contrast, the process of

microautophagy is mediated by the uptake of small portions of cytoplasm through the invagination of the lysosomal membrane. Both micro- and macro- autophagy can act as selective or nonselective mechanisms (Glick et al., 2010). Chaperone-mediated autophagy (CMA) is a selective form of autophagy, degrading proteins containing the KFERQ-like motif without formation of the autophagic vacuole. Substrates for CMA are recognized by Hsp70, Hsp90 and several co-chaperones, which mediate delivery of substrates to the lysosomes, where they are transported across membrane by the LAMP2 (Lysosomal associated membrane glycoprotein 2) receptor (Damme et al., 2014; Johansen and Lamark, 2011).

Autophagy begins with the phagophore formation, which represents an isolation membrane, possibly derived from the ER, *trans* Golgi, endosomes or nuclear membrane, although its exact origin is still controversial. The isolation membrane curves into double-membraned autophagosome containing isolated cargo. Autophagosome matures through fusion with endosomal and lysosomal vesicles to form amphisome and autolysosome, respectively, where the cargo is degraded by acid proteases. Amino acids and by-products of degradation are recycled and re-used for energy production and/or biosynthesis (Glick et al., 2010). In macroautophagy, autophagosome formation is initiated by the inactivation of nutrient and metabolism sensing mTORC1 complex (Mammalian target of rapamycin complex 1) which activates the Ulk1/Ulk2 complex (Unc-51-like kinase1/2). Ulk1/Ulk2 forms a complex with Atg13 (Autophagy-related protein 13) and FIP200 (a focal adhesion kinase family-interacting protein of 200 kDa) which is essential for autophagosome formation. Under nutrient rich conditions, mTORC1 associates with this complex and inactivates it by phosphorylation of Ulk1/2 and Atg13. In case of nutrient starvation, mTORC1 dissociates from Ulk complex, resulting in autophagy activation (Damme et al., 2014; Hosokawa et al., 2009). Phagophore elongation is mediated by the activation of class III phosphatidyl inositol 3-kinase (PI3KC3) complex, especially Vps34 (Vesicular protein sorting 34) and its binding partner Beclin-1. When bound to Beclin-1, Vps-34 uses phosphatidylinositol (PI) as a substrate to generate phosphatidyl inositol triphosphate (PI3P), which in turn recruits other PI3P binding proteins, connected to the formation of specialized ER subdomain, where autophagosome biogenesis occurs. In addition, growing phagophore membrane recruits Atg12-Atg5 complex. The whole process is performed in an ubiquitin-like manner; Atg-12 is activated by Atg7 and transferred to Atg10, which enables covalent linkage of Atg12 to Atg5. Further on, Atg12-Atg5 complex binds Atg16L1. The localization of Atg12-Atg5 complex determines where the lipidation of LC3 (Microtubule-associated protein 1 light chain 3) occurs. During lipidation, cytosolic LC3-I (Atg4-processed LC3) is conjugated to phosphatidyl ethanolamine (PE) on the autophagosomal membrane, giving rise to LC3-II. The related protein GABARAP (Gamma-aminobutyric acid receptor-associated protein) undergoes similar processing during autophagy and colocalizes with autophagosomal LC3-II. It has even been proposed that both, LC3 and GABARAP, are indispensable for autophagy in mammalian cells. After the closure of autophagosomal membrane, Atg12-Atg5-/Atg16L1 dissociates from membrane, while LC3-II stays bound to both sides of autophagosomal membrane, as well as (though to lesser extent) to the autolysosome (Damme et al., 2014; Glick et al., 2010; Yang and Klionsky, 2009). It is important to mention that alternative, Atg5/Atg7-independent autophagy has also been identified. Unlike the classical pathway of autophagy, this one is not associated with LC3 processing, but rather involves autophagosome formation by fusion of isolation membranes with vesicles derived from the late endosome and *trans* Golgi, in a Rab9-dependant manner. This process of macroautophagy was shown to be regulated by Ulk1 and Beclin-1 proteins (Nishida et al., 2009).

In mammalian cells, autophagosomes are often formed at the cell periphery, and later

transported along microtubules to the MTOC, where they fuse with lysosomes. Autophagosome-lysosome fusion is controlled by several Rab and SNARE proteins. It has been proposed that fusion of autophagosomes with early and late endosomes delivers cargo and components of the membrane fusion machinery, in addition to the vacuolar proton pump V-ATPase which lowers the pH of the autophagosomes, prior to delivery of lysosomal proteases. Inhibition of acidification (V-ATPase inhibition) prevents autophagosomal-lysosomal fusion. During the fusion, autophagosomal membrane also acquires lysosomal membrane proteins, such as LAMP1 and LAMP2 (Damme et al., 2014; Glick et al., 2010; Lamark and Johansen, 2012).

Autophagy has been viewed as a random, non-selective process for many years. However, a number of recent reports suggest selective autophagic degradation of various organelles like mitochondria (mitophagy), excessive ER (reticulophagy), peroxisosmes (pexophagy), ribosomes (ribophagy), bacteria and viruses (xenophagy) and aggregation-prone/misfolded proteins (aggrephagy) (Johansen and Lamark, 2011). Selective uptake is believed to be mediated by the adaptor molecules that bind to selected targets on one side and LC3-II protein on phagophore, on the other side. Therefore, autophagy receptors are themselves degraded by autophagy simultaneously with bound substrates. The first known and best characterized example of such adaptor protein is p62/SQSTM1, a multifunctional protein that promotes formation and degradation of polyubiquitinated protein aggregates by autophagy/aggrephagy (Bjorkoy et al., 2005; Glick et al., 2010). The p62 protein is commonly found in cellular inclusion bodies and cytosolic protein aggregates in various chronic, toxic and degenerative diseases, including Levy bodies in Parkinson disease, neurofibrillary tangles in Alzheimer disease and Huntington aggregates in Huntington disease. p62 is able to bind ubiquitin or polyubiquitin via its C-terminal UBA domain and LC3 or GABARAP/GABARAP-like proteins via its N-terminal LIR domain. Specific binding of LIR-containing proteins to the inner surface of autophagosomes results in their degradation by autophagy (Su and Lau, 2009). Moreover, p62 was recently shown to mediate autophagic degradation of some substrates in ubiquitin-independent manner (Gal et al., 2009). Later on, yet another protein with similar characteristics to the p62, named NBR1 (Neighbor of BRCA1 gene) has also been found to be a cargo receptor (Kirkin et al., 2009). Besides, ALFY (Autophagy linked FYVE protein), a PI3P binding protein, acts as a bridge between ubiquitin-positive protein inclusions and selective macroautophagy machinery. ALFY co-localizes and interacts with p62 and NBR1 positive proteins, and directly interacts with autophagic effectors Atg5, Atg12, Atg16L and LC3. No requirement for ALFY in nutrient deprivation-induced autophagy has been found, however, it is essential for autophagic clearance of aggregated proteins (Clausen et al., 2010; Gal et al., 2009).

Another important system for selective degradation of misfolded or oxidized proteins is CMA, where selectivity is based on recognition of the KFERQ peptide (or related sequence) in substrate proteins, which are recognized by the cytosolic Hsp70 chaperone complex (Bozaykut et al., 2014; Dice, 2007). Chaperones interacting with Hsp70 include Hsp40, Hip (Hsp70-interacting protein), Hsp90, Hop (Hsp70-Hsp90 organizer protein) and BAG1 (BAG family molecular chaperone regulator 1) protein and regulate its activity or act as chaperones themselves (Demand et al., 1998; Dice, 2007; Hohfeld et al., 1995; Terada and Mori, 2000). In CMA, there is no need for vesicle formation or major changes in the lysosomal membrane. Selected substrate is targeted to the lysosomal membrane, unfolded with the assistance of Hsp70 (Salvador et al., 2000) and transferred across the lysosomal membrane through the putative translocon formed by the multiple LAMP2A transmembrane segments (Agarraberes and Dice, 2001; Cuervo and Dice, 1996). Translocation into the lysosomal lumen is assisted by the lysosome resident Hsp70 chaperone. Once inside the lumen of lysosome, the selected substrate is rapidly degraded

by lysosomal proteases (Agarraberes and Dice, 2001). Since substrates are transported across the lysosomal membrane and not engulfed by a vesicle, CMA can degrade proteins but not organelles (Bozaykut et al., 2014).

Moreover, recently the term chaperone-assisted selective autophagy (CASA) has been introduced to describe selective autophagy of misfolded proteins following a chaperone-mediated formation of protein aggregates that are targeted to autophagosomes (Arndt et al., 2010). The CASA complex comprises the molecular chaperone HspB8 (Heat shock protein beta-8) and the co-chaperones BAG3 and CHIP. CHIP-mediated ubiquitination of the chaperone-bound client induces recruitment of the adaptor protein p62. The adaptor simultaneously interacts with the ubiquitinated client and autophagosome membrane precursors, thereby inducing the autophagic engulfment of the substrate. The formed autophagosomes finally fuse with lysosomes, resulting in substrate degradation. CASA is thus distinct from CMA, which was shown to facilitate ubiquitin-independent, direct translocation of a client across the lysosomal membrane (Arndt et al., 2010; Ulbricht et al., 2013).

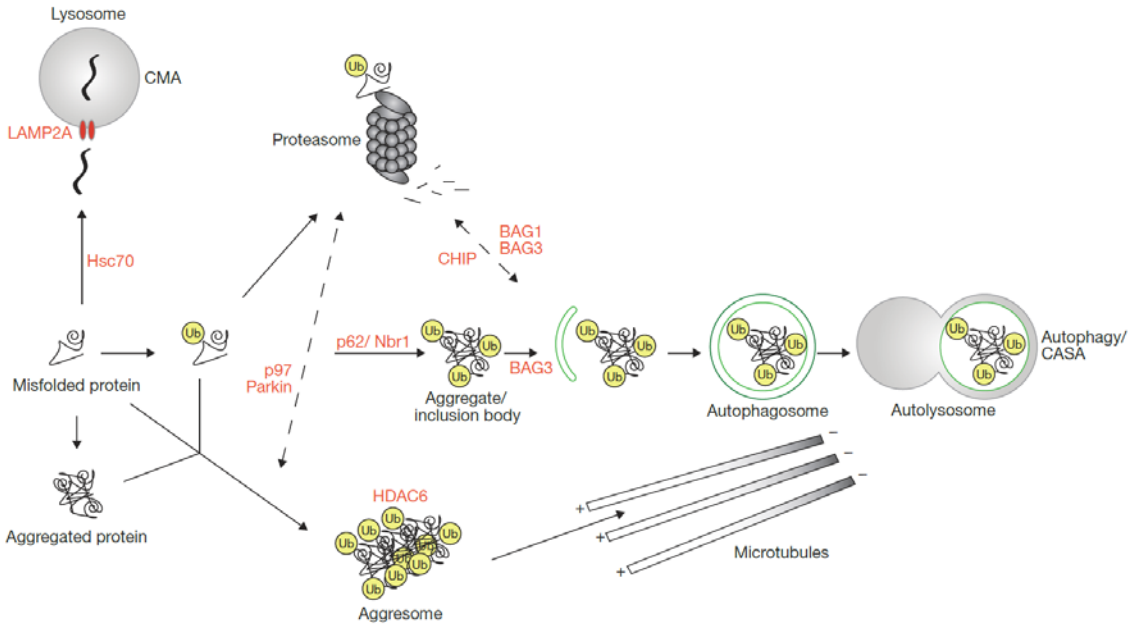

Figure 3: *Crosstalk between different degradation systems* (indicated by dashed arrows). Misfolded and aggregated proteins can be degraded by proteasome. If not, they may aggregate and form different deposits, which could be subjected to selective or non-selective macroautophagy, chaperone-mediated autophagy (CMA) or chaperone-assisted selective autophagy (CASA). Except for the case of CMA, substrates for degradation are often polyubiquitinated (Ub), which can serve as a recognition signal for both degradation systems, depending on the type of polyubiquitination (Kraft et al., 2010). Components coordinating different steps of the degradation routes are marked in red described in the text.

Since there is a distinct advantage of increased autophagy in various physiological and stress conditions, it has been suggested that autophagy represents an important adaptive mechanism that attempts to rescue cells from death. In other words, the presence of autophagic vesicles in dying cells may reflect an adaptive response to maintain cell survival under stress conditions rather than a reflection of “autophagic cell death’’ (Elmore, 2007).

1.2 Lysosomal storage diseases

Lysosomal storage diseases (LSDs) are inherited genetic diseases, caused by mutations in genes that encode lysosomal hydrolases, lysosomal membrane proteins, non-enzymatic lysosomal soluble proteins and proteins involved in processing, trafficking and targeting of lysosomal proteins, including some proteins residing in the ER, Golgi apparatus or the endosomal pathway (Ballabio and Gieselmann, 2009). So far, 58 genetically inherited LSDs have been identified, and the number is continuously growing. Common to all LSD is accumulation of specific storage material in the organelles of endosomal-lysosomal and autophagic system, leading to the lysosomal dysfunction and accumulation of undigested material. Nevertheless, number of disease symptoms indicates that many secondary biochemical and cellular pathways must be activated at the same time. LSDs are classified according to the nature of primary stored material or according to the type of protein deficiency. Clinical features depend on the cell type, the organs involved and the level of residual enzyme activity. The most affected are tissues and organs which synthesize the substrate or acquire it by an active mechanism, such as phagocytosis and those, in which substrate turnover is physiologically high (Alroy et al., 2014; Platt et al., 2012). Some of the well-known groups of LSDs and their respective storage materials are mucopolysaccharidoses (mucopolysaccharides), sphingolipidoses (ceramid, sphingomyelin and glycolipids), oligosaccharidoses and glycoproteinoses (glycogen and other autophagic components), diseases caused by defects in integral membrane proteins and neuronal ceroid lipofuscinoses (NCLs, autofluorescent lipofuscin and subunit c of mitochondrial ATP synthase) (Futerman and van Meer, 2004; Platt et al., 2012). Treatments of LSD may involve gene therapy, enzyme-replacement therapy, substrate-reduction therapy, general treatments, design of small molecules to reactivate defective enzymes (chemical chaperones) and specific drug therapy (Futerman and van Meer, 2004).

1.2.1 Neuronal ceroid lipofuscinoses

The neuronal ceroid lipofuscinoses (NCLs) comprise a group of inherited, severe neurodegenerative disorders with variable age of onset. The incidence (affected persons per live newborns) of disease in USA and Scandinavian countries is 1:12500, while the world incidence is reported to be 1:20000 - 1:100000 (Hachiya et al., 2006; Kyttala et al., 2006). NCLs are characterized by accumulation of autofluorescent ceroid lipopigments, subunit c of the mitochondrial ATP synthase or sphingolipid activator proteins A and D in the lysosomes. The central nervous system (CNS) is the most dramatically affected organ, however, accumulation of autofluorescent material can also occur in extraneuronal cells. Classification of NCLs is based on the onset of clinical symptoms and range from infantile, late infantile and juvenile, to adult forms of the

Table 1: *Classification of* the *NCLs*. (Haltia and Goebel, 2013; Jalanko and Braulke, 2009; Kollmann et al., 2013; Palmer et al., 2013; Schulz et al., 2013)

Gene	Protein	Eponym	Disease onset	Protein localization	Main storage material[a]
CLN1	Palmitoyl-protein thioesterase 1 (PPT1)	Haltia-Santavuori	Infantile, also late infantile, juvenile and adult	Lysosomal matrix, extralysosomal vesicules, extracellular	Saposins A and D
CLN2	Tripeptidyl-peptidase 1 (TPP1)	Jansky–Bielschowsky	Late infantile, juvenile	Lysosomal matrix	Subunit c of mitochondrial ATP synthase
CLN3	Battenin (CLN3)	Batten/ Spielmeyer-Sjögren	Juvenile	Late endosomal/lysosomal membrane, presynaptic vesicles	Subunit c of mitochondrial ATP synthase
CLN4	DnaJ homolog subfamily C member 5 (DNAJC5)	Parry disease	Adult	Cytosolic, associate to vesicular membranes	Saposins A and D
CLN5	Ceroid-lipofuscinosis neuronal protein 5 (CLN5)	Finnish variant late infantile	Late infantile, juvenile and adult (Finnish variant)	Lysosomal matrix	Subunit c of mitochondrial ATP synthase
CLN6	Ceroid-lipofuscinosis neuronal protein 6 (CLN6)	Lake-Cavanagh early juvenile /Indian variant late infantile, adult Kufs type A	Late infantile and adult	ER membrane	Subunit c of mitochondrial ATP synthase
CLN7	Major facilitator superfamily domain-containing protein 8 (MFSD8)	Turkish variant late infantile	Late infantile (Turkish variant)	Lysosomal membrane	Subunit c of mitochondrial ATP synthase
CLN8	Protein CLN8 (CLN8)	Northern epilepsy/ progressive epilepsy with mental retardation	Late infantile	ER membrane	Subunit c of mitochondrial ATP synthase
CLN9	Unknown	Juvenile variant	Juvenile	-	Subunit c of mitochondrial ATP synthase
CLN10	Cathepsin D (CTSD)	Congenital	Congenital, late infantile and adult	Lysosomal matrix, extracellular	Saposins A and D, Subunit c of mitochondrial ATP synthase
CLN11	Granulin (GRN)	Adult variant	Adult	Extracellular	n.d.
CLN12	Probable cation-transporting ATPase 13A2 (ATP13A2)	Juvenile variant	Juvenile	Lysosomal membrane	Uncharacterized non-neuronal storage
CLN13	Cathepsin F (CTSF)	Adult Kufs type B	Adult	Lysosomal matrix	n.d.
CLN14	BTB/POZ domain-containing protein KCTD7 (KCTD7)	Infantile	Infantile	Cytosolic, partially associate to membranes	Subunit c of mitochondrial ATP synthase

[a]In addition to the common lipopigment storage; n.d., not described

disease, although several so-called variant forms were also recognized (Jalanko and Braulke, 2009; Kollmann et al., 2013; Kyttala et al., 2006). Different forms of NCL share many similar pathological features but result from mutations in different genes (designated as CLN1-14; see Table 1), most of which encode soluble and transmembrane proteins localized to the endoplasmic reticulum or endosomal-lysosomal compartment and directly or indirectly regulate lysosomal function. Clinical symptoms of NCLs include photoreceptor- and neurodegeneration, epilepsy, dementia, progressive mental retardation, neuroinflammation and reduced lifespan (Jalanko and Braulke, 2009; Kollmann et al., 2013; Kyttala et al., 2006). At autopsy, massive neuronal loss with characteristic storage material is usually found. For now, none of the NCLs are treatable and the only clinical option is remedy of signs and symptoms (Bennett and Rakheja, 2013). Neurons appear to die due to the increased rate of apoptosis and altered autophagy. Mechanisms from enzyme deficiency to cell death are poorly understood. Settembre and his co-workers found that lysosomal storage impairs delivery of autophagosomal content to the lysosomes, resulting in its inefficient degradation. This impairment leads to massive accumulation of polyubiquitinated proteins and dysfunctional mitochondria, which are putative mediators of cell death (Settembre et al., 2008).

1.2.1.1 Kufs disease

Initial signs and symptoms of adult NCL usually appear around age 30 years, although some symptoms may be visible as early as age 11 years. Death is usually occurring around age 40 years (Mole and Williams, 2013). Among adult forms of NCLs, Kufs disease is the most common, representing between 1.3-10% of NCL cases, however, in general it is a rare and poorly characterized disease. Kufs disease is subdivided into two groups, depending on the dominant clinical symptoms: type A (connected to tonic-clonic seizures, progressive myoclonic epilepsy, dysarthria and ataxia; linked to mutations in CLN6), and type B (with dementia, extrapyramidal and cerebellar signs and behavioral changes, including psychosis and cognitive decline; linked to mutations in CLN13/CTSF) (Berkovic et al., 1988; Josephson et al., 2001; Lewandowska et al., 2009). Thus, Kufs disease is different from early onset forms of NCLs in the way that it lacks visual symptoms. In general, diagnosis of Kufs disease is very challenging, since the same symptoms may occur due to the variety of other disorders. In addition, it is also very demanding to distinguish between abnormal ceroid (lipofuscin) and normal age pigment, thus leaving diagnostic doubts. Confirmed cases of Kufs disease are either sporadic or occur with an autosomal recessive (mainly) or a dominant pattern (Parry type) of inheritance (Sadzot et al., 2000). Type B Kufs disease is genetically heterogeneous and poorly characterized, and therefore very difficult to diagnose based on clinical and ultrastructural examination (Lewandowska et al., 2009; Smith et al., 2013). Recently, missense mutations in the cathepsin F gene were identified by exome sequencing of samples from two families with the recessive type B Kufs disease and additional 22 unrelated individuals with suspected recessive Kufs disease (Smith et al., 2013). Pathological similarities of different NCLs and the fact that the same patients have mutations in different CLN genes, suggests that more NCL proteins function in the same biological pathway (Getty and Pearce, 2011).

1.2.1.2 Cell biology of NCL

Routine microscopic examinations of sections from the adult onset NCL brain show numerous swollen neurons containing abundant storage material, extended from the nucleus to the periphery of the cell (Sadzot et al., 2000). Immunostaining also often revealed astroglial proliferation (astrogliosis) in some areas of the NCL brain (Sadzot et al., 2000; Tang et al., 2006). Stored material in the cytoplasm of neurons and non-neuronal cells is autofluorescent lipopigment, chemically characterized as ceroid (Seehafer and Pearce, 2006). The stored granular pigment is colourless on unstained sections, yellow-brown with hematoxylin and eosin staining, dark blue with luxol-fast blue, lightly stained with oil-red and pale yellow autofluorescent in UV light. By contrast, lipofuscin, which accumulates during the normal aging is yellow-brown on unstained sections and shows orange fluorescence in UV light (Sadzot et al., 2000). Besides, accumulated inclusions in NCLs are period acid Schiff (PAS) positive (Josephson et al., 2001). Lipofuscin is perinuclear, highly oxidized cross-linked aggregate, consisting of oxidized protein (30-58%) and lipid (19-51%) clusters, it is insoluble and cannot be degraded by lysosomal enzymes or UPS (Jung et al., 2007). In general, mechanism of ceroid formation differs from the mechanism of lipofuscin formation (Katz and Robison, 2002). It is assumed that lipofuscin formation starts either with oxidative damage to cytosolic structures (e.g. proteins) or with mitochondrial oxidative stress. If the cellular degradation systems (autophagy and UPS) fail to remove oxidized proteins and damaged giant mitochondria, lipofuscin may form and accumulate, leading to the lysosomal rupture and release of toxic products to the cytosol (Jung et al., 2007). At the ultrastructural level NCL ceroid can be seen as more structured, like fingerprint deposit (FP), curvilinear profile (CP), rectilinear profile (RP) or granular osmophilic deposit (GROD), as well as typical lipofuscin deposit or microtubular aggregate (Figure 4). It was proposed that type of storage material roughly correlates with the age of NCLs onset (Lewandowska et al., 2009; Mole et al., 2005). The accumulated pigment may react with antibodies against some epitopes of amyloid-β precursor protein, suggesting defects in the processing of this protein (Sadzot et al., 2000; Westlake et al., 1995). Besides, storage material is also immunoreactive for ubiquitin (Smith et al., 2013). Granular osmophilic deposits can be mixed with small lipid droplets (Josephson et al., 2001; Tang et al., 2006). This could be a consequence of altered lipid trafficking, which has been shown in some LSDs (Vitner et al., 2010). Moreover, sometimes an assemblage of mitochondria, among which some were swollen and showed changed shape, was found near fingerprint inclusions (Lewandowska et al., 2009). Accumulation of ATPase subunit c was variable in different diagnosed cases (Sadzot et al., 2000; Tang et al., 2006).

Physiological effects of lipofuscin implicate formation of free radicals (Brunk and Terman, 2002) and decline in the efficiency of proteasome and certain lysosomal proteases due to its accumulation in the lysosomes (Terman and Brunk, 2004). Owing to the chemically very reactive surface, lipofuscin is able to bind metals, coming from the metal-containing proteins, including mitochondrial proteins. The consequence is a redox-active surface of lipofuscin particles, enhancing production of reactive oxygen species (ROS) in Fenton reaction, driving to lipid peroxidation, protein and DNA oxidation (Jung et al., 2007). In such a way, lipofuscin also influences the lysosomal membrane integrity and destabilizes the lysosomal compartment, finally leading to cell death (Wihlmark et al., 1997). On the other hand, moderate levels of lipofuscin were shown to have a protective role and increase the resistance of ageing fibroblasts to cell death (Stroikin et al., 2007).

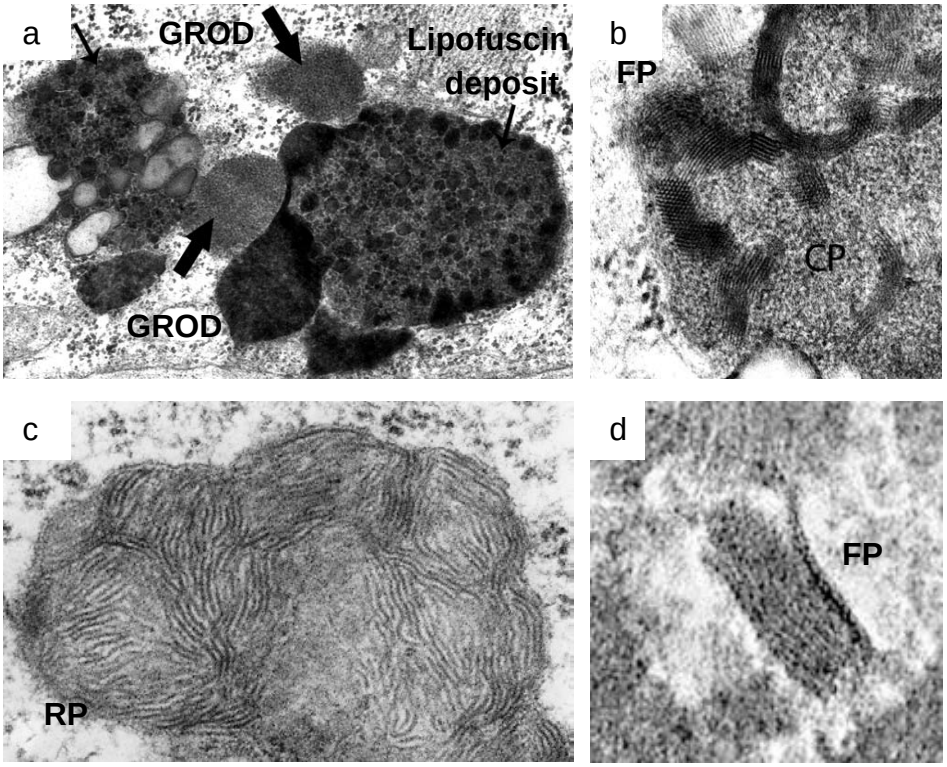

Figure 4: *Examples of storage material profiles, as seen under electron microscope*. (a) Typical lipofuscin deposit and granular osmophilic deposits; GROD. (b) Fingerprint (FP) and curvilinear (CP) profiles (Lewandowska et al., 2009). (c) Rectilinear profile (RP). (d) Fingerprint profile (FP) (Smith et al., 2013).

In lysosomal storage diseases, the size of the lysosomes can increase several fold as a result of accumulation of undigested material. Lysosomal proliferation and swelling could be an attempt of the cells to cope with the accumulated storage material. Observations show progressive increasing in number and size of storage vesicles with age in affected tissues of animal models. Swelling of lysosomes increases the intra-lysosomal pH, due to the failure of the proton pumps in the lysosomal membrane to maintain the H^+ gradient. Since lysosomal enzymes are less active at elevated pH, this may in turn lead to increased formation and deposition of lipofuscin, which is again, most prominently affecting post-mitotic cells (Heard et al., 2010; Hesselink et al., 2003; Parkinson-Lawrence et al., 2010).

Another possible explanation of LSD pathology would be that accumulation of undegraded material in lysosomes block intracellular transport to or from lysosomes, due to the lysosomal »overload« and change in the vacuolar pH. This was indeed found in some types of LSDs (Futerman and van Meer, 2004). Lysosomes are also key organelles in the autophagy system, therefore storage material may impact degradation of autophagosomal and endocytic material, leading to accumulation of excessive levels of undegraded macromolecules, catabolic products and formation of high molecular weight aggregates. Reduced autophagic flux leads to the persistence of giant, dysfunctional mitochondria, which is highly pronounced in NCLs (Ballabio, 2009; Raben et al., 2009). It should be noted that mitochondria are involved in signaling pathways regulating Ca^{2+}

homeostasis, apoptosis and innate immunity too (Futerman and van Meer, 2004). In addition, reduced autophagic flux can set off a cascade of events that impacts also other organelles, including the ER, Golgi, peroxisomes, proteasomal activity, protein turnover and overall cell function (Figure 5) (Platt et al., 2012). Finally, this process may lead to the accumulation of numerous autophagosomes as well as endo/autolysosomes and autophagosome-associated proteins, such as LC3II and p62 (Cao et al., 2006; Settembre et al., 2008).

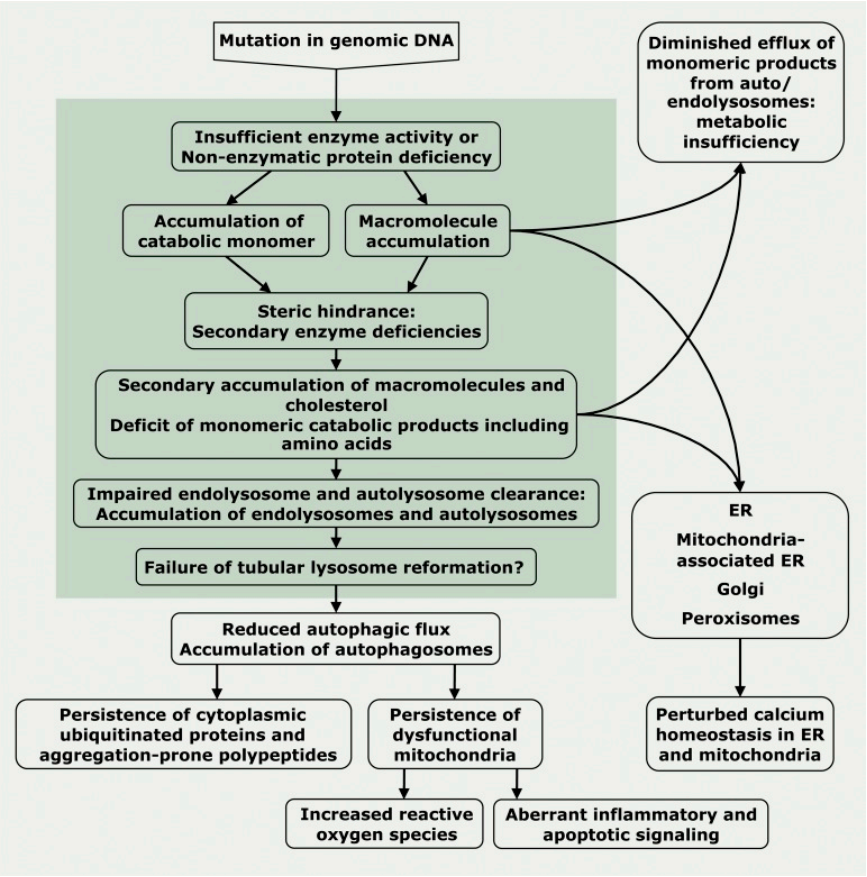

Figure 5: *Hypothetical cascade of events in LSD pathology.* Scheme presents the downstream effects of gene mutations observed in numerous (but not necessarily all) LSDs. Endo/autolysosomal events are confined within green background, whereas processes taking place in cytoplasm that affect other organelles are presented on light background (Platt et al., 2012).

Calcium plays vital roles in regulating a variety of cellular events, and impaired calcium homeostasis leads to ER stress, ER-mediated apoptosis through caspase-12 activation and oxidative stress. In addition, depletion of ER calcium stores interferes with proper folding of proteins in the ER lumen, leading to the UPR. Elevated cytosolic Ca^{2+} may result in activation of mitochondrial apoptotic pathway. However, ER stress has not been reported very often in LSDs. Instead, lipid storage disorders mainly impact ER calcium regulation, leading to the elevated cytosolic Ca^{2+} (Platt et al., 2012). Defective intracellular calcium signaling is recognized as a common pathway in LSDs. The cause of impaired calcium homeostasis is different in each LSD and depends on the organelle, where defective signaling is observed. For example, in CLN3-deficient mouse neurons calcium homeostasis is altered by modulation of a plasma membrane voltage-gated

calcium channel, leading to the higher intracellular Ca^{2+} (Luiro et al., 2006; Vitner et al., 2010).

Increased ROS production, oxidative stress-induced membrane lipid peroxidation, activation of caspases and subsequent DNA fragmentation was found in several cases of late infantile and juvenile NLC (Hachiya et al., 2006; Vidal-Donet et al., 2013). In NCLs, elevated ROS and superoxide dismutase levels were suggested to be downstream to ER stress (Kim et al., 2006). A significant increase in superoxide dismutase activity was also detected in fibroblasts and brain extracts from CLN6 sheep (Heine et al., 2003). Oxidative stress in LSDs is suggested to be most likely activated as a secondary biochemical pathway, rather than as a direct result of accumulation of the primary substrate. Since it plays a central role in other, better studied neurodegenerative conditions, it may be of real significance in delineating LSD pathology too (Vitner et al., 2010). Anyhow, as already mentioned, increased ROS production may initiate or facilitate further formation of lipofuscin (Jung et al., 2007).

Numerous cases of NCL report significant decrease of brain masses with predominant cerebral and cerebellar cortices atrophy, as a consequence of neuronal cell loss (Josephson et al., 2001; Lewandowska et al., 2009; Sadzot et al., 2000; Tang et al., 2006). Some of the possible mechanisms, leading to cell death have already been mentioned above, although the precise cues that activate cell death are not yet fully understood. Neuronal cell death can occur by diverse mechanisms; among them, apoptotic cell death seems to be the main mechanism of cell death in NCLs, according to the studies in mouse models (Mitchison et al., 2004).

1.3 Cell death

As aggregated proteins or their precursors, namely oligomers or fibrils may be cytotoxic, their efficient disposal is essential for cell survival. Therefore, failure to degrade misfolded proteins or prolonged ER stress may lead to a cell death. In fact, this is a dominant contributing factor to neuronal cell death in many neurodegenerative diseases. However, as described later in this chapter, misfolded proteins or ER stress are just one of the numerous activators of cell death (Kopito, 2000). In addition to cytotoxic protein aggregates, oxidative stress and different storage materials may induce cell death through various mechanisms and signaling pathways (Galluzzi et al., 2007). There are several different types of cell death, which may be programmed (genetically controlled), regulated (influenced, at least to some extent, by specific pharmacologic or genetic interventions) or »accidental«. Cell death modes may be classified according to the morphological appearance or molecular definitions (Galluzzi et al., 2012). Based on functional and biochemical parameters cell death modes can be classified to caspase-dependant or independent intrinsic apoptosis, extrinsic apoptosis by death receptors or dependence receptors, necroptosis, autophagic cell death, mitotic catastrophe, necrosis and others (Galluzzi et al., 2015; Galluzzi et al., 2012; Kroemer et al., 2009).

1.3.1 Apoptosis

Apoptosis is morphologically defined by rounding up of the cell, reduction of cellular and

nuclear volume (pyknosis), retraction of pseudopods, nuclear fragmentation (karyorrhexis), minor modification of cytoplasmic organelles and plasma membrane blebbing (but maintenance of its integrity until the final stages of the process). As a result of progressive cellular condensation and budding, small round apoptotic bodies that are surrounded by membranes and contain intact cytoplasmic organelles or fragments of the nucleus, are formed. These apoptotic bodies are quickly taken up by nearby phagocytic cells *in vivo* and degraded within their lysosomes, usually with no associated inflammation (Kroemer et al., 2009). In addition, apoptotic cells exhibit several biochemical features, which comprise protein cleavage by different types of proteases (e.g. caspases, cathepsins and granzymes), DNA breakdown by Ca^{2+} and Mg^{2+} dependant endonucleases and expression of cell surface markers (e.g. phosphatidylserine (PS), Annexin I, calreticulin) (Elmore, 2007). Cell death with apoptotic morphology can be triggered by several stimuli; the response depends on the type of stimuli and/or the degree of stimuli that determines the mode of cell death (Elmore, 2007). Different stimuli can be mediated by death receptor on the cell surface or intracellular stress. In accordance with this, there are two major signalling pathways that mediate apoptosis: (i) the death receptor-dependant or *extrinsic* and (ii) the mitochondria-dependant or *intrinsic* apoptotic pathways. However, these two pathways are linked and can influence each other (Galluzzi et al., 2012).

The *extrinsic* apoptotic pathway is activated by cell surface death receptors binding their respective cytokine ligands. Apoptosis-inducing death receptors are members of the TNF receptor superfamily among which best characterized ligands and their corresponding death receptors are FasL (CD95L)/FasR, TNFα/TNFR1 and TRAIL/TRAILR1/2. Ligand binding to the extracellular death receptor domain stabilizes pre-assembled receptor oligomers, leading to the aggregation of the intracellular motif of death receptor, the death domain (DD). This complex of aggregated receptor domains recruits adaptor proteins containing DDs. Thus, binding of Fas ligand to Fas receptor results in the binding of the adaptor FAS-associated death domain (FADD). The resulting supramolecular complex, described as death-inducing signalling complex (DISC), is a platform for activation of caspase-8 (or-10). DISC formation facilitates a high local concentration of procaspase molecules and thereby promotes the auto-activation of caspase-8. Activated initiator caspases in turn process and activate the downstream executioner caspases, including caspase-3, -6 and -7, which execute the destruction of the cell. Similarly, binding of TNFα ligand to TNFR1 require binding of the TNFR1-associated death domain protein (TRADD), which recruit FADD and caspase-8 (Lavrik and Krammer, 2012; Scott et al., 2009; Vermeulen et al., 2005). Death receptor-mediated apoptosis can be inhibited by proteins recruited to receptor DD and include proteins like c-FLIP (cellular caspase-8 (FLICE)-like inhibitory protein), which binds to the DISC and c-IAP-1 or c-IAP-2 (cellular inhibitor of apoptosis), which binds to RIP1 and TRAF2 on the TNFR1. In this case several non-apoptotic signaling pathways can also originate from the association of adaptor proteins with the receptor, which generally results in the activation of MAPK- and/or NF-κB-mediated survival signals (Guicciardi and Gores, 2009; Lavrik et al., 2005).

For CD95 signalling pathway, two distinct prototypic cell types have been identified. In type I cells, caspase-8 is activated upon death receptor ligation at the DISC in quantities sufficient to directly activate downstream effector caspases such as caspase-3. In type II cell, however, the amount of active caspase-8 generated at the DISC is insufficient to activate caspase-3 and a mitochondrial amplification loop, in which caspase-8 may cleave and activate pro-apoptotic BH3-only protein Bid, leading to the mitochondrial outer membrane-permeabilizing fragment tBID (Guicciardi and Gores, 2009; Scaffidi et al., 1998).

The *intrinsic* apoptotic pathway is mediated by intrinsic signals that converge at the mitochondria in response to diverse intracellular stressors. The intrinsic pathway is activated by non-receptor stimuli, such as UV radiation, gamma irradiation, hypertermia, toxins, virulence factors, the majority of DNA-damaging agents, hypoxia, accumulation of unfolded proteins in the ER, deregulated mitochondrial calcium homeostasis and activation of some oncogenic factors, in addition to the absence of certain growth factors, hormones and cytokines (Elmore, 2007; Galluzzi et al., 2012). The mitochondrial outer membrane permeabilization (MOMP) that commits the cell to apoptosis acts as a central regulator of the intrinsic apoptotic pathway. MOMP prompts the cytosolic release of various signalling molecules that are normally confined to the mitochondrial intermembrane space (IMS). Importantly, cytochrome c leaks into the cytosol and binds to apoptosis protease-activating factor 1 (Apaf-1) in a dATP-dependent manner to form a complex that recruits procaspase-9. The formation of this complex, known as the apoptosome, facilitates oligomerization and activation of caspase-9. Activated caspase-9, in turn, processes and activates the executioner caspases-3, -6, and -7, which drive the execution of the cell (Bratton and Salvesen, 2010; Ow et al., 2008; Repnik and Turk, 2010; Riedl and Salvesen, 2007). Mitochondrial integrity and consequently the fate of cell is actually determined by the balance between the levels of anti-apoptotic Bcl2 family members (such as Bcl-2, Bcl-XL, Bcl-W, MCL,-1), pro-apoptotic Bcl-2 members (BAX and BAK) and pro-apoptotic BH3-only proteins (such as BID, PUMA, BIM, NOXA, BAD and BIK). BH3-only proteins are able to activate BAX and BAK, which form oligomers in mitochondrial outer membrane, finally leading to MOMP, due to the formation of pores (Brenner and Mak, 2009; Kim et al., 2009).

Besides cytochrome c release, the Bcl-2 family proteins have also been reported to control the release of other proteins from mitochondria including certain caspases (caspase-2, caspase-3 and caspase-9), apoptosis inducing factor (AIF), second mitochondria-derived activator of caspase/direct IAP-binding protein with low PI (Smac/Diablo), Omi/HtrA2, endonucleases G and CAD. AIF translocate to the nucleus and causes DNA fragmentation and chromatin condensation. Endonucleases G translocate to the nucleus during apoptosis and similarly to AIF induce caspase-independent DNA fragmentation. Smac/Diablo can interact with the inhibitors of apoptosis (IAPs) like X-linked inhibitor of apoptosis (XIAP) and prevent their activity. Omi/HtrA2 is a serine protease that contributes to caspase-dependent and caspase-independent cell death and also interacts with IAPs or cleaves a wide array of cellular substrates, including cytoskeletal proteins. CAD translocate to the nucleus, where after cleavage by caspase-3 leads to oligonucleosomal DNA fragmentation and chromatin condensation. In addition, MOMP can also cause inhibition of respiratory chain, eliciting reactive oxygen species (ROS) overproduction and caspase-independent apoptosis (Galluzzi et al., 2012; Vande Walle et al., 2008; Wu et al., 2000).

Moreover, there has been accumulating experimental evidences that suggest also involvement of lysosomes or lysosomal constituents in some cell death programs. Several mechanisms have been proposed that may connect the *lysosomal pathway* of cell death to other well documented cell death pathways (Ferri and Kroemer, 2001; Guicciardi et al., 2004; Repnik and Turk, 2010; Stoka et al., 2005). The involvement of lysosomes and lysosomal proteases in apoptosis has been confirmed in several systems. For induction of apoptosis, lysosomal contents must be released into the cytosol. Lysosomes can undergo membrane permeabilization in response to extralysosomal or intralysosomal stimuli. Direct stimuli may involve lysosomotropic agents, photo damage, sphingosine, D-galactosamine, reactive oxygen species (ROS) and compounds that activate p53-independent apoptosis, whereas indirect stimuli may involve binding of a ligand TNFα to its receptor, thus activating caspase-8 (Stoka et al., 2005). The molecular mechanisms of

lysosomal membrane breakdown and the release of lysosomal content into the cytosol are still poorly understood. However, low levels of stress have been suggested to cause only partial lysosomal permeabilization and thereby a limited release of lysosomal contents into the cytoplasm followed by apoptosis or apoptosis-like cell death. In contrast, high stress levels have been suggested to lead to a generalized lysosomal rupture and rapid cellular necrosis (Repnik and Turk, 2010). Lysosome-mediated apoptosis has been reported to be either death receptor-dependent or- independent, however, it is believed to proceed through mitochondria (Repnik and Turk, 2010; Turk and Stoka, 2007). Lysosomal cathepsins that are released into the cytosol after lysosomal membrane destabilization can cleave various protein substrates. Cathepsins B, H, K, L and S exert their effect through the cleavage of BID to generate tBID and by degradation of the anti-apoptotic Bcl-2 molecules Bcl-2, Bcl-XL and MCL-1. Cysteine cathepsins can also act downstream of mitochondria, by degrading XIAP and perhaps other members of IAPs, thereby facilitating executioner caspase activation (Repnik and Turk, 2010). On the other hand, the aspartic cathepsin D activates Bax, thus inducing a selective release of AIF and apoptosis. Another very special example is cathepsin C-mediated activation of the serine protease granzyme B which leads to direct caspase-3 activation. A direct, cathepsin-independent pathway has also been suggested, involving the lysosomal protein lactoferrin. It is thus clear that there is no conserved pathway of lysosome-mediated apoptosis; rather, the pathways differ being stimulus and cell type-dependent (Stoka et al., 2005).

1.4 Cathepsins

For efficient degradation of diverse types of macromolecules, lysosomes contain many different hydrolases, including proteases, amylases, lipases and nucleases (Turk et al., 2012). Based on the catalytic mechanism, proteolytic enzymes can be classified into aspartic, cysteine, glutamic, metallo, asparagine, serine, threonine and mixed catalytic type proteases. Among lysosomal proteases, cysteine cathepsins play an important role (Turk et al., 2012). According to the MEROPS classification (Rawlings et al., 2014) these group of proteases belong to the clan CA (cysteine peptidases), papain family C1 and subfamily C1A. Eleven cysteine cathepsins have been found in humans, including cathepsin B, C, F, H, K, L, O, S, V, W, X (Rossi et al., 2004; Turk and Turk, 2009). These papain-related proteases share conserved folds and similar sequences. Most of them are monomers with a M_r of 20-35 kDa, with the exception of cathepsin C, being a tetrameric enzyme with M_r of ~200 kDa. Papain-like enzymes consist of two (left and right) domains, with V-shaped active site cleft among them (Figure 6). Active site cleft consists of Cys25 and His159 (papain numbering) residues (Turk et al., 2000; Turk et al., 2001).

Cysteine cathepsins are synthesized as inactive precursors with a signal peptide and N-terminal propeptide. The role of signal peptide is to direct the protein to the endoplasmic reticulum (ER) during its synthesis. In the ER, the signal is removed and the protein folds with assistance of the propeptide, which is also responsible for the stability and control of the enzyme's proteolytic activity (Brix et al., 2008). Enzymes are activated in slightly acidic pH of the late endosomes or lysosomes by proteolytic removal of the propeptide. *In vitro* this can be facilitated by activation by other proteases or by autocatalytic activation by an intermolecular process at acidic pH or in the presence of various glycosaminoglycans (Turk et al., 2000; Turk et al., 2012; Turk et al., 2001).

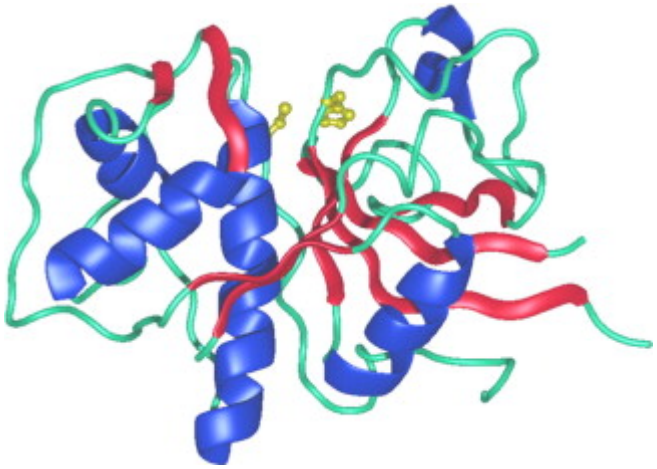

Figure 6: *Typical fold of the mature form of cysteine cathepsin – endopeptidase (example of cathepsin L).* Green ribbon representation is used to show fold of two-chain form cathepsin L. Elements of secondary structures are presented in blue (α-helices) and red (β-sheets) color. The side chain of catalytic residues Cys25 and His163 are shown in ball-and-stick representation (yellow) (Turk et al., 2012).

Activity of cysteine cathepsins can be thus regulated by zymogen processing, pH and inhibition by endogenous protein inhibitors, including stefins, cystatins, kininogens, thyropins, serpins and others. Besides, their functioning can be controlled by regulation of their synthesis (Turk et al., 2000; Turk and Turk, 2009; Turk et al., 2012; Turk et al., 2001; Vasiljeva and Turk, 2008). Most cysteine cathepsins exhibit a predominantly endopeptidase activity, whereas cathepsin B and H are both endo- and exopeptidases and cathepsins X and C are exopeptidases only (Barrett, 1998; Turk et al., 2012; Turk et al., 2001).

Sequence analysis revealed two distinct subfamilies of cysteine cathepsins, namely cathepsin B-like (cathepsin B) and cathepsin L-like (cathepsins L, V, K, S, W, F and H) proteases, although Wang and Wex with their colleagues proposed cathepsins F and W to be divided in a new subgroup named cathepsin F-like (Wang et al., 1998; Wex et al., 1999). The main difference between them is in the sequence and the length of the propeptide. Cathepsin L-like proteases contain a highly conserved ER(F/W)NIN motif, whereas cathepsin B subfamily and the propeptides of cathepsins C, O, and X lack this motif (Karrer et al., 1993; Turk et al., 2012; Wex et al., 1999). In contrast, cathepsin F and W possess ERFNAQ motif (Wang et al., 1998; Wex et al., 1999).

From the ER, cysteine cathepsins are targeted to the acidic environment of late endosomes and lysosomes through addition of mannose-6-phospahete (M6P) on N-linked oligosaccharides in *cis* Golgi network. M6P is recognized by mannose-6-phospahete receptor (M6PR) in *trans* Golgi network. M6PR are later released as the pH drops in the late endosomes and reused in Golgi (Alberts, 2002; Hasilik et al., 2009). Slightly acidic pH (4-6) of the lysosomes is an optimal environment for the activity of most cysteine cathepsins. Some of them, namely cathepsin L, B, H, K, F are unstable at neutral pH,

whereas cathepsin S was found to be stable at neutral or slightly alkaline pH (Turk et al., 1995; Turk et al., 1993; Turk et al., 2000). Therefore, they were initially considered to be localized exclusively in the lysosomes for many years, since they can be relatively rapidly irreversibly inactivated at neutral pH (Turk et al., 2000; Turk et al., 2012; Turk et al., 2001). Nevertheless, despite their stability issues outside of lysosomes, cysteine cathepsins can be active at neutral pH for a short time, which is sufficient for a cleavage of a limited subset of substrates, thus participating in transduction of cellular signals (Turk and Stoka, 2007; Turk and Turk, 2009; Turk et al., 2012). Therefore, they were believed to be localized exclusively in the lysosomes for many years, since they can be relatively rapidly irreversibly inactivated at neutral pH. Nevertheless, despite their stability problems, cysteine cathepsins can be active at neutral pH for a short time, which is sufficient for a cleavage of a limited subset of substrates, thus participating in transduction of cellular signals. However, it was found that cathepsins can also translocate to other organelles inside of the cells (nucleus, mitochondria, cytosol), at the plasma membrane or in the extracellular milieu, where they can play important functions (Goulet et al., 2004; Jane et al., 2006; Muntener et al., 2004; Roshy et al., 2003; Vasiljeva and Turk, 2008). Moreover, truncated forms of some cysteine cathepsins (e.g. cathepsin B, L and H) have been shown to have altered trafficking and subcellular localization, while preserving their catalytic activity (Goulet et al., 2004; Muntener et al., 2003; Muntener et al., 2004; Waghray et al., 2002). Nevertheless, the majority of underlying trafficking mechanisms and sorting signals have not yet been identified (Brix et al., 2008).

Cysteine cathepsins were initially considered as only lysosomal proteases, performing degradation and turnover of cellular proteins, however, this view is rapidly changing and many novel functions were uncovered (Turk et al., 2012). Besides, there is also a lot of redundancy among their functions, as none of the single cathepsin knockouts have defects in protein degradation (Turk and Turk, 2009). Processing of major histocompatibility complex class II molecule and antigen presentation (Nakagawa et al., 1998; Shi et al., 1999), bone remodeling (Saftig et al., 1998), wound healing and prohormone processing (Brix et al., 2008), cancer progression (Jedeszko and Sloane, 2004; Mohamed and Sloane, 2006; Turk et al., 2012; Vasiljeva et al., 2007; Vasiljeva and Turk, 2008), arthritis and cardiovascular diseases (Turk, 2006; Vasiljeva et al., 2007), obesity and diabetes (Reiser et al., 2010), neurological disorders (Pislar and Kos, 2014), inflammation (Colbert et al., 2009; Conus and Simon, 2008) and cell death (Stoka et al., 2001; Stoka et al., 2005; Turk and Turk, 2009) are just some of their known functions (Table 2). The majority of cysteine cathepsins, namely cathepsin B, H, L, C, X, F and O are also ubiquitously expressed in human tissues in contrast to tissue specific distribution of cathepsin K, V, W and S (Turk and Turk, 2009; Turk et al., 2012).

Table 2: *Properties of human cysteine cathepsins.* (Fonovic and Turk, 2014; Pislar and Kos, 2014; Reiser et al., 2010; Turk et al., 2001)

Name	Synonyms	Substrate cleavage mode	Expression	Involvement in diseases (evidence form human and animal studies)
Cathepsin B	Cathepsin B1	Endopeptidase Carboxydipeptidase	Ubiquitous	Cancer and metastasis, lung diseases, rheumatoid arthritis, osteoarthritis, neurological disorders
Cathepsin C	Dipeptidyl peptidase I Cathepsin J	Aminodipeptidase	Ubiquitous	Immune defects
Cathepsin F	-	Endopeptidase	Ubiquitous	Neurological disorders, cancer and metastasis
Cathepsin H	Cathepsin I	Endopeptidase Aminopeptidase	Ubiquitous	Cancer and metastasis, lung diseases, neurological disorders
Cathepsin K	Cathepsin O Cathepsin O2	Endopeptidase	Predominant in osteoclasts and synovial fibroblasts	Atherosclerosis, cancer and metastasis, metabolic syndrome (obesity and type II diabetes), lung diseases, rheumatoid arthritis, osteoarthritis
Cathepsin L	-	Endopeptidase	Ubiquitous	Atherosclerosis, cancer and metastasis, metabolic syndrome (obesity and type II diabetes), lung diseases, immune defects rheumatoid arthritis, osteoarthritis, neurological disorders
Cathepsin O	-	n.d.	Ubiquitous	-
Cathepsin S	-	Endopeptidase	Predominant in professional antigen-presenting cells	Atherosclerosis, cancer and metastasis, metabolic syndrome (obesity and type II diabetes), lung diseases, immune defects rheumatoid arthritis, osteoarthritis, neurological disorders
Cathepsin V	Cathepsin L2 Cathepsin U	Endopeptidase	Thymus, testis	Cancer and metastasis, immune defects
Cathepsin W	Lymphopain	n.d.	Cytotoxic lympho-cytes	-
Cathepsin X	Cathepsin Z Cathepsin P Cathepsin Y	Carboxypeptidase	Ubiquitous	Cancer and metastasis, neurological disorders

n.d., not determined

1.4.1 Cathepsin F

Cathepsin F (CTSF) was identified in alveolar lung macrophage cDNA library and further on cloned from skeletal muscle cDNA library as a sequence encoding 302 amino acids long polypeptide (Wang et al., 1998). This sequence was later found to be only a part of a complete, 484 amino acids long cysteine proteinase belonging to the papain family (Santamaria et al., 1999). Cathepsin F has the same domain organization as other cysteine proteinases, including a hydrophobic signal sequence, a prodomain, and a catalytic region (Santamaria et al., 1999). Nevertheless, this protein shares a relatively low degree of protein sequence identity with cathepsin L- and B-like subfamilies. Since it shares the closest identity (42% identity within mature region and 41% within propeptide) with cathepsin W, it was suggested that these two proteins form a subfamily of cathepsin F-like cysteine proteases (Wang et al., 1998; Wex et al., 1999). The unusually long prodomain, which can be divided into three regions, namely, a N-terminal domain predicted to adopt a cystatin-like fold, a flexible linker and a C-terminal domain similar to that in cathepsin L-like enzymes, makes cathepsin F unique among cysteine protease zymogens (Nagler et al., 1999). The presence of the signal sequence and five potential N-glycosylation sites (Asn^{160}, Asn^{195}, Asn^{367}, Asn^{378}, Asn^{440}) suggest that the enzyme may be targeted to the endosomal/lysosomal compartment via M6P receptor pathway (Nagler et al., 1999; Santamaria et al., 1999). After cleavage of the 19 amino acids long signal peptide, the proenzyme can be subsequently processed autocatalytically or by other lysosomal cysteine or aspartate proteases into the mature, catalytically active, enzyme (Rawlings, 2013; Wang et al., 1998).

Cathepsin F is an endopeptidase with specificity similar to those of cathepsin L, S and K, preferring either phenylalanine or leucine over valine or arginine in P_2 position (Wang et al., 1998). Recombinant human cathepsin F has 90% of maximal activity in the pH range between 5.2 and 6.8, and low pH stability at cytosolic pH (Wang et al., 1998). In addition to its own propeptide, this enzyme has been shown to be inhibited by cystatins (cystatin C, chicken cystatin, L-kininogen, stefin A and stefin B), thyropin (equistatin), propeptide of cruzipain and vinyl sulfones (Fonovic et al., 2004; Reis et al., 2007; Shi et al., 2000; Somoza et al., 2002).

Northern blot analysis showed variable levels of CTSF mRNA expression in different human tissues. High levels were observed in heart, brain, skeletal muscle testis and ovary; kidney, pancreas, placenta, liver and colon express moderate levels, whereas lung, spleen and small intestine produce low levels of CTSF mRNA (Nagler et al., 1999; Santamaria et al., 1999; Wang et al., 1998).

There is not much known about the physiological and pathological role of cathepsin F. Nuclear activity of rat cathepsin F was linked to transcriptional regulation of hepatic stellate cell activation markers. This activity was confirmed to be regulated by nuclear cystatin B and the same nuclear localization was observed also in human hepatic stellate cells (Maubach et al., 2008). Expression of CTSF gene was found in mouse macrophages but not in dendritic cells or splenocytes and recombinant human protein was shown to process major histocompatibility complex class II-associated invariant chain from cathepsin S (CTSS) KO mouse splenocytes (Shi et al., 2000). However, no differences in invariant chain processing could later be found between the CTSF KO mice and wild type (wt) or CTSF/S double KO mice (Tang et al., 2006). Further on, various results suggest a role for cathepsin F in different stages of atherosclerosis, due to its ability of proteolytic modification of apolipoprotein A-I and B-100 *in vitro*. Indeed, cathepsin F was also found to be secreted by cultured macrophages and localized in macrophage-rich areas of the human coronary atherosclerotic plaques, where it may participate in the remodeling of extracellular matrix (Lindstedt et al., 2003; Oorni et al., 2004). Increased mRNA

expression and secretion by cultured human monocyte-derived macrophages can be stimulated by angiotensin II, a relevant factor in the pathogenesis of atherosclerosis (Kaakinen et al., 2007). Overexpression of CTSF in the cervical carcinoma tumor tissues and cell lines in comparison to the normal, HPV negative cervical specimens was revealed by cDNA and tissue microarrays, thus suggesting a possible role of this protein in the pathogenesis of cervical cancer (Vazquez-Ortiz et al., 2005). Moreover, functional implication of CTSF in late adenovirus type 12 infection was proposed (Dorn et al., 2005).

Among cysteine cathepsins, cathepsin F is the only one whose inactivation alone causes a lysosomal storage defect and progressive neurological features in mice (Tang et al., 2006). Mice lacking CTSF developed progressive hind leg weakness, poor balance, tremors, some spontaneous seizures and decline in motor coordination at 12 to 16 months of age. These symptoms were followed by significant body weight loss, ultimately leading to death. Analysis of brain sections from CTSF KO mice demonstrated abundance of neurons accumulating large amounts of autofluorescent lipofuscin, a characteristic of the neurodegenerative disease named neuronal ceroid lipofuscinosis (NCL), thus suggesting cathepsin F to be a candidate for adult-onset NCL. Autofluorescent neurons were observed throughout the brain, including cerebral cortex, hypothalamus, cerebellum (Purkinje cells) and anterior horn cells. Analysis also demonstrated striking accumulation of cytoplasmic eosinophilic granules in most neurons and some glial cells of spinal cord, but not in visceral organs, beginning as early as 6 weeks of age. Ultrastructural assessment of spinal cord motor neurons from CTSF KO mice revealed substantial accumulation of membrane-bound lamellar inclusions with mixed fingerprint and lamellar profiles. In addition, pronounced gliosis, an indicator of neuronal stress and neurodegeneration was also observed in older mice. However, no difference in accumulation of mitochondrial ATP synthase subunit c (a major constituent of lamellar inclusions in most human NCLs) has been observed in spinal cord extracts of cathepsin F KO mice, compared to the WT mice (Tang et al., 2006). Although initial prompts to find similar NCL-related loss-of-function or a mutation of cathepsin F in human patients failed (Tang et al., 2006), a correlation between CTSF and type B Kufs disease, a rare, but most common adult form of NCL has been recently found (Smith et al., 2013). Four missense mutations and one frameshift mutation were identified in cathepsin F gene by exome sequencing of samples from two families with recessive type B Kufs disease and additional 22 unrelated individuals with suspected recessive Kufs disease. The four missense mutations p.Gln321Arg (exon 7), p.Gly458Ala (exon 12), p.Ser480Leu (exon 13), p.Tyr231Cys (exon 5) affect highly conserved amino acids and secondary structure elements and are therefore predicted to be probably damaging for the enzyme. Single nucleotide deletion in exon 7 (p.Ser319Leufs*27) results in a frameshift and a subsequent nonsense mutation that truncates the protein on its C-terminus to approximately three-quarters of its usual length. *In silico* modeling predicted these mutations would alter protein structure and function, thus proposing cathepsin F as a highly plausible candidate mechanism for at least some of cases of type B Kufs disease (Smith et al., 2013). Moreover, some unexplained adult onset peripheral neuropathies were linked to the chromosomal region from 11q12 to 11q14, loci encompassing 11q13, where cathepsin F was mapped to (Macedo-Souza et al., 2005; Windpassinger et al., 2003).

2 Aims and Hypothesis

As human cathepsin F was initially found in its N-terminally truncated form (Wang et al., 1998), we aimed to get an in-depth into the structure-function relationship of published (Δ^{146}CatF) and two additional (Δ^{19}CatF and Δ^{125}CatF) N-terminally truncated forms, in comparison to the wild type (wtCatF) protein. Since all of these three forms lack signal peptide and/or cystatin-like domain, we hypothesize (i) their trafficking and subcellular localization is altered, (ii) they are probably misfolded and prone to aggregation, besides, (iii) expression of such protein could activate cell death pathways. Therefore, we studied expression pattern, subcellular localization, propensity for aggregation and potential activation of cell death program upon their overexpression in human cells.

In the second part of this work we aimed to characterize four point (Y231C, Q321R, G458A and S480L) and one frameshift (S319Lfs*27) mutations, found in cathepsin F gene of patients with type B Kufs disease (Smith et al., 2013). We hypothesize that (i) mutations (i) induce loss-of-function effect, (ii) expression of such mutants may affect cellular homeostasis, resulting in impaired lysosomal function and cytotoxicity. We also hypothesize that (iii) frameshift mutation may cause protein misfolding. In order to evaluate our hypothesis, we focused our attention to the cellular pathways that have been found to be deregulated or impaired in many NCLs; namely lysosomal accumulation and function, autophagic flux and clearance, ROS generation and accumulation of autofluorescent lipopigment. As for the N-terminal mutants, we additionally study expression pattern and subcellular localization, upon overexpression of mutated and wild type protein in human neuronal cells.

3 Materials and Methods

3.1 Materials

All reagents were of an analytical grade and were purchased from Sigma-Aldrich (St. Louis, MO, USA) unless otherwise stated. The human embryonic kidney 293T (HEK 293T) cell line was purchased from LGC Standards GmbH (Wesel, Germany), the human neuroblastoma SH-SY5Y cells were from European Collection of Cell Cultures (ECACC, Salisbury, UK). Phosphate-buffered saline (PBS), Dulbecco's modified Eagle's medium (MEM), Ham's F12, Dulbecco's modified Eagle's medium (DMEM), Fetal bovine serum, L-glutamine, non-essential amino acids and Penicillin/Streptomycin were from PAA (Piscataway, NJ, USA). Poly-L-lysine, the protein inhibitor cocktail, Wortmannin, Menadione and Bafilomycin A1 were from Sigma-Aldrich (St. Louis, MO, USA). The Xfect transfection reagent was purchased from Clontech (Mountin View, CA, USA). The pcDNA3 and pcDNA4/myc-His vectors, non-animal cell dissociation reagent TrypLE Select, ProLong Gold antifade reagent, SlowFade Gold antifade reagent with DAPI and LysoTracker® Green DND-26 were purchased from Invitrogen, Life Technologies (Grand Island, NY, USA). The StrataClone PCR cloning kit was from Agilent Technologies (Santa Clara, CA, USA). The restriction enzymes HindIII, EcoRI and EcoRV-HF and N-Glycosidase F (PNGase F) were from New England Biolabs (Ipswich, MA, USA). The 15-mm round glass cover slips were from Electron Microscopy Sciences (Hatfield, PA, USA). The caspase substrate Ac-Asp-Glu-Val-Asp-AFC and pan-caspase inhibitor Z-Val-Ala-DL-Asp(OMe)-fluoromethylketone were purchased from Bachem AG (Bubendorf, Switzerland). Stock solutions of the substrates and the inhibitors were prepared in dimethylsulfoxide (DMSO) and stored at -20ºC until use. ProteoStat® Aggresome Detection kit was from Enzo Life Sciences (Plymouth Meeting, PA, USA). ECL Plus Western blotting detection reagent was from GE Healthcare Bio-Sciences AB (Uppsala, Sweden). TURBO DNA-free kit and PureLink® RNA Mini Kit were from Ambion, Life technologies (Foster City, CA). MitoSOX™ Red mitochondrial superoxide indicator, Fluo-4 AM calcium indicator and Bodipy 581/591 C_{11} was from Molecular Probes, Life technologies (Eugene, OR, USA) Precision nanoScript™ Reverse Transcription kit, 2x Precision MasterMix, GeNormPLUS reference gene selection kit and all gene specific primers for qPCR were purchased from Primerdesign Ltd (Southampton, UK). Proteasome inhibitor MG-132 was purchased from Santa Cruz Biotechnology (Dallas, Texas, USA).

3.2 Methods

3.2.1 Cloning

Full-length human cathepsin F (wtCatF) was obtained from Martina Klarić, Jožef Stefan Institute. Briefly, the construct was cloned using a PCR reaction and the StrataClone Blunt PCR Cloning kit. The pPCR-Script plasmid containing full-length cathepsin F was used as a template. The cloning was performed using the following oligonucleotides for full-length human cathepsin F: the forward primer 5'-ggaaagcttaaaatggcgccctggctg-3' and the reverse primer 5'-atgaattctcagtccaccaccgccg-3'. N-terminally truncated form was obtained from the wtCatF, namely, Pro126-Asp484 (Δ^{125}CatF) was cloned using 5'-ggaaagcttatgccagtggacaccaag-3' forward primer and and the reverse primer 5'-atgaattctcagtccaccaccgccg-3'. For the Ala20-Asp484 (Δ^{19}CatF) and Met147-Asp484 (Δ^{146}CatF) 5'-ggaaagcttatggcccccgcccagc-3' and 5'-ggaaagcttatgatttcttctctgtccc-3' forward primers and 5'-atgaattctcagtccaccaccgcc-3' reverse primer were used. The full-length cathepsin F and truncated constructs were inserted into the mammalian expression vector pcDNA3 using HindIII and EcoRI restriction enzymes.

For the purpose of comparative analysis of Kufs mutants (Y231C, Q321R, G458A, S480L and S319Lfs*27) and wtCatF, wtCatF was subcloned to the pcDNA4/myc-His A and pEGFP-N2 vectors, using HindIII and EcoRI restriction enzymes. Y231C, Q321R, G458A, S480L were obtained by side-directed mutagenesis using the following primers: for the Y231C 5'-ccgtggcacagctcagtgtggagtcacc-3' (forward primer) and 5'-ggtgactccacactgagctgtgccacgg-3' (reverse primer), for the Q321R 5'-tctccctctctgaacgggagctcttggactg-3' (forward primer) and 5'-cagtccaagagctcccgttcagagagggaga-3' (reverse primer), for the G458A 5'-gggcactgactgggctgagaagggttact-3' (forward primer) and 5'-agtaacccttctcagcccagtcagtgccc-3' (reverse primer), for the S480L mutant 5'-gaacaccatggccagcttggcggtggt-3' (forward primer) and 5'-accaccgccaagctggccatggtgttc-3' (reverse primer) and wtCatF in pcDNA4/myc-His A or pEGFP-N2 vectors (respectively) as a template. Similarly, side-directed mutagenesis was used for the S319Lfs*27 construct, where 5'-ccctgctctccctcctgaacaggagctc-3' (forward primer) and 5'-gagctcctgttcaggagggagagcaggg-3' (reverse primer) were used. In order to eliminate stop codon, forward primer 5'-ggaaagcttaaaatggcgccctggctg-3' and reverse primer 5'-cgttgatatctggccgagtaggcat-3' were used in PCR reaction. To enable the right open reading frame, PCR product was further subcloned to the pcDNA4/myc-His B vector, using HindIII and EcoRV HF restriction enzymes. For cloning of the S319Lfs*27 into the pEGFP-N2 vector, the same procedure was used, except that HindIII and EcoRI restriction enzymes and 5'-cgttgaattctggccgagtaggcat-3' reverse primer were used in the last two steps.

3.2.2 Cell cultures and transient transfection

Human embryonic kidney HEK 293T cells were grown in DMEM medium, supplemented with 10% (v/v) fetal bovine serum, 2 mM L-glutamine, 100 U/ml penicillin/streptomycin at 37ºC in a humidified atmosphere with 5% CO2. Human neuroblastoma SH-SY5Y cells were grown in the MEM/F12 (1:1) medium mixture, supplemented with 15% (v/v) fetal bovine serum, 1% non-essential amino acids (NEAA)

and 100 U/ml penicillin/streptomycin, at the same environmental conditions. Cells were evenly seeded and grown overnight before treatment. For the immunofluorescence labeling and aggresome detection studies, cells were grown on poly-L-lysine-coated coverslips.

The plasmids were transfected into the cells using Xfect transfection reagent following the manufacturer's instructions and grown in complete growth media for 48 h before the analysis. When transfecting two different plasmids (double transfection), 1:1 ratio of both DNA was used in the same amounts as for the single transfection.

3.2.3 Cell lysates and determination of whole protein concentration

The cells were harvested 48 h after transfection using TrypLE Select, washed twice with PBS and centrifuged for 5 min at 1,000 × g. The supernatant was discarded, and the pellet was resuspended in ice-cold RIPA buffer (50 mM Tris, 100 mM NaCl, 0.1% (w/v) SDS, 1% (v/v) NP-40, 0.5% (w/v) deoxycholic acid, 1 mM EDTA pH8). A cocktail of inhibitors was added to the RIPA buffer to prevent protein degradation before Western blotting. The cells were lysed by a 1 hour incubation period on ice and spun for 10 min at 16,000 × g using a refrigerated microcentrifuge. The supernatant (soluble fraction) was collected and used either immediately or stored at -20°C for later use. The pellets were solubilized in 50 µl of 1% (v/v) SDS in PBS for 10 min at room temperature, followed by addition of 50 µl RIPA buffer and sonified for 10 s with a tip sonicator (insoluble fraction).

The protein concentration was estimated using the Bio-Rad Protein assay, based on the Bradford method, following the manufacturer's instructions (Bio-Rad, Hercules, CA, USA).

3.2.4 Cathepsin F deglycosylation

In order to determine N-linked glycosylation of cathepsin F 50µg of total protein was combined with Glycoprotein Denaturing Buffer and heated at 100°C for 10 minutes. After this step G7 Reaction Buffer, NP40 and PNGaseF were added in a total reaction volume of 50µL and incubated at 37°C for 1 hour, as recommended by the manufacturer. 50µg of total protein, subjected to the same reaction conditions except PNGase F treatment, was used as a negative control. Decrease of molecular masses was assessed by Western blotting.

3.2.5 SDS-PAGE and Western blotting

Cells grown in full growth medium alone or (only SH-SY5Y) supplemented with 30 nM bafilomycin A1 or cell permeable proteasome inhibitor 5µM MG-132 (24 hours after transfection) were harvested and lysed 48 hours after transfection. A total of 50 or 100 µg of protein extract was loaded and resolved in 12.5% SDS-PAGE gels, which were run

under reducing conditions using 25 mM Tris, 0.2 M glycine, 0.1% (w/v) SDS running buffer (35mA constant per gel). The gels were then electro-transferred to nitrocellulose membrane (Serva Electrophoresis GmbH, Heidelberg, Germany) at 250 mA constant over 120 min in buffer containing 25 mM Tris, 8 mM glycine and 20% (v/v) methanol. After a blocking step, the membranes were probed with goat polyclonal anti human cathepsin F #ab36161 (Abcam, Cambridge, UK), mouse monoclonal anti myc #R950-25 (Invitrogen, Paisley, UK) or rabbit polyclonal anti human LC3B #ab51520 (Abcam, Cambridge, UK) primary antibodies (final conc. 0.2−0.5 μg/ml) for 3 h. Loading of equivalent amounts of protein was assessed by mouse monoclonal anti β-actin antibodies # A1978 (Sigma, St. Louis, MO, USA). After a washing step, the membrane was incubated with horseradish peroxidase-conjugated secondary antibodies for 1 h at room temperature. Following a washing step, the antigen-antibody complexes were detected using ECL Plus Western blotting detection reagents according to the manufacturer's instructions. The membranes were exposed to a Kodak BioMax Light autoradiography film and developed using a Konica Minolta SRX - 101A automatic X-ray film processor.

3.2.6 Caspase activity

For this purpose, HEK293T cells were grown in full medium, supplemented with 15 μM Z-VAD(OMe)-FMK after transfection. Caspase (DEVDase) activities were assessed from 50 μg of total protein. Briefly, the cleavage of the fluorogenic substrate Ac-DEVD-AFC was measured continuously in a 96-well plate reader (Tecan Infinite M1000 pro) at excitation and emission wavelengths of 400 nm and 505 nm, respectively. The steady-state rates of substrate hydrolysis were extrapolated from the linear phase of the progress curves.

3.2.7 Analysis of free Ca^{2+} in the cell

For evaluation of free intracellular Ca^{2+} in the SH-SY5Y cells, transfected cells were stained with Fluo-4 AM, which exhibits increase in fluorescence intensity after calcium binding. 2 μM Fluo-4 AM in DMEM supplemented with 1% fetal bovine serum was incubated with cells for 30 minutes on 37 °C cells and washed with Ca^{2+} mobilization buffer (HBSS, 20 mM HEPES, 2.5 mM Probenecid and 0.1% (v/v) BSA). For negative control cells were treated with 100 nM EGTA, whereas for positive control 100 μM ionomycin was used. Fluorescence signal was measured immediately after addition of EGTA and ionomycin, continuously for at least 30 minutes in a 96-well plate reader (Tecan Infinite M1000 pro). Excitation and emission wavelengths of 380 nm and 460 nm, respectively 380 nm were used. One experiment on three biological replicates was done.

3.2.8 Flow cytometry (FACS)

SH-SY5Y cells were stained 48 hours after transfection with 40 nM LysoTracker® Green

DND-26 in the growth medium for 10 minutes, washed with PBS, centrifuged, resuspended in PBS and analyzed by flow cytometry on FACSCaliburTM (BD Biosciences, Franklin Lakes, NJ, USA) with CellQuest software (version 3.3). For positive control cells were incubated with 30 nM bafilomycin A1, for 1 hour. At least 10000 cells were acquired for each measurement with three biological replicates. LysoTracker® Green DND-26 fluorescence was excited a 488 Ar-Ion laser and detected in FL1 (515 – 545 nm) channel. LysoTracker® Green DND-26 is a green fluorescent dye that stains acidic compartments in live cells. Decrease in the fluorescence signal is indicative of increased pH of acidic organelles and *vice versa*.

3.2.9 Oxidative stress

Oxidative stress was assessed 48 hours after transfection in SH-SY5Y cells by MitoSOX^{TM} Red (5 μM, 30 minutes) and Bodipy 581/591 C_{11} (2 μM, 30 minutes). Once in mitochondria, MitSOX^{TM} Red reagent is oxidized by superoxide anion and exhibits red fluorescence. Oxidation product also becomes highly fluorescent upon binding to nucleic acids. On the other hand, Bodipy 581/591 C_{11} is sensitive fluorescence reporter for lipid peroxidation. Upon oxidation in live cells, fluorescence emission peak shifts from ~590 nm to ~510 nm after interaction with peroxyl radicals, providing ratiometric indication of lipid peroxidation. This increase or shift in fluorescence was detected under the confocal fluorescent microscope as described in section 3.2.12. Mitosox was excited using the 510 nm lines from WLL (white light laser). Emission light was detected within the range of 528 – 681 nm. Bodipy 581/591 C_{11} fluorescence was excited using the 488 and 581 nm lines from WLL, while emission was detected within the ranges of 493 – 574 nm and 587 – 723 nm, respectively. For positive control in MitoSOX^{TM} Red staining, cells were incubated 1 hour with 100 μM menadione, whereas 1 mM H_2O_2 (1 hour) was used as a positive control in Bodipy 581/591 C_{11} staining.

3.2.10 Immunocytochemistry and autofluorescence

Cells were grown on poly-L-lysine coated round glass coverslips. For lysosomal localization SH-SY5Y cells were incubated for 24 hours in growth medium supplemented with 5 μM wortmannin, one day after transfection. Similarly, growth medium was supplemented with 5 μM MG-132 for analysis of p62-mediate clearance of overexpressed proteins. For immunofluorescence labeling cells were fixed and permeabilized in methanol on ice for 13 min and rinsed in PBS and further incubated in 3% BSA solution for 30 min on shaker. Cells were then incubated with primary antibodies (final conc. 1 μg/ml), for 2 hours and washed with PBS. Further cells were incubated with Alexa Fluor conjugated secondary antibodies (final conc. 0.8 μg/ml) for 1 hour and again washed with PBS. Used primary and belonging secondary antibodies are listed in Table 2. At the end slides were mounted with ProLong Gold antifade reagent or Slowfade antifade reagent with DAPI. Washing steps were performed on shaker and whole procedure, except fixation was done at room temperature. All immunolabeled proteins were detected and visualized with confocal laser scanning microscope LEICA TCS SP5 X as described in section 3.2.12, unless otherwise stated.

For visualization of autofluorescence SH-SY5Y cells were fixed, washed and unstained mounted with ProLong Gold antifade reagent. Autofluorescence was visualized using an Olympus IX81 microscope (Olympus, Tokyo, Japan) with a motorized fluorescence unit. The emission signal was filtered using U-N41002 (red fluorescence), U-N49002 (green fluorescence) and U-MNUA2 (UV) filter cube. Micrographs were taken using a Hamamatsu ORCA-R2 cooled digital CCD camera (Hamamatsu, Hamamatsu City, Japan), and Olympus Cell F software (Olympus, Tokyo, Japan) was used to evaluate the signal. For the final image, signal from red, green and blue fluorescence was combined and converted to black and white image for better visualization.

Table 3: Primary and secondary antibodies used in immunocytochemistry.

Antibody	#Cat. No.	Producer
rabbit polyclonal anti human Cathepsin F	sc-13987	Santa Cruz Biotechnology, Dallas, Texas, USA
goat polyclonal anti human Cathepsin F	ab36161	Abcam, Cambridge, UK
rabbit polyclonal anti human LC3B	ab51520	Abcam, Cambridge, UK
mouse monoclonal anti human p62, clone 11C9.2	MABC32	Merck Millipore, Darmstadt, Germany
mouse monoclonal anti human LAMP2 [H4B4]	ab25631	Abcam, Cambridge, UK
mouse monoclonal anti human PDI	ADI-SPA-891	Farmingdale, NY, USA
goat anti rabbit IgG, Alexa Fluor 488	A-11034	Molecular Probes, Eugene, OR, USA
goat anti mouse IgG, Alexa Fluor 546	A- 11030	Molecular Probes, Eugene, OR, USA
donkey anti goat IgG, Alexa Fluor 546	A-11056	Molecular Probes, Eugene, OR, USA
goat anti mouse IgG, Alexa Fluor 488	A-11029	Molecular Probes, Eugene, OR, USA
goat anti rabbit IgG, Alexa Fluor 546	A-11035	Molecular Probes, Eugene, OR, USA

3.2.11 Aggresome detection

Cellular aggresomes were detected using the ProteoStat® Aggresome Detection kit according to the manufacturer's instructions. HEK 293T and SH-SY5Y cells were grown on poly-L-lysine coated coverslips and transfected as described in Section 3.2.2. Cells incubated for 12 (HEK293T) or 24 (SH-SY5Y) hours with a cell permeable proteasome inhibitor, MG-132 (5 µM), were used as a positive control. Afterwards, the cells were washed with PBS and fixed in 4% paraformaldehyde for 30 min at room temperature. The cells were then permeabilized in permeabilizing solution (0.5% Triton X-100, 3 mM EDTA, pH 8.0 in 1× assay buffer) with gentle shaking on ice for 30 min. After this step, cells were washed again in PBS and stained using the ProteoStat® Aggresome Detection Reagent and Hoechst 33342 Nuclear Stain for 30 min at room temperature protected from

light. The microscope slides were mounted using the ProLong Gold antifade reagent and aggressomes were visualized using an Olympus IX81 microscope (Olympus, Tokyo, Japan) with a motorized fluorescence unit. The emission signal was filtered using U-N41002 (red fluorescence) filter cube. Micrographs were taken using a Hamamatsu ORCA-R2 cooled digital CCD camera (Hamamatsu, Hamamatsu City, Japan), and Olympus Cell F software (Olympus, Tokyo, Japan) was used to evaluate the specific labeling signal.

3.2.12 Fluorescence confocal microscopy

Fluorescence microscopy and optical slicing were performed using an inverted confocal laser scanning microscope LEICA TCS SP5 X with white light laser (WLL) at an excitation source in the range from 470 nm to 670 nm and a 405 nm diode laser for DAPI excitation. The excitation lines were selected using an acousto-optical tunable filter (AOTF) as indicated below. An oil objective HCX PL APO 60× (N.A. = 1.4) was used. Optical sections in the z-direction were obtained and the emission signal was separated using an acousto-optical beam splitter (AOBS) and captured with one PMT and two hybrid detectors (HyD). Immunolabeled proteins were excited using the 488 nm and 546 nm lines from WLL. Sequential scanning was strictly applied when multiple fluorescence signals were examined and the emission light was detected within the range of (1) 413 nm – 457 nm for fluorescence in the blue spectrum, (2) 498 nm – 550 nm for fluorescence in the green spectrum, and (3) 559 nm – 617 nm for fluorescence in the red spectrum. Leica software LAS AF was used to evaluate the obtained fluorescence signals and colocalization of labeled proteins, respectively.

3.2.13 Transmission electron microscopy (TEM)

SH-SY5Y cells were fixed with 4 % paraformaldehyde at room temperature for 2 h. Mixture of growth medium and fixative was removed with a series of centrifugation steps and the pellet of cells embedded in 10 % gelatin. Gelatin was solidified on ice and cells excised and cut into small blocks (1 mm3). Blocks of cells were then immersed in 2.6 M sucrose (cryoprotectant) in 0.1 M phosphate buffer and infiltrated at 4 ºC overnight. Finally, cryoprotected cells were mounted on aluminum specimen carriers and stored in liquid nitrogen. Trimming and sectioning of frozen blocks were performed on Leica EM FC6 ultramicrotome for cryosectioning. Frozen specimen blocks were trimmed at –90 °C and ultrathin cryosections (70 nm) were cut at –120 °C using diamond 35° angle cryo-immuno knife (Diatome, Biel, Switzerland). Sections were collected and thawed on droplets of pick-up solution, i.e. 1:1 mixture of 2.3 M sucrose and 2 % methyl cellulose. Retrieved ultrathin sections of cells were put on carbon-coated Formvar film spread over copper grids (Agar Scientific, Elektron Technology UK Ltd., Essex, UK). Prior to uranyl acetate staining gelatin was removed from sections and grids rinsed on droplets of ultra-pure water. Sections were contrasted with 0.4 % uranyl acetate in solution with 1.8 % methyl cellulose (pH 4). Uranyl contrasted the cell proteins but not the lipids so the membranes appeared white on TEM micrographs. Contrasted cells were observed at 150 kV with JEM-2100 LaB6 transmission electron microscope at the Centre for Electron

Microscopy, Jožef Stefan Institute, Ljubljana, Slovenia. Micrographs were taken using Gatan digital camera and DigitalMicrographTM software (Gatan, Inc., Pleasanton, CA, USA).

3.2.14 RNA isolation and quantitative real time PCR (qPCR)

We isolated RNA and quantify mRNA expression of selected genes as described in (Maher et al., 2014). Namely, total RNA was isolated from the SH-SY5Y cells with the PureLink® RNA Mini Kit and treated with TURBO DNA-free kit for genomic DNA elimination. RNA quality (A260/230 and A260/280 ratios) was assessed spectrophometrically, whereas RNA integrity was confirmed by 1.2% gel electrophoresis. RNA was further reverse transcribed into cDNA with a random nanomer primers using Precision nanoScript™ Reverse Transcription kit. mRNA expression levels of analyzed genes were detected by SYBR green detection chemistry using 2x Precision MasterMix. Most stable expressed reference genes for normalization were chosen by GeNormPLUS reference gene selection kit and their geometric mean was used to calculate the relative mRNA expression of individual genes. Quantitative real-time PCR reaction was run on Mx3005P Real-time PCR system (Agilent, Stratagene products) using the following conditions: 95°C for 10 min (an initial denaturation step) followed by 40 cycles of 95°C for 15 sec and 60°C for 1 min (annealing and extension). Additionally, melting curve was performed at the end of each run. Sequences of gene specific primers are listed in Table 3. REST (Relative Expression Software Tool) 2009 was used for group-wise comparison and statistical analysis of relative expression results as described by Pfaffl et al. (Pfaffl et al., 2002). The relative expression ratios of target genes were calculated considering their real-time PCR efficiencies and the crossing point difference between control and treated samples. For up-regulation, the factor of regulation is equal to the given value, while for down-regulation, the regulation factor is illustrated as a reciprocal value (1/expression ratio). Randomization test randomly reallocates the observed values in different sample groups to the values in the control group. Relative expression is then estimated for each of the new groups and the effect of randomization in each group is evaluated.
The hypothesis test P (H1) performed 2000 pairwise fixed reallocations of control and sample group. $P<0.05$ was considered as statistically significant.

Table 4: List of primers used in qPCR analysis

Gene name	**Official gene symbol**	**Prime sequence** F: forward primer R: reverse primer
DNA-damage-inducible transcript 3, transcript variant 1 (human)	DDIT3 (CHOP)	F: GTGGCTACTGACTACCCTCTC R: ACCTTTCCTTTTGTCTACTCCAA
78 kDa glucose-regulated protein (human)	HSPA5 (BiP)	F: CAGGCTGGTGTGCTCTCT R: TCCTTGGAATCAGTTTGGTCAT
ER degradation enhancer, mannosidase alpha-like 1 (human)	EDEM1	F: GGGAACTACTCATTGACTCTTGT R: CTTGGACGGTGGAATCTTTGT
Calreticulin (human)	CALR	F: GGCACCATCTTTGACAACTTC R: CTCTGCTCCTCGTCCTGTT
Cathepsin F (human)	CTSF	F: ACAAGATGAAGCAAGCCAAGT R: CACACATGCCCTGGTCTTTG
Ecto-NOX disulfide-thiol exchanger 2 (human)	ENOX2	part of the human geNormPLUS kit (Primerdesign Ltd, Southampton, UK)
Spermatogenesis-defective protein 39 homolog (human)	VIPAR	part of the human geNormPLUS kit (Primerdesign Ltd, Southampton, UK)

3.2.15 Statistical analysis

For statistical analyses we used Office Analysis ToolPak. Student's t-test was employed for the calculation of P value. Graphs represent the mean and standard deviation of three biological replicates or independent experiments unless otherwise stated.

4 Results

4.1 Characterization of N-terminally truncated forms of human cathepsin F

Truncated forms of some cysteine cathepsins have been shown to encounter altered trafficking and subcellular localization, while preserving their catalytic activity (Goulet et al., 2004; Muntener et al., 2003; Muntener et al., 2004; Waghray et al., 2002). Human cathepsin F was initially thought to encompass only 302 amino acids (according to the by authors' opinion most probable putative translation start site) (Wang et al., 1998). Nevertheless, the same authors raised the possibility of the other putative translation start site, resulting in the 338 amino acids long transcript from smooth muscles and deposited it to the GeneBank under the accession number »AF071748«. We aimed to research the consequences of such N-terminal truncation for the protein expression and behavior. Therefore, we cloned three different N-terminally truncated variants of human cathepsin F, namely Δ^{19}CatF (Ala^{20} – Asp^{484}), Δ^{125}CatF (Pro^{126} – Asp^{484}) and Δ^{146}CatF (Met^{147} – Asp^{484}) in addition to the wild type (wtCatF) protein (Figure 7) in pcDNA3 vector, and expressed them in HEK293T cells. Δ^{19}CatF thus lacks the signal peptide, Δ^{125}CatF lacks signal peptide and cystatin like domain, whereas Δ^{146}CatF lacks in addition 20 amino acids of linker.

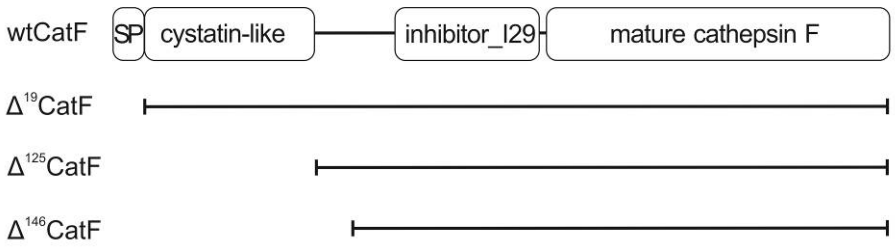

Figure 7: *Schematic representation of human cathepsin F and its N-terminally truncated forms.* Top panel represents the domain composition of the wild type human cathepsin F. Below is a scaled representation of Δ^{19}CatF, Δ^{125}CatF and Δ^{146}CatF boundaries.

4.1.1 N-terminally truncated forms of human cathepsin F have distinct subcellular localization to the wild type protein

Wild type cathepsin F has been proposed to be targeted to the lysosomal compartment (Nagler et al., 1999; Santamaria et al., 1999). Similarly the 302 amino acids long truncated variant was proposed to have vesicular pattern and to be targeted to the lysosomes via M6P-independent pathway, however, we predict that lack of the signal

peptide will alter trafficking and subcellular localization of our mutants. Therefore we assessed the lysosomal localization of the expressed proteins by examination of the protein colocalization with the endosomal/lysosomal marker LAMP2, 48 hours after transfection in HEK293T cells. Immunolabeling of cathepsin F revealed vesicular staining and colocalization of the wtCatF with the LAMP2 marker (Figure 8). On the other hand, Δ^{19}CatF, Δ^{125}CatF and Δ^{146}CatF exhibited more massive, perinuclear and aggregate-like appearance of staining, which was mainly not colocalized with the LAMP2.

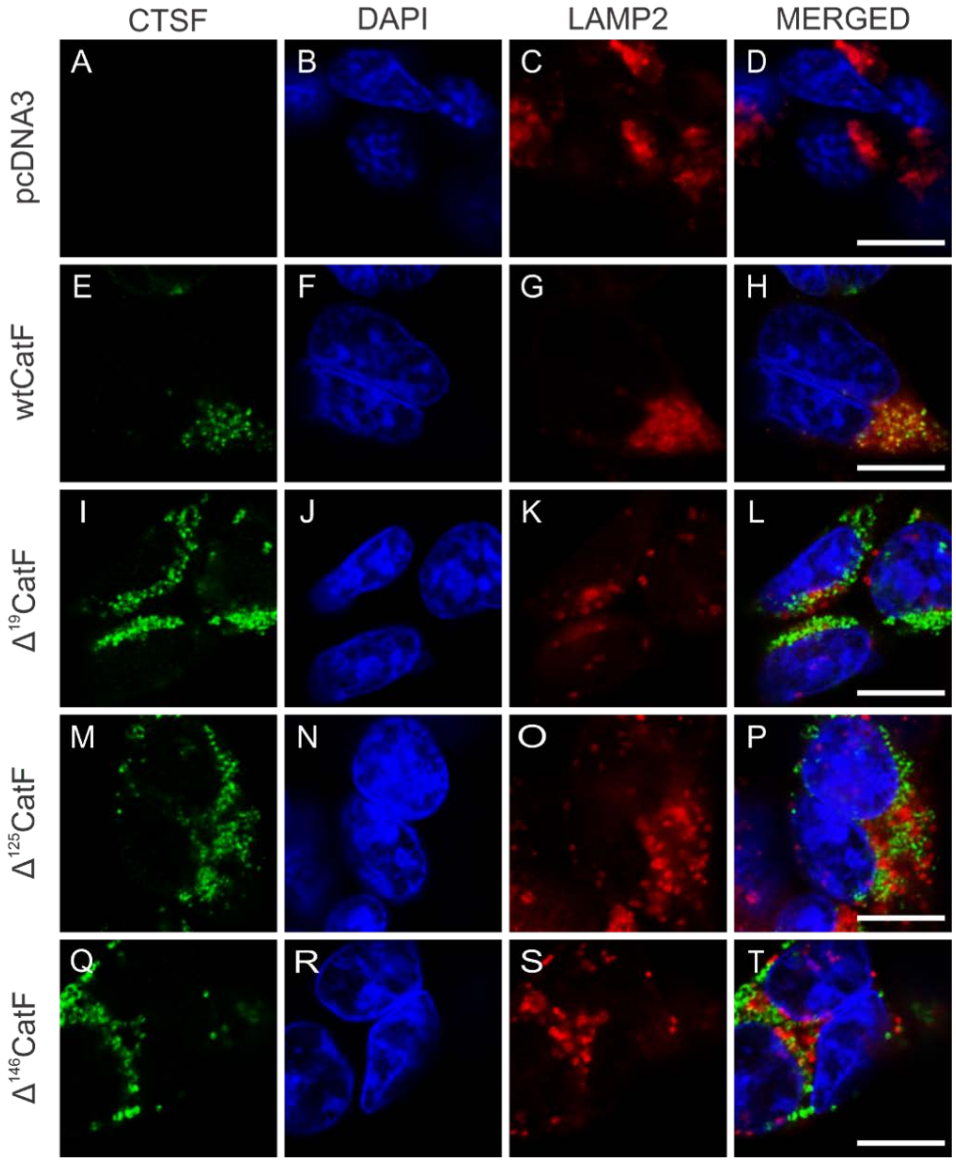

Figure 8: *Subcellular localization of human cathepsin F (wtCatF) and its N-terminally truncated forms (Δ^{19}CatF, Δ^{125}CatF and Δ^{146}CatF).* Subcellular localization was assessed using confocal microscopy 48 h after transfection in HEK 293T cells. Immunolabeling was done using rabbit polyclonal anti cathepsin F and mouse monoclonal anti LAMP2 primary antibodies, followed by Alexa Fluor-labeled secondary antibodies as described in Section 3.2.10. Confocal images showed expression pattern of cathepsin F (CTSF) labeled with green fluorescence (A, E, I, M, Q) and the lysosomal marker LAMP2 labeled with red fluorescence (C, G, K, O, S). Merged images represent overlapping immunoreactivity in yellow (D, H, L, P, T). The nucleus was counterstained for DNA using DAPI (blue fluorescence: B, F, J, N, R). Negative controls included the non-transfected, mock-transfected and pcDNA3 empty vector-transfected cells. Since very similar pattern was obtained under all of these three conditions, a representative example, the pcDNA3 (A –D) is shown only. Scale bar = 10 μm.

4.1.2 Expression pattern and deglycosylation of the wild type cathepsin F and its N-terminally truncated variants

We studied expression pattern of N-terminally truncated variants in comparison to the wild type cathepsin F following their overexpression in HEK293T cells. 48 hours after transfection cell lysates were obtained and analyzed by Western blotting (Figure 9). Surprisingly, only two bands of the wild type protein (wtCatF) at approximately 70 and 30 kDa were detected in the soluble fraction (Figure 9A). This led us to the evaluation of insoluble fraction (Figure 9B) of the same cell lysate, which uncovered the bands of all three N-terminally truncated variants. Δ^{19}CatF resulted in a major band of ~60 kDa and additional two minor bands of ~52 and ~45 kDa, respectively. Δ^{125}CatF and Δ^{146}CatF were detected as single bands of ~40 and ~38 kDa, respectively.

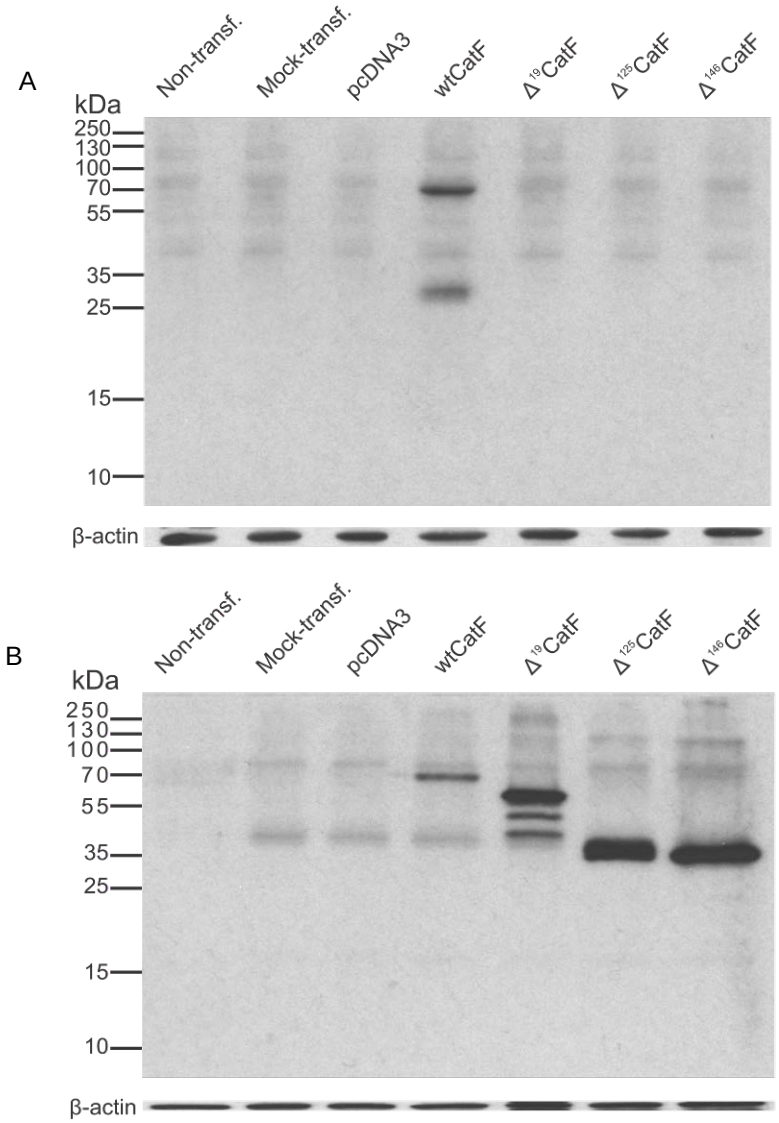

Figure 9: *Expression of human cathepsin F and its N-terminally truncated forms in HEK293T cells.* HEK293T cells were transfected with pcDNA3 plasmids containing wtCatF, Δ^{19}CatF, Δ^{125}CatF and Δ^{146}CatF and lysed 48 hours later to obtain soluble (A) and insoluble (B) fractions of whole cell protein extracts, as described in section 3.2.3. Expression of cathepsin F was evaluated by Western blotting using an anti-human cathepsin F antibody (described in section 3.2.5). Negative controls included the non-transfected, mock-transfected and pcDNA3 empty vector-transfected cells. Loading of equivalent amounts of protein was assessed with β-actin (lower blot).

Asparagine-linked glycosylation properties of the wtCatF, Δ^{19}CatF, Δ^{125}CatF and Δ^{146}CatF were obtained by exposure of the proteins to the peptide-N-glycosidase F (PNGase F), an enzyme that hydrolyzes all classes of N-linked glycans (Figure 10). Extracts were further subjected to the Western blotting. As expected, we observed differences in the molecular weight after deglycosylation of the wild type protein but not also the truncated variants. We demonstrated a ~6 kDa decrease in the Mw of both, the full-length and mature form of the wild type cathepsin F, respectively.

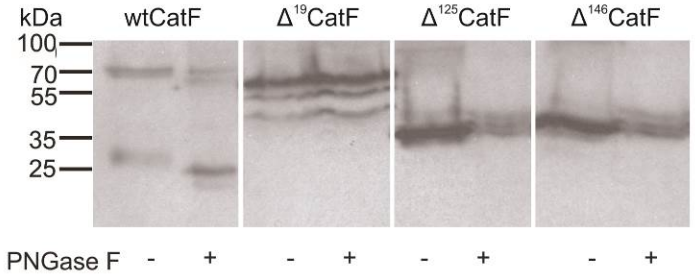

Figure 10: *Deglycosylation of human cathepsin F and its N-terminally truncated forms.* Whole cell protein extracts of wtCatF, Δ^{19}CatF, Δ^{125}CatF and Δ^{146}CatF-expressing HEK293T cells was subjected to the PNGase F treatment as described in section 3.2.4. Eventual decrease in Mw of the treated proteins after deglycosylation was assessed by Western blotting.

4.1.3 N-terminally truncated forms of human cathepsin F accumulate in aggresome-like inclusions

The fact that Δ^{19}CatF, Δ^{125}CatF and Δ^{146}CatF form aggregated insoluble structures that do not localize to the lysosomes, encouraged us to inspect the possibility of the aggresome formation. With this purpose, we stained HEK293T cells overexpressing our constructs with the Proteostat®, which is a red fluorescent molecular rotor dye detecting aggregated proteins within the aggresome and aggresome-like structures (Shen et al., 2011). Staining with Proteostat® revealed the presence of perinuclear aggresome-like structures in cells overexpressing Δ^{19}CatF, Δ^{125}CatF and Δ^{146}CatF proteins or cells treated with 5 μM proteasomal inhibitor MG-132 (positive control), (Figure 11). Contrary, overexpression the wtCatF or transfection of the cells with empty vector did not result in positive Proteostat® staining.

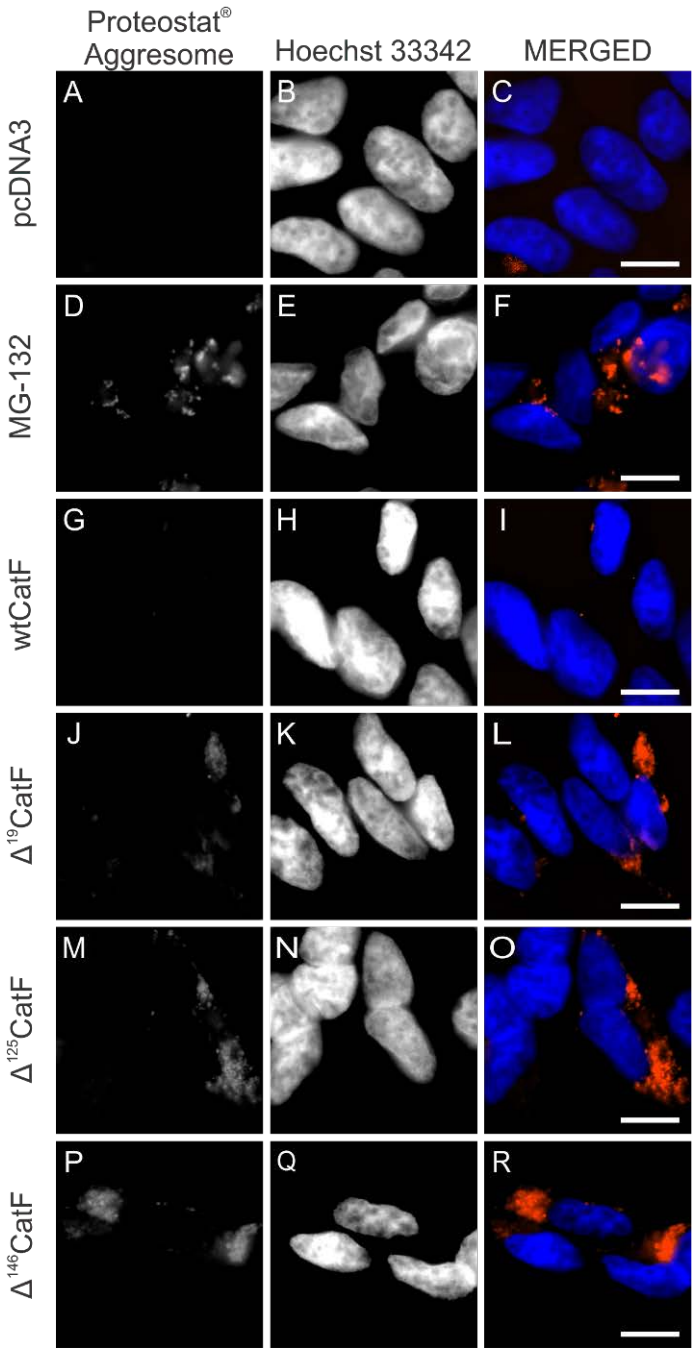

Figure 11: *Accumulation of aggregated N-terminally truncated forms of Δ[19]CatF, Δ[125]CatF and Δ[146]CatF in aggresomes.* HEK293T cells were stained with Proteostat® 48 hours after transfection with pcDNA3 plasmids containing wtCatF (G – I), Δ^{19}CatF (J – L), Δ^{125}CatF (M – O) and Δ^{146}CatF (P – R). Nuclei were counterstained with DNA-staining Hoechst 33342 (blue fluorescence). Negative controls included non-transfected, mock-transfected and empty vector-transfected cells. Due to the similar pattern, only the representative image of pcDNA3 (A – C) is included. For positive control, cells were treated with 5 μM proteasomal inhibitor MG-132 (D – F), 12 hours before staining. Scale bar = 10 μm.

4.1.4 N-terminally truncated Δ^{19}CatF, Δ^{125}CatF and Δ^{146}CatF are p62 positive inclusions, cleared by autophagy

Autophagy is the most often used route by cells for degradation and elimination of aggregated proteins due to the limited capacity of ubiquitin-proteasome system in degradation of protein aggregates. Ubiquitinated proteins are bound by the p62/SQSTM1 adaptor protein that promotes formation of the aggresomes as well as ALIS and their degradation by autophagy and/or aggrephagy (Bjorkoy et al., 2005; Glick et al., 2010). Using anti human p62/SQSTM1 antibodies, we demonstrated that Δ^{19}CatF, Δ^{125}CatF and Δ^{146}CatF often colocalize with p62 (Figure 12). This was, however, not the case for the wtCatF, where also the basic level of p62 protein expression was much lower.

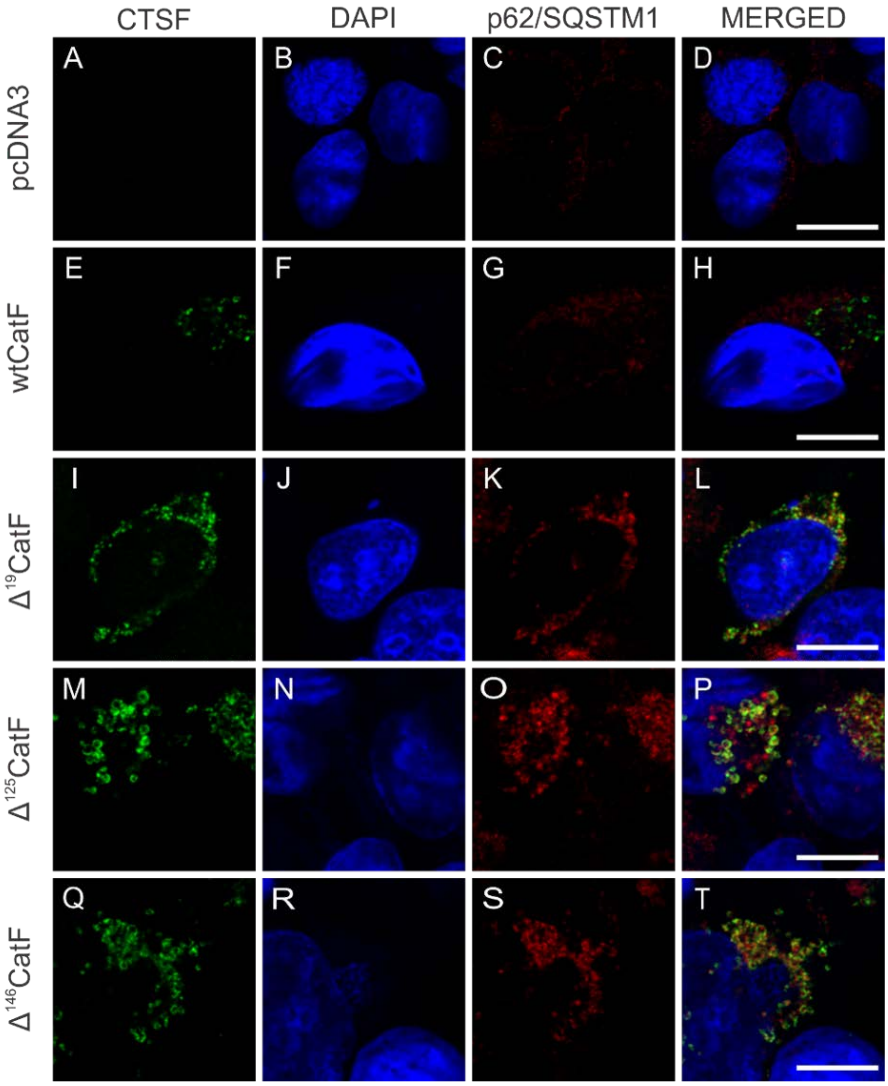

Figure 12: N-terminally truncated Δ^{19}CatF (I – L), Δ^{125}CatF (M – P) and Δ^{146}CatF (Q – T), but not also the wtCatF (E – H) are p62 positive inclusions. HEK293T cells were transfected with the wild type and N-terminally truncated constructs and 48 later immunolabeled with rabbit polyclonal anti human cathepsin F (CTSF; green fluorescence) and mouse monoclonal anti human p62 (p62/SQSTM1; red fluorescence) antibodies. Merged images (in yellow) represent the combined fluorescence. Nuclei were counterstained with DNA-staining DAPI (blue fluorescence). Negative controls included non-transfected, mock-transfected and empty vector-transfected cells. Due to the similar pattern under all three conditions, only, the representative image of pcDNA3 (A – D) is included. Scale bar = 10 μm.

Further, we assessed whether protein aggregates of the N-terminally truncated proteins colocalize with the autophagosomal marker microtubule-associated protein 1A/1B light chain 3B (LC3B). Transfection of cells with N-terminally truncated forms induced formation of the aggregated LC3B puncta which were larger, yet fewer in number, compared to more numerous but vesicular, cytoplasmic puncta when cells were transfected with the wild type protein (Figure 13). Nevertheless, Δ^{19}CatF, Δ^{125}CatF and Δ^{146}CatF displayed strong colocalization with the LC3B, which was othewise only minor in the cells expressing wtCatF. Transfection of HEK293T cells with the empty vector or mock transfection displayed only a weak signal of baseline autophagy, similar to non-transfected cells.

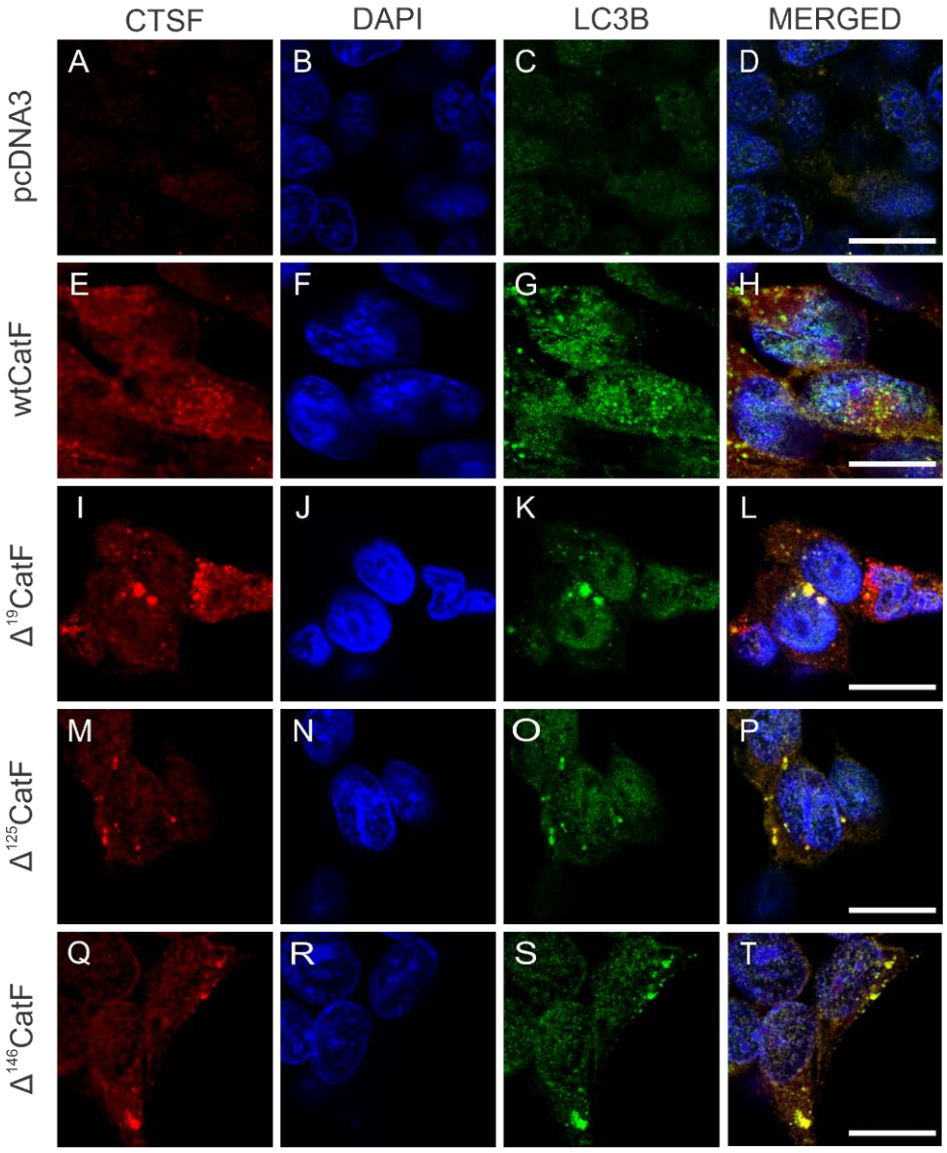

Figure 13: Colocalization of LC3B with overexpressed cathepsin F variants in HEK293T cells. Cells were immunolabeled with goat polyclonal anti cathepsin F (CTSF; green fluorescence) and rabbit polyclonal anti LC3B (LC3B; red fluorescence) primary antibodies. Confocal images showed colocalization of cathepsin F and autophagosomal marker LC3B (yellow) in cells transfected with pcDNA3 plasmids containing wtCatF (E – H), Δ^{19}CatF (I – L), Δ^{125}CatF (M – P) and Δ^{146}CatF (Q – T). Nuclei were counterstained with DAPI (blue fluorescence). Representative negative control is pcDNA3 (A – D). Scale bar = 10 μm.

4.1.5 N-terminally truncated forms of human cathepsin F induce caspase activation

Accumulation of protein aggregates may lead to caspase activation and apoptosis, if not degraded or removed from the cells (Grenier et al., 2006; Kristiansen et al., 2005). Using a fluorogenic substrate Ac-DEVD.AFC (c-Asp-Glu-Val-Asp-7-amino-4-trifluoromethylcoumarin), we demonstrated a significant 2 – 3 fold increase in caspase activation in HEK293T cells transfected by N-terminally truncated variants compared to the empty vector transfected cells (Figure 14). In contrast, cells overexpressing the wild type cathepsin F exhibited similar signal level to the one, obtained in the negative controls. Signal increase was blocked by pan-caspase inhibitor Z-VAD(OMe)-FMK in all tested samples, thus confirming specificity of the detected signal.

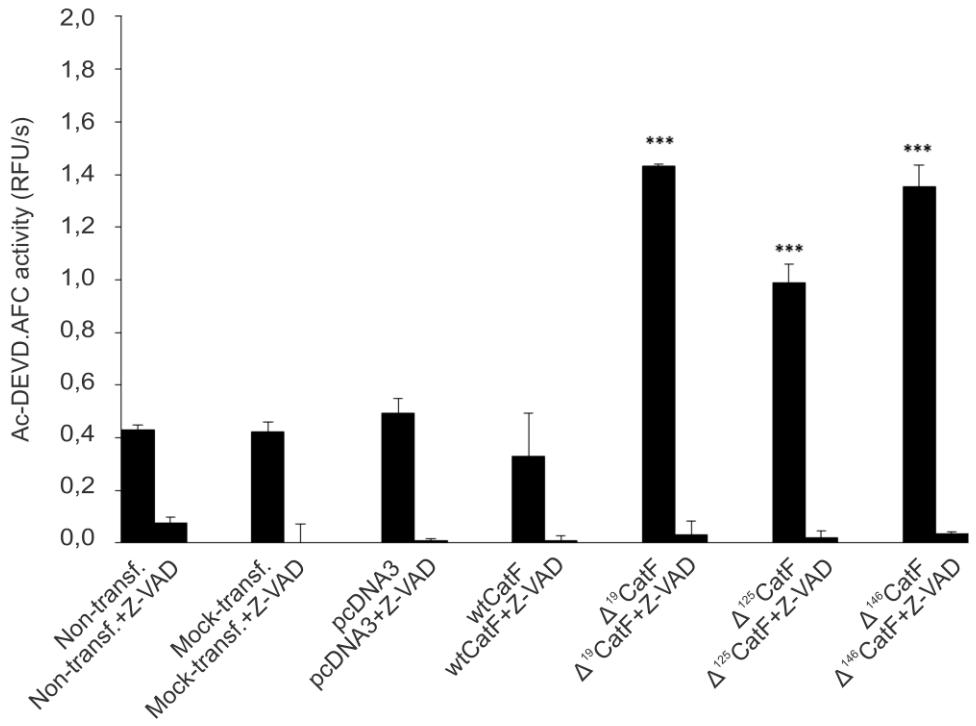

Figure 14: Overexpression of the N-terminally truncated forms of human cathepsin F, but not the wild-type protein, induces caspase activation. DEVDase activity was monitored by kinetics 48 h post-transfection with human cathepsin F and its N-terminally truncated forms Δ^{19}CatF, Δ^{125}CatF and Δ^{146}CatF. For this purpose, HEK293T cells were grown in full medium, supplemented with 15 μM Z-VAD(OMe)-FMK after transfection. Caspase (DEVDase) activities were assessed from 50 μg of total protein as described in section 3.2.6. Negative control experiments included non-transfected, mock-transfected and pcDNA3 empty vector-transfected cells. The results are given as the means ± SD of three independent experiments. ***, $p<0.001$ compared to pcDNA3.

4.2 CLN13 mutations induce alterations in cellular homeostasis that resemble characteristics of NCL disease

The purpose of the second part of this work was to characterize four point (Y231C, Q321R, G458A and S480L) and one frameshift (S319Lfs*27) mutations (Figure 15), found in cathepsin F (designated as CLN13) gene of patients with type B Kufs disease (Smith et al., 2013). Mutations were predicted to be probably damaging for the function of the affected protein by the same authors, but not also experimentally confirmed. Characterization of deleterious functional effects is limited due to the limited knowledge of physiological substrates and lack of specific inhibitors. Therefore, we rather focused our attention to the consequences of the expression of Y231C (p.Tyr231Cys), Q321R (p.Gln321Arg), G458A (p.Gly458Ala), S480L (p.Ser480Leu) and S319Lfs*27 (p.Ser319Leufs*27) mutants in the neuronal cell line SH-SY5Y compared to the effects of the wild type protein. We paid our special attention to changes in the cellular pathways or processes that have been found deregulated or impaired in many NCLs, namely accumulation of undegraded material in lysosomes, autophagic flux and clearance, ROS generation and accumulation of autofluorescent lipopigment. CLN13 mutants were obtained by side directed mutagenesis from wild type human cathepsin F (wtCatF) and cloned into the pcDNA4/myc-His and pEGFP vectors. The frameshift mutation results in the 344 amino acids long, C-terminally truncated, protein due to the premature stop codon.

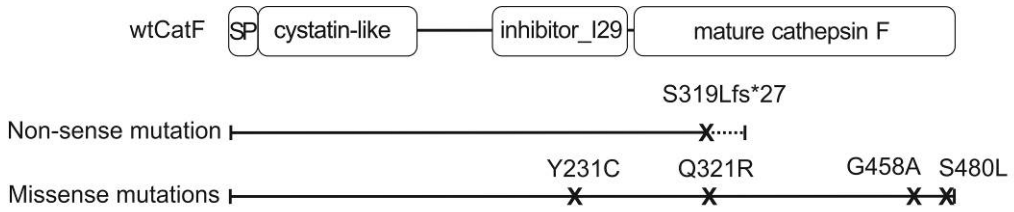

Figure 15: *Schematic representation of human cathepsin F (CLN13) and its type B Kufs mutants.* Top panel represents the domain composition of the wild type human cathepsin F. Positions of S319Lfs*27, Y231C, Q321R, G458A and S480L mutations are indicated in a scaled representation. Dashed line represents frameshift and the new amino acid sequence in the protein.

4.2.1 Expression pattern and potential degradation pathway

Firstly, we evaluated expression pattern of the CLN13 mutants and the wild type protein after their overexpression in human neuroblastoma SH-SY5Y cell line. In addition, we strived to determine the dominant degradation pathway of expressed proteins by monitoring their accumulation after inhibition of the lysosomal degradation (autophagy) or UPS pathway, respectively. SH-SY5Y cells were transfected with pcDNA4/myc-His vector containing either the wtCatF or Y231C, Q321R, G458A, S480L and S319Lfs*27, respectively and 24 hours later treated with bafilomycin A1, a known inhibitor of autophagy or MG-132 (Z-Leu-Leu-Leu-CHO), a cell-permeable reversible proteasome inhibitor (Lee and Goldberg, 1998). Bafilomycin A1 prevents maturation of autophagic

vacuoles by inhibiting fusion between autophagosomes and lysosomes, through inhibition of the vacuolar H^+ ATPase (V-ATPase) (Yamamoto et al., 1998). Soluble and insoluble fractions were prepared from cell lysates, 48 hours after transfection and assessed by Western blotting, as described in section 3.2.3 and 3.2.5, respectively.

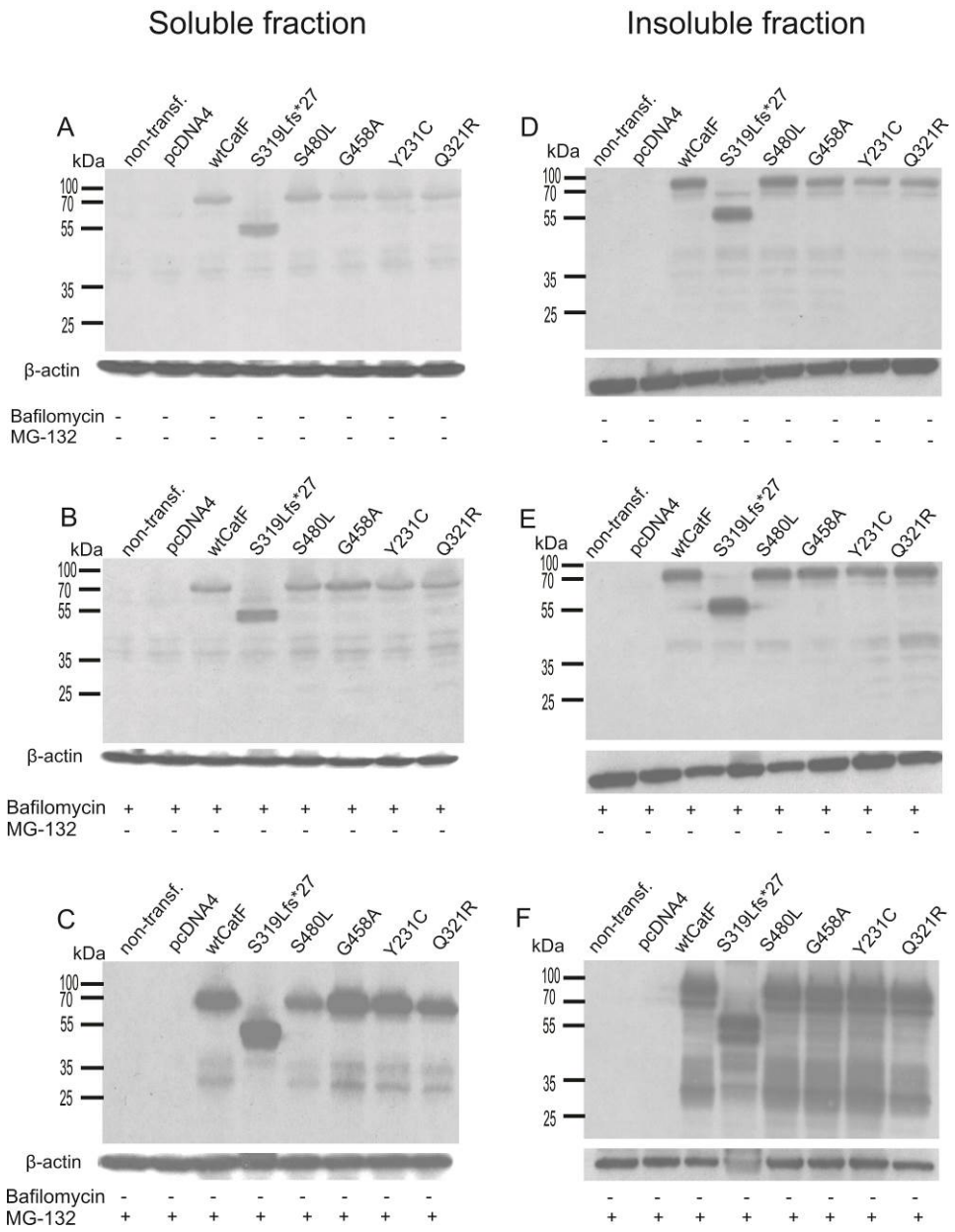

Figure 16: *Expression of human cathepsin F (CLN13) and its type B Kufs mutants in SY-SY5Y cells.* Cells were transfected with pcDNA4/myc-His-containing wtCatF, S319Lfs*27, S480L, G458A, Y231C and Q321R mutants and 24 hours later left untreated (A, D) or exposed to 30 nM bafilomycin (B, E) or 5 μM MG-132 (C, D) for further 24 hours. Soluble (A – C) and insoluble (D – E) fractions of whole protein extracts were evaluated by Western blotting using anti myc tag antibodies. Loading of equivalent amounts of protein was assessed against β-actin (lower blot).

All transfected constructs were successfully expressed and found in the soluble fraction (Figure 16 A – C). wtCatF and missense mutants were detected as a single band of ~70 kDa by Western blot analysis, whereas expression of the frame shift mutant S319Lfs*27 resulted in two close bands of ~50 and ~52 kDa. Although we could not observe increased amounts of insoluble fraction (pellet size), like in the case of N-terminally truncated cathepsin F variants (which were completely insoluble), we surprisingly detected bands of all expressed proteins also in the insoluble fraction (Figure 16 D – E). Detected proteins in the insoluble fraction had slightly higher Mw (~85 kDa for the wtCatF and missense mutations and ~60 kDa for the frameshift mutation, respectively), compared to those observed in the soluble fraction. After proteasomal inhibition by MG-132, additional bands of slightly lower (~70 kDa) Mw for the wtCatF and missense mutants emerged in the insoluble fraction (Figure 16F). These bands were reminiscent of those observed in the soluble fraction of the same treatment (Figure 16C), since they had the same Mw. Overall, we could note slight accumulation of the expressed proteins after autophagy inhibition and major accumulation after proteasomal inhibition.

4.2.2 Y231C, Q321R, G458A, S480L but not also S319Lfs*27 are expressed in the lysosomes

Potential lysosomal localization of CLN13 mutants was assessed after their overexpression in SH-SY5Y using anti LAMP2 antibodies. For this purpose wtCatF, Y231C, Q321R, G458A, S480L and S319Lfs*27 were cloned in pEGFP-N2 vector. Fluorescence microscopy revealed S319Lfs*27 to be prevalently expressed as aggregates in opposite to dispersed, vesicular expression of the wtCatF protein and missense mutants (Figure 17, left panel G – I). Immunostaining indicated colocalization of all investigated proteins (CTSF-EGFP) with the lysosomal/endosomal marker LAMP2 (Figure 17, left panel). Although all of the expressed proteins contain signal peptide for lysosomal targeting, mutated and aggregated proteins could be localized to the lysosomes as a consequence of their autophagic clearance. Therefore, we re-evaluated lysosomal localization after treatment of the cells with 5 μM wortmannin, a phosphatidyl inositol 3-kinase inhibitor (Blommaart et al., 1997), thereby inhibiting autophagosome formation and sequestration of the expressed proteins into the autophagosomes (Figure 17, right panel). Truly, wortmannin abolished colocalization of EGFP- tagged S319Lfs*27 with LAMP2 (Figure 17, right panel G – I), suggesting its delivery to the lysosomes via autophagy. S319Lfs*27 also induced swelling of LAMP-2 positive vesicles (Figure 17, left panel H and I). This effect was sometimes also observed within cells expressing other mutants, but less prominently (Figure 17, left panel K or T).

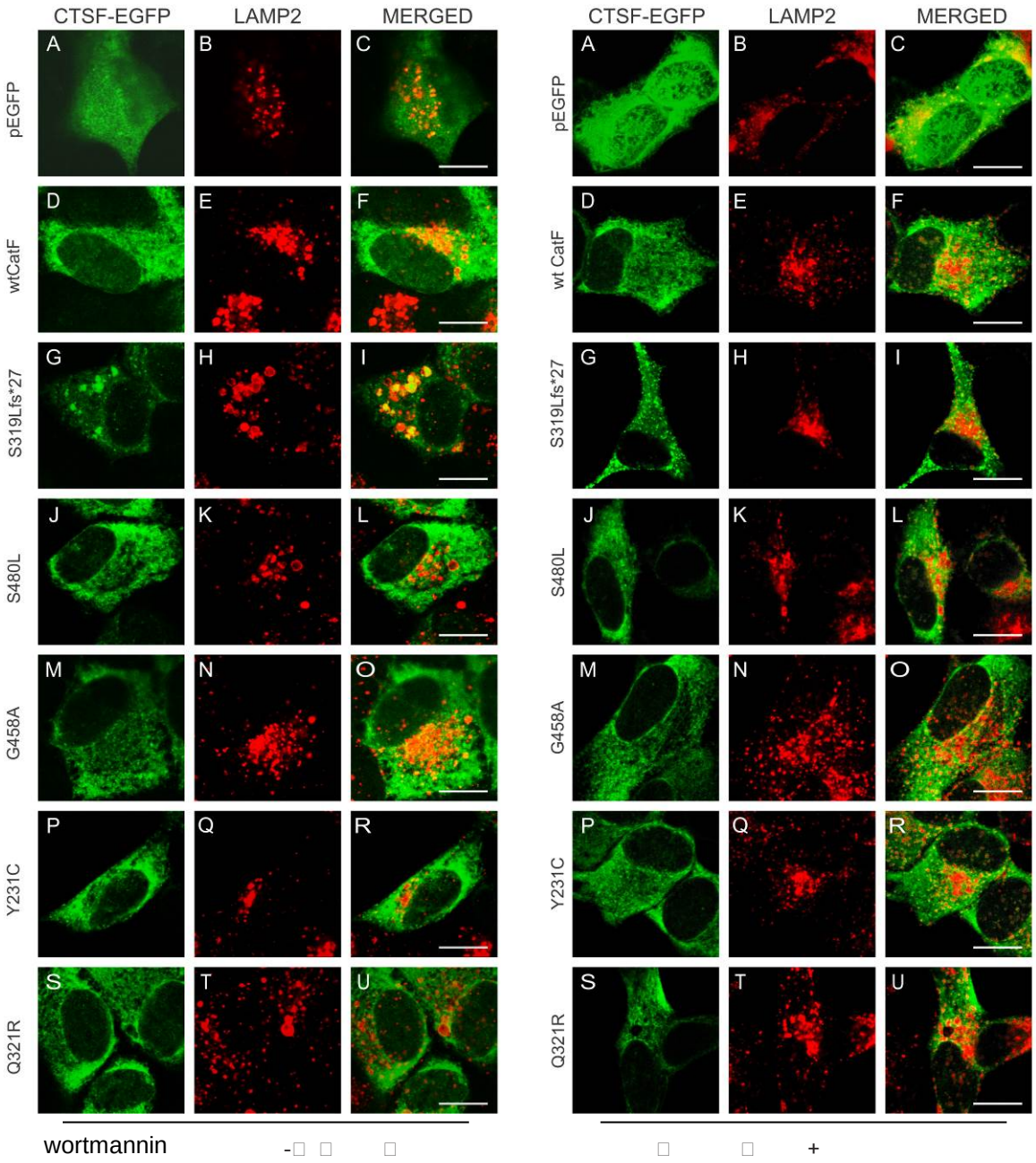

Figure 17: *CLN13 mutation S319Lfs*27 induces its aggregation and non-lysosomal targeting.* SH-SY5Y cells were transfected with pEFGP-containing wtCatF (D – F), S319Lfs*27 (G – I), S480L (J – L), G458A (M – O), Y231C (P – R) and Q321R (S – U) mutants (CTSF-EGFP, green fluorescence) and 24 hours later either left untreated (left panel) or exposed to 5 μM wortmannin (right panel). Using Alexa Fluor 546 labeled mouse monoclonal anti LAMP2 antibodies (red fluorescence), cells were immunolabeled 48 hours after transfection and examined by confocal microscopy. Merged images represent overlapping fluorescence in yellow. Scale bar = 10 μm.

4.2.3 Aggregation of S319Lfs*27 mutant is not held in the endoplasmic reticulum

Accumulation of mutated, misfolded proteins in the ER or the presence of undegraded material can lead to ER stress and UPR, a pathogenic condition in many neurodegenerative diseases (Lindholm et al., 2006; Tessitore et al., 2004; Zhang et al., 2006).

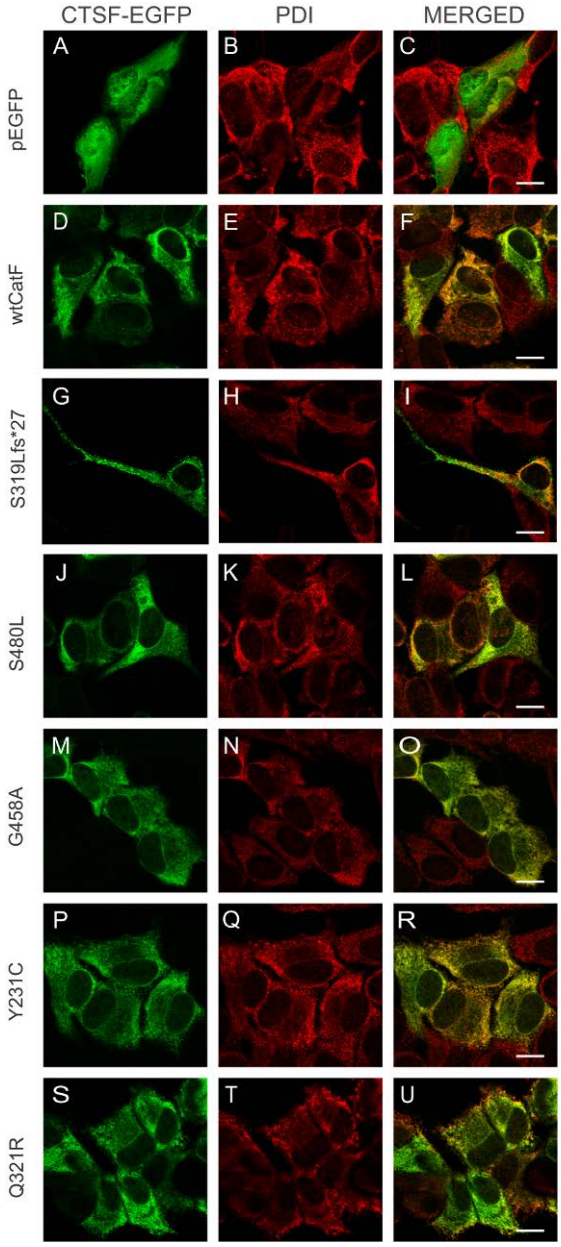

Figure 18: *S319Lfs*27 aggregates do not localize to the endoplasmic reticulum.* SH-SY5Y cells were transfected with the wild type and mutant CLN13 (CTSF-EGFP, green fluorescence). 48 hours after transfection endoplasmic reticulum was immunolabeled with mouse monoclonal anti PDI antibodies (red fluorescence) and examined by confocal microscopy. Merged images represent overlapping fluorescence in yellow. Scale bar = 10 μm.

All of the expressed proteins with vesicular pattern colocalized with the ER marker PDI (protein disulfide isomerase). This was, however, not observed for the S319Lfs*27 aggregates (Figure 18). These findings suggest that misfolded S319Lfs*27 proteins are most likely not retained in the ER, but rather translocated to the cytoplasm where they aggregate.

4.2.4 Terminal misfolding of the S319Lfs*27 may lead to its accumulation in the aggresomes

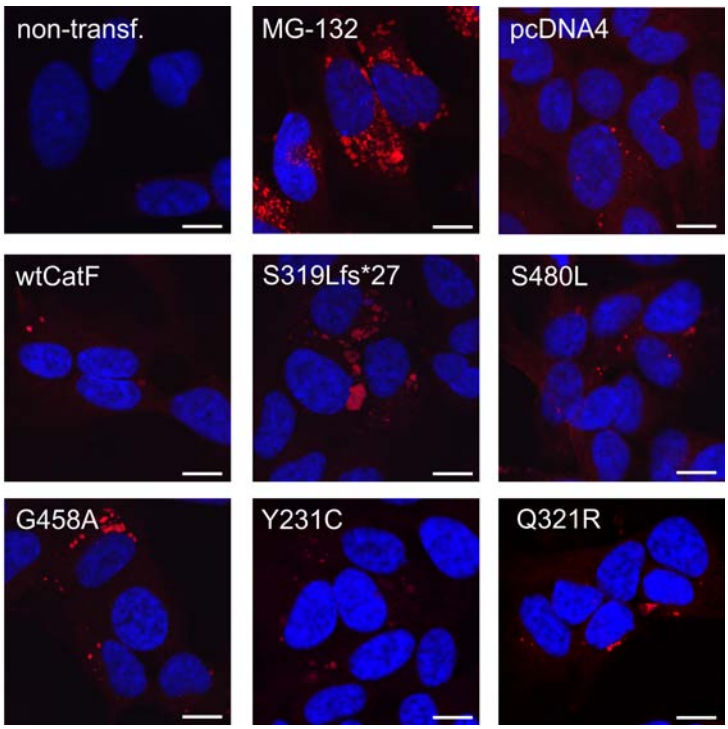

Figure 19: *S319Lfs*27 aggregates accumulate in aggresomes-like inclusions.* SH-SY5Y cells were stained with Proteostat® 48 hours after transfection with pcDNA4/myc-His plasmids containing wtCatF, S319Lfs*27, S480L, G458A, Y231C and Q321R. Nuclei were counterstained with DNA-staining Hoechst 33342 (blue fluorescence). Negative controls included non-transfected, mock-transfected and empty vector-transfected cells. For positive control, cells were treated with 5 μM proteasomal inhibitor MG-132, 24 hours before staining. Scale bar = 10 μm.

Since immunoblotting revealed that all of the CLN13 mutants could be found in the soluble and insoluble fraction, it is tempting to consider that they may be misfolded to a certain extent. These terminally misfolded proteins may aggregate together and cells may sequester such aggregates in different soluble or insoluble deposits. We also observed that frameshift mutant S319Lfs*27 aggregates upon its overexpression in SH-SY5Y cells (Figure 17). Therefore, we wondered if expression of the protein with single amino acid

mutation or frameshift mutation could increase aggregation propensity and consequently induce aggresome formation in neuronal cells after their overexpression. Staining with Proteostat® molecular rotor dye revealed translocation of mainly dispersed S319Lfs*27 aggregates to the perinuclear aggresome-like inclusions (Figure 19). Although some aggresome-like inclusions were observed in G458A, no significant or stronger signal was observed in cells transfected with the wtCatF or missense mutants S480L, Y231C and Q321R, compared to the signals in empty vector transected cells.

4.2.5 Evaluation of CLN13-induced changes in autophagy pathway

Accumulation of non-degraded material in lysosomes, block of intracellular transport to or from lysosomes, due to the lysosomal »overload« and change in the vacuolar pH are frequently observed phenomena of the LSDs (Futerman and van Meer, 2004). Perturbations in the lysosomal function may further lead to reduced autophagic flux and accumulation of numerous autophagosomes as well as endo/autolysosomes and autophagosome-associated proteins, such as LC3II and p62 (Cao et al., 2006; Settembre et al., 2008).

Enlarged LAMP2 positive vesicles were observed in previous experiments (Figure 17, left panel), especially in cells loaded with large S319Lfs*27 aggregates. Therefore we evaluated whether the expression of CLN13 mutants influences the biosynthesis or pathogenesis of lysosomes. We used LysoTracker® Green DND-26, a green fluorescent dye that stains acidic compartments in live cells. Organelles with lower pH accumulate higher amounts of LysoTracker® Green and thereby produce higher intensity of the fluorescence when quantified by e.g. flow cytometry. Lower number of acidic vesicles or higher number of organelles with increased pH would conversely result in decreased fluorescence signal. Since no significant difference in the number of LAMP2 positive vesicle could be observed between transfected or non-transfected cells by immunocytochemistry, we concluded that any possible shift in the fluorescence signal between examined samples would very likely account for changes in the pH of the stained vesicles. Indeed, we found a significant decrease of LysoTracker® Green DND-26 fluorescence in the cells overexpressing CLN13 mutants, but not also in cells overexpressing the wild type cathepsin F, compared to the empty vector transfected cells (Figure 20). For positive control, cells were treated with 30 nM bafilomycin A1 for 1 hour, before staining. Non-transfected cells represent negative control.

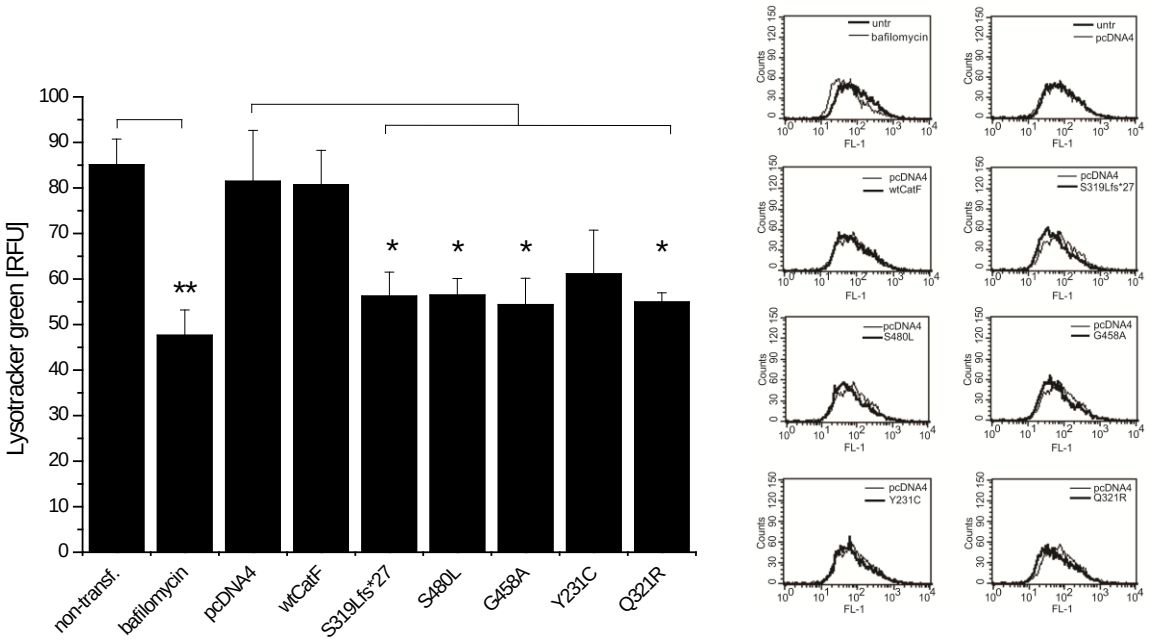

Figure 20: *Expression of CLN13 mutants decrease pH of acidic organelles.* 48 hours after transfection SH-SY5Y cells were stained for 30 min with 40 nM LysoTracker® Green DND-26 probe, which accumulates in acidic organelles. 1hour bafilomycin A1 (baf, 30 nM) treatment was used as a positive control. Shift in fluorescence was measured by flow cytometry. Lower values denote higher pH of vesicles. Bars on the graph represent the geometrical means of fluorescence intensity ± SD of two independent experiments. *p<0,05; **p<0,01 compared to the pcDNA4. On the right side representative histograms are shown.

We further analyzed whether observed increased pH of the acidic organelles influences the autophagic flux in our experimental system. By analysis of changes in LAMP2 and LC3B colocalization we can monitor changes in the fusion of autophagosomes and lysosomes. Less colocalization of LAMP2 and LC3B was found in cells overexpressing the CLN13 mutants (marked by arrowheads) in comparison to the cells transfected with the wtCatF (Figure 21). We also observed that LC3 puncta in cells transfected with S319Lfs*27 were fewer in number but larger in size (Figure 21K).

Finally, we also examined whether autophagic clearance is p62/SQSTM1 mediated using immunocytochemical labeling with anti p62 antibodies. Though we observed some colocalization of the wtCatF and mutant proteins with p62/SQSTM1, this was not the case for the larger S319Lfs*27 aggregates (Figure 22). There was, however, some colocalization with dispersed S319Lfs*27-EGFP signal, which could represent misfolded but not yet aggregated species. No significant increase in p62 expression was observed in any of the transfected samples.

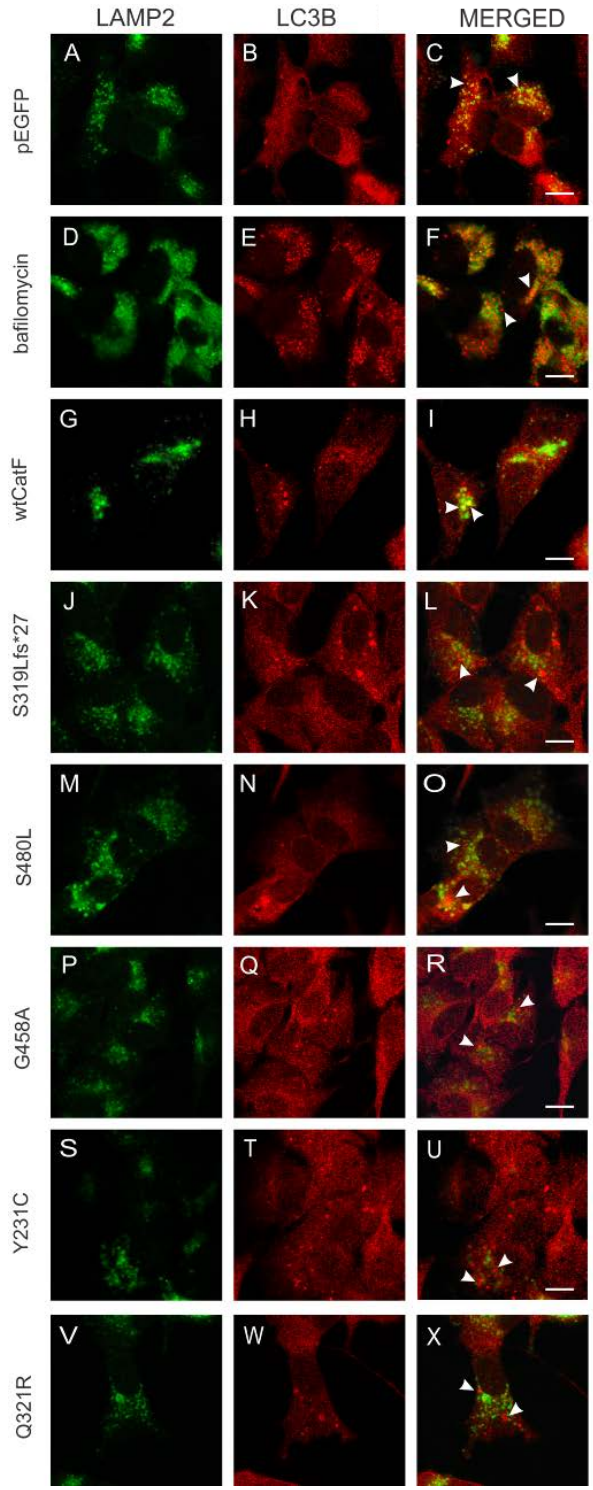

Figure 21: *CLN13 mutants decrease autophagic flux.* SH-SY5Y were immunolabeled 48 hours after transfection with mouse monoclonal anti LAMP2 (LAMP2; green fluorescence) and rabbit polyclonal anti LC3B (LC3B; red fluorescence) primary antibodies. Confocal images showed reduced colocalization of LAMP2 and autophagosomal marker LC3B (yellow) in cells transfected with S319Lfs*27 (J – L), S480L (M – O), G458A (P – R), Y231C (S – U) and Q321R (V – X). More overlapping signal of LAMP2 and LC3B was observed in pEGFP (A – C) and wtCatF (G – I) transfected cells. For positive control cells were treated with 30nM bafilomycin for 24 hours (D – E). Colocalization was assessed only in the transfected (EGFP positive) cells (indicated by arrowheads). Scale bar = 10 μm.

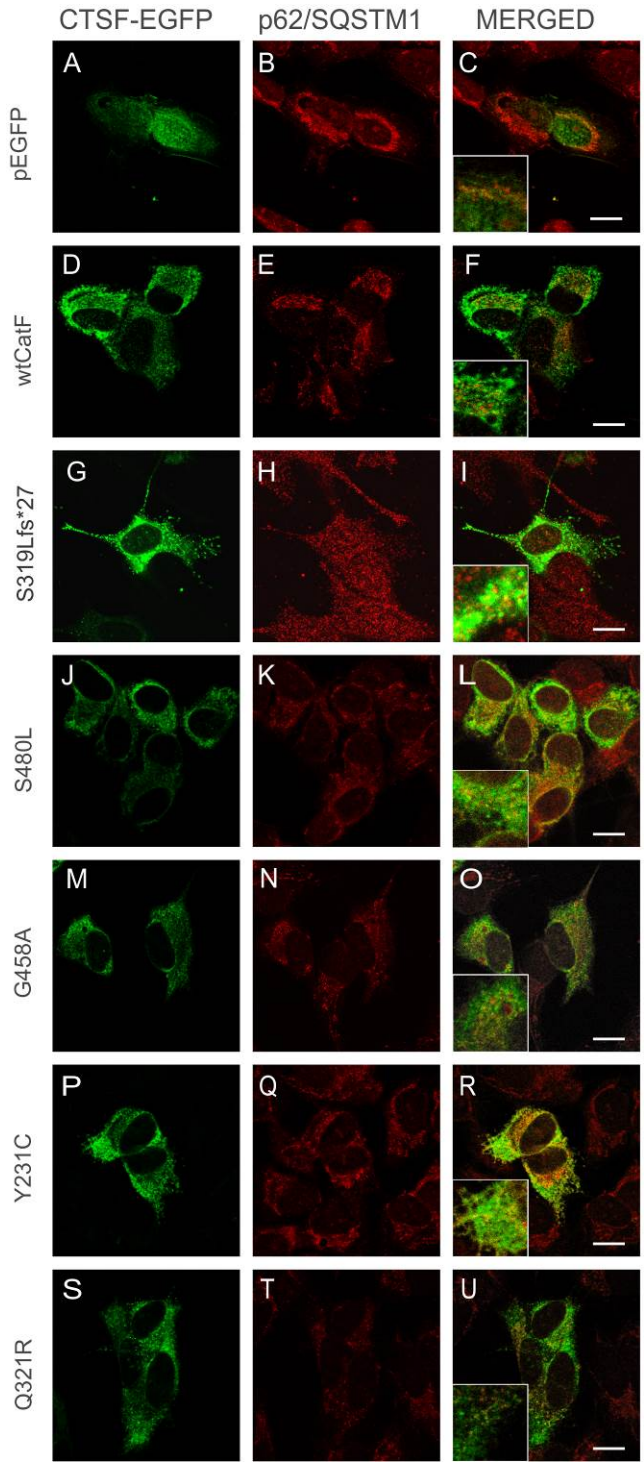

Figure 22: *Non aggregated CLN13 mutants are p62 positive.* SH-SY5Y cells were transfected for 48 hours with the EGFP-tagged wild type cathepsin F and CLN13 mutants S319Lfs*27, S480L, G458A, Y231C and Q321R (CTSF-EGFP, green fluorescence) and immunolabeled with mouse monoclonal anti human p62 (p62/SQSTM1; red fluorescence) antibodies. Images were obtained with confocal laser scanning microscope. Merged images (in yellow) represent combined fluorescence. Insertions represent selected enlarged area for better visualization. Scale bar = 10 μm.

4.2.6 Expression of S319Lfs*27 induce increased accumulation of autofluorescent perinuclear material

NCL diseases are characterized by the accumulation of the autofluorescent lipopigment in the cytoplasm (Seehafer and Pearce, 2006). Our results have shown that cells expressing the C-terminally truncated frameshift mutant S319Lfs*27 accumulate higher levels of uncharacterized perinuclear autofluorescent pigment or material, compared to the empty vector, wtCatF or S480L, G458A, Y231C and Q321R-transfected cells (Figure 23). Essentially no autofluorescent signal could be detected in non-transfected cells.

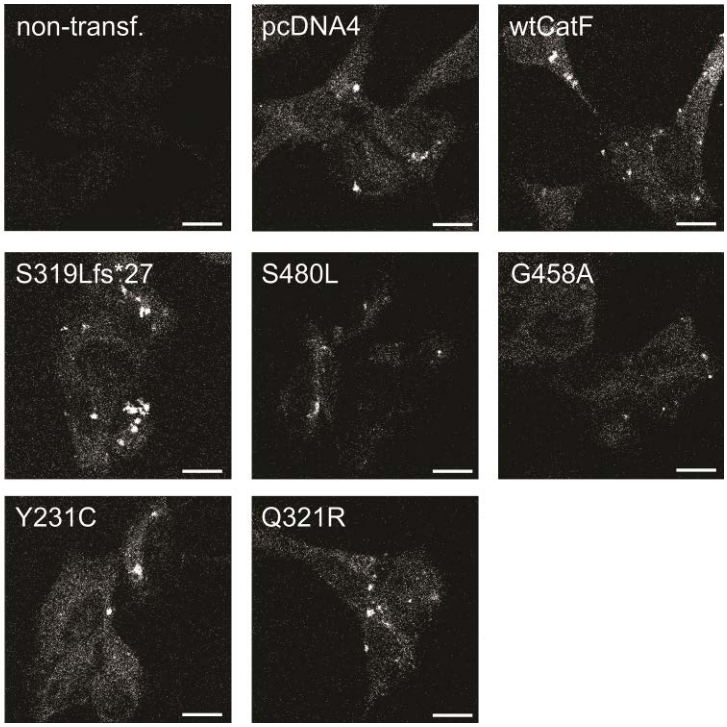

Figure 23: *Accumulation of autofluorescent material.* SH-SY5Y cells were fixed and analysed without staining 48 hours after transfection with either wtCatF or CLN13 mutants. Images were obtained by confocal scanning microscope. White dots represent overlaid blue, red and green fluorescence emission. Scale bar = 10 μm.

4.2.7 Ultrastructural analysis by TEM

Accumulation of autofluorescent material in SH-SY5Y cells expressing S319Lfs*27 led us to examination at the ultra-structural level. Electron microscopy of our samples revealed increased accumulation of lipids throughout the cell, around the nuclear (Figure 25F) and vesicular membranes (Figure 25D, 24E, 24H) and sometimes also near the mitochondria (Figure 25C, 24G) or the ER membrane (Figure 25I), in cells transfected with the S319Lfs*27 (Figure 25), compared to the cells transfected with the wtCatF or non-transfected cells (Figure 24). We also found some lamellar inclusions in vesicles of S319Lfs*27-expressing cells (Figure 25A, 24B left insert) and some (more infrequent) damaged mitochondria (Figure 25C, 24G). In addition, vesicles loaded with electronically-dense material (proteins) were often observed in these cells (Figure 25 A, B, E, H).

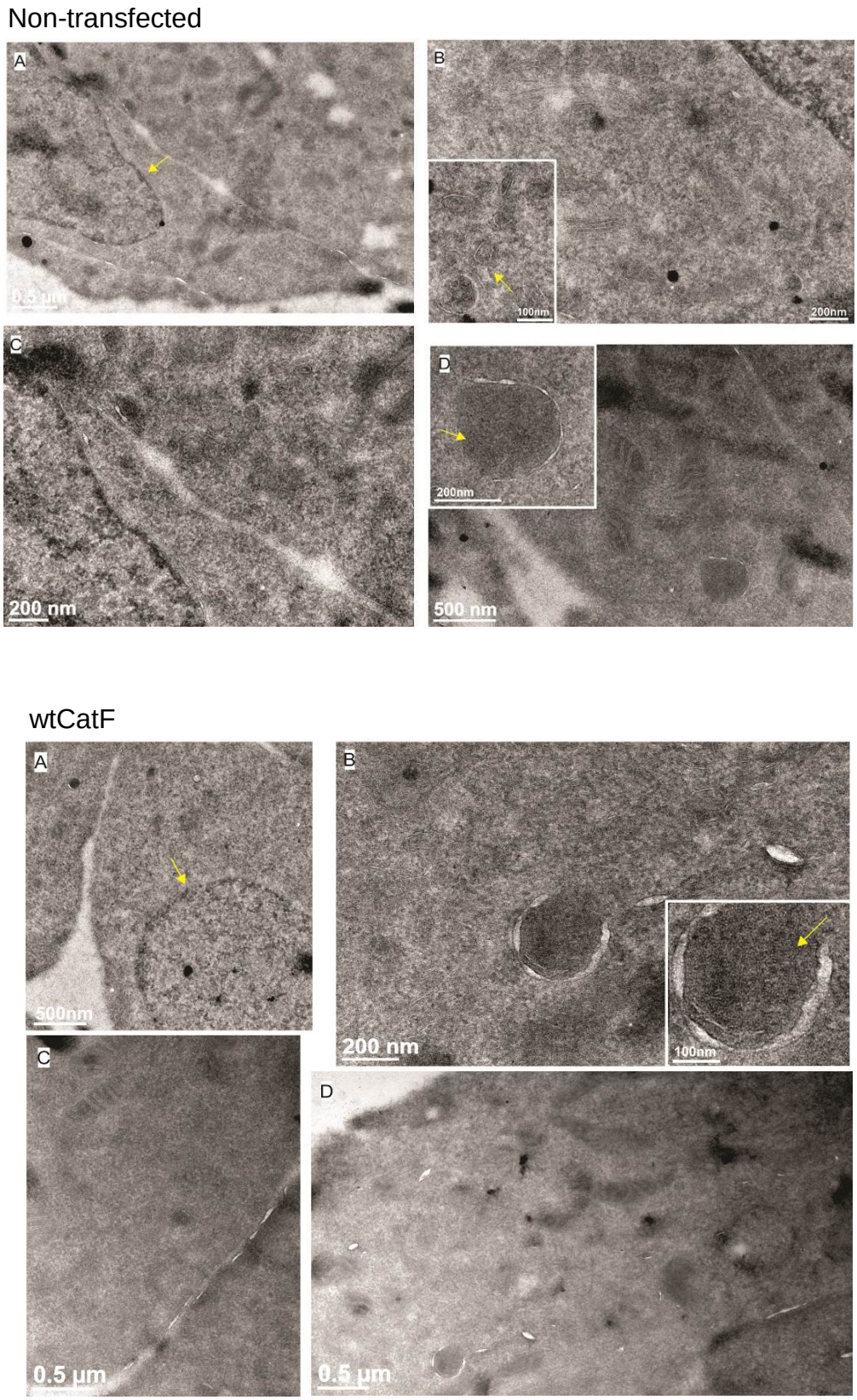

Figure 24: *Transmission electron microscopy of non-transfecetd and wtCatF-transfected SH-SY5Y cells.* Non-transfected cells or cells transfected with the wtCatF or S319Lfs*27 mutant were fixed with 4 % paraformaldehyde, embedded in 10 % gelatin and cryoprotected in 2.6 M sucrose. Cryosected slices were contrasted with 0.4 % uranyl acetate and analysed by TEM. Uranyl contrasted the cell proteins but not the lipids so the membranes appear white. Inserts show details of the zoomed structures.

S319Lfs*27

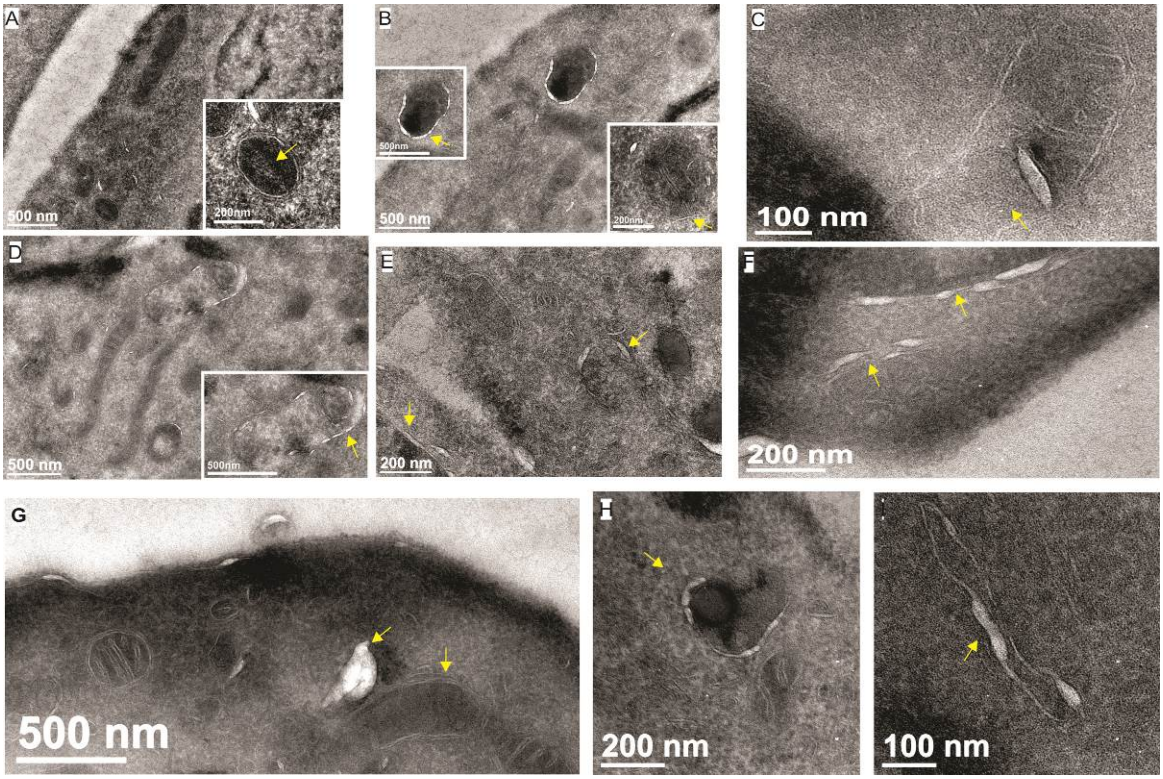

Figure 25: *Transmission electron microscopy of S319Lfs*27-transfected SH-SY5Y cells.* Non-transfected cells or cells transfected with the wtCatF or S319Lfs*27 mutant were fixed with 4 % paraformaldehyde, embedded in 10 % gelatin and cryoprotected in 2.6 M sucrose. Cryosected slices were contrasted with 0.4 % uranyl acetate and analysed by TEM. Uranyl contrasted the cell proteins but not the lipids so the membranes appear white. Inserts show details of the zoomed structures.

4.2.8 Does expression of CLN13 induce ER stress?

ER is the major reservoir of cellular Ca^{2+}, and lipid storage disorders were shown to impact ER calcium regulation, leading to the elevated cytosolic Ca^{2+} (Platt et al., 2012). With regard to the observed ER localization of the wtCatF and CLN13 mutants expressed in SH-SY5Y cells (Figure 18), we also tested transfected cells for the signs of the ER stress. Firstly, we measured free intracellular Ca^{2+} with Fluo-4 AM reagent, which exhibits increase in fluorescence intensity after calcium binding. Obtained results displayed no significant difference between the wtCatF, mutant CLN13-transfected cells and negative control (EGTA) (Figure 26). For positive control cells were treated with the ionomycin, a well-known ionophore.

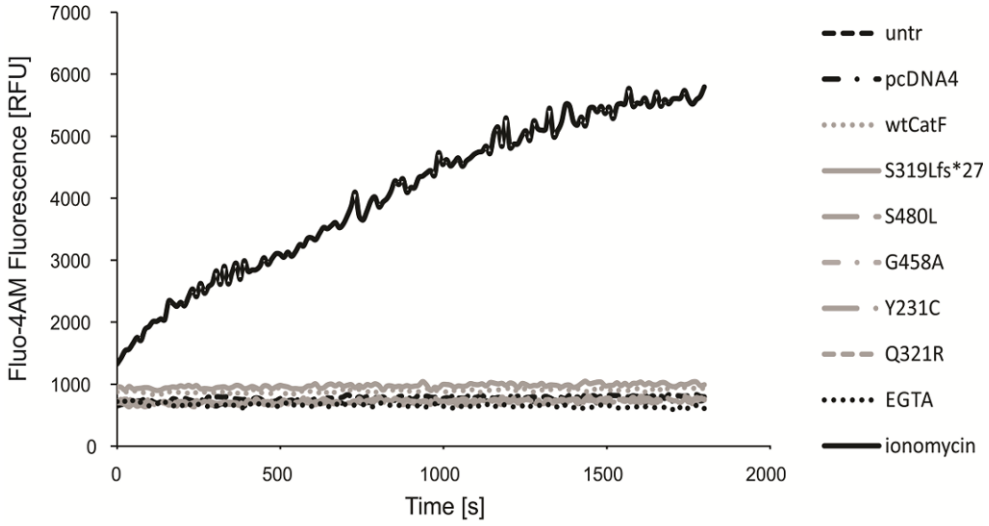

Figure 26: *Evaluation of free intracellular* Ca^{2+}. Transfected SH-SY5Y cells were stained with Fluo-4 AM, as described in section 3.2.7. For negative control cells were treated with 100 nM EGTA, whereas for positive control 100 µM ionomycin was used. Fluorescence signal was measured continuously for at least 30 minutes using Tecan Infinite M1000 pro. One experiment on three biological replicates was done.

Further investigation led us to the inspection of yet another ER stress-inducible mechanism, the unfolded protein response (UPR), which promotes protein folding through the up-regulation of the genes encoding ER chaperones, and components of the ER-associated degradation (ERAD) machinery for the degradation of misfolded proteins (Ding et al., 2007). Hence, we evaluated relative mRNA expression of the BiP (78 kDa glucose-regulated protein), CALR (calreticulin), CHOP (DNA damage-inducible transcript 3 protein) and EDEM1 (ER degradation-enhancing alpha-mannosidase-like protein 1) genes in cells overexpressing the wild type cathepsin F or the S319Lfs*27 mutant. For positive control, cells were treated 24 hours with 1.5 µM thapsigargin which is known to disrupt intracellular Ca^{2+} stores (Verma et al., 1990). RNA was isolated and reversed transcribed 24 and 36 hours after transfection, as described in section 3.2.14. Gene expression was analysed using the qPCR technique and primers listed in Table 3. Similar results were obtained for both time points, thus only the graph for 36 hours is presented here. Transfection efficiency was confirmed by analysis of CTSF mRNA expression. Biologically significant up-regulation (relative to the empty vector-transfected cells) was detected only for BiP and CHOP genes. Nevertheless, observed up-regulation of relative expression of BiP and CHOP was very similar for the wtCatF and S319Lfs*27 mutant (Figure 27), suggesting that observed shift in expression could be attributed to the overexpression by itself, rather than specific response to the wild type or mutant CLN13 expression, as such.

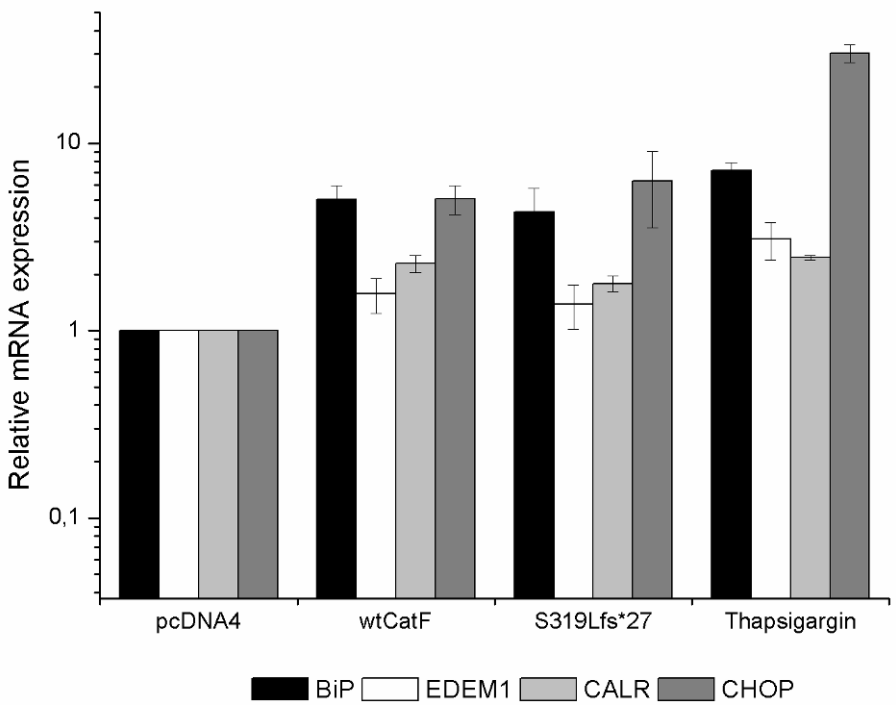

Figure 27: *Evaluation of CLN13-induced ER stress by qPCR.* RNA was isolated from the SH-SY5Y cells transfected with the empty vector, wtCatF or S319Lfs*27 and reverse transcribed to the cDNA. cDNA was evaluated for the relative mRNA expression of the BiP, EDEM1, CALR and CHOP genes using SYBR Green qPCR chemistry. Expression of genes of interest was calculated using REST 2009 software and normalized to the expression of ENOX2 and VIPAR. Graph represents mean values of fold changes (relative to pcDANA4) and ±SD of three biological replicates. For positive control, cells were treated with 1.5 μM thapsigargin (24 hours).

4.2.9 CLN13 mutants induced slight increase in mitochondrial superoxide and lipid peroxidation

Increased ROS production and oxidative stress-induced membrane lipid peroxidation were found in NCL diseases (Hachiya et al., 2006; Vidal-Donet et al., 2013). Observed elevated ROS and superoxide dismutase levels were suggested to be downstream to ER stress (Kim et al., 2006). We analyzed whether the expression of CLN13 mutants induces superoxide production or lipid peroxidation. For this reason cells were stained with two different reagents, namely MitoSOX™ Red and BODIPY® 581/591 C11. The first one is a fluorogenic dye, targeted to mitochondria of live cells, where it may exhibit red fluorescence upon oxidation by superoxide but not other ROS. Oxidation product also becomes highly fluorescent upon binding to nucleic acids. On the other hand, BODIPY® 581/591 C_{11} indicates lipid peroxidation. Upon oxidation (interaction with peroxyl radicals) in live cells, its fluorescence emission peak shifts from ~590 nm (red) to ~510 nm (green). Examination by confocal microscopy has shown a slight increase in mitochondrial superoxide formation in cells overexpressing CLN13 mutants, compared to the cells expressing empty vector (Figure 28). We also found some, but weaker signal in cells expressing the wild type protein. For positive control 1 hour treatment with 100 μM menadione, a known free radical inducing agent was used. BODIPY® 581/591 revealed lipid peroxidation in cells transfected with S480L, G458A, Y231C, Q321R or S319Lfs*27, but not in wtCatF-transfected cells (Figure 29).

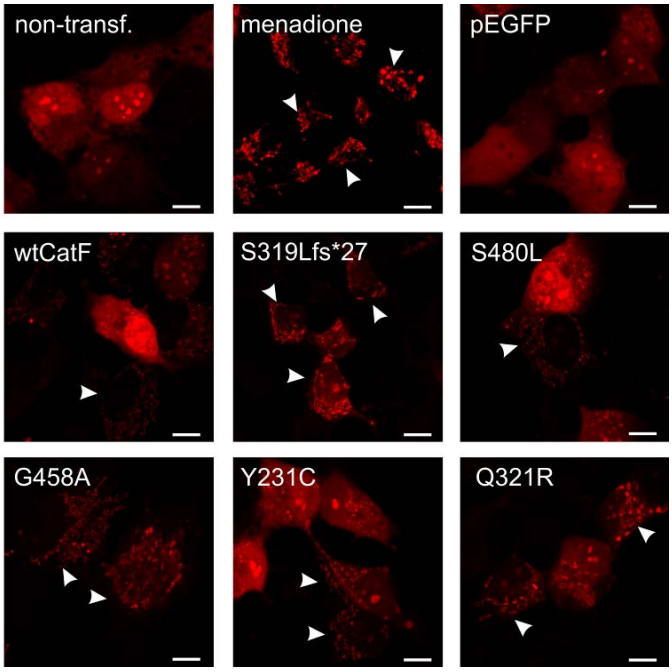

Figure 28: *Detection of superoxide anion formation by MitoSOXTM Red.* Cells were transfected with wtCatF and CLN13 mutants and 48 hours later stained with MitoSOX™ Red (5 µM, 30 minutes). 100µM menadione (1hour) was used as a positive control. MitoSOX™ Red reagent is oxidized by superoxide but not other ROS and exhibits red fluorescence. Images of live cells were taken by confocal microscope. Arrowheads indicate signal in transfected (EGFP positive) cells only. Scale bar = 10µM.

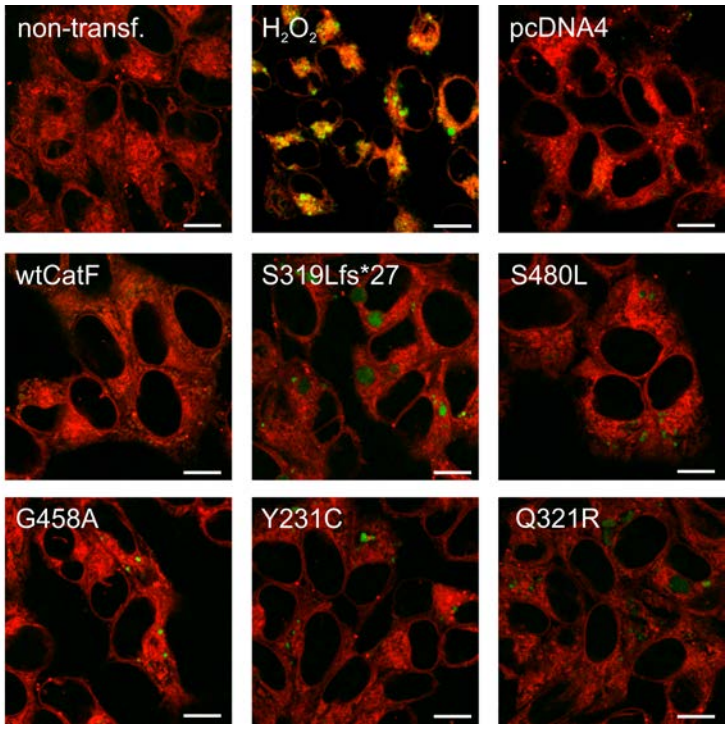

Figure 29: *CLN13 mutants induce lipid peroxidation.* Cells were transfected with wtCatF and CLN13 mutants and stained with BODIPY® 581/591 C_{11} (2 µM, 30 minutes), 48 hours after transfection. 1mM H_2O_2 (1 hour) was used as a positive control. Upon oxidation in live cells, fluorescence shift from red to green occurs, providing indication of lipid peroxidation. Images were obtained by confocal microscopy. Scale bar = 10µM.

5 Discussion

Among eleven human cysteine cathepsins, cathepsin F is the only one exhibiting unusually long N-terminal proregion, containing a signal peptide, cystatin-like domain, and linker (Nagler et al., 1999; Santamaria et al., 1999). The role of cystatin-like domain is still not known and remains a matter of discussion. Due to the presence of the signal sequence and five potential N-glycosylation sites, cathepsin F was suggested to be targeted to the endosomal/lysosomal compartment via M6P receptor pathway (Nagler et al., 1999; Santamaria et al., 1999), similarly to other cysteine cathepsins. However, initially only part of the sequence belonging to cathepsin F was found and two different putative translation start sides, resulting in either 302 or 338 amino acids long protein from smooth muscle mRNA were predicted (Wang et al., 1998). The 302 amino acids long protein was proposed to be targeted to the lysosomal compartment via M6P-independent pathway and even shown to possess enzymatic activity, in spite of the fact that isolated cDNA sequence lacks signal peptide (Wang et al., 1998). Although also some other truncated forms of cysteine cathepsins B, L and H, lacking the whole or a part of signal peptide, have been shown to preserve their catalytic activity (Goulet et al., 2004; Goulet et al., 2007; Mehtani et al., 1998; Waghray et al., 2002), these data are not very convincing. Namely, it should be noted that some of these activities (e.g. for truncated cathepsin F and B) were measured with recombinant purified truncated proteins or *in vitro* translation products, under specific conditions (Mehtani et al., 1998; Wang et al., 1998), which may have altered characteristics due to the nature of methodology. On the other hand, the group of Goulet and his colleagues (Goulet et al., 2007) acknowledge that short cathepsin L isoforms devoid of signal peptide do not fold properly in an *in vitro* expression system and do not exhibit catalytic activity. In addition, later publications prove that Δ^{51}CB (cathepsin B lacking second and third exon) has no regular cathepsin B enzymatic activity (Muntener et al., 2005; Muntener et al., 2004) and rather uses an alternative mechanism by which it is able to induce cell death (Bestvater et al., 2005). Further, experimental data on CA1 cysteine peptidase's prodomains in correct intracellular targeting and assistance in folding of the mature enzyme have been shown (Wiederanders, 2003). All these data led us to the broader research of real behavior of the N-terminally truncated forms of human cathepsin F (Jeric et al., 2013).

On the other hand, 344 amino acids long C-terminally truncated variant of human cathepsin F has been found together with four other missense mutations in patients suffering from type B Kufs disease, an adult-onset neuronal ceroid lipofuscinosis (NCL) (Smith et al., 2013). Clinically Type B Kufs disease is manifested as adult onset dementia and motor disturbances rather than epilepsy, in addition to the characteristic abnormal accumulation of ceroid lipopigment in the lysosomes. Nevertheless, exact molecular basis of this disease remains unknown (Smith et al., 2013). According to the obtained results and the fact that murine cathepsin F deficiency has also been found to cause late-onset NCL (Tang et al., 2006), Smith and her colleagues proposed that dysfunction of this protein could be a mechanism for type B Kufs disease. Five (four missense and one frameshift) mutations found in CTSF were predicted to be probably damaging for the function of the protein (Smith et al., 2013) but not yet experimentally confirmed. On the basis of these published data, we prepared single mutations and expressed them in the

neuronal cell line. Their behavior and consequences of their expression on in NCL deregulated cellular pathways has been compared to the effects of the wild type protein.

5.1 Analysis of N-terminally truncated forms of human cathepsin F in HEK293T cells

We cloned three different N-terminally truncated variants of human cathepsin F and expressed them in human embryonic kidney (HEK293T) cells. Δ^{19}CatF (Ala^{20} – Asp^{484}) is devoid of signal peptide only, Δ^{125}CatF (Pro^{126} – Asp^{484}) lacks signal peptide and cystatin like domain, while the variant found in skeletal muscle cDNA by the group of Wang (Wang et al., 1998) lacks signal peptide, cystatin like domain and additional 20 amino acids of linker (Δ^{146}CatF; Met^{147} – Asp^{484}). In this way we aimed to estimate the contribution of the signal peptide and cystatin like domain to the enzyme trafficking and re-evaluate the possibility of the lysosomal targeting of these N-terminally truncated variants. A schematic representation of the wild type protein (wtCatF) and its N-terminally truncated variants used in this study is shown in Figure 7.

Soluble proteins are directed to the ER by the N-terminal signal sequence, where they fold and later travel further through the secretory pathway to their final location (Schroder and Kaufman, 2005). Lysosomal targeting of cysteine cathepsins is mediated by M6P, attached to the N-linked oligosaccharides in *cis* Golgi network, which is recognized by mannose-6-phospahete receptor in *trans* Golgi network (Alberts, 2002; Hasilik et al., 2009). Since all of our three N-terminally truncated forms lack signal peptide, we expected their trafficking and subcellular localization will be altered. The fact that they would not follow the cysteine cathepsins classical biosynthetic and folding pathway through the ER strongly suggests they would probably not fold correctly and would be subsequently enzymatically inactive (Schroder and Kaufman, 2005; Tao et al., 1994). On the other hand all of three expressed truncated variants contain at least part of the prodomain (Figure 7), which could assist in their proper folding. Moreover, existence of M6P-independent trafficking of the lysosomal proteins has been suggested (Wiederanders, 2003). As expected, expression of the truncated forms of human cathepsin F (Δ^{19}CatF, Δ^{125}CatF and Δ^{146}CatF) in HEK293T cells revealed that the deletion of at least the signal peptide prevents them from significant lysosomal localization (Figure 8 L, P, T). This was contrary to the wtCatF, which expectedly colocalized with the endosomal/lysosomal marker LAMP2 (Figure 8H). Moreover, immunolabeling of cathepsin F displayed vesicular staining of the wtCatF (Figure 8E), while Δ^{19}CatF, Δ^{125}CatF and Δ^{146}CatF exhibited more condensed, aggregated, perinuclear appearance (Figure 8 I, M, Q).

Review of the literature dealing with the N-terminally truncated cathepsin H or alternatively spliced cathepsin B, lacking the signal peptide, revealed that both of them were also found in the cytoplasm, perinuclear but not in the ER. After expression in human cell lines, cathepsin B has been found to be associated with the nuclei and localized on the cytosolic side of the intracellular membranes (Mehtani et al., 1998), later identified as mitochondria (Muntener et al., 2003; Muntener et al., 2004). Short artificial cathepsin B constructs were even localized to the nucleus and in the midbodies of dividing cells (Bestvater et al., 2005). On the other hand, cathepsin H has been found in perinuclear compartments and secreted (Waghray et al., 2002). Wang and colleagues described vesicular, predominantly juxtanuclear expression of 302 amino acids long N-

terminally truncated cathepsin F after its expression in COS-7 cells (Wang et al., 1998). They have found their staining pattern similar to the one for the truncated cathepsin B, observed by (Mehtani et al., 1998). Comparing microscopic images of our Δ^{19}CatF, Δ^{125}CatF and Δ^{146}CatF variants and those from Wang and colleagues, we could also describe our pattern to be vesicular. However, the term »vesicular« is wide and cells may sequester expressed proteins in many different vesicles ranging from the endosomal/lysosomal system to the autolysomes, formed in autophagic degradation or even deposits of misfolded or aggregated proteins, like aggresomes. It is therefore always useful to characterize observed vesicular pattern with the existent markers for at least some of the cell organelles/vesicles and evaluate whether this is their primary or secondary location. For example, observed lysosomal localization could be a consequence of autophagic clearance of the expressed protein.

Western blot analysis of soluble fraction disclosed only a major band of ~70 kDa and a minor band of ~30 kDa, belonging to the wtCatF, whereas N-terminally truncated form Δ^{19}CatF, Δ^{125}CatF and Δ^{146}CatF were essentially undetectable (Figure 9A). Endogenous human cathepsin F from HEK293T cells was also not detected. Theoretical Mw assessed from protein sequence as described in (Jeric et al., 2013) of the full length and mature form of human cathepsin F is 53.3 and 23.6 kDa, respectively. The higher values observed by Western blotting could be attributed to the presence of five potential N-linked glycosylation sides, from which two of them (Asn160 and Asn195) are located in the propeptide and three of them (Asn367, Asn378, Asn440) in the mature form (Ho et al., 2002; Nagler et al., 1999; Wang et al., 1998). Indeed, treatment of cell lysate obtained from transfected cells with the PNGase F that hydrolyzes all classes of N-linked glycans (Tarentino et al., 1985), decreased the Mw of the full length protein to ~60 kDa and Mw of mature form to ~24 kDa, as assessed by Western blot (Figure 9). Wang and colleagues observed approximately 9 and 5 kDa decrease in Mw of the proenzyme and mature enzyme, respectively after treatment of recombinant enzyme by endoglycosidases H and F *in vitro* (Wang et al., 1998). This is close to our results if we consider that the exact Mw cannot be assessed completely accurately from the Western blot analysis and that glycosylation pattern of the same protein may vary between different expression systems (Fonovic et al., 2004; Wang et al., 1998). Anyhow, it should also be pointed that the Wang used α-pheromone in the procedure of expression and purification of truncated cathepsin F in *Pichia pastoris* (Wang et al., 1998). This is a signal sequence for the extracellular targeting of the protein which leads expressed protein through the classical secretory pathway »ER-Golgi-secretory vesicles« (Julius et al., 1984), thereby also enabling it to encounter glycosylation.

The absence of the N-terminally truncated variants in the soluble fraction led us to the inspection of the insoluble, membrane fraction of the cell lysates. Surprisingly, all of the truncated forms were found in the insoluble fraction (Figure 9B). Δ^{19}CatF resulted in a major band of ~60 kDa and additional two minor bands of ~52 and ~45 kDa, respectively. Δ^{125}CatF and Δ^{146}CatF were detected as single bands of ~40 and ~38 kDa, respectively. Calculated predicted Mw for the Δ^{19}CatF, Δ^{125}CatF and Δ^{146}CatF from protein sequences are 51.5, 40.0 and 37.9, respectively. Thus, observed Mw for the Δ^{125}CatF and Δ^{146}CatF correlates with the predictions, whereas major band of Δ^{19}CatF position approximately 8 kDa higher on the Western blot. While lower, minor bands could be attributed to the degradation of the protein by cytoplasmic proteases, higher Mw could be attributed to the glycosylation which was, however, not expected for this construct, considering that it is most probably not routed to the classical biosynthetic pathway. Nevertheless we tested this option experimentally. As expected, no decrease in Mw of the expressed N-terminally truncated variants Δ^{19}CatF, ^{125}CatF and Δ^{146}CatF was observed (Figure 10),

indicating they do not include N-linked glycans. Noteworthy, truncated cathepsin B, lacking exons 2 and 3 was similarly found in the membrane fraction by the Western blot analysis (Muntener et al., 2004).

We have shown that Δ^{19}CatF, Δ^{125}CatF and Δ^{146}CatF form aggregated, perinuclear insoluble structures that did not localize to the lysosomes. Besides, human cathepsin F has been found to contain three natively disordered regions inside the enzyme's propeptide and aggregation prone regions, containing amino acid stretches with high fibrillation propensity (Jeric et al., 2013). This encouraged us to inspect whether truncated variants reside inside aggresome or aggresome-like structures. Aggresomes are juxtanuclear structures where insoluble misfolded or otherwise unsuccessfully refolded proteins could be targeted to (Johnston et al., 1998). It is initiated by the packing of aggregated proteins into larger, insoluble aggregates, which oligomerize and then multimerize into even larger insoluble inclusions or aggregates (Grune et al., 2004; Hyttinen et al., 2014). Stability of aggresome inclusions is enabled by intermediate filaments such as vimentin, keratin or neurofilaments, which prevent them from non-specific interactions (Hyttinen et al., 2014; Johnston et al., 1998). We used Proteostat®, a red fluorescent molecular rotor dye enabling detection of aggregated proteins within the aggresome and aggresome-like structures (Shen et al., 2011). Staining with Proteostat® revealed the presence of perinuclear aggresome-like structures in cells overexpressing Δ^{19}CatF, Δ^{125}CatF and Δ^{146}CatF (Figure 11 L, O, R) proteins. Signal intensity was of similar extent to the cells treated with known reversible and cell-permeable inhibitor of ubiquitin-proteasome pathway MG-132, which reduces degradation of ubiquitinated proteins (Lee and Goldberg, 1998). Contrary, no red fluorescence could be observed after overexpression of the wtCatF (Figure 11I) or transfection of cells with the empty vector (Figure 11F). Whether these structures are aggresomes or aggresome-like inclusions is a matter of further investigation. It has been suggested that aggresomes do not represent a general response to protein misfolding (Beaudoin et al., 2008), although they have been initially proposed to be a general cell response to the accumulation of aggregation-prone misfolded proteins and proteasome inhibition (Johnston et al., 1998).

Proteins and protein aggregates inside aggresomes are often but not necessary tagged by ubiquitin moieties (Johnston et al., 2000), enabling binding of adaptor proteins like p62/SQSTM1 (Iwata et al., 2005b; Lamark and Johansen, 2012). p62 (Sequestosome-1) has been shown to facilitate the formation of aggresome-like induced structures (ALIS) and their degradation by autophagy (Bjorkoy et al., 2005; Clausen et al., 2010; Glick et al., 2010). Selective uptake of p62 targets is mediated by the binding of ubiquitin or polyubiqutin via its C-terminal UBA domain and LC3 or GABARAP/GABARAP-like proteins via its N-terminal LIR domain, thereby targeting them to the phagophores (Su and Lau, 2009). Besides, p62 may also mediate autophagic degradation of some substrates in ubiquitin-independent manner (Gal et al., 2009). We examined whether the N-terminally truncated forms of human cathepsin F colocalize with the p62 protein. Results revealed that Δ^{19}CatF, Δ^{125}CatF and Δ^{146}CatF (Figure 12 L, P, T), but not the wtCatF (Figure 12H) form p62 positive inclusions, thereby suggesting their removal by p62-mediated autophagy pathway. Moreover, increased levels of p62 were observed in cells overexpressing N-terminally truncated variants of cathepsin F, compared to very low levels of p62 in empty vector or wtCatF-transfected cell.

We assessed the possibility of autophagic clearance by colocalization with the autophagy marker microtubule-associated protein 1A/1B light chain 3B (LC3B). All three N-terminally truncated forms strongly colocalized with LC3B (Figure 13 L, P, T), indicating their clearance by autophagy pathway. Similarly, wtCatF (Figure 13H) seems

to be, at least partially, degraded by autophagy. Nevertheless, expression of N-terminally truncated forms induced formation of aggregated LC3B puncta which were larger, yet fewer in number (Figure 13 K, O, S), compared to more numerous but vesicular puncta in cells expressing the wild type protein (Figure 13G). LC3B puncta accumulation could be observed either due to the increased *de novo* autophagosome formation after autophagy induction or due to its delayed/reduced degradation in the autolysosomes (Vergarajauregui et al., 2008). According to the observed elevated levels of p62, these results could altogether suggest a decrease in autophagic degradation. This could be due to the overexpression of the proteins by itself or due to the overload of the cells by accumulated aggregates. The former variant seems to be less plausible, since cells overexpressing the wtCatF display neither p62 accumulation nor autophagosomes/autolysosomes accumulation, as assed by immunocytochemistry. On the other hand, observed LC3B puncta might also represent clusters of autophagosomes, which may be later dispersed in live cells (Ganley et al., 2011).

Truncated cathepsin B, lacking a part of the N-terminal region (exons 2 and 3), has been shown to trigger nuclear fragmentation and induce apoptotic cell death (Muntener et al., 2003; Muntener et al., 2004). Due to the lack of regular cathepsin B enzymatic activity, it was proposed that alternative mechanism of cell death induction was activated (Bestvater et al., 2005). Furthermore, accumulation of toxic cytosolic proteins or aggresomes may lead to the caspase activation and apoptotic cell death (Kristiansen et al., 2005; Wang et al., 2009). Therefore, we evaluated the potential contribution of the N-terminally truncated cathepsin F to the apoptosis, induced by caspase activation. For this reason, fluorogenic substrate Ac-DEVD.AFC (c-Asp-Glu-Val-Asp-7-amino-4-trifluoromethylcoumarin), a reporter of general caspase activation was used. We demonstrated significant 2 – 3 fold increase in DEVDase activity in HEK293T cells transfected by Δ^{19}CatF, Δ^{125}CatF or Δ^{146}CatF, compared to the empty vector or wtCatF transfected cells (Figure 14). Measured signal was blocked by pan-caspase inhibitor Z-VAD(OMe)-FMK in all tested samples, thus confirming the specificity of the detected signal. Nevertheless, observed caspase activation was not sufficient to induce apoptotic cell death as assessed by annexinV/propidium iodide staining and detection using flow cytometry (Jeric et al., 2013), thus further suggesting a protective and pro-survival role of aggresome-like inclusions and their autophagic elimination in our experimental system.

5.2 Characterization of CLN13 mutants in SH-SY5Y cells

The neuronal ceroid lipofuscinoses (NCLs) comprise a group of inherited progressive degenerative disorders characterized by intellectual and motor deterioration, seizures, visual loss, dementia and early death. To date, fourteen CLN-related genes have been identified, most of which encode for soluble and transmembrane proteins localized to the ER or endosomal/lysosomal compartment. Dysfunction of CLN genes may lead to characteristic lysosomal accumulation of autofluorescent ceroid lipopigments and undegradable substrates or metabolites (Kollmann et al., 2013; Mole and Williams, 2013). Recently, Smith and her colleagues (Smith et al., 2013) found four missense (c.1439C>T, c.1373G>C, c.692A>G, c.962A>G) and one frameshift mutation (c.954delC) in human cathepsin F (CLN13) gene linked to type B Kufs diseases. The mutations lead to protein changes p.(S480L), p.(G458A), p.(Y231C), p.(G321A) and p.(S319Lfs*27), respectively. Individuals whose genotypes were analyzed had mutations either on one or both alleles. In some cases each of the affected alleles had a different mutation. If and which affected alleles were actually expressed on protein level was not investigated. Nevertheless, the mutations affect highly conserved amino acids and secondary structure elements and are therefore predicted to damage the protein function (Smith et al., 2013). Moreover, the frameshift mutation leads to the premature stop codon and results in a truncation of C-terminal part of the protein, which subsequently lacks three-quarters of the mature part (Figure 15).

Due to the lack of suitable human neuronal model for *in vitro* studies, we decided to express our single mutants in human SH-SY5Y neuroblastoma cell line. SH-SY5Y cells are generally considered as immature neuroblasts at different stages of neuronal differentiation (Constantinescu et al., 2007). Nevertheless, these cells have neuronal origin and express tyrosine hydroxylase and dopamine β-hydroxylase, both of which are specific for catecholaminergic neurons (Constantinescu et al., 2007; Ross et al., 1983). In addition, receptors and transporters for dopamine and acetylcholine have been found to be expressed in SH-SY5Y cells (Biedler et al., 1978; Constantinescu et al., 2007; Willets et al., 1995). They also express genes associated with neuronal differentiation, including neurofilament proteins and neuron specific enolase (Constantinescu et al., 2007).

Successful transfection of CLN13 mutants was demonstrated by Western blot analysis. Wild type cathepsin F (wtCatF) and all CLN13 mutants (S319Lfs*27, Y231C, Q321R, G458A and S480L) were detected in soluble fraction of cell lysates (Figure 16A). wtCatF and missense mutants were detected as a single band of ~70 kDa by Western blot analysis, whereas expression of the frame shift mutant S319Lfs*27 resulted in two close bands of ~50 and ~52 kDa. myc/His tag increased the Mw of all expressed proteins for additional 3 kDa. Besides, higher Mw could be attributed to the glycosylation. None of the missense mutations affected potential glycosylation sites. Contrary, potential N-glycosylation pattern changed strongly in the frameshift mutant. Namely, this protein is devoid of all three (Asn367, Asn378 and Asn440) potential glycosylation sites in the mature form; however, new potential N-linked glycosylation site was formed at the Asn320. Two potential glycosylation sites in the propeptide region (Asn160 and Asn19) remained unaffected. Theoretical Mw of S319Lfs*27 is 38.1 kDa, as assessed from its amino acid sequence. Higher Mw observed on Western blots could be therefore attributed to the glycosylation which is initiated in the ER and myc/His tag. Glycosylation also increases protein solubility due to its hydrophilic nature (Aebi, 2013; Schroder and Kaufman, 2005; Wormald and Dwek, 1999). This could explain solubility of S319Lfs*27 aggregates, which are described later on in the discussion. Unexpectedly, all of the expressed proteins were also observed in the insoluble (membrane) fraction (Figure 16D).

Explanation for this phenomenon could reside inside the methodology (possible contamination of insoluble fraction with soluble proteins, impact of SDS on the protein concentration quantification and subsequent differences in protein loading between soluble in insoluble fraction etc.). Since also the wtCatF is present in insoluble fraction, it could be possible as well that a larger portion of the expressed proteins is not folded properly due to the overload of the cells with protein overexpression. Moreover, detected proteins in the insoluble fraction had a slightly higher Mw (~85 kDa for the wtCatF and missense mutations and ~60 kDa for the frameshift mutation, respectively), compared to those observed in the soluble fraction. This shift in Mw could be attributed to the fact that by folding machinery-unprocessed products are very likely (multi)ubiquitinated and targeted for proteasomal degradation. Overload of the proteasome by overexpression may lead to the accumulation of the ubiquitinated, high molecular weight derivates (Johnston et al., 1998; Kim et al., 1997). Higher Mw bands could also represent some other posttranslational modifications that may increase their hydrophobicity (Greaves et al., 2012) or smaller MG-132 induced-aggregates.

Anyhow, inhibition of lysosomal (autophagic) degradation using bafilomycin A1 (Figure 16 B and E) or inhibition of the proteasomal degradation by MG-132 (Figure 16 C and F), argues that expressed proteins are degraded by both, autophagy and ubiquitin-proteasome pathway. Bafilomycin A1 prevents maturation of autophagic vacuoles by inhibiting fusion between autophagosomes and lysosomes through inhibition of the vacuolar H^+ ATPase (Yamamoto et al., 1998), whereas MG-132 is a cell-permeable reversible proteasome inhibitor (Lee and Goldberg, 1998). There was, however, much more remarkable protein accumulation after proteasomal inhibition in comparison to the inhibition of lysosomal degradation. These results suggest ubiquitin-proteasome is the major degradation pathway for the CLN13 mutants and wtCatF. However, ubiquitin-proteasome pathway is complemented by the autophagic degradation. Autophagy activation may also occur in response to endoplasmic reticulum stress caused by misfolded proteins during proteasome inhibition (Ding et al., 2007).

All of the expressed proteins contain signal sequence for the lysosomal localization; therefore they have been expected to be targeted to the lysosomes. On the other hand, changes in glycosylation sites of the S319Lfs*27 could potentially disrupt classical M6P receptor-dependent lysosomal targeting of this mutated protein. Lysosomal localization of the wtCatF and CLN13 mutants was experimentally assessed by confocal microscopy and evaluation of EGFP-tagged protein – LAMP2 colocalization. As expected all of the expressed proteins colocalized with LAMP2 (Figure 17, left panel). However, prevalent aggregate-like expression of S319Lfs*27 (Figure 17, left panel G) was opposite to dispersed, vesicular expression of the wtCatF protein and missense mutants (Figure 17, left panel D, J, M, P, S), raised our attention. LAMP2 colocalization is open to several interpretations, therefore we tested the possibility that aggregates may be delivered to the lysosomes by autophagosomes. This hypothesis was confirmed using wortmannin, a phosphatidyl inositol 3-kinase inhibitor (Blommaart et al., 1997), thereby inhibiting autophagosome formation and sequestration of the expressed proteins into the autophagosomes (Figure 17, right panel). Colocalization of EGFP-tagged S319Lfs*27 with LAMP2 was thus largely abolished, suggesting that intralysosomal S319Lfs*27 result from its autophagic uptake. Considering that immunoblotting (Figure 16) suggests proteasome-mediated degradation to dominate autophagic clearance, we assumed that properly folded and misfolded proteins are most probably degraded by proteasome. In case of overload or when misfolded proteins begin to aggregate (such as S319Lfs*27), this function is probably overtaken by autophagy. Similarly, differential roles of the proteasome system and autophagy were observed in clearance of soluble and aggregated

TDP-43 species (a major pathological protein in amyotrophic lateral sclerosis), where they have found that soluble TDP-43 is degraded primarily by the UPS, whereas the clearance of aggregated TDP-43 requires autophagy (Scotter et al., 2014).

We extra examined potential ER retention of the expressed wild type protein and CLN13 mutants (Figure 18). Wild type protein as well as all of the CLN13 mutants with vesicular pattern colocalized with the ER marker protein disulfide isomerase (PDI). Adversely, S319Lfs*27 aggregates were not observed in the ER. Together with the fact that S319Lfs*27 do not reach lysosomes on its biosynthetic pathway, misfolded proteins are very likely retro translocated to the cytosol from the ER (possibly by the ER-associated degradation mechanism), where they may aggregate, if are not degraded. Colocalization of other expressed proteins (the wtCatF and missense mutants Y231C, Q321R, G458A and S480L) with the ER may be observed due the fact that this is their normal expression and folding start point, which is not synchronized for all of the expressed proteins. Nonetheless, as we observed these proteins also in the insoluble fraction of cell lysates, it could, however, also be possible that they are held in the ER for a prolonged time due to the overload of folding machinery by their overexpression.

Accumulation of the misfolded proteins in the ER can lead to ER stress (Lindholm et al., 2006; Tessitore et al., 2004; Zhang et al., 2006). Besides, ER stress can be induced by multiple other factors, such as the changes in calcium homeostasis, redox status and glycosylation (Schroder and Kaufman, 2005). Lipid storage disorders were often shown to impact intracellular calcium regulation, leading to the elevated cytosolic Ca^{2+} (Futerman and van Meer, 2004; Platt et al., 2012). The cause of impaired calcium homeostasis is different in each storage disease and depends on the organelle, where defective signaling is observed. For example, in CLN3-deficient mouse neurons calcium homeostasis is altered by modulation of a plasma membrane voltage-gated calcium channel, leading to the higher intracellular Ca^{2+} (Luiro et al., 2006; Vitner et al., 2010). Moreover, aberrant disturbed ER calcium regulation may impact mitochondria, resulting in mitochondria-mediated apoptosis (Platt et al., 2012). Nevertheless, although defective intracellular calcium signaling is common to e.g. Gaucher and Niemann-Pick disease (Vitner et al., 2010), it has not yet been reported in neuronal ceroid lipofuscinoses. According to the observed ER localization of the CLN13 mutants and the wild type protein, we decided to test their impact on intracellular Ca^{2+} levels. Using Fluo-4 AM, a reagent which exhibits increase in fluorescence intensity after calcium binding, no significant difference between the wtCatF, mutant CLN13-transfected cells and negative control (Figure 26) was observed. Results thus prove that expression of either the wild type protein or CLN13 mutants did not impact cellular Ca^{2+} levels to the measurable extent.

Besides the release of the Ca^{2+} to the cytosol, ER stress can also be reflected in regulation of genes expression involved in the unfolded protein response (UPR), which can promote protein folding or degradation of the misfolded proteins (Ding et al., 2007).We evaluated relative mRNA expression of the BiP (78 kDa glucose-regulated protein), CALR (calreticulin), CHOP (DNA damage-inducible transcript 3 protein) and EDEM1 (ER degradation-enhancing alpha-mannosidase-like protein 1) genes. All of these proteins are involved either in protein folding, ER stress and subsequent UPR or ER-associated degradation (ERAD). Namely, BiP (GRP78) facilitates translocation and folding of the proteins in the ER. In addition it prevents their aggregation. CALR is a chaperone that promotes folding, assembly and quality control of the monoglucosylated glycoproteins in the ER. CHOP is a transcription factor that induces apoptosis in response to ER stress. EDEM1 eliminates misfolded glycoproteins from the calnexin cycle, and is involved in ERAD which targets misfolded proteins for degradation in the cytoplasm

(Caramelo and Parodi, 2007; Noack et al., 2014; Olzmann et al., 2013; Walter and Ron, 2011). Approximately 4-, 5- and 7-fold up-regulation (relative to the empty vector-transfected cells) was detected for BiP and approximately 6-, 5- and 30-fold up-regulation for CHOP genes in cells transfected with the S319Lfs*27, wtCatF or thapsigargin-treated cells, respectively (Figure 27). Although no measurable changes in intracellular Ca^{2+} could be detected in transfected cells, cells treated with thapsigargin, a known inhibitor of the ER Ca^{2+} ATPase (Verma et al., 1990), and cell overexpressing cathepsin F protein displayed similar expression profile of the analyzed genes. This is somehow expected since depletion of ER calcium stores interferes with proper folding of proteins in the ER, thus leading to the UPR (Platt et al., 2012). Up-regulation of the BiP chaperone could be attributed to the increased folding demands of transfected cells, whereas CHOP up-regulation could indicate activation of apoptotic pathways, activated through the PERK signalling pathway (Walter and Ron, 2011). Overall, no significant difference in the expression of the UPR or ERAD-related genes could be found between the cells expressing wild type cathepsin F and those expressing its C-terminally truncated mutant S319Lfs*27. We therefore concluded that observed up-regulation of genes is most likely only a consequence of milder ER stress, activated by protein overexpression by itself. In conclusion, mutations in CLN13 do not induce ER stress in our system.

If not degraded, terminally misfolded proteins may aggregate together and cells may sequester such aggregates in different soluble or insoluble deposits. The initial aggregates are usually soluble, but gradually became insoluble as they exceed a certain size and solubility limits (Dobson, 2003; Stefani and Dobson, 2003; Wang, 2005). Link between protein misfolding, aggregation and neurodegeneration is already well known for disorders like Alzheimer's disease, Parkinson's disease, Huntington's disease, amyotrophic lateral sclerosis, prion diseases, lysosomal storage disease, etc. (Beaudoin et al., 2008; Roussel et al., 2013; Takalo et al., 2013). Accumulating evidence also implies that cellular toxicity is associated with non-native soluble species, rather than large aggregates. Large soluble aggregates can be protective and promote cell survival (Stefani and Dobson, 2003). The sequestration of misfolded proteins into separated compartments can thus protect cellular environment and facilitate their clearance (Arrasate et al., 2004; Zhang and Qian, 2011). Moreover, it is becoming evident that protein aggregation is not an uncontrolled process but rather directed, specific cellular defense (Tyedmers et al., 2010; Zhang and Qian, 2011). Formed protein aggregates may be sequestered into different quality control compartments, such as juxtanuclear quality control compartment (JUNQ), insoluble protein deposit (IPOD), aggresomes or aggresome-like induced structures (ALIS). Based on their ubiquitination status, aggregation state and solubility they may be even partitioned from one to another compartment (Kaganovich et al., 2008; Takalo et al., 2013). Aggregation of the frameshift mutant S319Lfs*27 upon its expression in SH-SY5Y cells was hereby confirmed immunocytochemically. Collected data further encouraged us to explore the nature of this aggregates. Since S319Lfs*27 aggregates were also found in soluble fraction and displayed dispersed morphology, they were not expected to form aggresomes. Especially since aggresomes are generally considered as insoluble juxtanuclear deposits (Johnston et al., 1998). Nevertheless, their positive staining with Proteostat®, which is a red fluorescent molecular rotor dye and claimed to detect aggregated proteins within the aggresome and aggresome-like structures (Shen et al., 2011), suggested that mainly dispersed S319Lfs*27 aggregates can be translocated to the perinuclear aggresome-like inclusions (Figure 19). On the other hand, no significant staining for aggresomes was observed in cells transfected with the wtCatF and other CLN13 mutants, although they were also found in the insoluble fraction by immunoblotting. According to microscopy and immunoblotting results it is more

tempting to designate S319Lfs*27 aggregates as aggresome-like structures, rather than aggresomes. Moreover, the extent of Proteostat® dye specificity is not very well established. On the other hand, it is known that aggresomes arise proteins that are transported on microtubules to the juxtanuclear microtubule organizing center (MTOC) by HDAC6, BAG3 or p97/VCP-mediated transport (Kawaguchi et al., 2003; Tresse et al., 2010; Zhang and Qian, 2011). It may, however, also be possible that aggresomes represent only a part of the observed aggregates or that aggresomes observed in S319Lfs*27-expressing cells are only a consequence of proteasomal inhibition by accumulation of protein aggregates. Prion protein was, for example, similarly shown to form aggresomes or dispersed aggregates in different cell lines; the formation of dispersed aggregates was insensitive to HDAC6 inhibitors and does not result in cytoskeleton rearrangements. Moreover, level of protein expression or proteasome inhibition had no effect on the formation of dispersed aggregates (Beaudoin et al., 2008). According to the fact that no other expressed protein was observed to aggregate, it is clear that aggregation of the S319Lfs*27 mutant is not a general consequence of protein overexpression, although the exact identity of these aggregates remains to be elucidated.

A phenomena of enlarged (swollen) LAMP-2 positive vesicles (lysosomes) was also evident in SH-SY5Y cells expressing S319Lfs*27 mutant (Figure 17, left panel H) and rarely, but less prominently also within cells expressing other mutants (Figure 17, left panel K N, Q, T). Enlarged lysosomes could result from accumulation of the undegraded material or decreased rate of fusion with other organelles (Alroy et al., 2014; Damme et al., 2014; Platt et al., 2012; Settembre et al., 2008; Vidal-Donet et al., 2013). Lysosomal proliferation and swelling could be an attempt of the cells to cope with the accumulated storage material. Swelling of lysosomes consequently increases the intra-lysosomal pH, due to the failure of the proton pumps in the lysosomal membrane to maintain the H^+ gradient (Heard et al., 2010; Hesselink et al., 2003; Parkinson-Lawrence et al., 2010; Yue et al., 2009). Indeed, we confirmed the increase in pH of acidic vesicles in CLN-13, but not also wtCatF-transfected cells using LysoTracker® Green DND-26 (Figure 20). This could potentially also explain less massive accumulation of expressed mutants after autophagic inhibition in comparison to proteasomal inhibition (Figure 16). Due to the increased pH in the lysosomes, their fusion with aggresomes may be decreased and degradation inhibited. In lysosomal storage diseases, the size of the lysosomes can increase several fold as a result of accumulation of undigested material (Futerman and van Meer, 2004). Moreover, block of one pathway (e.g. autophagy) stimulates the compensatory (e.g. proteasomal) pathway (Yue et al., 2009). Increase in lysosomal pH and subsequent alterations in macroautophagy has been linked to CLN3 as well (Vidal-Donet et al., 2013).

Perturbations in the lysosomal function may further lead to reduced autophagic flux (autophagosomal-lysosomal fusion) and accumulation of numerous autophagosomes as well as endo/autolysosomes and autophagosome-associated proteins, such as LC3II and p62 (Cao et al., 2006; Settembre et al., 2008). We therefore further analyzed whether the observed increase in the pH of the acidic organelles influences the autophagic flux in our experimental system, by analysis of LAMP2 and LC3B colocalization (Figure 21). Less colocalization of LAMP2 and LC3B (marked by arrowheads) was observed in cells overexpressing CLN13 mutants S480L, G458A, Y231C, G321A and S319Lfs*27 in comparison to the cells transfected with the wtCatF. These data support the idea that observed decrease in the autophagic flux in cells expressing CLN13 mutants results from the increased pH of acidic vesicles. Altogether, this can again explain the fact of the dominating proteasomal rather than autophagic degradation, observed by immunoblotting.

We also observed that LC3 puncta were fewer in number but larger in size, a phenomena hereby already observed and discussed for N-terminally truncated variants of human cathepsin F. Large LC3 puncta were most prominent in cells transfected with S319Lfs*27 (Figure 21K), thus additionally suggesting distinct autophagosomal-lysosomal fusion. It has been shown that accumulation of large LC3 structures results from decreased flux rather than induction of autophagy (Jaber et al., 2012).

Finally, we also examined whether autophagic clearance is p62/SQSTM1-mediated using immunolabeling with anti p62 antibodies. Although some colocalization of the wtCatF and mutant proteins with p62/SQSTM1 was observed, this was not the case for the larger S319Lfs*27 aggregates (Figure 22). Nevertheless, it should be noted that some colocalization with dispersed S319Lfs*27-EGFP signal, which could represent misfolded but not yet aggregated species, was observed. One could conclude from these results that clearance of S319Lfs*27 aggregates may not be p62-mediated. Although we have no experimental evidence, it could be possible that cells might use other (p62-independent) way of autophagic clearance in this case. Nevertheless, it is intriguing that no significant increase in p62 expression was observed in any of the transfected samples with regard to the fact that we observed a decreased autophagic flux. On the other hand immunocytochemistry is not a quantitative method allowing researcher to detect small changes in protein level.

Abnormalities in autophagic pathways have been linked to the accumulation of storage material (Cao et al., 2006; Cao et al., 2011; Settembre et al., 2008). NCL diseases are particularly characterized by the accumulation of the autofluorescent lipopigment resembling ceroid and age pigment lipofuscin (Palmer et al., 2013; Seehafer and Pearce, 2006). Ceroid is known to consist of proteins and lipids with a profile attributable to a lysosomal/endosomal origin (Palmer et al., 2013; Palmer et al., 1988). Since no sign of intrinsic fluorophore has been found, it has been concluded that autofluorescence is a consequence of accumulated protein aggregates and not intrinsic property or result of lipid peroxidation (Palmer et al., 2002). In addition, high levels of dolichols, dolichyl pyrophosphoryl oligosaccharides and 4-hydroxynonenal, a secondary product of lipid peroxidation, have also been found in storage bodies (Granier et al., 2000; Hall et al., 1991; Wolfe et al., 1983).

Our results have shown that the expression of C-terminally truncated frameshift mutant S319Lfs*27 led to the accumulation of higher levels of uncharacterized perinuclear autofluorescent pigment compared to the empty vector, wtCatF or S480L, G458A, Y231C and Q321R-transfected cells (Figure 23). This led us to further examination at the ultra-structural level. At the ultrastructural level, NCL ceroid can be seen as (membrane bound) lamellar inclusions with different profiles, including fingerprint deposit, curvilinear profile, rectilinear profile or granular osmophilic deposit, as well as typical lipofuscin deposit or microtubular aggregate (Figure 4). Lamellar inclusions are also often mixed with small lipid droplets. In addition, swollen or damaged mitochondria were found near fingerprint inclusions (Josephson et al., 2001; Lewandowska et al., 2009; Mole et al., 2005). Transmission electron microscopy (TEM) analysis of our samples revealed increased accumulation of lipids throughout the cell, around the nuclear and vesicular membranes and sometimes also near the mitochondria or the ER membrane after S319Lfs*27 expression (Figure 25), compared to wtCatF or non-transfected cells (Figure 24). We also found some lamellar inclusions in vesicles of S319Lfs*27-expressing cells, profile of which is hard to determine due to the low resolution of obtained images. Less frequently some damaged mitochondria were observed. In addition, vesicles loaded with electronically-dense material (proteins/protein aggregates) were often observed in these cells (Figure 25). These data indicate that

expression of S319Lfs*27 mutant led to the abnormal accumulation of lipids which were especially prone to load on the membranes of the intracellular organelles (predominantly vesicles and nuclear membrane) and probably in a longer term also to the formation of lamellar inclusions. According to the research, glycosphingolipids, phospholipids and cholesterol are among the most frequently found and studied storage lipids (Walkley and Vanier, 2009). Although the origin of lipids in our system and exact cause of their accumulation is unknown, these results suggest that S319Lfs*27 expressions lead to the aberrant lipid metabolism or trafficking. Accumulation of these uncharacterized lipids may also represent a secondary storage material, which may be involved in disease pathogenesis as well (Walkley and Vanier, 2009). Similarly, Tang and colleagues reported prominent presence of lipid droplets within many of the lipofuscin containing lysosomes in cathepsin F knock out mice (Tang et al., 2006). However, they did not report on membrane lipid accumulation, as observed in our cells. On the other side Smith and collegues unfortunately did not provide enough data on the storage material of the analyzed families (Smith et al., 2013). The only reported case was accumulation of ubiquitin positive storage material with fingerprint profile in patient with G458A/S480L genotype for cathepsin F gene (Smith et al., 2013). The comparison of published image from electron microscopy (Figure 4d) of this patient with ours (insert of Figure 25 A and B) reveals resemblance in lamellar inclusions. Moreover, accumulation of vesicular protein material, which may occur as a consequence of observed reduced autophagic flux, is very reminiscent of characteristic accumulation of proteinaceous storage material in the lysosomes of different types of NCLs.

Abnormal lipid metabolism, increase in superoxide dismutase and lipid peroxidation have initially been proposed to explain the pathogenesis of NCL, although exact biochemical mechanisms are still unknown (Granier et al., 2000; Hall et al., 1991; Palmer et al., 2013; Palmer et al., 1988; Wolfe et al., 1983). Observed damaged mitochondria using TEM and decreased autophagic flux could eventually lead to the generation of reactive oxygen species (ROS) and oxidative damage. Experiments have revealed slight increase in mitochondrial superoxide formation in cells overexpressing CLN13 mutants, compared to the cells expressing empty vector, as assessed by MitoSOX™ Red reagent on confocal microscopy (Figure 28). While this increase was only minor and to a certain, although lower, extent appeared also in cells transfected with the wild type protein, BODIPY® 581/591 revealed clear cut differences. Cells transfected with S480L, G458A, Y231C, Q321R or S319Lfs*27 but not in wtCatF transfected cells displayed many larger areas of oxidized (green fluorescent) BODIPY® 581/591 C11 (Figure 29), thus indicating lipid peroxidation. Consistent with the majority of other obtained experimental data, the effect was again most prominent with S319Lfs*27 mutant. Observed lipid peroxidation is most probably a consequence of oxidative damage induced by increased mitochondrial ROS production, a side product of normal oxygen metabolism. The source of ROS and oxidative damage in our system could be both, mitochondria and alterations in autophagic flux (which could again lead to decreased degradation of damaged mitochondria). Both of them (disturbed autophagy and damaged mitochondria) are also the major contributor to lipofuscin formation (Brunk and Terman, 2002).

In this study we have attempted to verify the role of signal peptide and cystatin-like domain in correct folding of human cathepsin F. Besides, we firstly show the behavior of CLN13 mutations upon their overexpression in SH-SY5Y cells, where the C-terminally truncated mutant exhibited the most profound effects on the disruption of normal cellular homeostasis.

6 Conclusions

While lysosomal enzymes should not encounter appropriate folding conditions in the cytoplasm, their targeting to the endoplasmic reticulum and subsequently to the Golgi apparatus and lysosomes was believed to be very important. Nevertheless, enzymatically active truncated forms of human cathepsins, devoid of signal sequence, have been observed in physiological as well as pathological conditions. Among them, human cathepsin F was not an exception. Yet, the impact of used methodologies on obtained results should be considered before conclusions are made. Namely, many conclusions on the properties of truncated cathepsin have been done on the basis of recombinant and not endogenous proteins. In our study some crucial differences between N-terminally truncated human cathepsin F found in sceletal muscles and N-terminally truncated variants expressed in HEK293T cells have been found. Our results show that N-terminal removal of signal sequence prevents this protein from lysosomal localization and glycosylation. Although cysteine cathepsins prodomains were suggested to assist their folding, cystatin-like domain is not sufficient to prevent aggregation of cathepsin F lacking signal peptide. N-terminal truncation of human cathepsin F renders it insoluble and leads to its aggregation. Furthermore, p62-positive aggregates form perinuclear aggresome-like inclusions, cleared by autophagy pathway. Accumulation of these aggregates finally leads to the increase in caspase activity, which is however not sufficient to induce apoptotic cell death. We therefore conclude that deletion of at least signal peptide from human cathepsin F leads to the cytosolic expression of enzymatically non-functional protein, which is eliminated by cellular degradation system.

In this study we have also attempted to functionally characterize effects of four missense and one frameshift CLN13 mutations found in patients with type B Kufs disease. All of them were predicted to be probably damaging for the function of protein. Moreover, frameshift mutation leads to the C-terminal truncation of the protein. We examined the pathways that have been found to be deregulated in NCL diseases. Our results have shown that CLN13 mutants are mainly degraded by ubiquitin-proteasome system, which is complemented by the autophagic degradation. Mutation S319Lfs*27 prevents it from its lysosomal localization and leads to aggregation of the protein, when expressed in SH-SY5Y cells. At least part of these dispersed aggregates was able to form perinuclear aggresome-like structures. Contrary, S480L, G458A, Y231C and Q321R end up in the lysosomes, as expected. Accumulation of CLN13 mutants induces swelling of the LAMP2-positive vesicle, whereby accumulation of S319Lfs*27 aggregates exhibits most profound effects. We have shown that S319Lfs*27 aggregates accumulate in autolysosomes after their autophagosomal sequestration. Expression of CLN13 mutants leads to the increased pH of acidic organelles, which is the most plausible mechanism of the observed reduced autophagic flux. Moreover, S319Lfs*27 induces accumulation of autofluorescent perinuclear material, increased accumulation of lipids on intracellular membranes, formation of lamellar inclusions inside of electronically dense vesicles and damage of some mitochondria. Finally, slightly increased levels of mitochondrial superoxide and more prominent lipid peroxidation are very likely caused by mitochondrial damage and reduced autophagic flux. Overall, CLN13 mutations have been shown to induce changes in cellular homeostasis which resembles those, also observed in

many other NCL diseases.

7 Acknowledgements

First, I would like to thank to my PhD mentor Prof. Dr. Veronika Stoka for the scientific advice, ideas, time, knowledge and support during these past four years. Sometimes it was difficult, but everything happened only made me better scientist and stronger person.

I want to thank the members of my PhD committee, Prof. Ddr. Boris Turk, Prof. Dr. Ana Plemenitaš and Prof. Dr. Eva Žerovnik for the corrections and suggestions which improved this thesis.

My gratitude is also extended to the Head of our department Prof. Ddr. Boris Turk, Academic Prof. Dr. Vito Turk and the Slovenian Research Agency to enable me this research work.

I would also like to thank Asst. Prof. Dr. Tina Zavašnik-Bergant for the execution of transmission electron microscopy.

Special and big thanks go to my parents for all kinds of the support I constantly receive from their side. They have taught me about hard work, about persistence and about how to be independent. It was a good foundation with which to meet life. Thanks go also to my brother, sister and broader family for all support.

Words cannot express how grateful I am to my beloved husband Gašper. Thank you for your love, thank you for supporting me in everything, and especially I cannot thank you enough for encouraging me throughout this experience. Thank you also for all the weekends that you spent next to me in the lab. Your complete and unconditional love has changed me for the better and carries me through always. Thank you with all my heart and soul.

To all my friends, especially Katarina, Katja, Jaka, Marta, Gašper, Matej, Iztok, Klemen and Alja. There was not a lot of time to hang around in past four years, but those precious moments that we spent together helped me to relax and gave me fresh energy for this work. Thank you for your care, listening and advices. I greatly value for supporting me through this entire process and your friendship.

Last, but certainly not least, I was lucky to be a part of a great team of coworkers which supported and encouraged me. When the times were tough, their humor and friendliness allowed me to laugh and lighten my perspective. Together, we have laughed and cried, discussed experiments and our lives. Many thanks to Maruša, Barbara, Katarina M., Nežka, Katarina P., Ajda, Miha, Gabi and all others.

8 References

Acosta-Alvear, D.; Zhou, Y.; Blais, A.; Tsikitis, M.; Lents, N.H.; Arias, C.; Lennon, C.J.; Kluger, Y.; Dynlacht, B.D. XBP1 controls diverse cell type- and condition-specific transcriptional regulatory networks. *Mol Cell* 27, 53-66. (2007)

Aebi, M. N-linked protein glycosylation in the ER. *Biochim Biophys Acta* 1833, 2430-2437. (2013)

Agarraberes, F.A.; Dice, J.F. A molecular chaperone complex at the lysosomal membrane is required for protein translocation. *Journal of cell science* 114, 2491-2499. (2001)

Alberts, B., Johnson, A., Lewis, J., Raff, M., Roberts, K., Walter, P. (2002). Molecular Biology of the Cell, 4th edn (New York, Garland Science).

Alroy, J.; Garganta, C.; Wiederschain, G. Secondary biochemical and morphological consequences in lysosomal storage diseases. *Biochemistry (Mosc)* 79, 619-636. (2014)

Arndt, V.; Dick, N.; Tawo, R.; Dreiseidler, M.; Wenzel, D.; Hesse, M.; Furst, D.O.; Saftig, P.; Saint, R.; Fleischmann, B.K., *et al.* Chaperone-assisted selective autophagy is essential for muscle maintenance. *Current biology : CB* 20, 143-148. (2010)

Arrasate, M.; Mitra, S.; Schweitzer, E.S.; Segal, M.R.; Finkbeiner, S. Inclusion body formation reduces levels of mutant huntingtin and the risk of neuronal death. *Nature* 431, 805-810. (2004)

Ballabio, A. Disease pathogenesis explained by basic science: lysosomal storage diseases as autophagocytic disorders. *International journal of clinical pharmacology and therapeutics* 47 Suppl 1, S34-38. (2009)

Ballabio, A.; Gieselmann, V. Lysosomal disorders: from storage to cellular damage. *Biochim Biophys Acta* 1793, 684-696. (2009)

Barrett, A.J., Rawlings, N.D., Woessner, J.F., ed. (1998). Handbook of Proteolytic Enzymes, 2nd edn (London, Academic Press).

Beaudoin, S.; Goggin, K.; Bissonnette, C.; Grenier, C.; Roucou, X. Aggresomes do not represent a general cellular response to protein misfolding in mammalian cells. *BMC Cell Biol* 9, 59. (2008)

Benaroudj, N.; Tarcsa, E.; Cascio, P.; Goldberg, A.L. The unfolding of substrates and ubiquitin-independent protein degradation by proteasomes. *Biochimie* 83, 311-318. (2001)

Bennett, M.J.; Rakheja, D. The neuronal ceroid-lipofuscinoses. *Dev Disabil Res Rev* 17, 254-259. (2013)

Berkovic, S.F.; Andermann, F.; Andermann, E.; Carpenter, S.; Wolfe, L. Kufs disease: clinical features and forms. *Am J Med Genet Suppl* 5, 105-109. (1988)

Bestvater, F.; Dallner, C.; Spiess, E. The C-terminal subunit of artificially truncated human cathepsin B mediates its nuclear targeting and contributes to cell viability. *BMC Cell Biol* 6, 16. (2005)

Bhatia, R.; Lin, H.; Lal, R. Fresh and globular amyloid beta protein (1-42) induces rapid cellular degeneration: evidence for AbetaP channel-mediated cellular toxicity. *Faseb J* 14, 1233-1243. (2000)

Biedler, J.L.; Roffler-Tarlov, S.; Schachner, M.; Freedman, L.S. Multiple neurotransmitter synthesis by human neuroblastoma cell lines and clones. *Cancer research* 38, 3751-3757. (1978)

Bjorkoy, G.; Lamark, T.; Brech, A.; Outzen, H.; Perander, M.; Overvatn, A.; Stenmark, H.; Johansen, T. p62/SQSTM1 forms protein aggregates degraded by autophagy and has a protective effect on huntingtin-induced cell death. *J Cell Biol* 171, 603-614. (2005)

Blommaart, E.F.; Krause, U.; Schellens, J.P.; Vreeling-Sindelarova, H.; Meijer, A.J. The phosphatidylinositol 3-kinase inhibitors wortmannin and LY294002 inhibit autophagy in isolated rat hepatocytes. *European journal of biochemistry / FEBS* 243, 240-246. (1997)

Boyault, C.; Gilquin, B.; Zhang, Y.; Rybin, V.; Garman, E.; Meyer-Klaucke, W.; Matthias, P.; Muller, C.W.; Khochbin, S. HDAC6-p97/VCP controlled polyubiquitin chain turnover. *Embo J* 25, 3357-3366. (2006)

Bozaykut, P.; Ozer, N.K.; Karademir, B. Regulation of protein turnover by heat shock proteins. *Free Radic Biol Med*. (2014)

Bratton, S.B.; Salvesen, G.S. Regulation of the Apaf-1-caspase-9 apoptosome. *Journal of cell science* 123, 3209-3214. (2010)

Brenner, D.; Mak, T.W. Mitochondrial cell death effectors. *Curr Opin Cell Biol* 21, 871-877. (2009)

Brix, K.; Dunkhorst, A.; Mayer, K.; Jordans, S. Cysteine cathepsins: cellular roadmap to different functions. *Biochimie* 90, 194-207. (2008)

Brunk, U.T.; Terman, A. The mitochondrial-lysosomal axis theory of aging: accumulation of damaged mitochondria as a result of imperfect autophagocytosis. *European journal of biochemistry / FEBS* 269, 1996-2002. (2002)

Calfon, M.; Zeng, H.; Urano, F.; Till, J.H.; Hubbard, S.R.; Harding, H.P.; Clark, S.G.; Ron, D. IRE1 couples endoplasmic reticulum load to secretory capacity by processing the XBP-1 mRNA. *Nature* 415, 92-96. (2002)

Cao, Y.; Espinola, J.A.; Fossale, E.; Massey, A.C.; Cuervo, A.M.; MacDonald, M.E.; Cotman, S.L. Autophagy is disrupted in a knock-in mouse model of juvenile neuronal ceroid lipofuscinosis. *J Biol Chem* 281, 20483-20493. (2006)

Cao, Y.; Staropoli, J.F.; Biswas, S.; Espinola, J.A.; MacDonald, M.E.; Lee, J.M.; Cotman, S.L. Distinct early molecular responses to mutations causing vLINCL and JNCL presage ATP synthase subunit C accumulation in cerebellar cells. *PLoS One* 6, e17118. (2011)

Caramelo, J.J.; Parodi, A.J. How sugars convey information on protein conformation in the endoplasmic reticulum. *Seminars in Cell & Developmental Biology* 18, 732-742. (2007)

Caughey, B.; Lansbury, P.T. Protofibrils, pores, fibrils, and neurodegeneration: separating the responsible protein aggregates from the innocent bystanders. *Annu Rev Neurosci* 26, 267-298. (2003)

Clausen, T.H.; Lamark, T.; Isakson, P.; Finley, K.; Larsen, K.B.; Brech, A.; Overvatn, A.; Stenmark, H.; Bjorkoy, G.; Simonsen, A., *et al.* p62/SQSTM1 and ALFY interact to facilitate the formation of p62 bodies/ALIS and their degradation by autophagy. *Autophagy* 6, 330-344. (2010)

Colbert, J.D.; Matthews, S.P.; Miller, G.; Watts, C. Diverse regulatory roles for lysosomal proteases in the immune response. *Eur J Immunol* 39, 2955-2965. (2009)

Constantinescu, R.; Constantinescu, A.T.; Reichmann, H.; Janetzky, B. Neuronal differentiation and long-term culture of the human neuroblastoma line SH-SY5Y. *J Neural Transm Suppl*, 17-28. (2007)

Conus, S.; Simon, H.U. Cathepsins: key modulators of cell death and inflammatory

responses. *Biochem Pharmacol* 76, 1374-1382. (2008)
Conway, K.A.; Lee, S.J.; Rochet, J.C.; Ding, T.T.; Williamson, R.E.; Lansbury, P.T., Jr. Acceleration of oligomerization, not fibrillization, is a shared property of both alpha-synuclein mutations linked to early-onset Parkinson's disease: implications for pathogenesis and therapy. *Proc Natl Acad Sci U S A* 97, 571-576. (2000)
Cuervo, A.M.; Dice, J.F. A receptor for the selective uptake and degradation of proteins by lysosomes. *Science* 273, 501-503. (1996)
Damme, M.; Suntio, T.; Saftig, P.; Eskelinen, E.L. Autophagy in neuronal cells: general principles and physiological and pathological functions. *Acta Neuropathol*. (2014)
Dantuma, N.P.; Bott, L.C. The ubiquitin-proteasome system in neurodegenerative diseases: precipitating factor, yet part of the solution. *Front Mol Neurosci* 7, 70. (2014)
Demand, J.; Luders, J.; Hohfeld, J. The carboxy-terminal domain of Hsc70 provides binding sites for a distinct set of chaperone cofactors. *Mol Cell Biol* 18, 2023-2028. (1998)
Dice, J.F. Chaperone-mediated autophagy. *Autophagy* 3, 295-299. (2007)
Ding, W.X.; Ni, H.M.; Gao, W.; Yoshimori, T.; Stolz, D.B.; Ron, D.; Yin, X.M. Linking of autophagy to ubiquitin-proteasome system is important for the regulation of endoplasmic reticulum stress and cell viability. *Am J Pathol* 171, 513-524. (2007)
Dobson, C.M. Protein folding and misfolding. *Nature* 426, 884-890. (2003)
Dorn, A.; Zhao, H.; Granberg, F.; Hosel, M.; Webb, D.; Svensson, C.; Pettersson, U.; Doerfler, W. Identification of specific cellular genes up-regulated late in adenovirus type 12 infection. *Journal of virology* 79, 2404-2412. (2005)
Ellgaard, L.; Helenius, A. Quality control in the endoplasmic reticulum. *Nat Rev Mol Cell Biol* 4, 181-191. (2003)
Elmore, S. Apoptosis: a review of programmed cell death. *Toxicol Pathol* 35, 495-516. (2007)
Ferri, K.F.; Kroemer, G. Organelle-specific initiation of cell death pathways. *Nat Cell Biol* 3, E255-263. (2001)
Fink, A.L. Protein aggregation: folding aggregates, inclusion bodies and amyloid. *Fold Des* 3, R9-23. (1998)
Fonovic, M.; Bromme, D.; Turk, V.; Turk, B. Human cathepsin F: expression in baculovirus system, characterization and inhibition by protein inhibitors. *Biol Chem* 385, 505-509. (2004)
Fonovic, M.; Turk, B. Cysteine cathepsins and extracellular matrix degradation. *Biochim Biophys Acta* 1840, 2560-2570. (2014)
Futerman, A.H.; van Meer, G. The cell biology of lysosomal storage disorders. *Nature reviews. Molecular cell biology* 5, 554-565. (2004)
Gal, J.; Strom, A.L.; Kwinter, D.M.; Kilty, R.; Zhang, J.; Shi, P.; Fu, W.; Wooten, M.W.; Zhu, H. Sequestosome 1/p62 links familial ALS mutant SOD1 to LC3 via an ubiquitin-independent mechanism. *J Neurochem* 111, 1062-1073. (2009)
Galluzzi, L.; Bravo-San Pedro, J.M.; Vitale, I.; Aaronson, S.A.; Abrams, J.M.; Adam, D.; Alnemri, E.S.; Altucci, L.; Andrews, D.; Annicchiarico-Petruzzelli, M., *et al.* Essential versus accessory aspects of cell death: recommendations of the NCCD 2015. *Cell Death Differ* 22, 58-73. (2015)
Galluzzi, L.; Maiuri, M.C.; Vitale, I.; Zischka, H.; Castedo, M.; Zitvogel, L.; Kroemer, G. Cell death modalities: classification and pathophysiological implications. *Cell Death Differ* 14, 1237-1243. (2007)
Galluzzi, L.; Vitale, I.; Abrams, J.M.; Alnemri, E.S.; Baehrecke, E.H.; Blagosklonny, M.V.; Dawson, T.M.; Dawson, V.L.; El-Deiry, W.S.; Fulda, S., *et al.* Molecular definitions of cell death subroutines: recommendations of the Nomenclature

Committee on Cell Death 2012. *Cell Death Differ* 19, 107-120. (2012)
Ganley, I.G.; Wong, P.M.; Gammoh, N.; Jiang, X. Distinct autophagosomal-lysosomal fusion mechanism revealed by thapsigargin-induced autophagy arrest. *Mol Cell* 42, 731-743. (2011)
Getty, A.L.; Pearce, D.A. Interactions of the proteins of neuronal ceroid lipofuscinosis: clues to function. *Cell Mol Life Sci* 68, 453-474. (2011)
Glick, D.; Barth, S.; Macleod, K.F. Autophagy: cellular and molecular mechanisms. *J Pathol* 221, 3-12. (2010)
Glover, J.R.; Lindquist, S. Hsp104, Hsp70, and Hsp40: a novel chaperone system that rescues previously aggregated proteins. *Cell* 94, 73-82. (1998)
Goulet, B.; Baruch, A.; Moon, N.S.; Poirier, M.; Sansregret, L.L.; Erickson, A.; Bogyo, M.; Nepveu, A. A cathepsin L isoform that is devoid of a signal peptide localizes to the nucleus in S phase and processes the CDP/Cux transcription factor. *Mol Cell* 14, 207-219. (2004)
Goulet, B.; Sansregret, L.; Leduy, L.; Bogyo, M.; Weber, E.; Chauhan, S.S.; Nepveu, A. Increased expression and activity of nuclear cathepsin L in cancer cells suggests a novel mechanism of cell transformation. *Mol Cancer Res* 5, 899-907. (2007)
Granier, L.A.; Langley, K.; Leray, C.; Sarlieve, L.L. Phospholipid composition in late infantile neuronal ceroid lipofuscinosis. *Eur J Clin Invest* 30, 1011-1017. (2000)
Greaves, J.; Lemonidis, K.; Gorleku, O.A.; Cruchaga, C.; Grefen, C.; Chamberlain, L.H. Palmitoylation-induced aggregation of cysteine-string protein mutants that cause neuronal ceroid lipofuscinosis. *J Biol Chem* 287, 37330-37339. (2012)
Grenier, C.; Bissonnette, C.; Volkov, L.; Roucou, X. Molecular morphology and toxicity of cytoplasmic prion protein aggregates in neuronal and non-neuronal cells. *J Neurochem* 97, 1456-1466. (2006)
Grune, T.; Jung, T.; Merker, K.; Davies, K.J. Decreased proteolysis caused by protein aggregates, inclusion bodies, plaques, lipofuscin, ceroid, and 'aggresomes' during oxidative stress, aging, and disease. *Int J Biochem Cell Biol* 36, 2519-2530. (2004)
Guicciardi, M.E.; Gores, G.J. Life and death by death receptors. *Faseb J* 23, 1625-1637. (2009)
Guicciardi, M.E.; Leist, M.; Gores, G.J. Lysosomes in cell death. *Oncogene* 23, 2881-2890. (2004)
Hachiya, Y.; Hayashi, M.; Kumada, S.; Uchiyama, A.; Tsuchiya, K.; Kurata, K. Mechanisms of neurodegeneration in neuronal ceroid-lipofuscinoses. *Acta Neuropathol* 111, 168-177. (2006)
Hall, N.A.; Lake, B.D.; Patrick, A.D. Recent biochemical and genetic advances in our understanding of Batten's disease (ceroid-lipofuscinosis). *Dev Neurosci* 13, 339-344. (1991)
Haltia, M.; Goebel, H.H. The neuronal ceroid-lipofuscinoses: a historical introduction. *Biochim Biophys Acta* 1832, 1795-1800. (2013)
Hammond, C.; Braakman, I.; Helenius, A. Role of N-linked oligosaccharide recognition, glucose trimming, and calnexin in glycoprotein folding and quality control. *Proc Natl Acad Sci U S A* 91, 913-917. (1994)
Han, X.; Zhou, J.; Zhang, P.; Song, F.; Jiang, R.; Li, M.; Xia, F.; Guo, F.J. IRE1alpha dissociates with BiP and inhibits ER stress-mediated apoptosis in cartilage development. *Cell Signal* 25, 2136-2146. (2013)
Harding, H.P.; Zhang, Y.; Ron, D. Protein translation and folding are coupled by an endoplasmic-reticulum-resident kinase. *Nature* 397, 271-274. (1999)
Hasilik, A.; Wrocklage, C.; Schroder, B. Intracellular trafficking of lysosomal proteins and lysosomes. *International journal of clinical pharmacology and therapeutics*

47 Suppl 1, S18-33. (2009)
Haze, K.; Yoshida, H.; Yanagi, H.; Yura, T.; Mori, K. Mammalian transcription factor ATF6 is synthesized as a transmembrane protein and activated by proteolysis in response to endoplasmic reticulum stress. *Mol Biol Cell* 10, 3787-3799. (1999)
He, C.H.; Gong, P.; Hu, B.; Stewart, D.; Choi, M.E.; Choi, A.M.; Alam, J. Identification of activating transcription factor 4 (ATF4) as an Nrf2-interacting protein. Implication for heme oxygenase-1 gene regulation. *J Biol Chem* 276, 20858-20865. (2001)
Heard, J.M.; Bruyere, J.; Roy, E.; Bigou, S.; Ausseil, J.; Vitry, S. Storage problems in lysosomal diseases. *Biochemical Society transactions* 38, 1442-1447. (2010)
Hegde, A.N.; Upadhya, S.C. Role of ubiquitin-proteasome-mediated proteolysis in nervous system disease. *Biochim Biophys Acta* 1809, 128-140. (2011)
Heine, C.; Tyynela, J.; Cooper, J.D.; Palmer, D.N.; Elleder, M.; Kohlschutter, A.; Braulke, T. Enhanced expression of manganese-dependent superoxide dismutase in human and sheep CLN6 tissues. *The Biochemical journal* 376, 369-376. (2003)
Hesselink, R.P.; Wagenmakers, A.J.; Drost, M.R.; Van der Vusse, G.J. Lysosomal dysfunction in muscle with special reference to glycogen storage disease type II. *Biochim Biophys Acta* 1637, 164-170. (2003)
Ho, J.D.; Meltser, Y.; Buggy, J.J.; Palmer, J.T.; Elrod, K.C.; Chan, H.; Mortara, K.D.; Somoza, J.R. Expression, purification, crystallization and preliminary X-ray diffraction studies of human cathepsin F complexed with an irreversible vinyl sulfone inhibitor. *Acta Crystallogr D Biol Crystallogr* 58, 2187-2190. (2002)
Hohfeld, J.; Minami, Y.; Hartl, F.U. Hip, a novel cochaperone involved in the eukaryotic Hsc70/Hsp40 reaction cycle. *Cell* 83, 589-598. (1995)
Hosokawa, N.; Hara, T.; Kaizuka, T.; Kishi, C.; Takamura, A.; Miura, Y.; Iemura, S.; Natsume, T.; Takehana, K.; Yamada, N., *et al.* Nutrient-dependent mTORC1 association with the ULK1-Atg13-FIP200 complex required for autophagy. *Mol Biol Cell* 20, 1981-1991. (2009)
Huyer, G.; Longsworth, G.L.; Mason, D.L.; Mallampalli, M.P.; McCaffery, J.M.; Wright, R.L.; Michaelis, S. A striking quality control subcompartment in Saccharomyces cerevisiae: the endoplasmic reticulum-associated compartment. *Mol Biol Cell* 15, 908-921. (2004)
Hyttinen, J.M.; Amadio, M.; Viiri, J.; Pascale, A.; Salminen, A.; Kaarniranta, K. Clearance of misfolded and aggregated proteins by aggrephagy and implications for aggregation diseases. *Ageing Res Rev* 18C, 16-28. (2014)
Ishida, T.; Kinoshita, K. Prediction of disordered regions in proteins based on the meta approach. *Bioinformatics* 24, 1344-1348. (2008)
Iwata, A.; Christianson, J.C.; Bucci, M.; Ellerby, L.M.; Nukina, N.; Forno, L.S.; Kopito, R.R. Increased susceptibility of cytoplasmic over nuclear polyglutamine aggregates to autophagic degradation. *Proc Natl Acad Sci U S A* 102, 13135-13140. (2005a)
Iwata, A.; Riley, B.E.; Johnston, J.A.; Kopito, R.R. HDAC6 and microtubules are required for autophagic degradation of aggregated huntingtin. *J Biol Chem* 280, 40282-40292. (2005b)
Jalanko, A.; Braulke, T. Neuronal ceroid lipofuscinoses. *Biochim Biophys Acta* 1793, 697-709. (2009)
Jane, D.T.; Morvay, L.; Dasilva, L.; Cavallo-Medved, D.; Sloane, B.F.; Dufresne, M.J. Cathepsin B localizes to plasma membrane caveolae of differentiating myoblasts and is secreted in an active form at physiological pH. *Biol Chem* 387, 223-234. (2006)
Jansen, G.; Maattanen, P.; Denisov, A.Y.; Scarffe, L.; Schade, B.; Balghi, H.; Dejgaard,

K.; Chen, L.Y.; Muller, W.J.; Gehring, K., *et al.* An interaction map of endoplasmic reticulum chaperones and foldases. *Mol Cell Proteomics* 11, 710-723. (2012)

Jedeszko, C.; Sloane, B.F. Cysteine cathepsins in human cancer. *Biol Chem* 385, 1017-1027. (2004)

Jeric, B.; Dolenc, I.; Mihelic, M.; Klaric, M.; Zavasnik-Bergant, T.; Guncar, G.; Turk, B.; Turk, V.; Stoka, V. N-terminally truncated forms of human cathepsin F accumulate in aggresome-like inclusions. *Biochim Biophys Acta* 1833, 2254-2266. (2013)

Jimenez, J.L.; Nettleton, E.J.; Bouchard, M.; Robinson, C.V.; Dobson, C.M.; Saibil, H.R. The protofilament structure of insulin amyloid fibrils. *Proc Natl Acad Sci U S A* 99, 9196-9201. (2002)

Johansen, T.; Lamark, T. Selective autophagy mediated by autophagic adapter proteins. *Autophagy* 7, 279-296. (2011)

Johnston, J.A.; Dalton, M.J.; Gurney, M.E.; Kopito, R.R. Formation of high molecular weight complexes of mutant Cu, Zn-superoxide dismutase in a mouse model for familial amyotrophic lateral sclerosis. *Proc Natl Acad Sci U S A* 97, 12571-12576. (2000)

Johnston, J.A.; Ward, C.L.; Kopito, R.R. Aggresomes: a cellular response to misfolded proteins. *J Cell Biol* 143, 1883-1898. (1998)

Josephson, S.A.; Schmidt, R.E.; Millsap, P.; McManus, D.Q.; Morris, J.C. Autosomal dominant Kufs' disease: a cause of early onset dementia. *J Neurol Sci* 188, 51-60. (2001)

Julius, D.; Schekman, R.; Thorner, J. Glycosylation and processing of prepro-alpha-factor through the yeast secretory pathway. *Cell* 36, 309-318. (1984)

Jung, T.; Bader, N.; Grune, T. Lipofuscin: formation, distribution, and metabolic consequences. *Annals of the New York Academy of Sciences* 1119, 97-111. (2007)

Kaakinen, R.; Lindstedt, K.A.; Sneck, M.; Kovanen, P.T.; Oorni, K. Angiotensin II increases expression and secretion of cathepsin F in cultured human monocyte-derived macrophages: an angiotensin II type 2 receptor-mediated effect. *Atherosclerosis* 192, 323-327. (2007)

Kaganovich, D.; Kopito, R.; Frydman, J. Misfolded proteins partition between two distinct quality control compartments. *Nature* 454, 1088-1095. (2008)

Kakoi, S.; Yorimitsu, T.; Sato, K. COPII machinery cooperates with ER-localized Hsp40 to sequester misfolded membrane proteins into ER-associated compartments. *Mol Biol Cell* 24, 633-642. (2013)

Kamhi-Nesher, S.; Shenkman, M.; Tolchinsky, S.; Fromm, S.V.; Ehrlich, R.; Lederkremer, G.Z. A novel quality control compartment derived from the endoplasmic reticulum. *Mol Biol Cell* 12, 1711-1723. (2001)

Karrer, K.M.; Peiffer, S.L.; DiTomas, M.E. Two distinct gene subfamilies within the family of cysteine protease genes. *Proc Natl Acad Sci U S A* 90, 3063-3067. (1993)

Katz, M.L.; Robison, W.G., Jr. What is lipofuscin? Defining characteristics and differentiation from other autofluorescent lysosomal storage bodies. *Archives of gerontology and geriatrics* 34, 169-184. (2002)

Kawaguchi, Y.; Kovacs, J.J.; McLaurin, A.; Vance, J.M.; Ito, A.; Yao, T.P. The deacetylase HDAC6 regulates aggresome formation and cell viability in response to misfolded protein stress. *Cell* 115, 727-738. (2003)

Kim, H.; Tu, H.C.; Ren, D.; Takeuchi, O.; Jeffers, J.R.; Zambetti, G.P.; Hsieh, J.J.; Cheng, E.H. Stepwise activation of BAX and BAK by tBID, BIM, and PUMA initiates mitochondrial apoptosis. *Mol Cell* 36, 487-499. (2009)

Kim, S.J.; Zhang, Z.; Lee, Y.C.; Mukherjee, A.B. Palmitoyl-protein thioesterase-1 deficiency leads to the activation of caspase-9 and contributes to rapid neurodegeneration in INCL. *Hum Mol Genet* 15, 1580-1586. (2006)

Kim, T.W.; Pettingell, W.H.; Hallmark, O.G.; Moir, R.D.; Wasco, W.; Tanzi, R.E. Endoproteolytic cleavage and proteasomal degradation of presenilin 2 in transfected cells. *J Biol Chem* 272, 11006-11010. (1997)

Kirkin, V.; Lamark, T.; Sou, Y.S.; Bjorkoy, G.; Nunn, J.L.; Bruun, J.A.; Shvets, E.; McEwan, D.G.; Clausen, T.H.; Wild, P., *et al.* A role for NBR1 in autophagosomal degradation of ubiquitinated substrates. *Mol Cell* 33, 505-516. (2009)

Kollmann, K.; Uusi-Rauva, K.; Scifo, E.; Tyynela, J.; Jalanko, A.; Braulke, T. Cell biology and function of neuronal ceroid lipofuscinosis-related proteins. *Biochim Biophys Acta* 1832, 1866-1881. (2013)

Kopito, R.R. Aggresomes, inclusion bodies and protein aggregation. *Trends in cell biology* 10, 524-530. (2000)

Kraft, C.; Peter, M.; Hofmann, K. Selective autophagy: ubiquitin-mediated recognition and beyond. *Nat Cell Biol* 12, 836-841. (2010)

Kristiansen, M.; Messenger, M.J.; Klohn, P.C.; Brandner, S.; Wadsworth, J.D.; Collinge, J.; Tabrizi, S.J. Disease-related prion protein forms aggresomes in neuronal cells leading to caspase activation and apoptosis. *J Biol Chem* 280, 38851-38861. (2005)

Kroemer, G.; Galluzzi, L.; Vandenabeele, P.; Abrams, J.; Alnemri, E.S.; Baehrecke, E.H.; Blagosklonny, M.V.; El-Deiry, W.S.; Golstein, P.; Green, D.R., *et al.* Classification of cell death: recommendations of the Nomenclature Committee on Cell Death 2009. *Cell Death Differ* 16, 3-11. (2009)

Kyttala, A.; Lahtinen, U.; Braulke, T.; Hofmann, S.L. Functional biology of the neuronal ceroid lipofuscinoses (NCL) proteins. *Biochim Biophys Acta* 1762, 920-933. (2006)

Lamark, T.; Johansen, T. Aggrephagy: selective disposal of protein aggregates by macroautophagy. *Int J Cell Biol* 2012, 736905. (2012)

Lavrik, I.; Golks, A.; Krammer, P.H. Death receptor signaling. *Journal of cell science* 118, 265-267. (2005)

Lavrik, I.N.; Krammer, P.H. Regulation of CD95/Fas signaling at the DISC. *Cell Death Differ* 19, 36-41. (2012)

Lee, D.H.; Goldberg, A.L. Proteasome inhibitors: valuable new tools for cell biologists. *Trends in cell biology* 8, 397-403. (1998)

Lelouard, H.; Ferrand, V.; Marguet, D.; Bania, J.; Camosseto, V.; David, A.; Gatti, E.; Pierre, P. Dendritic cell aggresome-like induced structures are dedicated areas for ubiquitination and storage of newly synthesized defective proteins. *J Cell Biol* 164, 667-675. (2004)

Lelouard, H.; Gatti, E.; Cappello, F.; Gresser, O.; Camosseto, V.; Pierre, P. Transient aggregation of ubiquitinated proteins during dendritic cell maturation. *Nature* 417, 177-182. (2002)

Lewandowska, E.; Lipczynska-Lojkowska, W.; Modzelewska, J.; Wierzba-Bobrowicz, T.; Mierzewska, H.; Szpak, G.M.; Passenik, E.; Jachinska, K. Kufs' disease: diagnostic difficulties in the examination of extracerebral biopsies. *Folia Neuropathol* 47, 259-267. (2009)

Lilienbaum, A. Relationship between the proteasomal system and autophagy. *Int J Biochem Mol Biol* 4, 1-26. (2013)

Lindholm, D.; Wootz, H.; Korhonen, L. ER stress and neurodegenerative diseases. *Cell Death Differ* 13, 385-392. (2006)

Lindstedt, L.; Lee, M.; Oorni, K.; Bromme, D.; Kovanen, P.T. Cathepsins F and S block HDL3-induced cholesterol efflux from macrophage foam cells. *Biochem Biophys Res Commun* 312, 1019-1024. (2003)

Liu, X.D.; Ko, S.; Xu, Y.; Fattah, E.A.; Xiang, Q.; Jagannath, C.; Ishii, T.; Komatsu, M.; Eissa, N.T. Transient aggregation of ubiquitinated proteins is a cytosolic unfolded protein response to inflammation and endoplasmic reticulum stress. *J Biol Chem* 287, 19687-19698. (2012)

Luiro, K.; Kopra, O.; Blom, T.; Gentile, M.; Mitchison, H.M.; Hovatta, I.; Tornquist, K.; Jalanko, A. Batten disease (JNCL) is linked to disturbances in mitochondrial, cytoskeletal, and synaptic compartments. *Journal of neuroscience research* 84, 1124-1138. (2006)

Macedo-Souza, L.I.; Kok, F.; Santos, S.; Amorim, S.C.; Starling, A.; Nishimura, A.; Lezirovitz, K.; Lino, A.M.; Zatz, M. Spastic paraplegia, optic atrophy, and neuropathy is linked to chromosome 11q13. *Annals of neurology* 57, 730-737. (2005)

Maher, K.; Jeric Kokelj, B.; Butinar, M.; Mikhaylov, G.; Mancek-Keber, M.; Stoka, V.; Vasiljeva, O.; Turk, B.; Grigoryev, S.A.; Kopitar-Jerala, N. A role for stefin B (cystatin B) in inflammation and endotoxemia. *J Biol Chem* 289, 31736-31750. (2014)

Maubach, G.; Lim, M.C.; Zhuo, L. Nuclear cathepsin F regulates activation markers in rat hepatic stellate cells. *Mol Biol Cell* 19, 4238-4248. (2008)

Mehtani, S.; Gong, Q.; Panella, J.; Subbiah, S.; Peffley, D.M.; Frankfater, A. In vivo expression of an alternatively spliced human tumor message that encodes a truncated form of cathepsin B. Subcellular distribution of the truncated enzyme in COS cells. *J Biol Chem* 273, 13236-13244. (1998)

Merulla, J.; Fasana, E.; Solda, T.; Molinari, M. Specificity and regulation of the endoplasmic reticulum-associated degradation machinery. *Traffic* 14, 767-777. (2013)

Mitchison, H.M.; Lim, M.J.; Cooper, J.D. Selectivity and types of cell death in the neuronal ceroid lipofuscinoses. *Brain pathology* 14, 86-96. (2004)

Mohamed, M.M.; Sloane, B.F. Cysteine cathepsins: multifunctional enzymes in cancer. *Nat Rev Cancer* 6, 764-775. (2006)

Mole, S.E.; Williams, R.E. (2013). Neuronal Ceroid-Lipofuscinoses. In GeneReviews® [Internet], R.A. Pagon, Adam, M.P., Ardinger, H.H., Bird, T.D., Dolan, C.R., Fong C.T., Smith, R.J.H, Stephens, K., ed. (Seattle, University of Washington),

Mole, S.E.; Williams, R.E.; Goebel, H.H. Correlations between genotype, ultrastructural morphology and clinical phenotype in the neuronal ceroid lipofuscinoses. *Neurogenetics* 6, 107-126. (2005)

Muntener, K.; Willimann, A.; Zwicky, R.; Svoboda, B.; Mach, L.; Baici, A. Folding competence of N-terminally truncated forms of human procathepsin B. *J Biol Chem* 280, 11973-11980. (2005)

Muntener, K.; Zwicky, R.; Csucs, G.; Baici, A. The alternative use of exons 2 and 3 in cathepsin B mRNA controls enzyme trafficking and triggers nuclear fragmentation in human cells. *Histochem Cell Biol* 119, 93-101. (2003)

Muntener, K.; Zwicky, R.; Csucs, G.; Rohrer, J.; Baici, A. Exon skipping of cathepsin B: mitochondrial targeting of a lysosomal peptidase provokes cell death. *J Biol Chem* 279, 41012-41017. (2004)

Murata, S.; Minami, Y.; Minami, M.; Chiba, T.; Tanaka, K. CHIP is a chaperone-dependent E3 ligase that ubiquitylates unfolded protein. *EMBO Rep* 2, 1133-1138. (2001)

Nagler, D.K.; Sulea, T.; Menard, R. Full-length cDNA of human cathepsin F predicts the

presence of a cystatin domain at the N-terminus of the cysteine protease zymogen. *Biochem Biophys Res Commun* 257, 313-318. (1999)

Nakagawa, T.; Roth, W.; Wong, P.; Nelson, A.; Farr, A.; Deussing, J.; Villadangos, J.A.; Ploegh, H.; Peters, C.; Rudensky, A.Y. Cathepsin L: critical role in Ii degradation and CD4 T cell selection in the thymus. *Science* 280, 450-453. (1998)

Navon, A.; Ciechanover, A. The 26 S proteasome: from basic mechanisms to drug targeting. *J Biol Chem* 284, 33713-33718. (2009)

Nishida, Y.; Arakawa, S.; Fujitani, K.; Yamaguchi, H.; Mizuta, T.; Kanaseki, T.; Komatsu, M.; Otsu, K.; Tsujimoto, Y.; Shimizu, S. Discovery of Atg5/Atg7-independent alternative macroautophagy. *Nature* 461, 654-658. (2009)

Noack, J.; Brambilla Pisoni, G.; Molinari, M. Proteostasis: bad news and good news from the endoplasmic reticulum. *Swiss Med Wkly* 144, w14001. (2014)

Novoa, I.; Zeng, H.; Harding, H.P.; Ron, D. Feedback inhibition of the unfolded protein response by GADD34-mediated dephosphorylation of eIF2alpha. *J Cell Biol* 153, 1011-1022. (2001)

Olzmann, J.A.; Kopito, R.R.; Christianson, J.C. The mammalian endoplasmic reticulum-associated degradation system. *Cold Spring Harb Perspect Biol* 5. (2013)

Oorni, K.; Sneck, M.; Bromme, D.; Pentikainen, M.O.; Lindstedt, K.A.; Mayranpaa, M.; Aitio, H.; Kovanen, P.T. Cysteine protease cathepsin F is expressed in human atherosclerotic lesions, is secreted by cultured macrophages, and modifies low density lipoprotein particles in vitro. *J Biol Chem* 279, 34776-34784. (2004)

Outeiro, T.F.; Lindquist, S. Yeast cells provide insight into alpha-synuclein biology and pathobiology. *Science* 302, 1772-1775. (2003)

Ow, Y.P.; Green, D.R.; Hao, Z.; Mak, T.W. Cytochrome c: functions beyond respiration. *Nat Rev Mol Cell Biol* 9, 532-542. (2008)

Pahl, H.L. Signal transduction from the endoplasmic reticulum to the cell nucleus. *Physiol Rev* 79, 683-701. (1999)

Palmer, D.N.; Barry, L.A.; Tyynela, J.; Cooper, J.D. NCL disease mechanisms. *Biochim Biophys Acta* 1832, 1882-1893. (2013)

Palmer, D.N.; Martinus, R.D.; Barns, G.; Reeves, R.D.; Jolly, R.D. Ovine ceroid-lipofuscinosis. I: Lipopigment composition is indicative of a lysosomal proteinosis. *Am J Med Genet Suppl* 5, 141-158. (1988)

Palmer, D.N.; Oswald, M.J.; Westlake, V.J.; Kay, G.W. The origin of fluorescence in the neuronal ceroid lipofuscinoses (Batten disease) and neuron cultures from affected sheep for studies of neurodegeneration. *Archives of gerontology and geriatrics* 34, 343-357. (2002)

Parkinson-Lawrence, E.J.; Shandala, T.; Prodoehl, M.; Plew, R.; Borlace, G.N.; Brooks, D.A. Lysosomal storage disease: revealing lysosomal function and physiology. *Physiology* 25, 102-115. (2010)

Pastor, M.T.; Esteras-Chopo, A.; Serrano, L. Hacking the code of amyloid formation: the amyloid stretch hypothesis. *Prion* 1, 9-14. (2007)

Pereira, C.M.F. Crosstalk between Endoplasmic Reticulum Stress and Protein Misfolding in Neurodegenerative Diseases. *ISRN Cell Biology* 2013, 22 pages. (2013)

Pfaffl, M.W.; Horgan, G.W.; Dempfle, L. Relative expression software tool (REST) for group-wise comparison and statistical analysis of relative expression results in real-time PCR. *Nucleic Acids Res* 30, e36. (2002)

Pislar, A.; Kos, J. Cysteine cathepsins in neurological disorders. *Mol Neurobiol* 49, 1017-1030. (2014)

Platt, F.M.; Boland, B.; van der Spoel, A.C. The cell biology of disease: lysosomal storage disorders: the cellular impact of lysosomal dysfunction. *J Cell Biol* 199, 723-734. (2012)

Price, B.D.; Mannheim-Rodman, L.A.; Calderwood, S.K. Brefeldin A, thapsigargin, and AIF4- stimulate the accumulation of GRP78 mRNA in a cycloheximide dependent manner, whilst induction by hypoxia is independent of protein synthesis. *Journal of cellular physiology* 152, 545-552. (1992)

Raben, N.; Shea, L.; Hill, V.; Plotz, P. Monitoring autophagy in lysosomal storage disorders. *Methods in enzymology* 453, 417-449. (2009)

Rawlings, N.D., Salvesen G., ed. (2013). Handbook of Proteolytic Enzymes, 3rd edn (Amsterdam, Boston, Heidelberg, London, New York, Oxford, Paris, San Diego, San Francisco, Singapore, Sydney, Tokyo, Academic Press).

Rawlings, N.D.; Waller, M.; Barrett, A.J.; Bateman, A. MEROPS: the database of proteolytic enzymes, their substrates and inhibitors. *Nucleic Acids Res* 42, D503-509. (2014)

Reis, F.C.; Costa, T.F.; Sulea, T.; Mezzetti, A.; Scharfstein, J.; Bromme, D.; Menard, R.; Lima, A.P. The propeptide of cruzipain--a potent selective inhibitor of the trypanosomal enzymes cruzipain and brucipain, and of the human enzyme cathepsin F. *The FEBS journal* 274, 1224-1234. (2007)

Reiser, J.; Adair, B.; Reinheckel, T. Specialized roles for cysteine cathepsins in health and disease. *J Clin Invest* 120, 3421-3431. (2010)

Repnik, U.; Turk, B. Lysosomal-mitochondrial cross-talk during cell death. *Mitochondrion* 10, 662-669. (2010)

Riedl, S.J.; Salvesen, G.S. The apoptosome: signalling platform of cell death. *Nat Rev Mol Cell Biol* 8, 405-413. (2007)

Ron, D.; Walter, P. Signal integration in the endoplasmic reticulum unfolded protein response. *Nat Rev Mol Cell Biol* 8, 519-529. (2007)

Roshy, S.; Sloane, B.F.; Moin, K. Pericellular cathepsin B and malignant progression. *Cancer Metastasis Rev* 22, 271-286. (2003)

Ross, R.A.; Spengler, B.A.; Biedler, J.L. Coordinate morphological and biochemical interconversion of human neuroblastoma cells. *J Natl Cancer Inst* 71, 741-747. (1983)

Rossi, A.; Deveraux, Q.; Turk, B.; Sali, A. Comprehensive search for cysteine cathepsins in the human genome. *Biol Chem* 385, 363-372. (2004)

Roussel, B.D.; Kruppa, A.J.; Miranda, E.; Crowther, D.C.; Lomas, D.A.; Marciniak, S.J. Endoplasmic reticulum dysfunction in neurological disease. *Lancet Neurol* 12, 105-118. (2013)

Rutishauser, J.; Spiess, M. Endoplasmic reticulum storage diseases. *Swiss Med Wkly* 132, 211-222. (2002)

Sadzot, B.; Reznik, M.; Arrese-Estrada, J.E.; Franck, G. Familial Kufs' disease presenting as a progressive myoclonic epilepsy. *J Neurol* 247, 447-454. (2000)

Saftig, P.; Hunziker, E.; Wehmeyer, O.; Jones, S.; Boyde, A.; Rommerskirch, W.; Moritz, J.D.; Schu, P.; von Figura, K. Impaired osteoclastic bone resorption leads to osteopetrosis in cathepsin-K-deficient mice. *Proc Natl Acad Sci U S A* 95, 13453-13458. (1998)

Salvador, N.; Aguado, C.; Horst, M.; Knecht, E. Import of a cytosolic protein into lysosomes by chaperone-mediated autophagy depends on its folding state. *J Biol Chem* 275, 27447-27456. (2000)

Santamaria, I.; Velasco, G.; Pendas, A.M.; Paz, A.; Lopez-Otin, C. Molecular cloning and structural and functional characterization of human cathepsin F, a new cysteine proteinase of the papain family with a long propeptide domain. *J Biol Chem* 274, 13800-13809. (1999)

Scaffidi, C.; Fulda, S.; Srinivasan, A.; Friesen, C.; Li, F.; Tomaselli, K.J.; Debatin, K.M.; Krammer, P.H.; Peter, M.E. Two CD95 (APO-1/Fas) signaling pathways. *Embo J*

17, 1675-1687. (1998)
Schallus, T.; Jaeckh, C.; Feher, K.; Palma, A.S.; Liu, Y.; Simpson, J.C.; Mackeen, M.; Stier, G.; Gibson, T.J.; Feizi, T., *et al.* Malectin: a novel carbohydrate-binding protein of the endoplasmic reticulum and a candidate player in the early steps of protein N-glycosylation. *Mol Biol Cell* 19, 3404-3414. (2008)
Schroder, M. Endoplasmic reticulum stress responses. *Cell Mol Life Sci* 65, 862-894. (2008)
Schroder, M.; Kaufman, R.J. ER stress and the unfolded protein response. *Mutat Res* 569, 29-63. (2005)
Schulz, A.; Kohlschutter, A.; Mink, J.; Simonati, A.; Williams, R. NCL diseases - clinical perspectives. *Biochim Biophys Acta* 1832, 1801-1806. (2013)
Scott, F.L.; Stec, B.; Pop, C.; Dobaczewska, M.K.; Lee, J.J.; Monosov, E.; Robinson, H.; Salvesen, G.S.; Schwarzenbacher, R.; Riedl, S.J. The Fas-FADD death domain complex structure unravels signalling by receptor clustering. *Nature* 457, 1019-1022. (2009)
Scotter, E.L.; Vance, C.; Nishimura, A.L.; Lee, Y.B.; Chen, H.J.; Urwin, H.; Sardone, V.; Mitchell, J.C.; Rogelj, B.; Rubinsztein, D.C., *et al.* Differential roles of the ubiquitin proteasome system and autophagy in the clearance of soluble and aggregated TDP-43 species. *Journal of cell science* 127, 1263-1278. (2014)
Seehafer, S.S.; Pearce, D.A. You say lipofuscin, we say ceroid: defining autofluorescent storage material. *Neurobiol Aging* 27, 576-588. (2006)
Settembre, C.; Fraldi, A.; Jahreiss, L.; Spampanato, C.; Venturi, C.; Medina, D.; de Pablo, R.; Tacchetti, C.; Rubinsztein, D.C.; Ballabio, A. A block of autophagy in lysosomal storage disorders. *Hum Mol Genet* 17, 119-129. (2008)
Shang, F.; Taylor, A. Ubiquitin-proteasome pathway and cellular responses to oxidative stress. *Free Radic Biol Med* 51, 5-16. (2011)
Shen, D.; Coleman, J.; Chan, E.; Nicholson, T.P.; Dai, L.; Sheppard, P.W.; Patton, W.F. Novel cell- and tissue-based assays for detecting misfolded and aggregated protein accumulation within aggresomes and inclusion bodies. *Cell Biochem Biophys* 60, 173-185. (2011)
Shi, G.P.; Bryant, R.A.; Riese, R.; Verhelst, S.; Driessen, C.; Li, Z.; Bromme, D.; Ploegh, H.L.; Chapman, H.A. Role for cathepsin F in invariant chain processing and major histocompatibility complex class II peptide loading by macrophages. *The Journal of experimental medicine* 191, 1177-1186. (2000)
Shi, G.P.; Villadangos, J.A.; Dranoff, G.; Small, C.; Gu, L.; Haley, K.J.; Riese, R.; Ploegh, H.L.; Chapman, H.A. Cathepsin S required for normal MHC class II peptide loading and germinal center development. *Immunity* 10, 197-206. (1999)
Shorter, J. The mammalian disaggregase machinery: Hsp110 synergizes with Hsp70 and Hsp40 to catalyze protein disaggregation and reactivation in a cell-free system. *PLoS One* 6, e26319. (2011)
Shringarpure, R.; Grune, T.; Davies, K.J. Protein oxidation and 20S proteasome-dependent proteolysis in mammalian cells. *Cell Mol Life Sci* 58, 1442-1450. (2001)
Smith, K.R.; Dahl, H.H.; Canafoglia, L.; Andermann, E.; Damiano, J.; Morbin, M.; Bruni, A.C.; Giaccone, G.; Cossette, P.; Saftig, P., *et al.* Cathepsin F mutations cause Type B Kufs disease, an adult-onset neuronal ceroid lipofuscinosis. *Hum Mol Genet* 22, 1417-1423. (2013)
Somoza, J.R.; Palmer, J.T.; Ho, J.D. The crystal structure of human cathepsin F and its implications for the development of novel immunomodulators. *J Mol Biol* 322, 559-568. (2002)
Sousa, M.C.; Ferrero-Garcia, M.A.; Parodi, A.J. Recognition of the oligosaccharide and

protein moieties of glycoproteins by the UDP-Glc:glycoprotein glucosyltransferase. *Biochemistry* 31, 97-105. (1992)

Sousa, M.M.; Cardoso, I.; Fernandes, R.; Guimaraes, A.; Saraiva, M.J. Deposition of transthyretin in early stages of familial amyloidotic polyneuropathy: evidence for toxicity of nonfibrillar aggregates. *Am J Pathol* 159, 1993-2000. (2001)

Stefani, M.; Dobson, C.M. Protein aggregation and aggregate toxicity: new insights into protein folding, misfolding diseases and biological evolution. *J Mol Med (Berl)* 81, 678-699. (2003)

Stoka, V.; Turk, B.; Schendel, S.L.; Kim, T.H.; Cirman, T.; Snipas, S.J.; Ellerby, L.M.; Bredesen, D.; Freeze, H.; Abrahamson, M., *et al.* Lysosomal protease pathways to apoptosis. Cleavage of bid, not pro-caspases, is the most likely route. *J Biol Chem* 276, 3149-3157. (2001)

Stoka, V.; Turk, B.; Turk, V. Lysosomal cysteine proteases: structural features and their role in apoptosis. *IUBMB life* 57, 347-353. (2005)

Stroikin, Y.; Johansson, U.; Asplund, S.; Ollinger, K. Increased resistance of lipofuscin-loaded prematurely senescent fibroblasts to starvation-induced programmed cell death. *Biogerontology* 8, 43-53. (2007)

Su, V.; Lau, A.F. Ubiquitin-like and ubiquitin-associated domain proteins: significance in proteasomal degradation. *Cell Mol Life Sci* 66, 2819-2833. (2009)

Szeto, J.; Kaniuk, N.A.; Canadien, V.; Nisman, R.; Mizushima, N.; Yoshimori, T.; Bazett-Jones, D.P.; Brumell, J.H. ALIS are stress-induced protein storage compartments for substrates of the proteasome and autophagy. *Autophagy* 2, 189-199. (2006)

Takalo, M.; Salminen, A.; Soininen, H.; Hiltunen, M.; Haapasalo, A. Protein aggregation and degradation mechanisms in neurodegenerative diseases. *Am J Neurodegener Dis* 2, 1-14. (2013)

Tan, J.M.; Wong, E.S.; Kirkpatrick, D.S.; Pletnikova, O.; Ko, H.S.; Tay, S.P.; Ho, M.W.; Troncoso, J.; Gygi, S.P.; Lee, M.K., *et al.* Lysine 63-linked ubiquitination promotes the formation and autophagic clearance of protein inclusions associated with neurodegenerative diseases. *Hum Mol Genet* 17, 431-439. (2008)

Tang, C.H.; Lee, J.W.; Galvez, M.G.; Robillard, L.; Mole, S.E.; Chapman, H.A. Murine cathepsin F deficiency causes neuronal lipofuscinosis and late-onset neurological disease. *Mol Cell Biol* 26, 2309-2316. (2006)

Tao, K.; Stearns, N.A.; Dong, J.; Wu, Q.L.; Sahagian, G.G. The proregion of cathepsin L is required for proper folding, stability, and ER exit. *Arch Biochem Biophys* 311, 19-27. (1994)

Tarentino, A.L.; Gomez, C.M.; Plummer, T.H., Jr. Deglycosylation of asparagine-linked glycans by peptide:N-glycosidase F. *Biochemistry* 24, 4665-4671. (1985)

Taylor, J.P.; Tanaka, F.; Robitschek, J.; Sandoval, C.M.; Taye, A.; Markovic-Plese, S.; Fischbeck, K.H. Aggresomes protect cells by enhancing the degradation of toxic polyglutamine-containing protein. *Hum Mol Genet* 12, 749-757. (2003)

Terada, K.; Mori, M. Human DnaJ homologs dj2 and dj3, and bag-1 are positive cochaperones of hsc70. *J Biol Chem* 275, 24728-24734. (2000)

Terman, A.; Brunk, U.T. Lipofuscin. *Int J Biochem Cell Biol* 36, 1400-1404. (2004)

Tessitore, A.; del, P.M.M.; Sano, R.; Ma, Y.; Mann, L.; Ingrassia, A.; Laywell, E.D.; Steindler, D.A.; Hendershot, L.M.; d'Azzo, A. GM1-ganglioside-mediated activation of the unfolded protein response causes neuronal death in a neurodegenerative gangliosidosis. *Mol Cell* 15, 753-766. (2004)

Thompson, M.J.; Sievers, S.A.; Karanicolas, J.; Ivanova, M.I.; Baker, D.; Eisenberg, D. The 3D profile method for identifying fibril-forming segments of proteins. *Proc Natl Acad Sci U S A* 103, 4074-4078. (2006)

Tresse, E.; Salomons, F.A.; Vesa, J.; Bott, L.C.; Kimonis, V.; Yao, T.P.; Dantuma, N.P.; Taylor, J.P. VCP/p97 is essential for maturation of ubiquitin-containing autophagosomes and this function is impaired by mutations that cause IBMPFD. *Autophagy* 6, 217-227. (2010)

Trombetta, E.S.; Helenius, A. Conformational requirements for glycoprotein reglucosylation in the endoplasmic reticulum. *J Cell Biol* 148, 1123-1129. (2000)

Tsolis, A.C.; Papandreou, N.C.; Iconomidou, V.A.; Hamodrakas, S.J. A consensus method for the prediction of 'aggregation-prone' peptides in globular proteins. *PLoS One* 8, e54175. (2013)

Turk, B. Targeting proteases: successes, failures and future prospects. *Nat Rev Drug Discov* 5, 785-799. (2006)

Turk, B.; Bieth, J.G.; Bjork, I.; Dolenc, I.; Turk, D.; Cimerman, N.; Kos, J.; Colic, A.; Stoka, V.; Turk, V. Regulation of the activity of lysosomal cysteine proteinases by pH-induced inactivation and/or endogenous protein inhibitors, cystatins. *Biol Chem Hoppe Seyler* 376, 225-230. (1995)

Turk, B.; Dolenc, I.; Turk, V.; Bieth, J.G. Kinetics of the pH-induced inactivation of human cathepsin L. *Biochemistry* 32, 375-380. (1993)

Turk, B.; Stoka, V. Protease signalling in cell death: caspases versus cysteine cathepsins. *FEBS letters* 581, 2761-2767. (2007)

Turk, B.; Turk, D.; Turk, V. Lysosomal cysteine proteases: more than scavengers. *Biochim Biophys Acta* 1477, 98-111. (2000)

Turk, B.; Turk, V. Lysosomes as "suicide bags" in cell death: myth or reality? *J Biol Chem* 284, 21783-21787. (2009)

Turk, V.; Stoka, V.; Vasiljeva, O.; Renko, M.; Sun, T.; Turk, B.; Turk, D. Cysteine cathepsins: from structure, function and regulation to new frontiers. *Biochim Biophys Acta* 1824, 68-88. (2012)

Turk, V.; Turk, B.; Turk, D. Lysosomal cysteine proteases: facts and opportunities. *Embo J* 20, 4629-4633. (2001)

Tyedmers, J.; Mogk, A.; Bukau, B. Cellular strategies for controlling protein aggregation. *Nat Rev Mol Cell Biol* 11, 777-788. (2010)

Ulbricht, A.; Eppler, F.J.; Tapia, V.E.; van der Ven, P.F.; Hampe, N.; Hersch, N.; Vakeel, P.; Stadel, D.; Haas, A.; Saftig, P., *et al.* Cellular mechanotransduction relies on tension-induced and chaperone-assisted autophagy. *Current biology : CB* 23, 430-435. (2013)

Vande Walle, L.; Lamkanfi, M.; Vandenabeele, P. The mitochondrial serine protease HtrA2/Omi: an overview. *Cell Death Differ* 15, 453-460. (2008)

Vasiljeva, O.; Reinheckel, T.; Peters, C.; Turk, D.; Turk, V.; Turk, B. Emerging roles of cysteine cathepsins in disease and their potential as drug targets. *Curr Pharm Des* 13, 387-403. (2007)

Vasiljeva, O.; Turk, B. Dual contrasting roles of cysteine cathepsins in cancer progression: apoptosis versus tumour invasion. *Biochimie* 90, 380-386. (2008)

Vazquez-Ortiz, G.; Pina-Sanchez, P.; Vazquez, K.; Duenas, A.; Taja, L.; Mendoza, P.; Garcia, J.A.; Salcedo, M. Overexpression of cathepsin F, matrix metalloproteinases 11 and 12 in cervical cancer. *BMC cancer* 5, 68. (2005)

Vergarajauregui, S.; Connelly, P.S.; Daniels, M.P.; Puertollano, R. Autophagic dysfunction in mucolipidosis type IV patients. *Hum Mol Genet* 17, 2723-2737. (2008)

Verma, A.; Hirsch, D.J.; Hanley, M.R.; Thastrup, O.; Christensen, S.B.; Snyder, S.H. Inositol trisphosphate and thapsigargin discriminate endoplasmic reticulum stores of calcium in rat brain. *Biochem Biophys Res Commun* 172, 811-816. (1990)

Vermeulen, K.; Van Bockstaele, D.R.; Berneman, Z.N. Apoptosis: mechanisms and

relevance in cancer. *Ann Hematol* 84, 627-639. (2005)
Vidal-Donet, J.M.; Carcel-Trullols, J.; Casanova, B.; Aguado, C.; Knecht, E. Alterations in ROS activity and lysosomal pH account for distinct patterns of macroautophagy in LINCL and JNCL fibroblasts. *PLoS One* 8, e55526. (2013)
Vitner, E.B.; Platt, F.M.; Futerman, A.H. Common and uncommon pathogenic cascades in lysosomal storage diseases. *J Biol Chem* 285, 20423-20427. (2010)
Waghray, A.; Keppler, D.; Sloane, B.F.; Schuger, L.; Chen, Y.Q. Analysis of a truncated form of cathepsin H in human prostate tumor cells. *J Biol Chem* 277, 11533-11538. (2002)
Walkley, S.U.; Vanier, M.T. Secondary lipid accumulation in lysosomal disease. *Biochim Biophys Acta* 1793, 726-736. (2009)
Walter, P.; Johnson, A.E. Signal sequence recognition and protein targeting to the endoplasmic reticulum membrane. *Annu Rev Cell Biol* 10, 87-119. (1994)
Walter, P.; Lingappa, V.R. Mechanism of protein translocation across the endoplasmic reticulum membrane. *Annu Rev Cell Biol* 2, 499-516. (1986)
Walter, P.; Ron, D. The unfolded protein response: from stress pathway to homeostatic regulation. *Science* 334, 1081-1086. (2011)
Wang, B.; Shi, G.P.; Yao, P.M.; Li, Z.; Chapman, H.A.; Bromme, D. Human cathepsin F. Molecular cloning, functional expression, tissue localization, and enzymatic characterization. *J Biol Chem* 273, 32000-32008. (1998)
Wang, G.; Gao, Y.; Li, L.; Jin, G.; Cai, Z.; Chao, J.I.; Lin, H.K. K63-linked ubiquitination in kinase activation and cancer. *Frontiers in oncology* 2, 5. (2012)
Wang, S.; Kaufman, R.J. The impact of the unfolded protein response on human disease. *J Cell Biol* 197, 857-867. (2012)
Wang, W. Protein aggregation and its inhibition in biopharmaceutics. *Int J Pharm* 289, 1-30. (2005)
Wang, X.; Dong, C.F.; Shi, Q.; Shi, S.; Wang, G.R.; Lei, Y.J.; Xu, K.; An, R.; Chen, J.M.; Jiang, H.Y., *et al.* Cytosolic prion protein induces apoptosis in human neuronal cell SH-SY5Y via mitochondrial disruption pathway. *BMB Rep* 42, 444-449. (2009)
Westlake, V.J.; Jolly, R.D.; Bayliss, S.L.; Palmer, D.N. Immunocytochemical studies in the ceroid-lipofuscinoses (Batten disease) using antibodies to subunit c of mitochondrial ATP synthase. *Am J Med Genet* 57, 177-181. (1995)
Wex, T.; Levy, B.; Wex, H.; Bromme, D. Human cathepsins F and W: A new subgroup of cathepsins. *Biochem Biophys Res Commun* 259, 401-407. (1999)
Wiederanders, B. Structure-function relationships in class CA1 cysteine peptidase propeptides. *Acta Biochim Pol* 50, 691-713. (2003)
Wihlmark, U.; Wrigstad, A.; Roberg, K.; Nilsson, S.E.; Brunk, U.T. Lipofuscin accumulation in cultured retinal pigment epithelial cells causes enhanced sensitivity to blue light irradiation. *Free Radic Biol Med* 22, 1229-1234. (1997)
Willets, J.M.; Lambert, D.G.; Lunec, J.; Griffiths, H.R. Studies on the neurotoxicity of 6,7-dihydroxy-1-methyl-1,2,3,4-tetrahydroisoquinoline (salsolinol) in SH-SY5Y cells. *Eur J Pharmacol* 293, 319-326. (1995)
Windpassinger, C.; Wagner, K.; Petek, E.; Fischer, R.; Auer-Grumbach, M. Refinement of the Silver syndrome locus on chromosome 11q12-q14 in four families and exclusion of eight candidate genes. *Human genetics* 114, 99-109. (2003)
Wolfe, L.S.; Ng Ying Kin, N.M.; Palo, J.; Haltia, M. Dolichols in brain and urinary sediment in neuronal ceroid lipofuscinosis. *Neurology* 33, 103-106. (1983)
Wormald, M.R.; Dwek, R.A. Glycoproteins: glycan presentation and protein-fold stability. *Structure* 7, R155-160. (1999)
Wu, G.; Chai, J.; Suber, T.L.; Wu, J.W.; Du, C.; Wang, X.; Shi, Y. Structural basis of IAP

recognition by Smac/DIABLO. *Nature* 408, 1008-1012. (2000)

Yamamoto, A.; Tagawa, Y.; Yoshimori, T.; Moriyama, Y.; Masaki, R.; Tashiro, Y. Bafilomycin A1 prevents maturation of autophagic vacuoles by inhibiting fusion between autophagosomes and lysosomes in rat hepatoma cell line, H-4-II-E cells. *Cell structure and function* 23, 33-42. (1998)

Yang, Z.; Klionsky, D.J. An overview of the molecular mechanism of autophagy. *Curr Top Microbiol Immunol* 335, 1-32. (2009)

Yue, Z.; Friedman, L.; Komatsu, M.; Tanaka, K. The cellular pathways of neuronal autophagy and their implication in neurodegenerative diseases. *Biochim Biophys Acta* 1793, 1496-1507. (2009)

Zhang, X.; Qian, S.B. Chaperone-mediated hierarchical control in targeting misfolded proteins to aggresomes. *Mol Biol Cell* 22, 3277-3288. (2011)

Zhang, Z.; Lee, Y.C.; Kim, S.J.; Choi, M.S.; Tsai, P.C.; Xu, Y.; Xiao, Y.J.; Zhang, P.; Heffer, A.; Mukherjee, A.B. Palmitoyl-protein thioesterase-1 deficiency mediates the activation of the unfolded protein response and neuronal apoptosis in INCL. *Hum Mol Genet* 15, 337-346. (2006)

Index of Figures

Figure 1: *Overview of the possible fates of a newly synthesized polypeptide chains.* See text for more details (Dobson, 2003)..... 6

Figure 2: *Different compartments of misfolded or aggregated proteins*. Misfolded proteins may form aggregates which may be sequestered into different quality control compartments, such as JUNQ, IPOD, aggresomes or ALIS, respectively. Sequestration strategy is presumably based on their ubiquitination status, aggregation state and solubility (Takalo et al., 2013)..... 9

Figure 3: *Crosstalk between different degradation systems* (indicated by dashed arrows). Misfolded and aggregated proteins can be degraded by proteasome. If not, they may aggregate and form different deposits, which could be subjected to selective or non-selective macroautophagy, chaperone-mediated autophagy (CMA) or chaperone-assisted selective autophagy (CASA). Except for the case of CMA, substrates for degradation are often polyubiquitinated (Ub), which can serve as a recognition signal for both degradation systems, depending on the type of polyubiquitination (Kraft et al., 2010). Components coordinating different steps of the degradation routes are marked in red described in the text..... 14

Figure 4: *Examples of storage material profiles, as seen under electron microscope*. (a) Typical lipofuscin deposit and granular osmophilic deposits; GROD. (b) Fingerprint (FP) and curvilinear (CP) profiles (Lewandowska et al., 2009). (c) Rectilinear profile (RP). (d) Fingerprint profile (FP) (Smith et al., 2013)..... 19

Figure 5: *Hypothetical cascade of events in LSD pathology.* Scheme presents the downstream effects of gene mutations observed in numerous (but not necessarily all) LSDs. Endo/autolysosomal events are confined within green background, whereas processes taking place in cytoplasm that affect other organelles are presented on light background (Platt et al., 2012). 20

Figure 6: *Typical fold of the mature form of cysteine cathepsin – endopeptidase (example of cathepsin L).* Green ribbon representation is used to show fold of two-chain form cathepsin L. Elements of secondary structures are presented in blue (α-helices) and red (β-sheets) color. The side chain of catalytic residues Cys25 and His163 are shown in ball-and-stick representation (yellow) (Turk et al., 2012)..... 25

Figure 7: *Schematic representation of human cathepsin F and its N-terminally truncated forms.* Top panel represents the domain composition of the wild type human cathepsin F. Below is a scaled representation of Δ^{19}CatF, Δ^{125}CatF and Δ^{146}CatF boundaries..... 43

Figure 8: *Subcellular localization of human cathepsin F (wtCatF) and its N-terminally truncated forms (Δ^{19}CatF, Δ^{125}CatF and Δ^{146}CatF).* Subcellular localization was assessed using confocal microscopy 48 h after transfection in HEK 293T cells. Immunolabeling was done using rabbit polyclonal anti cathepsin F and mouse monoclonal anti LAMP2 primary antibodies, followed by Alexa Fluor-labeled secondary antibodies as described in Section 3.2.10. Confocal images showed expression pattern of cathepsin F (CTSF) labeled with green fluorescence (A, E, I, M, Q) and the lysosomal marker LAMP2 labeled with red fluorescence (C, G, K, O, S). Merged images represent overlapping immunoreactivity in yellow (D, H, L, P, T). The nucleus was counterstained for DNA using DAPI (blue fluorescence: B, F, J, N, R). Negative controls included the non-transfected, mock-transfected and pcDNA3 empty vector-transfected cells. Since very similar pattern was obtained under all of these three conditions, a representative example, the pcDNA3 (A –D) is shown only. Scale bar = 10 μm. 44

Figure 9: *Expression of human cathepsin F and its N-terminally truncated forms in HEK293T cells.* HEK293T cells were transfected with pcDNA3 plasmids containing wtCatF, Δ^{19}CatF, Δ^{125}CatF and Δ^{146}CatF and lysed 48 hours later to obtain soluble (A) and insoluble (B) fractions of whole cell protein extracts, as described in section 3.2.3. Expression of cathepsin F was evaluated by Western blotting using an anti-human cathepsin F antibody (described in section 3.2.5). Negative controls included the non-transfected, mock-transfected and pcDNA3 empty vector-transfected cells. Loading of equivalent amounts of protein was assessed with β-actin (lower blot).....45

Figure 10: *Deglycosylation of human cathepsin F and its N-terminally truncated forms.* Whole cell protein extracts of wtCatF, Δ^{19}CatF, Δ^{125}CatF and Δ^{146}CatF-expressing HEK293T cells was subjected to the PNGase F treatment as described in section 3.2.4. Eventual decrease in Mw of the treated proteins after deglycosylation was assessed by Western blotting. 46

Figure 11: *Accumulation of aggregated N-terminally truncated forms of Δ^{19}CatF, Δ^{125}CatF and Δ^{146}CatF in aggresomes.* HEK293T cells were stained with Proteostat® 48 hours after transfection with pcDNA3 plasmids containing wtCatF (G – I), Δ^{19}CatF (J – L), Δ^{125}CatF (M – O) and Δ^{146}CatF (P – R). Nuclei were counterstained with DNA-staining Hoechst 33342 (blue fluorescence). Negative controls included non-transfected, mock-transfected and empty vector-transfected cells. Due to the similar pattern, only the representative image of pcDNA3 (A – C) is included. For positive control, cells were treated with 5 μM proteasomal inhibitor MG-132 (D – F), 12 hours before staining. Scale bar = 10 μm. 47

Figure 12: N-terminally truncated Δ^{19}CatF (I – L), Δ^{125}CatF (M – P) and Δ^{146}CatF (Q – T), but not also the wtCatF (E – H) are p62 positive inclusions. HEK293T cells were transfected with the wild type and N-terminally truncated constructs and 48 later immunolabeled with rabbit polyclonal anti human cathepsin F (CTSF; green fluorescence) and mouse monoclonal anti human p62 (p62/SQSTM1; red fluorescence) antibodies. Merged images (in yellow) represent the combined fluorescence. Nuclei were counterstained with DNA-staining DAPI (blue fluorescence). Negative controls included non-transfected, mock-transfected and empty vector-transfected cells. Due to the similar pattern under all three conditions, only, the representative image of pcDNA3 (A – D) is included. Scale bar = 10 μm. 48

Figure 13: Colocalization of LC3B with overexpressed cathepsin F variants in HEK293T cells. Cells were immunolabeled with goat polyclonal anti cathepsin F (CTSF; green fluorescence) and rabbit polyclonal anti LC3B (LC3B; red fluorescence) primary antibodies. Confocal images showed colocalization of cathepsin F and autophagosomal marker LC3B (yellow) in cells transfected with pcDNA3 plasmids containing wtCatF (E – H), Δ^{19}CatF (I – L), Δ^{125}CatF (M – P) and Δ^{146}CatF (Q – T). Nuclei were counterstained with DAPI (blue fluorescence). Representative negative control is pcDNA3 (A – D). Scale bar = 10 μm. 49

Figure 14: Overexpression of the N-terminally truncated forms of human cathepsin F, but not the wild-type protein, induces caspase activation. DEVDase activity was monitored by kinetics 48 h post-transfection with human cathepsin F and its N-terminally truncated forms Δ^{19}CatF, Δ^{125}CatF and Δ^{146}CatF. For this purpose, HEK293T cells were grown in full medium, supplemented with 15 μM Z-VAD(OMe)-FMK after transfection. Caspase (DEVDase) activities were assessed from 50 μg of total protein as described in section 3.2.6. Negative control experiments included non-transfected, mock-transfected and pcDNA3 empty vector-transfected cells. The results are given as the means ± SD of three independent experiments. ***, $p<0.001$ compared to pcDNA3. 50

Figure 15: *Schematic representation of human cathepsin F (CLN13) and its type B Kufs mutants.* Top panel represents the domain composition of the wild type human cathepsin F. Positions of S319Lfs*27, Y231C, Q321R, G458A and S480L mutations are indicated in a scaled representation. Dashed line represents frameshift and the new amino acid sequence in the protein. 51

Figure 16: *Expression of human cathepsin F (CLN13) and its type B Kufs mutants in SY-SY5Y cells.* Cells were transfected with pcDNA4/myc-His-containing wtCatF, S319Lfs*27, S480L, G458A, Y231C and Q321R mutants and 24 hours later left untreated (A, D) or exposed to 30 nM bafilomycin (B, E) or 5 μM MG-132 (C, D) for further 24 hours. Soluble (A – C) and insoluble (D – E) fractions of whole protein extracts were evaluated by Western blotting using anti myc tag antibodies. Loading of equivalent amounts of protein was assessed against β-actin (lower blot). 52

Figure 17: *CLN13 mutation S319Lfs*27 induces its aggregation and non-lysosomal targeting.* SH-SY5Y cells were transfected with pEFGP-containing wtCatF (D – F), S319Lfs*27 (G – I), S480L (J – L), G458A (M – O), Y231C (P – R) and Q321R (S – U) mutants (CTSF-EGFP, green fluorescence) and 24 hours later either left untreated (left panel) or exposed to 5 μM wortmannin (right panel). Using Alexa Fluor 546 labeled mouse monoclonal anti LAMP2 antibodies (red fluorescence), cells were immunolabeled 48 hours after transfection and examined by confocal microscopy. Merged images represent overlapping fluorescence in yellow. Scale bar = 10 μm. 54

Figure 18: *S319Lfs*27 aggregates do not localize to the endoplasmic reticulum.* SH-SY5Y cells were transfected with the wild type and mutant CLN13 (CTSF-EGFP, green fluorescence). 48 hours after transfection endoplasmic reticulum was immunolabeled with mouse monoclonal anti PDI antibodies (red fluorescence) and examined by confocal microscopy. Merged images represent overlapping fluorescence in yellow. Scale bar = 10 μm. 55

Figure 19: *S319Lfs*27 aggregates accumulate in aggresomes-like inclusions.* SH-SY5Y cells were stained with Proteostat® 48 hours after transfection with pcDNA4/myc-His plasmids containing wtCatF, S319Lfs*27, S480L, G458A, Y231C and Q321R. Nuclei were counterstained with DNA-staining Hoechst 33342 (blue fluorescence). Negative controls included non-transfected, mock-transfected and empty vector-transfected cells. For positive control, cells were treated with 5 μM proteasomal inhibitor MG-132, 24 hours before staining. Scale bar = 10 μm. 56

Figure 20: *Expression of CLN13 mutants decrease pH of acidic organelles.* 48 hours after transfection SH-SY5Y cells were stained for 30 min with 40 nM LysoTracker® Green DND-26 probe, which accumulates in acidic organelles. 1hour bafilomycin A1 (baf, 30 nM) treatment was used as a positive control. Shift in fluorescence was measured by flow cytometry. Lower values denote higher pH of vesicles. Bars on the graph represent the geometrical means of fluorescence intensity ± SD of two independent experiments. *p<0,05; **p<0,01 compared to the pcDNA4. On the right side representative histograms are shown.....58

Figure 21: *CLN13 mutants decrease autophagic flux.* SH-SY5Y were immunolabeled 48 hours after transfection with mouse monoclonal anti LAMP2 (LAMP2; green fluorescence) and rabbit polyclonal anti LC3B (LC3B; red fluorescence) primary antibodies. Confocal images showed reduced colocalization of LAMP2 and autophagosomal marker LC3B (yellow) in cells transfected with S319Lfs*27 (J – L), S480L (M – O), G458A (P – R), Y231C (S – U) and Q321R (V – X). More overlapping signal of LAMP2 and LC3B was observed in pEGFP (A – C) and wtCatF (G – I) transfected cells. For positive control cells were treated with 30nM bafilomycin for 24 hours (D – E). Colocalization was assessed only in the transfected (EGFP positive) cells (indicated by arrowheads). Scale bar = 10 μm. 59

Figure 22: *Non aggregated CLN13 mutants are p62 positive.* SH-SY5Y cells were transfected for 48 hours with the EGFP-tagged wild type cathepsin F and CLN13 mutants S319Lfs*27, S480L, G458A, Y231C and Q321R (CTSF-EGFP, green fluorescence) and immunolabeled with mouse monoclonal anti human p62 (p62/SQSTM1; red fluorescence) antibodies. Images were obtained with confocal laser scanning microscope. Merged images (in yellow) represent combined fluorescence. Insertions represent selected enlarged area for better visualization. Scale bar = 10 μm. 60

Figure 23: *Accumulation of autofluorescent material.* SH-SY5Y cells were fixed and analysed without staining 48 hours after transfection with either wtCatF or CLN13 mutants. Images were obtained by confocal scanning microscope. White dots represent overlaid blue, red and green fluorescence emission. Scale bar = 10 μm. 61

Figure 24: *Transmission electron microscopy of non-transfecetd and wtCatF-transfected SH-SY5Y cells.* Non-transfected cells or cells transfected with the wtCatF or S319Lfs*27 mutant were fixed with 4 % paraformaldehyde, embedded in 10 % gelatin and cryoprotected in 2.6 M sucrose. Cryosected slices were contrasted with 0.4 % uranyl acetate and analysed by TEM. Uranyl contrasted the cell proteins but not the lipids so the membranes appear white. Inserts show details of the zoomed structures.....62

Figure 25: *Transmission electron microscopy of S319Lfs*27-transfected SH-SY5Y cells.* Non-transfected cells or cells transfected with the wtCatF or S319Lfs*27 mutant were fixed with 4 % paraformaldehyde, embedded in 10 % gelatin and cryoprotected in 2.6 M sucrose. Cryosected slices were contrasted with 0.4 % uranyl acetate and analysed by TEM. Uranyl contrasted the cell proteins but not the lipids so the membranes appear white. Inserts show details of the zoomed structures..... 63

Figure 26: *Evaluation of free intracellular Ca^{2+}*. Transfected SH-SY5Y cells were stained with Fluo-4 AM, as described in section 3.2.7. For negative control cells were treated with 100 nM EGTA, whereas for positive control 100 μM ionomycin was used. Fluorescence signal was measured continuously for at least 30 minutes using Tecan Infinite M1000 pro. One experiment on three biological replicates was done..... 64

Figure 27: *Evaluation of CLN13-induced ER stress by qPCR.* RNA was isolated from the SH-SY5Y cells transfected with the empty vector, wtCatF or S319Lfs*27 and reverse transcribed to the cDNA. cDNA was evaluated for the relative mRNA expression of the BiP, EDEM1, CALR and CHOP genes using SYBR Green qPCR chemistry. Expression of genes of interest was calculated using REST 2009 software and normalized to the expression of ENOX2 and VIPAR. Graph represents mean values of fold changes (relative to pcDANA4) and ±SD of three biological replicates. For positive control, cells were treated with 1.5 μM thapsigargin (24 hours)..... 65

Figure 28: *Detection of superoxide anion formation by MitoSOXTM Red.* Cells were transfected with wtCatF and CLN13 mutants and 48 hours later stained with MitoSOX™ Red (5 μM, 30 minutes). 100μM menadione (1hour) was used as a positive control. MitoSOX™ Red reagent is oxidized by superoxide but not other ROS and exhibits red fluorescence. Images of live cells were taken by confocal microscope. Arrowheads indicate signal in transfected (EGFP positive) cells only. Scale bar = 10μM..... 66

Figure 29: *CLN13 mutants induce lipid peroxidation.* Cells were transfected with wtCatF and CLN13 mutants and stained with BODIPY® 581/591 C_{11} (2 μM, 30 minutes), 48 hours after transfection. 1mM H_2O_2 (1 hour) was used as a positive control. Upon oxidation in live cells, fluorescence shift from red to green occurs, providing indication of lipid peroxidation. Images were obtained by confocal microscopy. Scale bar = 10μM..... 66

Index of Tables

Table 1: *Classification of* the *NCLs*. (Haltia and Goebel, 2013; Jalanko and Braulke, 2009; Kollmann et al., 2013; Palmer et al., 2013; Schulz et al., 2013)..... 16
Table 2: *Properties of human cysteine cathepsins.* (Fonovic and Turk, 2014; Pislar and Kos, 2014; Reiser et al., 2010; Turk et al., 2001)..... 27
Table 3: Primary and secondary antibodies used in immunocytochemistry. 38
Table 4: List of primers used in qPCR analysis 41

Appendix

List of publications:

Jeric, B.; Dolenc, I.; Mihelic, M.; Klaric, M.; Zavasnik-Bergant, T.; Guncar, G.; Turk, B.; Turk, V.; Stoka, V. N-terminally truncated forms of human cathepsin F accumulate in aggresome-like inclusions. *Biochim Biophys Acta* 1833, 2254-2266. (2013)

Butinar, M.; Prebanda, M.T.; Rajkovic, J.; Jeric, B.; Stoka, V.; Peters, C.; Reinheckel, T.; Kruger, A.; Turk, V.; Turk, B., *et al.* Stefin B deficiency reduces tumor growth via sensitization of tumor cells to oxidative stress in a breast cancer model. *Oncogene* 33, 3392-3400. (2014)

Maher, K.; Jeric Kokelj, B.; Butinar, M.; Mikhaylov, G.; Mancek-Keber, M.; Stoka, V.; Vasiljeva, O.; Turk, B.; Grigoryev, S.A.; Kopitar-Jerala, N. A role for stefin B (cystatin B) in inflammation and endotoxemia. *J Biol Chem* 289, 31736-31750. (2014)

Maher, K.; Zavrsnik, J.; Jeric-Kokelj, B.; Vasiljeva, O.; Turk, B.; Kopitar-Jerala, N. Decreased IL-10 expression in stefin B-deficient macrophages is regulated by the MAP kinase and STAT-3 signaling pathways. *FEBS letters* 588, 720-726. (2014)

Biochimica et Biophysica Acta 1833 (2013) 2254–2266

Contents lists available at SciVerse ScienceDirect

Biochimica et Biophysica Acta

journal homepage: www.elsevier.com/locate/bbamcr

N-terminally truncated forms of human cathepsin F accumulate in aggresome-like inclusions☆☆

Barbara Jerič [a,b], Iztok Dolenc [a], Marko Mihelič [a,c], Martina Klarić [a,b], Tina Zavašnik-Bergant [a], Gregor Gunčar [d], Boris Turk [a,b,c,d], Vito Turk [a,b,c,*], Veronika Stoka [a,b,**]

[a] Department of Biochemistry and Molecular and Structural Biology, J. Stefan Institute, Jamova 39, SI-1000 Ljubljana, Slovenia
[b] Jožef Stefan International Postgraduate School, Jamova 39, SI-1000 Ljubljana, Slovenia
[c] Centre of Excellence for Integrated Approaches in Chemistry and Biology of Proteins (CIPKeBiP), Jamova 39, SI-1000 Ljubljana, Slovenia
[d] Department of Chemistry and Biochemistry, Faculty of Chemistry and Chemical Technology, University of Ljubljana, Cesta v Mestni log 88A, SI-1000 Ljubljana, Slovenia

ARTICLE INFO

Article history:
Received 19 November 2012
Received in revised form 6 May 2013
Accepted 7 May 2013
Available online 14 May 2013

Keywords:
Aggregation-prone
Aggresome
Aggresome-like inclusion
Autophagy
Caspase activation
Cathepsin F

ABSTRACT

The contribution of individual cysteine cathepsins as positive mediators of programmed cell death is dependent on several factors, such as the type of stimuli, intensity and duration of the stimulus, and cell type involved. Of the eleven human cysteine cathepsins, cathepsin F is the only cathepsin that exhibits an extended N-terminal proregion, which contains a cystatin-like domain. We predicted that the wild-type human cathepsin F contains three natively disordered regions within the enzyme's propeptide and various amino acid stretches with high fibrillation propensity. Wild-type human cathepsin F and its N-terminally truncated forms, Ala^{20}–Asp^{484} (Δ^{19}CatF), Pro^{126}–Asp^{484} (Δ^{125}CatF), and Met^{147}–Asp^{484} (Δ^{146}CatF) were cloned into the pcDNA3 vector and overexpressed in HEK 293T cells. Wild-type human cathepsin F displayed a clear vesicular labeling and colocalized with the LAMP2 protein, a lysosomal marker. However, all three N-terminally truncated forms of human cathepsin F were recovered as insoluble proteins, suggesting that the deletion of at least the signal peptides (Δ^{19}CatF), results in protein aggregation. Noteworthy, they concentrated large perinuclear–juxtanuclear aggregates that accumulated within aggresome-like inclusions. These inclusions showed p62-positive immunoreactivity and were colocalized with the autophagy marker LC3B, but not with the LAMP2 protein. In addition, an approximately 2–3 fold increase in DEVDase activity was not sufficient to induce apoptotic cell death. These results suggested the clearance of the N-terminally truncated forms of human cathepsin F via the autophagy pathway, underlying its protective and prosurvival mechanisms.
© 2013 The Authors. Published by Elsevier B.V. Open access under CC BY-NC-ND license.

1. Introduction

During the past decade, there has been an expansion of studies highlighting the importance of cysteine cathepsins under various physiological and pathological conditions [1]. Novel functions have been uncovered, and their involvement in the activation of programmed cell death (apoptosis) has been confirmed [2–7]. The contribution of cysteine cathepsins to apoptosis varies considerably and is dependent on the initiation of stimuli targeting in the mitochondria (*intrinsic* pathway) or activation of death receptors (*extrinsic* pathway) [8–13]. Studies aimed at dissecting the contribution of individual enzymes as positive mediators of apoptosis have also provided conflicting results. The transient overexpression of aspartic cathepsin D demonstrated several features of apoptosis, as assessed by cell morphology, DNA fragmentation and/or caspase-3 enzymatic activity [14]. In contrast, the transient overexpression of cysteine cathepsin B or cathepsin L did not demonstrate any significant features of apoptosis in either HeLa or rat hepatoma McA RH 7777 cell lines [15]. A 20-fold overexpression of these cysteine cathepsins or lysosomal permeabilization with the lysosomotropic detergent, *N*-dodecyl-imidazole, was insufficient to sensitize these cells to TNF-induced cell death [15]. In contrast, cathepsin B alternatively spliced variants and artificially truncated forms were found in various cellular compartments and induced apoptotic cell death [16–18]. Moreover, cysteine cathepsins B, H and L and the aspartic cathepsin D were detected in tubulovesicular structures surrounding the chromatoid bodies, which

Abbreviations: Δ^{19}CatF, truncated form of human cathepsin F (Ala^{20}–Asp^{484}); Δ^{125}CatF, truncated form of human cathepsin F (Pro^{126}–Asp^{484}); Δ^{146}CatF, truncated form of human cathepsin F (Met^{147}–Asp^{484}); HRP, horseradish peroxidase; Mw, molecular weight; wtCatF, wild-type cathepsin F

☆☆ This paper is dedicated to Prof. John A. Rupley at the Department of Chemistry and Biochemistry, University of Arizona, Tucson on the occasion of his 80th birthday.

* Correspondence to: V. Turk, J. Stefan Institute, Department of Biochemistry and Molecular and Structural Biology, Jamova 39, SI-1000 Ljubljana, Slovenia. Tel.: +386 1 477 3365; fax: +386 1 477 3984.
** Correspondence to: V. Stoka, J. Stefan Institute, Department of Biochemistry and Molecular and Structural Biology, Jamova 39, SI-1000 Ljubljana, Slovenia. Tel.: +386 1 477 3854; fax: +386 1 477 3984.
E-mail addresses: vito.turk@ijs.si (V. Turk), veronika.stoka@ijs.si (V. Stoka).

0167-4889 © 2013 The Authors. Published by Elsevier B.V. Open access under CC BY-NC-ND license.
http://dx.doi.org/10.1016/j.bbamcr.2013.05.007

displayed aggresome-like characteristics, and were confirmed to be a degradation site for unnecessary DNA, RNA, and proteins rather than a synthesis site [19]. Since cathepsin F (CTSF) has an unusually long N-terminal proregion [20,21] and is the only cysteine cathepsin whose inactivation alone results in a lysosomal storage defect and progressive neurological features in mice [22], we sought to determine whether this enzyme may also play a role in cell death.

In this study, wtCatF and its N-terminally truncated forms Ala^{20}–Asp^{484} (Δ^{19}CatF), Pro^{126}–Asp^{484} (Δ^{125}CatF) and Met^{147}–Asp^{484} (Δ^{146}CatF) were overexpressed in HEK 293T cells. We confirmed the protein's expression level, distinct subcellular localization and involvement in caspase activation and aggresome formation. In addition, a bioinformatic analysis highlighted the presence of natively disordered regions within the human cathepsin F sequence and its fibrillation propensity. Moreover, we demonstrated that all three N-terminally truncated forms of human cathepsin F accumulated in aggresome-like inclusions, and were confirmed as p62-positive aggregates, which differed from the wild-type protein.

2. Materials and methods

2.1. Reagents

All of the reagents were of an analytical grade and were purchased from Sigma-Aldrich (St. Louis, MO, USA) unless otherwise stated. The human embryonic kidney 293T (HEK 293T) cell line was purchased from LGC Standards GmbH (Wesel, Germany). Phosphate-buffered saline (PBS), Dulbecco's modified Eagle's medium (DMEM), fetal bovine serum, L-glutamine and penicillin/streptomycin were obtained from PAA (Piscataway, NJ, USA). Poly-L-lysine, the protein inhibitor cocktail and the mouse monoclonal anti-β-actin antibody clone AC-15 (#A1978) were obtained from Sigma-Aldrich (St. Louis, MO, USA). The Xfect transfection reagent was purchased from Clontech (Mountain View, CA, USA). The pcDNA3 vector, non-animal cell dissociation reagent TrypLE Select, ProLong Gold antifade reagent, SlowFade Gold antifade reagent with DAPI, goat anti-rabbit Alexa Fluor 488-conjugated secondary antibody, goat anti-mouse Alexa Fluor 546-conjugated secondary antibody and donkey anti-goat Alexa Fluor 546-conjugated secondary antibody were purchased from Life Technologies (Grand Island, NY, USA). The restriction enzymes HindIII and EcoRI and peptide: N-glycosidase (PNGase F) were obtained from New England Biolabs (Ipswich, MA, USA). The 15-mm round glass coverslips were obtained from Electron Microscopy Sciences (Hatfield, PA, USA). The Bio-Rad Protein assay was purchased from Bio-Rad (Hercules, CA, USA). The caspase substrate Ac-Asp-Glu-Val-Asp-AFC and pan-caspase inhibitor Z-Val-Ala-DL-Asp(OMe)-fluoromethylketone were purchased from Bachem AG (Bubendorf, Switzerland). Stock solutions of substrate and inhibitor were prepared in dimethylsulfoxide and stored at −20 °C until further use. ProteoStat® Aggresome Detection kit was obtained from Enzo Life Sciences (Plymouth Meeting, PA, USA). Rabbit anti-human cathepsin F polyclonal antibody (#sc-13987) was purchased from Santa Cruz Biotechnology (Santa Cruz, CA, USA) whereas the goat anti-human cathepsin F polyclonal antibody (#ab36161), mouse monoclonal anti-human LAMP2 antibody [H4B4] (#ab25631), rabbit polyclonal anti-human LC3B antibody (#ab51520) and donkey anti-goat HRP-conjugated secondary polyclonal antibody (#ab6885) were obtained from Abcam (Cambridge, MA, USA). Mouse monoclonal anti-human p62/SQSTM1, clone 11C9.2 antibody (#MABC32) was obtained from Merck Millipore (Darmstadt, Germany). Goat anti-mouse HRP-conjugated secondary polyclonal antibody (#115-035-068) was obtained from Jackson ImmunoResearch Laboratories (West Grove, PA, USA).

2.2. Plasmid construction

The pPCR-Script plasmid containing the wild-type human cathepsin F (IMAGE clone 3637189 (Invitrogen, Carlsbad, USA) was used as a template. The cloning was performed using the following oligonucleotide sequences for wild-type human cathepsin F (forward primer: 5′-ggaaagcttaaaatggcgccctggctg-3′, reverse primer: 5′-atgaattctcagtc caccaccgccg-3′) whereas for the N-terminally truncated forms Ala^{20}–Asp^{484} (Δ^{19}CatF) (forward primer: 5′-ggaaagcttatggcccccgcccagc-3′, reverse primer: 5′-atgaattctcagtccaccaccgcc-3′), Pro^{126}–Asp^{484} (Δ^{125}CatF) (forward primer: 5′-ggaaagcttatgccagtggacaccaag-3′, reverse primer: 5′-atgaattctcagtccaccaccgccg-3′), and Met^{147}–Asp^{484} (Δ^{146}CatF) (forward primer: 5′-ggaaagcttatgatttcttctctgtccc-3′, reverse primer: 5′-atgaattctcagtccaccaccgcc-3′). Wild-type human cathepsin F and the chimeric constructs were inserted into the mammalian expression vector pcDNA3 using HindIII and EcoRI restriction enzymes.

2.3. Cell culture and transfection

HEK 293T cells were grown in DMEM medium supplemented with 10% (v/v) fetal bovine serum, 2 mM L-glutamine, 100 U/ml penicillin and 100 μg/ml streptomycin at 37 °C in a humidified atmosphere with 5% CO_2. Cells were evenly seeded and grown overnight before treatment. For the immunofluorescence labeling and aggresome detection studies, HEK 293T cells were grown on poly-L-lysine-coated coverslips.

The plasmids were transfected into the cells using the Xfect transfection reagent according to the manufacturer's instructions and grown in complete growth media alone or supplemented with 15 μM Z-VAD(OMe)-FMK for 48 h prior to the analysis. Negative controls included non-transfected, mock and empty vector-transfected cells.

2.4. Preparation of whole cell extracts

The cells were harvested 48 h after transfection using TrypLE Select, washed twice with PBS and centrifuged for 5 min at 1000 ×*g*. The supernatant was discarded, and the pellet was resuspended in ice-cold RIPA buffer (50 mM Tris, 100 mM NaCl, 0.1% (w/v) SDS, 1% (v/v) NP-40, 0.5% (w/v) deoxycholic acid, 1 mM EDTA pH 8.0). A cocktail of inhibitors was added to the RIPA buffer to prevent protein degradation prior to Western blotting. The cells were disrupted by 1 h incubation period on ice and spun for 10 min at 16,000 ×*g* using a refrigerated microcentrifuge (Eppendorf 5415R). The supernatant (soluble fraction) was collected and either used immediately or stored at −20 °C for later use. The pellet (insoluble fraction) was further processed with slight modifications from Johnston et al. [23]. Briefly, the pellets were solubilized in 50 μl of 1% (v/v) SDS in PBS for 10 min at room temperature, followed by addition of 50 μl RIPA buffer and sonicated for 10 s using a tip sonicator Branson W-450D (Branson, Danbury, CT, USA).

2.5. Determination of protein concentration

The protein concentration was estimated using the Bio-Rad Protein assay, on the basis of the Bradford method, according to the manufacturer's instructions (Bio-Rad).

2.6. Cathepsin F deglycosylation

N-linked glycosylation of wtCatF was assessed upon treatment with peptide: N-glycosidase (PNGase F) according to the manufacturer's instructions (New England Biolabs). The glycoprotein denaturing buffer (final conc. 0.5% SDS, 40 mM DTT) was added to 20 μg total protein obtained from whole cell extracts and the mixture was heated at 100 °C for 10 min. Next, PNGase F (1500 U final) resuspended in 50 mM sodium phosphate buffer pH 7.5 containing 1% NP40 was added to the above mixture to a final reaction volume of 20 μl and incubated at 37 °C for 1 h. An analogous reaction was performed in the absence of PNGase F, which was used as a negative control. A decrease in

the molecular weight of the protein band upon deglycosylation was assessed using Western blotting as described in Section 2.8.

2.7. Caspase activity detection

Caspase (DEVDase) activities were assessed from 50 μg of total protein. Briefly, the cleavage of the fluorogenic substrate Ac-DEVD-AFC was continuously measured in a 96-well plate reader (Tecan Infinite M1000 PRO, Männedorf, Switzerland) at excitation and emission wavelengths of 400 nm and 505 nm, respectively. The steady-state rates of substrate hydrolysis were extrapolated from the linear phase of the progression curves.

2.8. SDS-PAGE and Western blotting

A total of 20 μg of protein extract was loaded and resolved in 12.5% SDS-PAGE gels, which were run under reducing conditions using 25 mM Tris, 0.2 M glycine, 0.1% (w/v) SDS running buffer (35 mA constant per gel). The gels were then electro-transferred on to nitrocellulose membrane (Serva Electrophoresis GmbH, Heidelberg, Germany) at 250 mA constant over 120 min in buffer containing 25 mM Tris, 8 mM glycine and 20% (v/v) methanol. After the blocking step, the membranes were probed using goat polyclonal anti-human cathepsin F antibody (final conc. 0.5 μg/ml) for 3 h. The membranes were washed and then incubated with donkey anti-goat HRP-conjugated polyclonal secondary antibody (final conc. 0.17 μg/ml) for 1 h at room temperature. Next, the antigen/antibody complexes were detected using ECL Plus Western blotting detection reagents according to the manufacturer's instructions (GE Healthcare Bio-Sciences AB, Uppsala, Sweden). The membrane was exposed to Kodak BioMax Light autoradiography film and developed using a Konica Minolta SRX-101A automatic X-ray film processor (Konica Minolta, Tokyo, Japan). Protein loading was assessed by reprobing the Western blots using mouse monoclonal antibody against β-actin (final conc. 0.5 μg/ml) and the goat anti-mouse HRP-conjugated polyclonal secondary antibody (final conc. 0.13 μg/ml).

2.9. Immunolabeling and confocal microscopy

HEK 293T cells were grown on poly-L-lysine-coated coverslips and transfected as previously described in Section 2.3. Prior to immunofluorescence labeling, the cells were fixed and permeabilized in ice-cold methanol for 13 min on ice, rinsed in PBS and further incubated in blocking buffer (3% BSA in PBS) for 30 min. Cells were then incubated with a polyclonal rabbit anti-human cathepsin F antibody, goat polyclonal anti-human cathepsin F antibody, mouse monoclonal anti-LAMP2 antibody [H4B4], rabbit polyclonal anti-human LC3B antibody or mouse monoclonal anti-human p62/SQSTM1 antibody at a final concentration of 1 μg/ml for 45 min for a single or double immunolabeling and washed with PBS. The cells were further incubated with the appropriate secondary antibody (goat anti-rabbit, goat anti-mouse or donkey anti-goat) conjugated either with Alexa Fluor 488 or Alexa Fluor 546 at a final concentration of 0.8 μg/ml for 45 min and washed several times with PBS. Labeled cells were mounted using the SlowFade Gold antifade reagent with DAPI (blue-fluorescent nuclear stain), which eliminated the need for a separate counterstaining step. The controls were processed in the absence of the primary antibody.

Fluorescence microscopy and optical slicing were performed using an inverted confocal laser scanning microscope LEICA TCS SP5 X with white light laser (WLL) at an excitation source in the range from 470 nm to 670 nm and a 405 nm diode laser for DAPI excitation. The excitation lines were selected using an acousto-optical tunable filter (AOTF) as indicated below. An oil objective HCX PL APO 60× (N.A. = 1.4) was used. Optical sections in the z-direction were obtained and the emission signal was separated using an acousto-optical beam splitter (AOBS) and captured with one PMT and two hybrid detectors (HyD). Immunolabeled cathepsin F, LAMP2, p62/SQSTM1 and LC3B were excited using the 488 nm and 546 nm lines from WLL. Sequential scanning was strictly applied when multiple fluorescence signals were examined and the emission light was detected within the range of (1) 413 nm–457 nm for fluorescence in the blue spectrum, (2) 498 nm–550 nm for fluorescence in the green spectrum, and (3) 559 nm–617 nm for fluorescence in the red spectrum. Leica software LAS AF was used to evaluate the obtained fluorescence signals and colocalization of labeled proteins, respectively.

2.10. Aggresome detection

Cellular aggresomes were detected using the ProteoStat® Aggresome Detection kit according to the manufacturer's instructions (Enzo Life Sciences). HEK 293T cells were grown on poly-L-lysine coated coverslips and transfected as previously described in Section 2.3. The cells incubated for 12 h with a cell permeable proteasome inhibitor MG-132 (5 μM), which was used as a positive control. Next, the cells were washed with PBS and fixed in 4% paraformaldehyde for 30 min at room temperature. The cells were then permeabilized in permeabilizing solution (0.5% Triton X-100, 3 mM EDTA, pH 8.0 in 1× assay buffer) with gentle shaking on ice for 30 min. After this step, the cells were washed again in PBS and stained using the ProteoStat® Aggresome Detection Reagent and Hoechst 33342 nuclear stain for 30 min at room temperature protected from light. The microscope slides were mounted using the ProLong Gold antifade reagent and the aggresomes were visualized using an Olympus IX81 microscope (Olympus, Tokyo, Japan) with a motorized fluorescence unit. The emission signal was filtered using U-N49002 (green fluorescence) and U-M41002 (red fluorescence) filter cubes. Oil immersion objective UPlanSApo 100× (N.A. = 1.35) was used. Micrographs were obtained using a Hamamatsu ORCA-R^2 CCD camera (Hamamatsu, Hamamatsu City, Japan), and the Olympus Cell F software (Olympus, Tokyo, Japan) was used to evaluate the fluorescence signals.

2.11. Bioinformatics analysis tools

2.11.1. Prediction of molecular weight

The theoretical average molecular weight for human cathepsin F and its truncated forms were calculated using the deposited protein sequence (UniProt ID: Q9UBX1), as previously described [24].

2.11.2. Prediction of protein disorder

The prediction of natively disordered regions within the human cathepsin F amino acid sequence was performed using a meta Protein Disorder Prediction System (metaPrDOS), which is a meta server that integrates the results of the following prediction algorithms: PrDOS, DISOPRED2, DisEMBL, DISOclust, DISpro, DISPROT (VSL2), IUpred and POODLE-S [25].

2.11.3. Prediction of aggregation-prone regions

The prediction of aggregation-prone regions in human cathepsin F was performed using the 3D profile method, which consisted of an ensemble of templates derived from the crystal structure of the peptide NNQQNY, a representative of cross-β spines [26,27]. Segments with binding energies below an empirical threshold value of −23 kcal/mol were predicted to form fibrils [26]. A high fibrillation propensity was referred to as a "steric-zipper" which are two self-complementary β-sheets that form the spine of an amyloid fibril [26,27].

2.11.4. 3D-protein modeling

Three dimensional atomic models of the truncated form of human cathepsin F (Pro^{126}–Asp^{484}) and procathepsin F (Ser^{176}–Asp^{484}) were generated using the iterative implementation of the Threading ASSEmbly Refinement (I-TASSER) program [28,29]. Briefly, the I-TASSER protocol consisted of the following steps: 1) threading, 2) structural assembly, 3)

model selection and refinement and 4) a structure-based functional annotation [29].

3. Results and discussion

3.1. Human cathepsin F contains three natively disordered regions and various amino acid stretches with high fibrillation propensity

The amino acid sequence might be a determinant of protein aggregation and/or amyloidogenicity [30,31]. Thus, we assessed the potential contribution of amino acid stretches indicative of natively disordered regions and/or a propensity for aggregation within the primary and tertiary structure of human cathepsin F. The prediction of intrinsically disordered regions was performed using the meta Protein Disorder Prediction System (metaPrDOS) server, which integrated the results of eight prediction algorithms [25]. The consensus approach suggested three natively disordered regions within the enzyme's propeptide (Fig. 1). Peak 1 was found within the cystatin-like domain and included the first 12 amino acid residues following the signal peptide (Arg^{20}–Arg^{31}). Peak 2 (Pro^{126}–Leu^{175}) and peak 3 (Arg^{245}–Leu^{270}) were found among the flexible linker regions. The latter connected the cystatin-like domain with the inhibitory_I29 domain and then with the peptidase C1A domain corresponding to the mature form of cathepsin F.

A detailed study involving a non-redundant set of ordered and disordered protein segments indicated significant differences between their amino acid compositions and sequence attribute values, i.e., coordination number, flexibility, aromaticity, net charge and hydropathy scales [32]. Moreover, a comparative study of the relationship between the protein structure and β-aggregation in globular and intrinsically disordered proteins (IDPs) demonstrated that globular proteins contained approximately three times as many aggregation nucleating regions, such as IDPs, whereas the formation of highly structured globular proteins occurred at the cost of a higher β-aggregation propensity due to their protein structure and aggregation properties, which obey very similar physico-chemical constraints [33].

Various sequence- and structure-based methods have been developed to predict the protein propensity for aggregation and/or amyloid-fibril formation [34,35]. A structure method based on the crystal structure of the cross-β spine steric zipper formed by the peptide NNQQNY enabled the identification of the fibril-forming segments of proteins that had been previously undetected [26]. A detailed structural study of 30 fibril-forming segments from 14 different proteins revealed eight classes of steric zippers where two identical β-sheets could be classified according to the orientation of their facing side chains (either 'face-to-face' or 'face-to-back'), the orientation of their strands (with both β-sheets having the same edge of the strand 'up', or one 'up' and the other 'down'), and whether the strands within the β-sheets were either parallel or antiparallel [36].

The amino acid sequence and location on the protein structure have been shown to be a determinant of aggregation and/or amyloid-fibril formation [37,38]. Thus, we generated a 3D model of Δ^{125}CatF. In addition, the location of the predicted natively disordered and aggregation-prone regions was labeled accordingly in the primary (Fig. 2A) and tertiary (Fig. 2B, C) structures of the protein.

Three-dimensional atomic models of Δ^{125}CatF were constructed from multiple threading alignments and iterative structural assembly simulations using I-TASSER, an integrated platform for protein structure prediction [28,29]. Although the protein topology of the best model was correctly assessed (TM score: 0.63 ± 0.14), the model's uncertainty predominantly relied on the first 60 amino acid residues due to the lack of sequence and structure conservation and the lack of appropriate templates (Fig. 2C). The latter was confirmed using a 3D model of procathepsin F (Ser^{176}–Asp^{484}), which was built in the absence of the 50-amino acid residue long linker region (Pro^{126}–Ile^{175}). The procathepsin F model provided a TM score value of 0.92 ± 0.06 and significantly improved the model's quality (46%).

The fibrillation propensity within human cathepsin F was assessed using a 3D profile [26] (Fig. 2A). This structure-based algorithm included contributions from apolar interactions, hydrogen bonds and steric overlaps, as well as retrieving amyloid-forming segments that might be undetected using property-based methods, i.e., hydrophobicity or β-strand propensity [26]. An energy per amino acid residue below −23 kcal/mol on the Rosetta Design energy scale was indicative of a high fibrillation propensity [26]. The findings obtained from the 3D profile were highlighted on the Δ^{125}CatF 3D model (Fig. 2B, C), where the aggregation-prone amino acid stretches were found to be solvent-exposed (Val^{181}–Ser^{185}, Gln^{143}–Ser^{150}) or mixed (Thr^{162}–Val^{166}). Additional aggregation-prone regions were predicted within the mature form of the enzyme (Fig. 2A), namely Gly^{281}–Ala^{282}, Ala^{341}–Ser^{343}, Ile^{400}–Ala^{403}, Ala^{432}–Val^{433} and Ala^{471}–Ala^{478}.

Although several factors have been shown to affect aggregation of proteins and peptides [32,39], various evolutionary strategies have been developed to prevent this from occurring (i) optimization of the thermodynamic stability of the protein is prevented burying the aggregation prone regions in solvent inaccessible regions of the structure, (ii) segregation between the folding nuclei and the aggregation nuclei

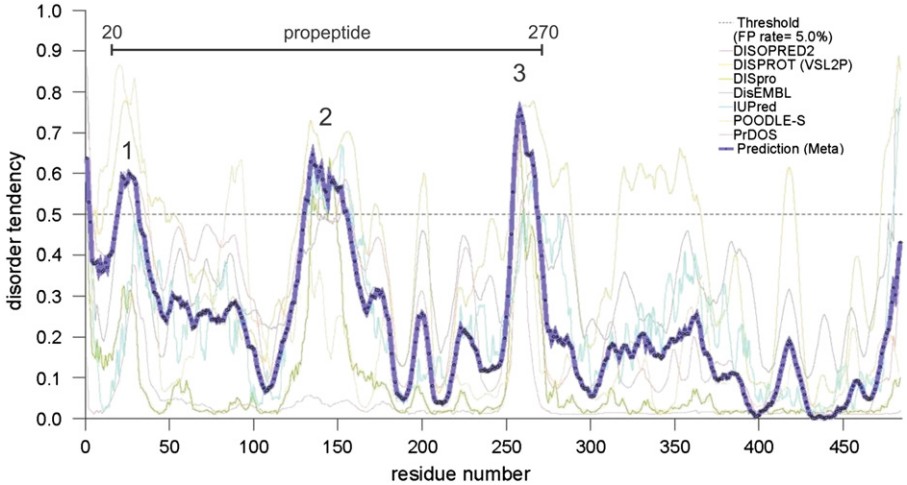

Fig. 1. Disorder profile of human cathepsin F. The probability of the disorder or disorder tendency within human cathepsin F was determined from its amino acid sequence using a consensus approach and a meta server (metaPrDOS) [25]. Three natively disordered regions (peaks 1–3) were found within the enzyme's propeptide region.

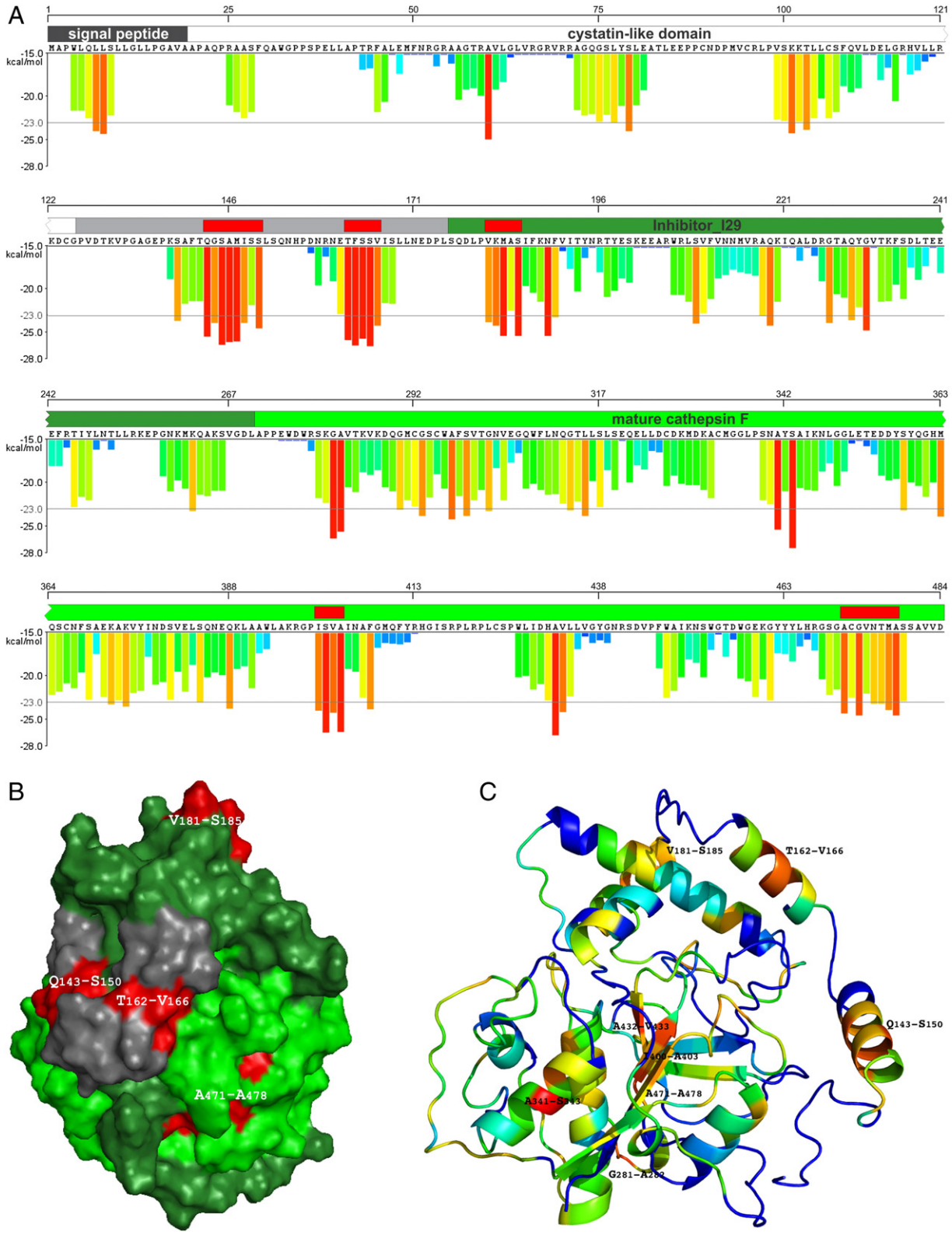

Fig. 2. Aggregation-prone regions of human cathepsin F. (A) The propensity for aggregation and/or amyloid fibril formation was determined using the 3D profile method [26]. The amino acid residues were colored according to their fibrillation propensity on a blue-to-red scale. The protein domain boundaries were indicated in the primary (A) and tertiary (B) structures of the protein. The non-conserved 50-amino acid residue region (P126–L175) is shown in dark gray, the inhibitor domain I29 (S176–L270) in dark green, and the mature form (A271–D484) in light green. Surface (B) and cartoon representation (C) of human Δ^{125}CatF. Δ^{125}CatF contains two exposed aggregation-prone amino acid stretches from positions Q143–S150 (energy range: −23.8 to −26.3 kcal/mol) and V181–S185 (energy range: −22.4 to −25.3 kcal/mol) and a mixed region at positions T162–V166 (energy range: −24.1 to −26.5 kcal/mol, mixed). Moreover, within the mature form of the enzyme, two major aggregation-prone regions were predicted from positions I400–A403 (energy range: −24.0 to −26.5 kcal/mol) and A471–A478 (energy range: −22.0 to −24.5 kcal/mol). These aggregation-prone amino acid stretches were highlighted in red in the primary (A) and tertiary (B) structures of the enzyme. The latter view (Fig. 2B) emphasizes their location at the enzyme's surface and is not the standard orientation used to display the structural data on the papain-like enzymes. The prediction of the 3D atomic model of Δ^{125}CatF was performed using the I-TASSER server [29]. A ribbon representation of the front view (standard orientation) of the best model is shown in panel C, which is labeled by their fibrillation propensity as assessed in panel A. The reliability of the model is indicated by a TM score: 0.63 ± 0.14. The molecular structure was generated using the molecular visualization system PyMOL [65].



Fig. 3. Schematic representation of human cathepsin F and its N-terminally truncated forms. The domain composition of wild-type human cathepsin F is indicated (top panel). The boundaries of the N-terminally truncated forms Ala^{20}–Asp^{484} (Δ^{19}CatF); Pro^{126}–Asp^{484} (Δ^{125}CatF) and Met^{147}–Asp^{484} (Δ^{146}CatF) are indicated accordingly in a scaled representation.

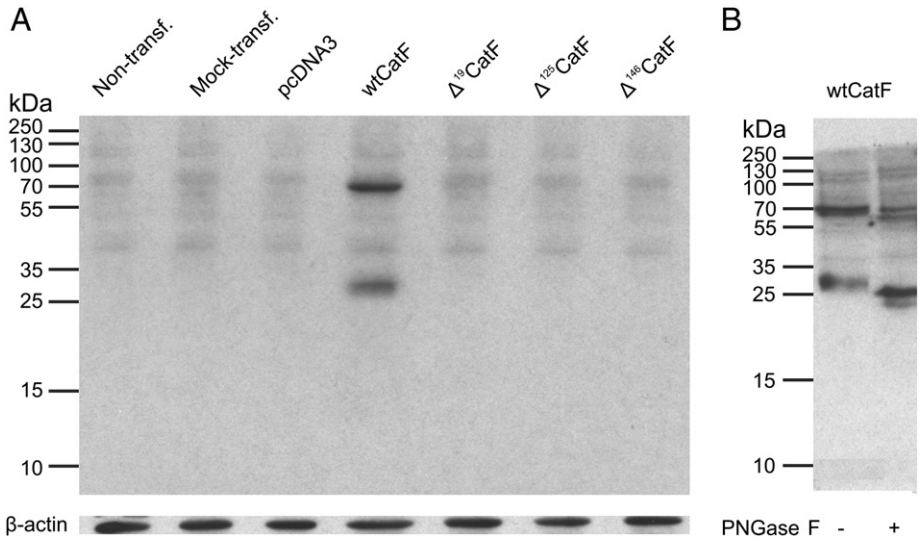

Fig. 4. (A) Expression of human cathepsin F and its N-terminally truncated forms in HEK 293T cells: soluble fraction. HEK 293T cells were transfected with pcDNA3-containing plasmids of human cathepsin F and its N-terminally truncated forms Δ^{19}CatF, Δ^{125}CatF and Δ^{146}CatF for 48 h. Next, whole cell protein extracts were evaluated by Western blotting analysis using an anti-human cathepsin F antibody (Abcam #ab36161). Negative controls included the non-transfected, mock-transfected and pcDNA3 empty vector-transfected cells. Loading of equivalent amounts of protein was assessed against β-actin (lower blot). (B) Deglycosylation of human cathepsin F by peptide: N-glycosidase (PNGase F). An extract of HEK 293T cells expressing wild-type human cathepsin F was treated with PNGase F and a decrease in Mw of the protein band upon N-deglycosylation was assessed by Western blotting.

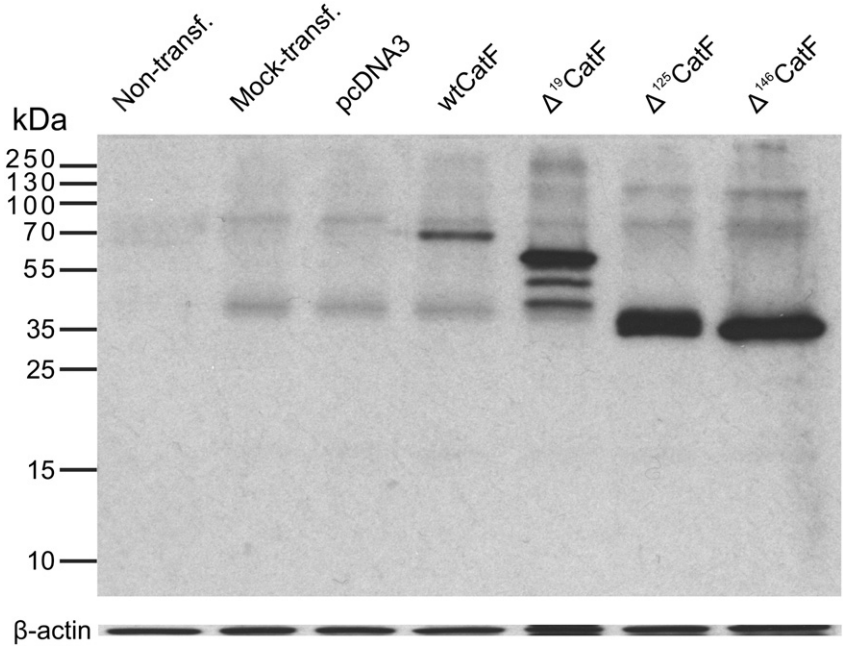

Fig. 5. Expression of human cathepsin F and its N-terminally truncated forms in HEK 293T cells: insoluble fraction. HEK 293T cells were transfected with pcDNA3-containing plasmids of human cathepsin F and its N-terminally truncated forms Δ^{19}CatF, Δ^{125}CatF and Δ^{146}CatF for 48 h. Next, whole cell protein extracts were evaluated by Western blotting analysis using an anti-human cathepsin F antibody (Abcam #ab36161). Negative controls included the non-transfected, mock-transfected and pcDNA3 empty vector-transfected cells. Loading of equivalent amounts of protein was assessed against β-actin (lower blot).

within a protein sequence, (iii) placement of gatekeeper residues at the flanks of aggregating segments, and (iv) molecular chaperones that directly target aggregation nucleating sequences in cellular environment [40]. Thus, the number of proteins that are capable of forming amyloid-like fibrils, which has been coined the "amylome" is limited, suggesting that chaperoning effects have evolved to constrain self-complementary segments from interacting with each other [27]. Moreover, functional interactions may act as a survival strategy against abnormal aggregations [41].

3.2. Distinct expression pattern of human cathepsin F compared to its N-terminally truncated forms following overexpression in HEK 293T cells

Wild-type human cathepsin F (wtCatF) and its N-terminally truncated forms Ala^{20}–Asp^{484} (Δ^{19}CatF), Pro^{126}–Asp^{484} (Δ^{125}CatF) and Met^{147}–Asp^{484} (Δ^{146}CatF) were cloned into a pcDNA3 vector and used for transient transfection experiments on HEK 293T cells. Two constructs were generated by deletion of the first 19 amino acid residues (SP), which represent the enzyme's signal peptide (Δ^{19}CatF) and the cystatin-like domain [20] (Δ^{125}CatF), whereas the third construct (Δ^{146}CatF) also lacks a 20-amino acid residue-long linker region and represents the naturally truncated form of human cathepsin F, which was first obtained from a λgt10-skeletal muscle cDNA library [42]. A schematic representation of wtCatF and its N-terminally truncated forms (Δ^{19}CatF, Δ^{125}CatF and Δ^{146}CatF) is shown in Fig. 3.

Western blotting analysis of the soluble fraction highlights the successful expression of the wild-type protein, which was detected as a major band of ~70 kDa and a minor band of 30 kDa (Fig. 4A lane 4). As assessed from the protein sequence, the predicted Mw of human cathepsin F (Δ^{19}CatF) was 51.4 kDa, whereas the mature form of the enzyme exhibited a theoretical average Mw of 23.6 kDa. Thus, the higher values assessed by Western blotting analysis (Fig. 4A) could be attributed to the presence of five potential N-linked glycosylation sites, two of which are located in the enzyme's 251-amino acid long propeptide (Asn160, Asn195) and three sites are present in its mature form

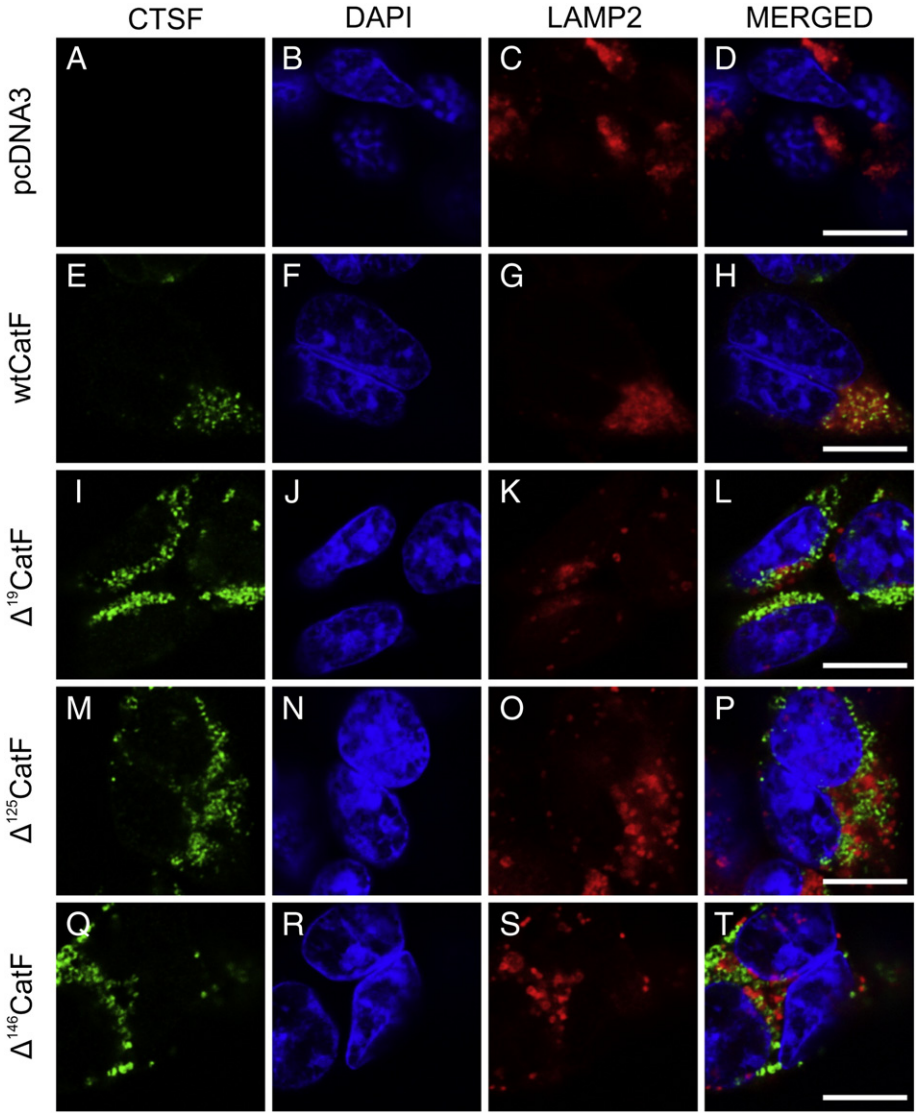

Fig. 6. Subcellular localization of human cathepsin F (E-H) and its N-terminally truncated forms Δ^{19}CatF (I–L), Δ^{125}CatF (M–P) and Δ^{146}CatF (Q–T). HEK 293T cells were transfected with wtCatF and its N-terminally truncated forms for 48 h. Their subcellular localizations were assessed using confocal microscopy and multiple immunofluorescence signals compared using anti-cathepsin F and anti-LAMP2 antibodies, followed by Alexa Fluor-labeled secondary antibodies as described in Section 2.9. Confocal images (optical sections) showed intracellular cathepsin F (CTSF) (green fluorescence: A, E, I, M, Q) together with the lysosomal marker LAMP2 (red fluorescence: C, G, K, O, S). Merged images showed overlapping immunoreactivity in yellow (D, H, L, P, T). The nucleus was counterstained for DNA using DAPI (blue fluorescence: B, F, J, N, R). Negative controls included the non-transfected, mock-transfected and pcDNA3 empty vector-transfected cells. Under these three conditions, a very similar pattern was obtained. Thus, as a representative example, only the pcDNA3 (A–D) example is shown. Scale bars = 10 μm.

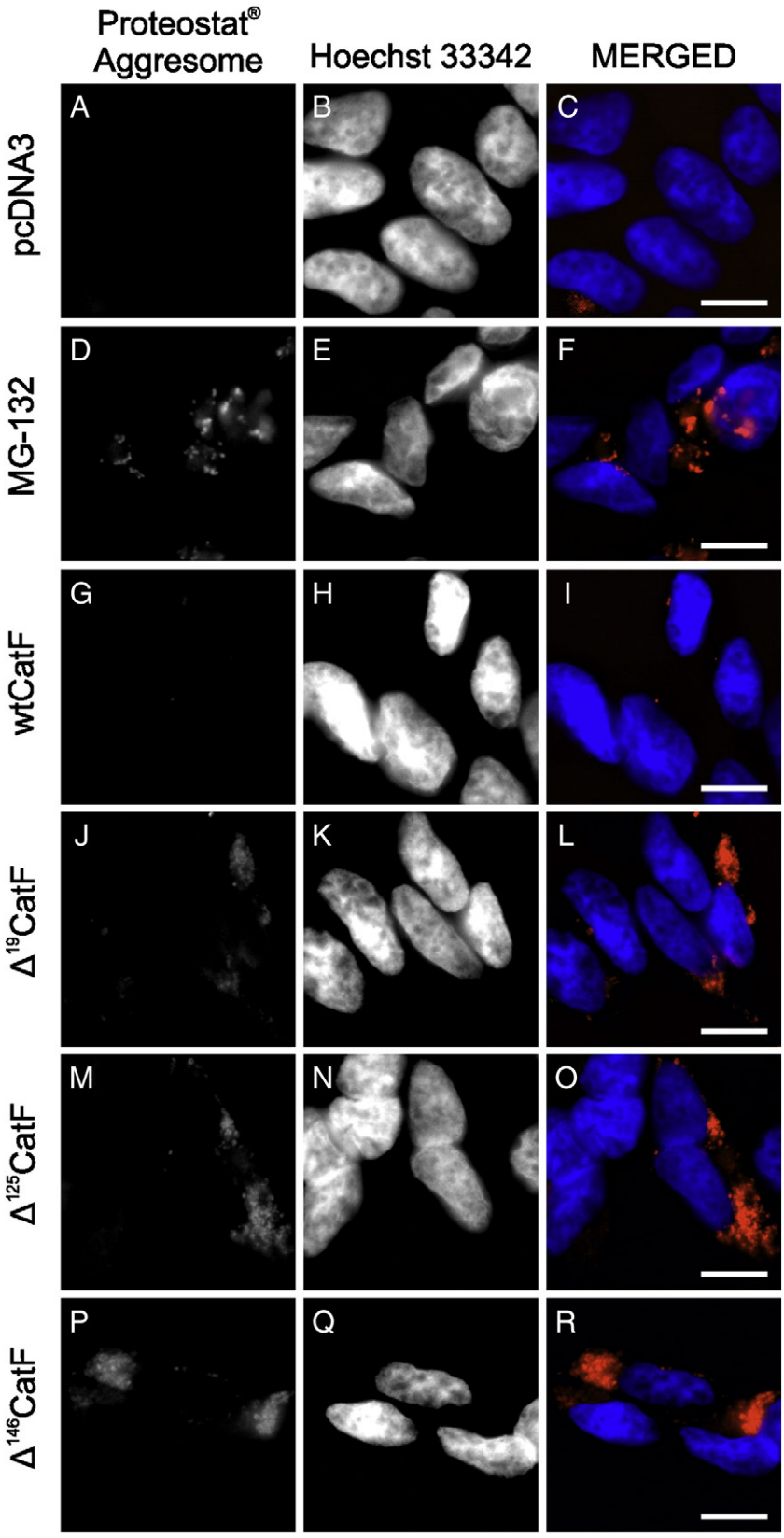

Fig. 7. Aggresome formation in HEK 293T cells 48 h post-transfection with pcDNA3-containing plasmids of human cathepsin F (G–I) and its N-terminally truncated forms Δ^{19}CatF (J–L), Δ^{125}CatF (M–O) and Δ^{146}CatF (P–R), as detected using the ProteoStat® aggresome detection dye. Δ^{19}CatF (J), Δ^{125}CatF (M) and Δ^{146}CatF (P) accumulated in aggresomes similar to cells pretreated with 5 μM of the proteasome inhibitor MG-132 (D). This was in contrast to the wild-type protein (wtCatF) (G) and empty vector-transfected negative control cells (A). The nucleus was counterstained for DNA using Hoechst 33342. Images were labeled with the ProteoStat® aggresome dye (A, D, G, J, M, P) and Hoechst 33342 nuclear stain (blue fluorescence: B, E, H, K, N, Q) and a merged view (C, F, I, L, O, R). The experiment was performed as previously described in Section 2.10. Negative controls included the non-transfected, mock-transfected and pcDNA3 empty vector-transfected cells. Under these three conditions, a very similar pattern was obtained. Thus, as a representative example, only the pcDNA3 (A–C) example is shown. Scale bars = 10 μm.

(Asn367, Asn378, Asn440) [20,42,43]. Using the peptide: N-glycosidase F (PNGase F), a potent enzyme with broader specificity that hydrolyzes all classes of asparagine-linked glycans [44], we demonstrated an approximate decrease of 6 kDa in the molecular mass of the full-length and mature forms of the enzyme, respectively (Fig. 4B). In vitro studies showed that treatment of the recombinant human cathepsin F zymogen with endoglycosidases H and F resulted in a decrease in the Mw of the proenzyme and mature form of approximately 9 kDa and 5 kDa, respectively [42,43]. Since PNGase F demonstrates an effect on most types of oligosaccharides, in particular, high mannose, hybrid, or complex type oligosaccharides [44], the observed differences were due to a different glycosylation pattern of recombinant human cathepsin F, which was produced in different expression systems [42,45]. Importantly, glycosylation pattern differences were found in proteins isolated from different tissues as well as transiently and permanently transfected cell lines [46,47].

Although all of the constructs were successfully transfected and the amount of protein loaded per lane was equivalent in all of the samples (20 μg), the N-terminally truncated forms of the enzyme, in particular, Δ^{19}CatF, Δ^{125}CatF and Δ^{146}CatF were nearly undetectable in the soluble fractions (Fig. 4A lanes 5–7). These results motivated the evaluation of the insoluble fraction. Interestingly, all of the evaluated N-terminally truncated forms of human cathepsin F were predominantly found in the insoluble fraction (Fig. 5 lanes 5–7), thus confirming that the deletion of at least the signal peptide (Fig. 5 lane 5), resulted in protein aggregation. Unexpectedly, Δ^{19}CatF was detected as a major band with a Mw of ~60 kDa, which was ~10 kDa smaller than its wild-type counterpart. In addition, two minor bands of 52 and 45 kDa, respectively, which were only observed in its truncated form (Fig. 5 lane 5). Moreover, Δ^{125}CatF and Δ^{146}CatF were detected as single bands with a Mw of 40 kDa (Fig. 5 lane 6) and 38 kDa (Fig. 5 lane 7), which were consistent with their theoretical average Mw of 39.9 kDa and 37.9 kDa, respectively.

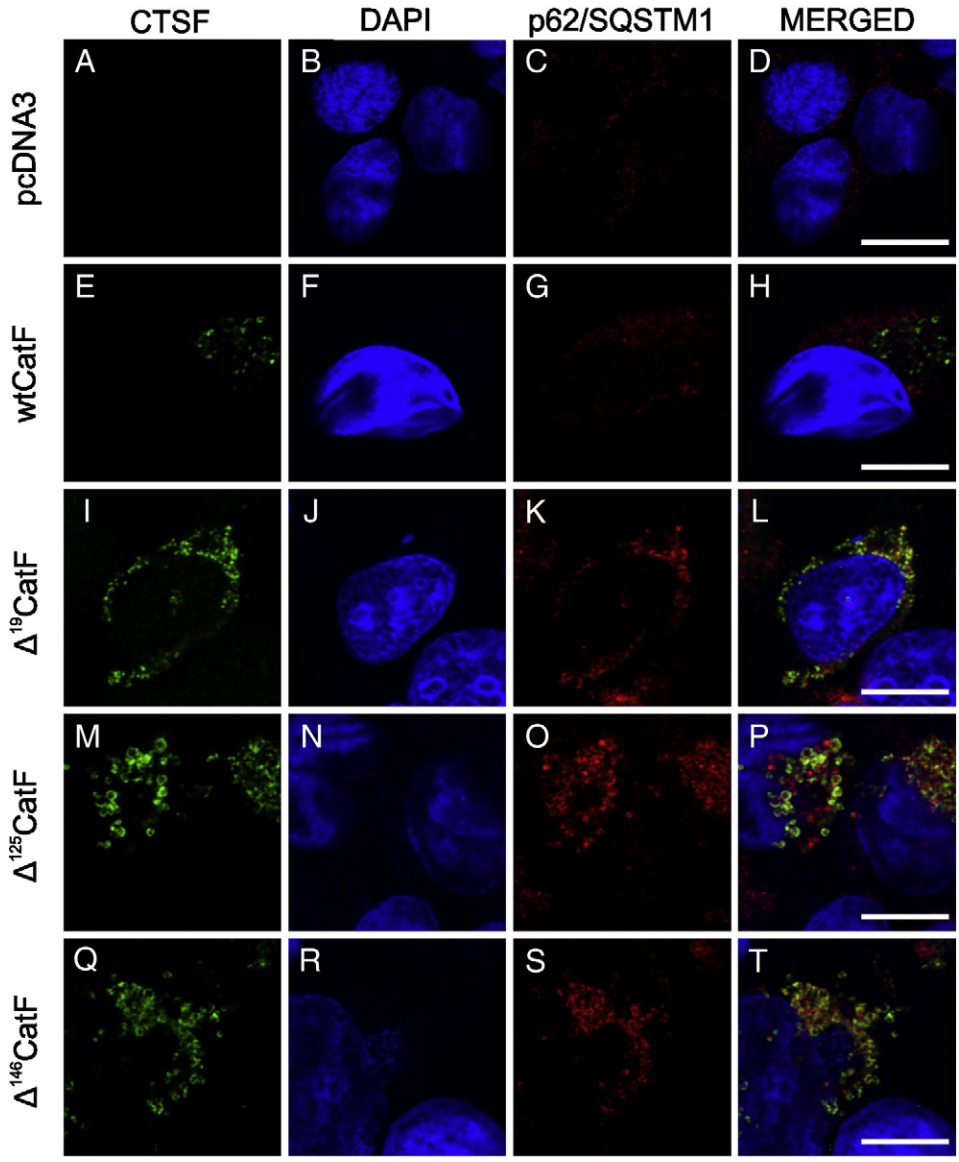

Fig. 8. N-terminally truncated forms of human cathepsin F Δ^{19}CatF (I–L), Δ^{125}CatF (M–P) and Δ^{146}CatF (Q–T) are p62-positive inclusions, which differ from the wild-type protein (E–H). HEK 293T cells were transfected with human cathepsin F and its N-terminally truncated forms for 48 h. Double immunolabeling with anti-cathepsin F and anti-p62/SQSTM1 antibodies, was performed as previously described in Section 2.9. Confocal images (optical sections) showed cathepsin F (CTSF) (green fluorescence: A, E, I, M, Q) and the p62/SQSTM1 marker (red fluorescence: C, G, K, O, S). Merged images showed overlapping immunoreactivity in yellow (D, H, L, P, T). The nucleus was counterstained for DNA using DAPI (blue fluorescence: B, F, J, N, R). Negative controls included the non-transfected, mock-transfected and pcDNA3 empty vector-transfected cells. Under these three conditions, a very similar pattern was obtained. Thus, as a representative example, only the pcDNA3 (A–D) example is shown. Scale bars = 10 μm.

3.3. N-terminally truncated forms of human cathepsin F in HEK 293T cells accumulated in aggresome-like inclusions and induce caspase activation, which differs from wild-type protein

Cysteine cathepsins require their propeptides for targeting and proper folding [48]. A strong correlation exists between the structural integrity of the propeptide, its inhibitory potency and its ability to catalyze the correct folding of the mature enzyme [48]. Similar to cathepsin L-like enzymes, human cathepsin F propeptide (Ser^{176}–Lys^{270}) [20] is present in Δ^{19}CatF and Δ^{125}CatF (as shown in this study) and the naturally occurring truncated form of the enzyme Met^{147}–Asp^{484} (Δ^{146}CatF) [42], suggesting that their folding properties are not compromised. Moreover, the latter has been confirmed to be catalytically active [42].

Transient transfections of wtCatF using HEK 293T cells showed a vesicular labeling pattern (Fig. 6E), which was characteristic of the lysosomal compartment (Fig. 6G) and was further confirmed by colocalization with LAMP2 (Fig. 6H). No fluorescence signal in green spectrum was detected with the empty vector-transfected cells (Fig. 6A, D). However, the N-terminally truncated forms Δ^{19}CatF, Δ^{125}CatF and Δ^{146}CatF were concentrated as large perinuclear–juxtanuclear aggregates (Fig. 6I, M, Q), which did not significantly colocalize with the lysosomal marker LAMP2 (Fig. 6L, P, T). Noteworthy, it was shown that the truncated forms of cathepsins B [18], H [49] and L [50], which contained a partial or total deletion of the signal peptide demonstrated altered trafficking and was thus targeted to the mitochondria, perinuclear, secreted, and nuclear sites, respectively.

The subcellular localization and labeling pattern observed for the N-terminally truncated forms of human cathepsin F motivated the hypothesis of whether the truncated forms reside within organelle-like structures, which are also known as aggresomes. Using a novel red fluorescent molecular rotor dye, which is essentially non-fluorescent until it binds to the structural features associated with aggregated protein

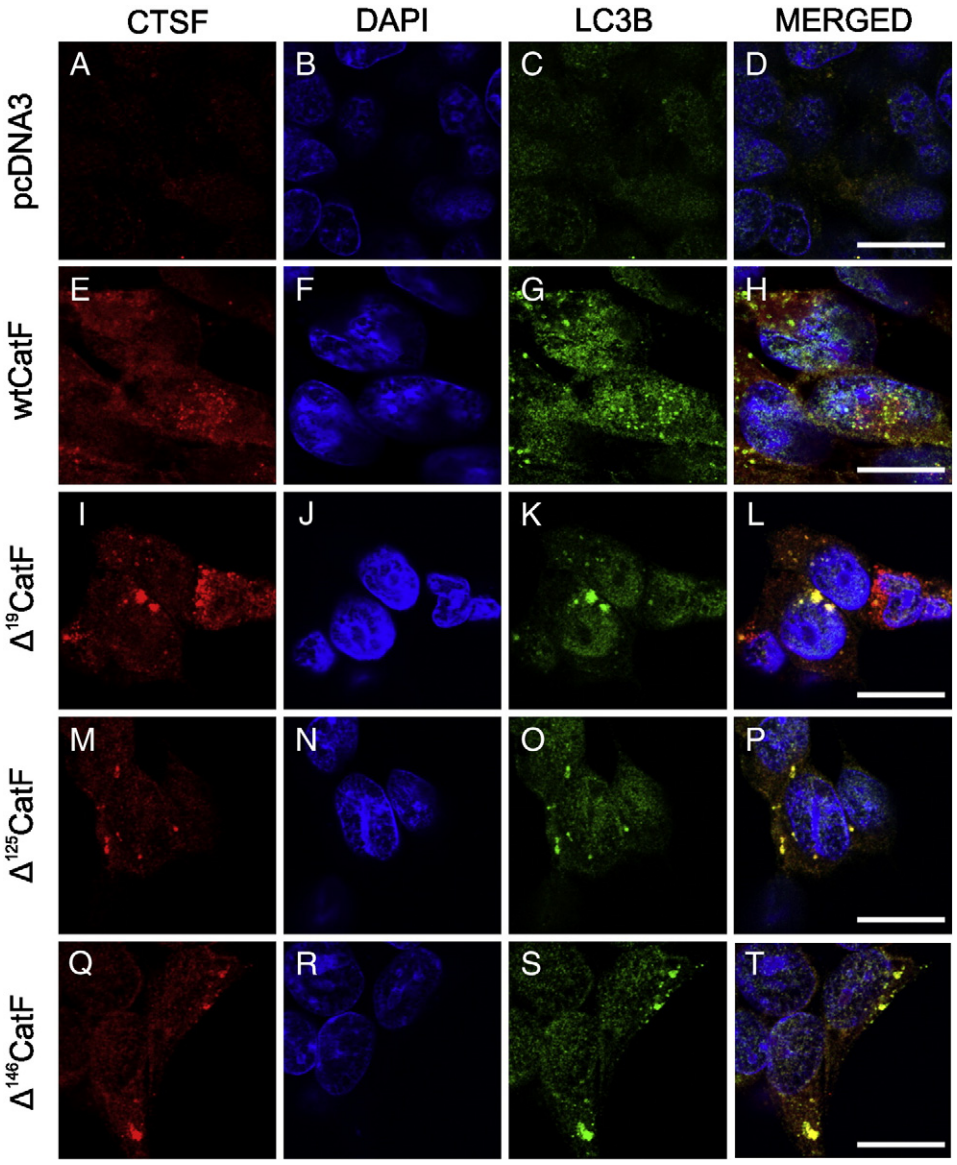

Fig. 9. Immunofluorescence of LC3B upon overexpression of human cathepsin F (E–H) and its N-terminally truncated forms Δ^{19}CatF (I–L), Δ^{125}CatF (M–P) and Δ^{146}CatF (Q–T). HEK 293T cells were transfected with human cathepsin F and its N-terminally truncated forms for 48 h. Double immunolabeling with anti-cathepsin F and anti-LC3B antibodies, was performed as described in Section 2.9. Confocal images (optical sections) showed human cathepsin F (CTSF) (red fluorescence: A, E, I, M, Q) and LC3B as marker of autophagy (green fluorescence: C, G, K, O, S). Merged images showed overlapping immunoreactivity in yellow (D, H, L, P, T). The nucleus was counterstained for DNA using DAPI (blue fluorescence: B, F, J, N, R). Negative controls included the non-transfected, mock-transfected and pcDNA3 empty vector-transfected cells. Under these three conditions, a very similar pattern was obtained. Thus, as a representative example, only the pcDNA3 (A–D) example is shown. Scale bars = 10 μm.

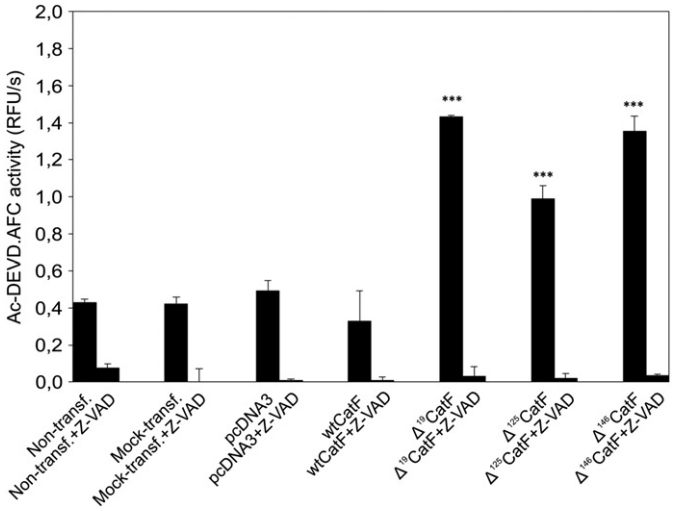

Fig. 10. Overexpression of the N-terminally truncated forms of human cathepsin F, but not the wild-type protein, induces caspase activation. DEVDase activity was monitored by kinetics 48 h post-transfection with pcDNA3-containing plasmids of human cathepsin F and its N-terminally truncated forms Δ^{19}CatF, Δ^{125}CatF and Δ^{146}CatF. Human cathepsin F (wtCatF) overexpression did not have an effect on caspase activation. In contrast, the N-terminally truncated forms Δ^{19}CatF, Δ^{125}CatF and Δ^{146}CatF induced an approximately 2–3 fold increase in DEVDase activity, which was blocked by the pan-caspase inhibitor Z-VAD(OMe)-FMK. Negative control experiments included non-transfected, mock-transfected and pcDNA3 empty vector-transfected cells. The results are given as the means ± SD of three independent experiments. ***, $p < 0.001$ compared to pcDNA3.

cargo [51], we demonstrated that the N-terminally truncated forms Δ^{19}CatF (Fig. 7J, L), Δ^{125}CatF (Fig. 7M, O) and Δ^{146}CatF (Fig. 7P, R) accumulated in aggresome-like inclusions. This was similar to observations made when autophagy was induced by treatment with the proteasome inhibitor MG-132 (Fig. 7D, F). In contrast, no effect was observed after the overexpression of wild-type protein (Fig. 7G, I) or empty vector-transfected cells (Fig. 7A, C). Next, we further examined whether the truncated forms of human cathepsin F might colocalize with an aggresome-related protein such as p62/SQSTM1. p62/SQSTM1 is a multifunctional polyubiquitin-binding protein that is commonly detected in cytoplasmic inclusions in diseases associated with protein aggregation [52]. In this study, all three human cathepsin F's N-terminally truncated forms (Fig. 8I, M, Q) had colocalized with p62/SQSTM1 (Fig. 8L, P, T), providing additional evidence that Δ^{19}CatF, Δ^{125}CatF and Δ^{146}CatF accumulated in aggresomes.

Aggresome formation was initially proposed as a general cellular response that occurred when the capacity of the proteasome was exceeded by the production of aggregation-prone misfolded proteins [23,53]. The aggregate-prone proteins would then be cleared from the cytosol by autophagy by removing the primary toxin (misfolded/aggregate-prone protein) and reducing its susceptibility to apoptotic insults [54]. However, recent evidence indicates that in mammalian cells, these aggresomes do not represent a general cellular response to protein misfolding [55,56].

To assess whether the protein aggregates induced by Δ^{19}CatF, Δ^{125}CatF and Δ^{146}CatF would be degraded and/or cleared via the autophagy pathway, we evaluated their potential colocalization with the autophagy marker, microtubule-associated protein 1A/1B-light chain 3 (LC3B) [57]. Interestingly, all three N-terminally truncated forms of cathepsin F (Fig. 9I, M, Q) were colocalized with LC3B (Fig. 9L, P, T), which indicated autophagy as a protective mechanism. In contrast, the wild-type protein exhibited a more diffuse vesicular pattern (Fig. 9H). Similarly, in huntingtin-induced cell death p62/SQSTM1 was shown to form protein aggregates that were degraded by autophagy [58]. Moreover, p62/SQSTM1 bound directly to Atg8/LC3 to facilitate the degradation of polyubiquitin-containing bodies by autophagy [59].

However, the accumulation of toxic proteins in the cytoplasm of neuronal and non-neuronal cells has also been linked to cytotoxicity and cell death by apoptosis [60–63]. Since Δ^{19}CatF, Δ^{125}CatF and Δ^{146}CatF accumulate in aggresome-like inclusions, we evaluated the potential contribution of apoptosis that was induced by caspase activation. An approximately 2–3 fold increase in DEVDase activity was evident in the samples transfected with the N-terminally truncated forms of the enzyme and was blocked by the general caspase inhibitor Z-VAD(OMe)-FMK (Fig. 10).

Transient overexpression of wtCatF did not induce caspase activation (Fig. 10), which is consistent with reports on cathepsins B and L [15]. Moreover, annexin V/propidium iodide staining and flow cytometry analysis 48 h post-transfection revealed that the number of apoptotic cells was below 5–10% after overexpression of wtCatF and its N-terminally truncated forms compared to non-transfected, mock-transfected and pcDNA3 empty vector-transfected cells (results not shown). Thus, the resulting DEVDase activity in our cellular model was not sufficient to induce apoptotic cell death. However, cathepsin B alternatively spliced variants [16,18] and its artificially truncated forms [17] resulted in nuclear fragmentation and cell death. Alternatively spliced variants and/or truncated forms of different cathepsins where found in different subcellular compartments i.e. aggresomes (this study), cytoplasm, mitochondria, nuclear, perinuclear and secreted [16–18,49,50]. Their effects on the cell were either deleterious, similar to reports for cathepsin B transcripts lacking exons 2 and 3 with and without the C-terminal propeptide and other aberrant forms [16–18] or did not manifest signs of cell death such as in cathepsin B transcripts with or without exon 2, in the presence of the C-terminal propeptide [16]. The N-terminally truncated forms of cathepsin F (in this study), showed many potential future avenues to pursue to gain insight into the role of cathepsins in pathophysiology. A genome-wide linkage mapping study of two families with recessive type B Kufs disease, an adult-onset neuronal ceroid lipofuscinosis, detected five rare or novel pathogenic mutations within human cathepsin F (CTSF). The authors proposed that CTSF should receive the locus designation CLN13 [64]. Moreover, the single nucleotide frameshift deletion in exon 7 (c.954delC [pSer319Leufs*27]) resulted in a nonsense mutation that truncated the protein to approximately three-quarters of its normal length [64].

4. Conclusion

In summary, we predicted that human cathepsin F contained three natively disordered regions within the enzyme's propeptide and various aggregation-prone amino acid stretches. Our results confirmed that the N-terminally truncated forms of human cathepsin F were found concentrated as large perinuclear-juxtanuclear aggregates, which accumulated within aggresome-like inclusions, and are cleared via the p62/SQSTM1-dependent autophagy pathway. In addition, an approximately 2–3 fold increase in DEVDase activity was not sufficient to induce apoptotic cell death. Furthermore, the truncated forms of cathepsins represent a wide signaling repertoire that is worth pursuing in future studies in order to gain insight into their role in pathophysiology.

Acknowledgements

The authors are grateful to Prof. Guy Salvesen (Sanford-Burnham Institute for Medical Research, La Jolla, CA, USA) and Dr. Urška Repnik for their valuable discussions. Confocal microscopy has been performed within Leica Reference Centre for confocal microscopy with white light laser (WLL) in Ljubljana. This study was supported by grants J1-9520 and J3-2258 to V.S., and P1-0140 to B.T obtained from the Slovenian Research Agency—ARRS.

References

[1] V. Turk, V. Stoka, O. Vasiljeva, M. Renko, T. Sun, B. Turk, D. Turk, Cysteine cathepsins: from structure, function and regulation to new frontiers, Biochim. Biophys. Acta 1824 (2012) 68–88.
[2] B. Turk, V. Stoka, J. Rozman-Pungerčar, T. Cirman, G. Droga-Mazovec, K. Orešić, V. Turk, Apoptotic pathways: involvement of lysosomal proteases, Biol. Chem. 383 (2002) 1035–1044.
[3] M.E. Guicciardi, M. Leist, G.J. Gores, Lysosomes in cell death, Oncogene 23 (2004) 2881–2890.
[4] P. Boya, G. Kroemer, Lysosomal membrane permeabilization in cell death, Oncogene 27 (2008) 6434–6451.
[5] T. Kirkegaard, M. Jäättelä, Lysosomal involvement in cell death and cancer, Biochim. Biophys. Acta 1793 (2009) 746–754.
[6] U. Repnik, V. Stoka, V. Turk, B. Turk, Lysosomes and lysosomal cathepsins in cell death, Biochim. Biophys. Acta 1824 (2012) 22–33.
[7] C. Tardy, P. Codogno, H. Autefage, T. Levade, N. Andrieu-Abadie, Lysosomes and lysosomal proteins in cancer cell death (new players of an old struggle), Biochim. Biophys. Acta 1765 (2006) 101–125.
[8] M.E. Guicciardi, J. Deussing, H. Miyoshi, S.F. Bronk, P.A. Svingen, C. Peters, S.H. Kaufmann, G.J. Gores, Cathepsin B contributes to TNF-α-mediated hepatocyte apoptosis by promoting mitochondrial release of cytochrome c, J. Clin. Invest. 106 (2000) 1127–1137.
[9] V. Stoka, B. Turk, S.L. Schendel, T.H. Kim, T. Cirman, S.J. Snipas, L.M. Ellerby, D. Bredesen, H. Freeze, M. Abrahamson, D. Brömme, S. Krajewski, J.C. Reed, X.M. Yin, V. Turk, G.S. Salvesen, Lysosomal protease pathways to apoptosis: cleavage of Bid, not pro-caspases, is the most likely route, J. Biol. Chem. 276 (2001) 3149–3157.
[10] L. Bojič, A. Petelin, V. Stoka, T. Reinheckel, C. Peters, V. Turk, B. Turk, Cysteine cathepsins are not involved in Fas/CD95 signalling in primary skin fibroblasts, FEBS Lett. 581 (2007) 5185–5190.
[11] P. Boya, K. Andreau, D. Poncet, N. Zamzami, J.L. Perfettini, D. Metivier, D.M. Ojcius, M. Jäättelä, G. Kroemer, Lysosomal membrane permeabilization induces cell death in a mitochondrion-dependent fashion, J. Exp. Med. 197 (2003) 1323–1334.
[12] G. Droga-Mazovec, L. Bojič, A. Petelin, S. Ivanova, R. Romih, U. Repnik, G.S. Salvesen, V. Stoka, V. Turk, B. Turk, Cysteine cathepsins trigger caspase-dependent cell death through cleavage of bid and antiapoptotic Bcl-2 homologues, J. Biol. Chem. 283 (2008) 19140–19150.
[13] M. Klarić, S. Tao, V. Stoka, B. Turk, V. Turk, Cysteine cathepsins are not critical for TNF-α-induced cell death in T98G and U937 cells, Biochim. Biophys. Acta 1794 (2009) 1372–1377.
[14] L.P. Deiss, H. Galinka, H. Berissi, O. Cohen, A. Kimchi, Cathepsin D protease mediates programmed cell death induced by interferon-γ, Fas/APO-1 and TNF-α, EMBO J. 15 (1996) 3861–3870.
[15] A. Gewies, S. Grimm, Cathepsin-B and cathepsin-L expression levels do not correlate with sensitivity of tumour cells to TNF-α-mediated apoptosis, Br. J. Cancer 89 (2003) 1574–1580.
[16] K. Müntener, R. Zwicky, G. Csucs, A. Baici, The alternative use of exons 2 and 3 in cathepsin B mRNA controls enzyme trafficking and triggers nuclear fragmentation in human cells, Histochem. Cell Biol. 119 (2003) 93–101.
[17] F. Bestvater, C. Dallner, E. Spiess, The C-terminal subunit of artificially truncated human cathepsin B mediates its nuclear targeting and contributes to cell viability, BMC Cell Biol. 6 (2005) 16.
[18] K. Müntener, R. Zwicky, G. Csucs, J. Rohrer, A. Baici, Exon skipping of cathepsin B: Mitochondrial targeting of a lysosomal peptidase provokes cell death, J. Biol. Chem. 279 (2004) 41012–41017.
[19] C.M. Haraguchi, T. Mabuchi, S. Hirata, T. Shoda, K. Hoshi, K. Akasaki, S. Yokota, Chromatoid bodies: aggresome-like characteristics and degradation sites for organelles of spermiogenic cells, J. Histochem. Cytochem. 53 (2005) 455–465.
[20] D.K. Nägler, T. Sulea, R. Ménard, Full-length cDNA of human cathepsin F predicts the presence of a cystatin domain at the N-terminus of the cysteine protease zymogen, Biochem. Biophys. Res. Commun. 257 (1999) 313–318.
[21] I. Santamaría, G. Velasco, A.M. Pendás, A. Paz, C. López-Otín, Molecular cloning and structural and functional characterization of human cathepsin F, a new cysteine proteinase of the papain family with a long propeptide domain, J. Biol. Chem. 274 (1999) 13800–13809.
[22] C.H. Tang, J.W. Lee, M.G. Galvez, L. Robillard, S.E. Mole, H.A. Chapman, Murine cathepsin F deficiency causes neuronal lipofuscinosis and late-onset neurological disease, Mol. Cell. Biol. 26 (2006) 2309–2316.
[23] J.A. Johnston, C.L. Ward, R.R. Kopito, Aggresomes: a cellular response to misfolded proteins, J. Cell Biol. 143 (1998) 1883–1898.
[24] E. Gasteiger, C. Hoogland, A. Gattiker, S. Duvaud, M.R. Wilkins, R.D. Appel, A. Bairoch, Protein identification and analysis tools on the ExPASy server, in: J.M. Walker (Ed.), The proteomics protocols handbook, Humana Press, 2005, pp. 571–607.
[25] T. Ishida, K. Kinoshita, Prediction of disordered regions in proteins based on the meta approach, Bioinformatics 24 (2008) 1344–1348.
[26] M.J. Thompson, S.A. Sievers, J. Karanicolas, M.I. Ivanova, D. Baker, D. Eisenberg, The 3D profile method for identifying fibril-forming segments of proteins, Proc. Natl. Acad. Sci. U. S. A. 103 (2006) 4074–4078.
[27] L. Goldschmidt, P.K. Teng, R. Riek, D. Eisenberg, Identifying the amylome, proteins capable of forming amyloid-like fibrils, Proc. Natl. Acad. Sci. U. S. A. 107 (2010) 3487–3492.
[28] Y. Zhang, I-TASSER server for protein 3D structure prediction, BMC Bioinformatics 9 (2008) 40.
[29] A. Roy, A. Kucukural, Y. Zhang, I-TASSER: a unified platform for automated protein structure and function prediction, Nat. Protoc. 5 (2010) 725–738.
[30] S. Ventura, Sequence determinants of protein aggregation: tools to increase protein solubility, Microb. Cell Fact. 4 (2005) 11.
[31] C. Wurth, W. Kim, M.H. Hecht, Combinatorial approaches to probe the sequence determinants of protein aggregation and amyloidogenicity, Protein Pept. Lett. 13 (2006) 279–286.
[32] A.K. Dunker, J.D. Lawson, C.J. Brown, R.M. Williams, P. Romero, J.S. Oh, C.J. Oldfield, A.M. Campen, C.M. Ratliff, K.W. Hipps, J. Ausio, M.S. Nissen, R. Reeves, C. Kang, C.R. Kissinger, R.W. Bailey, M.D. Griswold, W. Chiu, E.C. Garner, Z. Obradovic, Intrinsically disordered protein, J. Mol. Graph. Model. 19 (2001) 26–59.
[33] R. Linding, J. Schymkowitz, F. Rousseau, F. Diella, L. Serrano, A comparative study of the relationship between protein structure and beta-aggregation in globular and intrinsically disordered proteins, J. Mol. Biol. 342 (2004) 345–353.
[34] M. Belli, M. Ramazzotti, F. Chiti, Prediction of amyloid aggregation in vivo, EMBO Rep. 12 (2011) 657–663.
[35] S.J. Hamodrakas, Protein aggregation and amyloid fibril formation prediction software from primary sequence: towards controlling the formation of bacterial inclusion bodies, FEBS J. 278 (2011) 2428–2435.
[36] M.R. Sawaya, S. Sambashivan, R. Nelson, M.I. Ivanova, S.A. Sievers, M.I. Apostol, M.J. Thompson, M. Balbirnie, J.J.W. Wiltzius, H.T. McFarlane, A.Ø. Madsen, C. Riekel, D. Eisenberg, Atomic structures of amyloid cross-β spines reveal varied steric zippers, Nature 447 (2007) 453–457.
[37] F. Chiti, C.M. Dobson, Protein misfolding, functional amyloid, and human disease, Annu. Rev. Biochem. 75 (2006) 333–366.
[38] R. Nelson, D. Eisenberg, Recent atomic models of amyloid fibril structure, Curr. Opin. Struct. Biol. 16 (2006) 260–265.
[39] R.S. Harrison, P.C. Sharpe, Y. Singh, D.P. Fairlie, Amyloid peptides and proteins in review, Rev. Physiol. Biochem. Pharmacol. 159 (2007) 1–77.
[40] J. Reumers, F. Rousseau, J. Schymkowitz, Multiple evolutionary mechanisms reduce protein aggregation, Open Biol. 2 (2009) 176–184.
[41] L. Masino, G. Nicastro, L. Calder, M. Vendruscolo, A. Pastore, Functional interactions as a survival strategy against abnormal aggregation, FASEB J. 25 (2011) 45–54.
[42] B. Wang, G.P. Shi, P.M. Yao, Z. Li, H.A. Chapman, D. Brömme, Human cathepsin F. Molecular cloning, functional expression, tissue localization, and enzymatic characterization, J. Biol. Chem. 273 (1998) 32000–32008.
[43] J.D. Ho, Y. Meltser, J.J. Buggy, J.T. Palmer, K.C. Elrod, H. Chan, K.D. Mortara, J.R. Somoza, Expression, purification, crystallization and preliminary X-ray diffraction studies of human cathepsin F complexed with an irreversible vinyl sulfone inhibitor, Acta Crystallogr. D 58 (2002) 2187–2190.
[44] A.L. Tarentino, C.M. Gomez, T.H. Plummer, Deglycosylation of asparagine-linked glycans by peptide: N-glycosidase F, Biochemistry 24 (1985) 4665–4671.
[45] M. Fonovič, D. Brömme, V. Turk, B. Turk, Human cathepsin F: expression in baculovirus system, characterization and inhibition by protein inhibitors, Biol. Chem. 385 (2004) 505–509.
[46] C. Ohl, C. Albach, P. Altevogt, B. Schmitz, N-glycosylation patterns of HSA/CD24 from different cell lines and brain homogenates: a comparison, Biochimie 85 (2003) 565–573.
[47] . A.C. Vestrheim, A. Moen, W. Egge-Jacobsen, D.B. Bratlie, T.E. Michaelsen, Different glycosylation pattern of human IgG1 and IgG3 antibodies isolated from transiently as well as permanently transfected cell lines, Scand. J. Immunol. 77 (2013) 419–428.
[48] B. Wiederanders, Structure-function relationships in class CA1 cysteine peptidase propeptides, Acta Biochim. Pol. 50 (2003) 691–713.
[49] A. Waghray, D. Keppler, B.F. Sloane, L. Schuger, Y.Q. Chen, Analysis of a truncated form of cathepsin H in human prostate tumor cells, J. Biol. Chem. 277 (2002) 11533–11538.
[50] B. Goulet, A. Baruch, N.-S. Moon, M. Poirier, L.L. Sansregret, A. Erickson, M. Bogyo, A. Nepveu, A cathepsin L isoform that is devoid of a signal peptide localizes to the nucleus in S phase and processes the CDP/Cux transcription factor, Mol. Cell 14 (2004) 207–219.
[51] D. Shen, J. Coleman, E. Chan, T.P. Nicholson, L. Dai, P.W. Sheppard, W.F. Patton, Novel cell- and tissue-based assays for detecting misfolded and aggregated protein accumulation within aggresomes and inclusion bodies, Cell Biochem. Biophys. 60 (2011) 173–185.
[52] K. Zatloukal, C. Stumptner, A. Fuchsbichler, H. Heid, M. Schnoelzer, L. Kenner, R. Kleinert, M. Prinz, A. Aguzzi, H. Denk, p62 Is a common component of cytoplasmic inclusions in protein aggregation diseases, Am. J. Pathol. 160 (2002) 255–263.
[53] R. García-Mata, Z. Bebök, E.J. Sorscher, E.S. Sztul, Characterization and dynamics of aggresome formation by a cytosolic GFP-chimera, J. Cell Biol. 146 (1999) 1239–1254.
[54] A. Williams, L. Jahreiss, S. Sarkar, S. Saiki, F.M. Menzies, B. Ravikumar, D.C. Rubinsztein, Aggregate-prone proteins are cleared from the cytosol by autophagy: therapeutic implications, Curr. Top. Dev. Biol. 76 (2006) 89–101.
[55] S. Beaudoin, K. Goggin, C. Bissonnette, C. Grenier, X. Roucou, Aggresomes do not represent a general cellular response to protein misfolding in mammalian cells, BMC Cell Biol. 9 (2008) 59.
[56] E.S.P. Wong, J.M.M. Tan, W.E. Soong, K. Hussein, N. Nukina, V.I. Dawson, T.M. Dawson, A.M. Cuervo, K.L. Lim, Autophagy-mediated clearance of aggresomes is not a universal phenomenon, Hum. Mol. Genet. 17 (2008) 2570–2582.
[57] I. Tanida, T. Ueno, E. Kominami, LC3 and autophagy, Methods Mol. Biol. 445 (2008) 77–88.
[58] G. Bjørkøy, T. Lamark, A. Brech, H. Outzen, M. Perander, A. Øvervatn, H. Stenmark, T. Johansen, p62/SQSTM1 forms protein aggregates degraded by autophagy and has a protective effect on huntingtin-induced cell death, J. Cell Biol. 171 (2005) 603–614.
[59] S. Pankiv, T.H. Clausen, T. Lamark, A. Brech, J.-A. Bruun, H. Outzen, A. Øvervatn, G. Bjørkøy, T. Johansen, p62/SQSTM1 binds directly to Atg8/LC3 to facilitate degradation of ubiquitinated protein aggregates by autophagy, J. Biol. Chem. 282 (2007) 24131–24145.
[60] C. Grenier, C. Bissonnette, L. Volkov, X. Roucou, Molecular morphology and toxicity of cytoplasmic prion protein aggregates in neuronal and non-neuronal cells, J. Neurochem. 97 (2006) 1456–1466.

[61] M. Kristiansen, M.J. Messenger, P.C. Klöhn, S. Brandner, J.D.F. Wadsworth, J. Collinge, S.J. Tabrizi, Disease-related prion protein forms aggresomes in neuronal cells leading to caspase activation and apoptosis, J. Biol. Chem. 280 (2005) 38851–38861.
[62] X.L. Li, G.R. Wang, Y.Y. Jing, M.M. Pan, C.F. Dong, R.M. Zhou, Z.Y. Wang, Q. Shi, C. Gao, X.P. Dong, Cytosolic PrP induces apoptosis of cell by disrupting microtubule assembly, J. Mol. Neurosci. 43 (2011) 316–325.
[63] X. Wang, C.F. Dong, Q. Shi, S. Shi, G.R. Wang, Y.J. Lei, K. Xu, R. An, J.M. Chen, H.Y. Jiang, C. Tian, C. Gao, Y.J. Zhao, J. Han, X.P. Dong, Cytosolic prion protein induces apoptosis in human neuronal cell SH-SY5Y via mitochondrial disruption pathway, BMB Rep. 42 (2009) 444–449.
[64] K.R. Smith, H.-H.M. Dahl, L. Canafoglia, E. Andermann, J. Damiano, M. Morbin, A.C. Bruni, G. Giaccone, P. Cossette, P. Saftig, J. Grötzinger, M. Schwake, F. Andermann, J.F. Staropoli, K.B. Sims, S.E. Mole, S. Franceschetti, N.A. Alexander, J.D. Cooper, H.A. Chapman, S. Carpenter, S.F. Berkovic, M. Bahlo, Cathepsin F mutations cause type B Kufs disease, an adult-onset neuronal ceroid lipofuscinosis, Hum. Mol. Genet. 22 (2013) 1417–1423.
[65] W.L. DeLano, The PyMOL molecular graphics system, Computer Program, 2002, DeLano Scientific, San Carlos, CA, USA, 2002.

jbc The Journal of Biological Chemistry
AFFINITY SITES
ASBMB American Society for Biochemistry and Molecular Biology

Immunology:

A Role for Stefin B (Cystatin B) in Inflammation and Endotoxemia

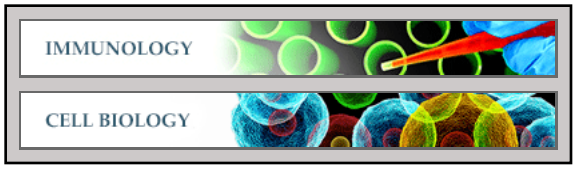

Katarina Maher, Barbara Jeric Kokelj, Miha Butinar, Georgy Mikhaylov, Mateja Mancek-Keber, Veronika Stoka, Olga Vasiljeva, Boris Turk, Sergei A. Grigoryev and Natasa Kopitar-Jerala

J. Biol. Chem. 2014, 289:31736-31750.
doi: 10.1074/jbc.M114.609396 originally published online October 6, 2014

Access the most updated version of this article at doi: 10.1074/jbc.M114.609396

Find articles, minireviews, Reflections and Classics on similar topics on the JBC Affinity Sites.

Alerts:
- When this article is cited
- When a correction for this article is posted

Click here to choose from all of JBC's e-mail alerts

This article cites 68 references, 22 of which can be accessed free at
http://www.jbc.org/content/289/46/31736.full.html#ref-list-1

Downloaded from http://www.jbc.org/ at Jozef Stefan Institut on January 20, 2015

THE JOURNAL OF BIOLOGICAL CHEMISTRY VOL. 289, NO. 46, pp. 31736–31750, November 14, 2014
© 2014 by The American Society for Biochemistry and Molecular Biology, Inc. Published in the U.S.A.

A Role for Stefin B (Cystatin B) in Inflammation and Endotoxemia*

Received for publication, September 5, 2014 Published, JBC Papers in Press, October 6, 2014, DOI 10.1074/jbc.M114.609396

Katarina Maher[‡§¶1,2], Barbara Jerič Kokelj[‡§1], Miha Butinar[‡§1], Georgy Mikhaylov[‡§], Mateja Manček-Keber[‖], Veronika Stoka[‡§], Olga Vasiljeva[‡], Boris Turk[‡ ‡‡§§], Sergei A. Grigoryev[¶], and Nataša Kopitar-Jerala[‡3]**

*From the [‡]Department of Biochemistry, Molecular and Structural Biology, Jožef Stefan Institute, Ljubljana SI-1000, Slovenia, the [§]Jožef Stefan International Postgraduate School, Jamova 39, Ljubljana SI-1000, Slovenia, the [‖]Department of Biotechnology, National Institute of Chemistry, Hajdrihova 19, Ljubljana SI-1000, Slovenia, the **EN-FIST Centre of Excellence, SI-1000 Ljubljana, Slovenia, the [‡‡]Centre of Excellence for Integrated Approaches in Chemistry and Biology of Proteins (CIPKeBiP), Jamova 39, SI-1000 Ljubljana, Slovenia, the [§§]Department of Chemistry and Biochemistry, Faculty of Chemistry and Chemical Technology, University of Ljubljana, Cesta v Mestni log 88A, SI-1000 Ljubljana, Slovenia, and the [¶]Department of Biochemistry and Molecular Biology, College of Medicine, Penn State University, Hershey, Pennsylvania 17033*

Background: The lack of cysteine cathepsin inhibitor, stefin B (cystatin B), results in progressive myoclonus epilepsy, type 1.
Results: Stefin B deficiency in macrophages resulted in increased inflammasome activation.
Conclusion: Stefin B-deficient mice are significantly more sensitive to e LPS-induced sepsis due to increased caspase-11 expression and mitochondrial damage.
Significance: Stefin B has an important role in limiting the inflammatory response during LPS-induced sepsis.

Stefin B (cystatin B) is an endogenous cysteine cathepsin inhibitor, and the loss-of-function mutations in the stefin B gene were reported in patients with Unverricht-Lundborg disease (EPM1). In this study we demonstrated that stefin B-deficient (StB KO) mice were significantly more sensitive to the lethal LPS-induced sepsis and secreted higher amounts of pro-inflammatory cytokines IL-1β and IL-18 in the serum. We further showed that increased caspase-11 gene expression and better pro-inflammatory caspase-1 and -11 activation determined in StB KO bone marrow-derived macrophages resulted in enhanced IL-1β processing. Pretreatment of macrophages with the cathepsin inhibitor E-64d did not affect secretion of IL-1β, suggesting that the increased cathepsin activity determined in StB KO bone marrow-derived macrophages is not essential for inflammasome activation. Upon LPS stimulation, stefin B was targeted into the mitochondria, and the lack of stefin B resulted in the increased destabilization of mitochondrial membrane potential and mitochondrial superoxide generation. Collectively, our study demonstrates that the LPS-induced sepsis in StB KO mice is dependent on caspase-11 and mitochondrial reactive oxygen species but is not associated with the lysosomal destabilization and increased cathepsin activity in the cytosol.

Sepsis, a systemic inflammatory response syndrome induced by infection, is characterized by multiple organ failures and hemodynamic shock (1). Lipopolysaccharide (LPS), a component on the surface of Gram-negative bacteria, is a potent inducer of sepsis and inflammation and acts by stimulating immune system cells to produce pro-inflammatory cytokines. Upon LPS binding and receptor homodimerization, the signal-transducing adaptor proteins become associated with the receptor and trigger the downstream signaling pathway leading to the activation of NF-κB (2, 3). Members of the NLR family (NLR proteins, Nlrp) and the adaptor ASC form multiprotein complexes, termed inflammasomes, that are required for the activation of the pro-inflammatory caspase-1 that processes pro-interleukin (IL)-1β and pro-IL-18 into mature forms (4, 5). The inflammasome activity should be tightly regulated to defend the host while limiting the excessive inflammation and immunopathology. Nlrp3 inflammasome is the best characterized as a central regulator of inflammation, which regulates caspase-1 and IL-1β production in myeloid cells (4, 5). In this pathway, TLR[4] signaling provides the priming step that up-regulates Nlrp3 and pro-IL-1β gene expression (6). Besides the priming step, there are three main cellular processes described in the literature that lead to Nlrp3 inflammasome activation (5, 7). The first is the pannexin-1 membrane pore formation via the ATP-gated P2X7 ion channel and K^+ efflux (8). The second way of Nlrp3 activation is the phagocytosis of crystalline or particulate structures. The proposed mechanism suggests that phagocytosis triggers lysosomal destabilization and subsequent release of the lysosomal content, including lysosomal cathepsin proteases, into the cytosol. However, it is not known yet whether the cathepsins interact directly with the inflammasome or whether the process involves molecules activated by the cathepsins (9, 10). The third model proposes that genera-

* This work was supported in part by Slovenian Research Agency Grants J3-0612 (to N. K. J.) and P-0140 (to B. T.) and Commissariat a l'Énergie Atomique et aux Énergies Alternatives France-Slovenia grant (to N. K. J.).
[1] Supported by the Slovenian Young Researcher Program.
[2] Recipient of EMBO Short Term Scholarship ASTF 50-2012 to visit the College of Medicine, Pennsylvania State University, Hershey, PA 17033.
[3] To whom correspondence should be addressed. Tel.: 386-1-4773510; Fax: 386-1-477-3984; E-mail: natasa.kopitar@ijs.si.

[4] The abbreviations used are: TLR, toll-like receptor; BMDM, bone marrow-derived macrophage; mtROS, mitochondrial reactive oxygen species; StB, stefin B-deficient; SEAP, secreted embryonic alkaline phosphatase; STS, staurosporin; Z, benzyloxycarbonyl; AMC, 7-amino-4-methylcoumarin hydrochloride; LDH, lactate dehydrogenase; TRIF, TIR domain-containing adapter-inducing IFN-β.

Downloaded from http://www.jbc.org/ at Jozef Stefan Institut on January 20, 2015

tion of the reactive oxygen species up-regulates activation of the Nlrp3 inflammasome. The role of mitochondria in the inflammasome activation has been recently elucidated by blocking the key enzymes of the respiratory chain, which resulted in the loss of mitochondrial membrane potential, a vast ROS generation and IL-1β secretion (11, 12). Recently, in addition to the canonical (LPS and ATP) Nlrp3 inflammasome signaling, a new noncanonical inflammasome pathway has been described, where caspase-11 is engaged in response to a number of Gram-negative bacteria. Caspase-11 is involved in Nlrp3-dependent activation of caspase-1 leading to IL-1β processing and secretion or in the Nlrp3- and caspase-1-independent pathway leading to cell death (13–16). It is worth noting that the mouse caspase-11 (gene name *Casp4*) has 46% similarities to caspase-1 and is orthologous to human caspases-4 and -5 (17). Endolysosomal cysteine cathepsins were first described as proteases involved in the protein breakdown within the lysosomes, but many studies revealed their important role in other cellular processes, such as apoptosis, cancer progression, inflammation, cell homeostasis, pathogen recognition, and its elimination (18, 19). Their activity is regulated by the interaction with the endogenous inhibitors, such as cystatins, tyrophins, and some of the serpins (20–23). Stefin B belongs to the type one cystatins and it is up-regulated in the activated macrophages (20, 22). In the nucleus stefin B interacts with the histones and cathepsin L (24). Mutations in the gene of stefin B are associated with the neurodegenerative disease known as the Unverricht-Lundborg disease or progressive myoclonus epilepsy of type 1 (EPM1) (25, 26). EPM1 is characterized by the cerebellar granule neuron apoptosis, progressive ataxia, and myoclonic epilepsy (25, 27). StB KO mice have increased apoptosis in the cerebellum and develop ataxia (28). Houseweart *et al.* (29) reported that the removal of cathepsin B from StB KO mice reduced the neuronal apoptosis but did not rescue the ataxia and seizure phenotype, suggesting that stefin B has alternative function(s) other than protease inhibition. Stefin B was found as a part of multiprotein complexes in the cerebellum; interestingly, none of the identified proteins interacting with stefin B was a protease (30). The precise mechanism by which stefin B influences the progression of the disease is not yet clear.

In this study, we describe a series of *in vivo* and *in vitro* experiments showing that stefin B deficiency profoundly influences the Nlrp3 inflammasome activation and viability of mice in response to LPS. In particular, the data strongly suggest that the lack of stefin B results in an increase of caspase-11 expression, pro-inflammatory cytokine IL-1β and IL-18 serum concentrations, and mitochondrial ROS formation. Thus, the traits observed in StB KO mice result from an increased sensitivity of these mice to inflammation rather than increased enzymatic activity of cathepsin proteases.

EXPERIMENTAL PROCEDURES

General Reagents

LPS from *Escherichia coli* (*E. coli* 055:B5, Sigma) was used at a final concentration of 100 ng/ml for the cellular studies. ATP was obtained from Sigma (A7699) and used at a final concentration of 5 mM ATP for 20 min. Recombinant mouse interferon-β (IFN-β) (eBioscience) was used at a final concentration of 100 units/ml. Antibodies used in Western blotting were purchased from Abcam, and anti-caspase-1 (ab108362), anti-caspase-11 (ab10454), anti-IL-18 (ab71495), anti-stefin B (ab53725), anti-STAT1 (ab3987), anti-STAT1 Y 701 (9171S) were from Cell Signaling. 3ZD anti-IL-1β mouse monoclonal antibodies were obtained from the National Cancer Institute-Frederick, MD (31). Anti-mouse IFNAR1 antibody (AF3039) was from R&D Systems. Recombinant mouse macrophage colony-stimulating factor (M-CSF) was purchased from eBioscience and used at a final concentration of 40 ng/ml. The cysteine protease inhibitor E-64d was purchased from the Peptide Research Institute and used at a final concentration of 15 μM.

Mice

Stefin B (cystatin B)-deficient mice were created as described previously (28) and were provided by Dr. R. M. Myers, Stanford University, and bred in our local colony. Mice (8–12 weeks of age) used in this study were wild type (WT) and StB KO, fully backcrossed to FVB/N background. All mouse studies were conducted in accordance with protocols approved by the Veterinary Administration of the Republic of Slovenia and the Government Ethical Committee. Procedures for animal care and use were in accordance with the "PHS Policy on Human Care and Use of Laboratory Animals" and the "Guide for the Care and Use of Laboratory Animals."

Preparation of Macrophages

Mouse primary bone marrow-derived macrophages (BMDMs) were obtained by *ex vivo* differentiation from mouse bone marrow progenitors in the presence of M-CSF over 7 days, as described previously (32). Cells were kept in DMEM supplemented with 20% FBS, 1% penicillin/streptomycin, 2 mM L-glutamine, and M-CSF.

Plasmid and Transfections

The cDNA clone for stefin B was obtained from Image (IMAGE, 3453675). It was PCR-amplified, tagged, and cloned into pcDNA3 vector (Invitrogen) at HindIII and XhoI restriction sites (24). Raw-blue cells (InvivoGen) were transiently transfected with pcDNA3 and pcDNA/stefin B-HisTag plasmid using Lipofectamine 2000 (Invitrogen), according to the manufacturer's instructions.

NF-κB Reporter Assay

Raw-blue cells (InvivoGen) were derived from the murine RAW 264.7 macrophages with chromosomal integration of a secreted embryonic alkaline phosphatase (SEAP) reporter construct inducible by NF-κB and AP-1. Cells were grown according to the manufacturer's protocol. Upon TLR activation, the signaling pathway leads to activation of the NF-κB-dependent secretion of SEAP. Quanti-blue medium (InvivoGen) was used for detection and quantification of SEAP, according to the manufacturer's protocol. SEAP activity was assessed by reading OD at 655 nm with a microplate reader (Tecan).

Stimulations and Systemic LPS Challenge in Vivo

BMDMs were prepared as described above and seeded in 6-well plates (10^6 cells/well) for lysate preparation or in 96-well

Downloaded from http://www.jbc.org/ at Jozef Stefan Institut on January 20, 2015

plates (10^5 cells/well) for supernatant collection. Cell were stimulated as indicated. Briefly, LPS (100 ng/ml) were primed for 4 h, washed with PBS, pH 7.2, and then ATP (5 mM) was applied for 20 min. For cytokine analysis in the serum, StB KO and WT mice were intraperitoneally injected with LPS at 10 mg/kg (*E. coli* 055:B5, Sigma). Blood was taken before (0 h) and 2, 4, and 6 h after the LPS administration. The serum was prepared by removing the clot by centrifuging at 2000 rpm for 10 min in a refrigerated centrifuge; the resulting supernatants were collected, and the serum levels of the cytokines were determined by flow cytometry. For the viability study, WT and StB KO mice were injected intraperitoneally with a high dose of LPS at 30 mg/kg (*E. coli* 055:B5, Sigma) and monitored six times daily over the 96 h.

Cell Lysate Preparation and Western Blot Analysis

Monolayer BMDMs at 80% confluence were first washed with ice-cold PBS, followed by the direct addition of the radioimmune precipitation assay lysis buffer supplemented with the Complete protease inhibitor mixture (Sigma) Cell lysates were prepared as described previously (33). The protein concentration of the cell lysates was measured using the Bradford reagent (Bio-Rad). The lysates were subjected to electrophoresis on 12.5% SDS-polyacrylamide gels followed by Western blotting as described previously (33). The proteins were visualized with ECL (Amersham Biosciences) according to the manufacturer's instructions.

Cathepsin Activity Measurements

The cytosolic cathepsin activity assay was performed in a 96-well plate by using sensitive fluorogenic substrates Z-Arg-Arg-AMC (Z-RR-AMC) and Z-Phe-Arg-AMC (Z-FR-AMC) (Bachem). The treated cells were partially lysed with an acetate buffer (50 mM sodium acetate, 150 mM NaCl, 0.5 mM EDTA, pH 5.6) containing 15 μg/ml digitonin (for the cytosolic cathepsin activity) for 12 min on ice as described (34). Immediately after the incubation on ice, the substrate (30 μM)-containing acetate buffer was added, and the liberation of AMC was measured using a fluorimeter (Tecan).

Quantitative Real Time PCR

Total RNA was isolated from the BMDMs after stimulation with LPS using PureLink RNA mini kit (Ambion), followed by DNase treatment using TURBO DNA-free kit (Ambion). RNA concentrations and A_{260}/A_{230} and A_{260}/A_{280} ratios were assessed spectrophotometrically using NanoDrop, whereas RNA integrity was confirmed by 1.2% gel electrophoresis. cDNA was synthesized from RNA with Precision nanoScript Reverse Transcription kit (Primer Design Ltd.) using random nanomer primers. The following primers designed by Primer Design were used for the real time quantitative PCR: IL-1β (*Il1b*) sense, 5′-GCTATGGCAACTGTTCCTGAA-3′, and antisense, 5′-ACAGCCCAGGTCAAAGGTT-3′; IL-18 (*Il18*) sense, 5′-CCAAGTTCTCTTCGTTGACAAAA-3′, and antisense, 5′-GTCCTCTTACTTCACTGTCTTTG-3′; caspase-1 (*Casp1*) sense, 5′-CTGCGGTGTAGAAAAGAAACG-3′, and antisense, 5′-TCCATTTATTGTCCCTATACTCACT-3′; caspase-11 (*Casp4*) sense, 5′-GCTACGATGTGGTGGTGAAA-3′, and antisense, 5′-GGAATGTGCTGTCTGATGTCT-3′. Real time PCR was run on Mx3005P system (Agilent, Stratagene products) using the following thermal profile: 95 °C for 10 min, followed by 40 cycles of 95 °C for 15 s and 60 °C for 1 min. Additionally, a melting curve (55–95 °C) was performed at the end of each run. The mRNA expressions of target genes were normalized to the expression of *Gapdh* and *B2m*, which were confirmed to be the most stably expressed reference genes by mouse geNorm reference gene selection kit (Primer Design). The mRNA expression of genes was calculated considering their real time PCR efficiencies using REST 2009 (Relative Expression Software Tool) and presented as a fold increase, relative to the unstimulated cells (control). The mRNA expression levels of genes in control samples were normalized to 1.0.

Chromatin Immunoprecipitation

WT and StB KO BMDMs were grown on six 10-cm culture dishes. The attached cells were washed two times with PBS on the dish and then overlaid with 10 ml of PBS with 1% formaldehyde for fixation at room temperature for 10–15 min with occasional shaking. After fixation, the dishes were washed once with PBS containing 125 mM glycine and two times with cold PBS, and then the cell nuclei were isolated as described (35) and resuspended in 3 mM $CaCl_2$, 50 mM Tris-HCl, pH 8.0. The nuclear preparation was digested with 60 units/ml micrococcal nuclease (Nuclease7, Roche Applied Science) at 37 °C for 30 min with occasional shaking to achieve ~150-bp-long mononucleosome fragments. The reaction was terminated by 10 mM EDTA. Nuclei were centrifuged for 5 min at 7500 rpm, and the pellet was resuspended in 1 ml of L-CHIP buffer (1% SDS, 10 mM EDTA, 50 mM Tris-HCl, pH 8.0), 1 mM PMSF, and Complete protease inhibitor mixture (Sigma) and sonicated once at setting 2 for 10 s on Sonic Dismembrator (Fisher, model 100). The lysate was centrifuged at 14,000 rpm for 5 min, and the protein concentration was adjusted to 1 mg/ml with L-CHIP buffer and subjected to immunoprecipitation with antibodies against histone H3 dimethyl K9 (Abcam, ab1220 ChIP grade) as described (36). Before immunoprecipitation, an aliquot of the nuclear lysate was saved for isolation of input DNA. Immunoprecipitated (ChIP) and input chromatin (Input) were treated with 0.5 mg/ml of proteinase K (Roche Applied Science) and RNase A (Roche Applied Science) at 37 °C for 30 min and uncross-linked by incubating at 65 °C overnight. DNA was extracted twice with phenol/chloroform and once with chloroform and ethanol precipitated with glycogen (Roche Applied Science) and sodium acetate. DNA was dissolved in 50 μl of water and used to prepare libraries with NEBNext ChIP-Seq Library Prep Reagent Set for Illumina (E6200). Libraries were sequenced on an Illumina HiSeq 2500 Genome Analyzer at the Pennsylvania State University Genomic Core Facility. ChIP-sequencing reads were mapped to the mouse genome with bowtie 0.12.9 software using the default parameters and the provided index NCBI37/mm9. Sequence reads mapped to multiple genomic locations were excluded from subsequent analysis. All sequence reads and input DNA reads were normalized to genome average, and the ratio of normalized ChIP sequence *versus* the nonfractionated input DNA was calculated for the promoter-containing region (1 kb upstream of the transcrip-

Downloaded from http://www.jbc.org/ at Jozef Stefan Institut on January 20, 2015

tional start site) and the open reading frame (1 kb downstream of the transcriptional start site) of the mouse caspase-11 gene (*Casp4*).

Flow Cytometry

Detection of Cytokines in Cell Supernatants and Serum—The levels of secreted cytokines in the BMDM culture supernatants and mice sera were quantified by bead-based multiplex immunoassay for the flow cytometer (FlowCytomix™, eBioscience), according to the manufacturer's instructions.

Analysis of Lysosome Integrity—Lysosomes in primed and stimulated BMDMs were stained with the fluorescent acidotropic probe LysoTracker Green probe (Invitrogen) according to the manufacturer's instructions, as described previously (37).

Analysis of Mitochondrial Membrane Potential—The mitochondrial membrane potential ($\Delta\Psi m$) in BMDMs was determined by the MitoTracker Red CMXRos (Invitrogen) uptake, as described previously (37).

Detection of Mitochondrion-derived ROS (mtROS)—MitoSOX Red (Invitrogen) was used as a mitochondrial superoxide indicator in WT and StB-deficient BMDMs. Upon 4 h of LPS treatment, cells were washed with warm PBS and loaded with 5 μM MitoSOX in PBS for 15 min at 37 °C. ATP was added thereafter for 20 min where indicated. Cells were harvested, pelleted at 1000 rpm for 5 min, immediately resuspended in PBS, and subjected to FACS analysis. According to the manufacturer, MitoSOX Red permeates live cells and is targeted to the mitochondria. The dye was rapidly oxidized by superoxide, which upon binding to nucleic acids emits red fluorescence, which was monitored by flow cytometer using excitation/emission = 488/564–606 nm. All samples were analyzed with the FACSCalibur flow cytometer (BD Biosciences), and fluorescence intensity plots were evaluated using the CellQuest acquisitions software (BD Biosciences), version 3.3. All flow cytometry analyses were performed following live cell gating from forward and side scatter profiles.

Cytotoxicity, Lactate Dehydrogenase Release

Release of the cytoplasmic enzyme lactate dehydrogenase (LDH) into the medium was determined by the cytotoxicity detection kit (Roche Applied Science) following the manufacturer's instruction. BMDMs were lysed with 2% Triton X-100 to obtain total LDH release. The cytotoxicity was expressed as the percent of the total LDH release.

Confocal Microscopy

WT BMDMs were seeded on coverslips, left untreated, or stimulated with LPS. After the indicated treatment, the cells were washed, probed with MitoTracker Red CMXRos (100 nM) in OptiMEM for 45 min at 37 °C, then fixed with 3.7% paraformaldehyde in PBS, pH 7.2, for 15 min, and permeabilized with 0.2% Triton X-100 for 10 min in PBS. Stefin B was labeled with rabbit anti-stefin B antibodies. Fluorescence microscopy was performed using the Carl Zeiss LSM 510 confocal microscope. Secondary antibodies conjugated with Alexa Fluor 488 or Alexa Fluor 546 and rhodamine were excited with an argon (488 nm) or He/Ne (543 nm) laser, and emission was filtered using a narrow band LP 505–530 nm (green fluorescence) and 560 nm (red fluorescence) filter, respectively. Carl Zeiss LSM image software 3.0 (Correlation Plots) was used to evaluate co-localization between the two labeled proteins (*i.e.* between red and green fluorescence signals).

Statistical Analysis

Average results are presented as the mean ± S.D. from the number of assays indicated. Statistical significance of the results was determined using unpaired Student's *t* test, assuming unequal variances. Survival rates were analyzed by the Kaplan-Meier method and compared by the log-rank test.

RESULTS

StB KO Mice Are More Sensitive to LPS-induced Lethal Endotoxicosis and Secrete High Levels of IL-1β and IL-18 in the Serum Post-LPS Administration—LPS, known as endotoxin, is found in the outer membrane of various Gram-negative bacteria, yet a small dose of LPS can cause severe inflammation and septic shock (38). Therefore, a high-dose LPS injection into mice is a useful model for the study of endotoxic shock and the associated inflammatory responses. To investigate the overall importance of stefin B during the LPS-induced lethal endotoxicosis, mice were intraperitoneally injected with a high dose of LPS (30 mg/kg weight), and survival was monitored over a 96-h period (Fig. 1*A*). StB KO mice were found to be significantly more susceptible to the LPS-induced sepsis. All StB KO mice thus succumbed to the high dose of LPS up to the 60-h time point, whereas a higher proportion of the WT mice survived LPS-induced endotoxicosis up to 92 h post-injection.

Furthermore, we challenged StB KO and WT mice (8–12 weeks of age) with a lower dose of LPS (10 mg/kg weight) and analyzed the pro-inflammatory cytokine profile in the serum (Fig. 1*B*). We determined a dramatic increase in the level of IL-1β and IL-18 in the serum of StB KO mice 4 and 6 h after LPS administration, whereas IL-6 serum levels remained comparable between the WT and StB KO mice. TNF-α release was significantly higher in the serum of StB KO mice only at the 2-h time point, but not at the 4- and 6-h post-LPS administration. These findings suggest that the lack of stefin B results in the greater susceptibility to sepsis, which is at least partly due to the increase of serum cytokines.

Transcription of Caspase-11 Is Up-regulated in LPS-stimulated StB KO BMDMs—The above results suggest that the molecular machinery regulating the IL-1 cytokine family secretion (IL-1β and IL-18), but not the IL-6 and TNF-α, is highly affected by the loss of stefin B. Our question was whether stefin B affects pro-inflammatory cytokine and caspase expression or activation. First, we examined the relative mRNA expression levels of caspases-1 and -11, IL-1β, and IL-18 4 h post-LPS stimulation in the BMDMs derived from StB KO and wild type mice (Fig. 2*A*). In line with the inducible IL-1β gene expression (39), we detected a dramatic up-regulation of the IL-1β gene expression in both WT and StB KO BMDMs in response to the LPS stimulation (50–90-fold induction). Moreover, the IL-18, caspase-1, and caspase-11 genes were also up-regulated, but to a much lesser extent. Stefin B deficiency had a minimal effect on the caspase-1, IL-1β, and IL-18 mRNA expression, whereas relative caspase-11 expression was significantly higher in StB KO

Downloaded from http://www.jbc.org/ at Jozef Stefan Institut on January 20, 2015

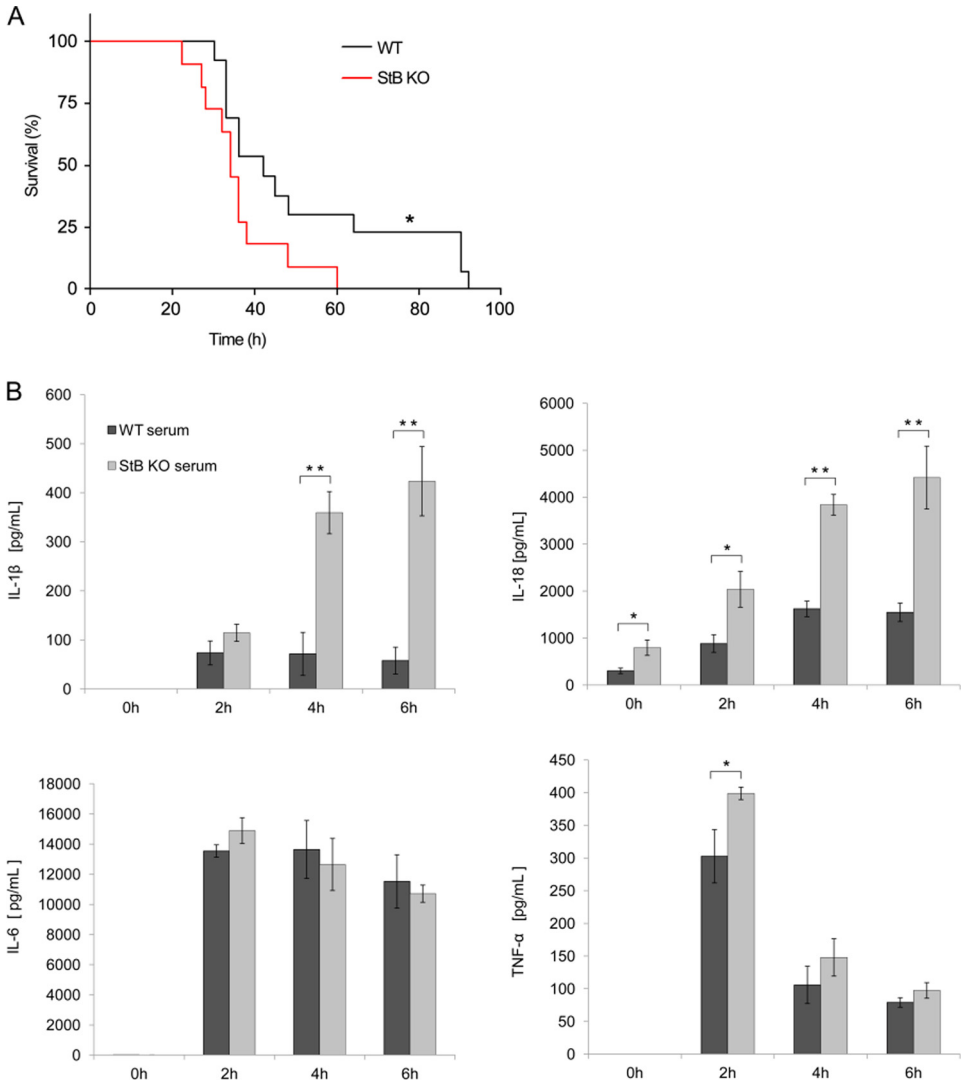

FIGURE 1. **LPS-induced lethality and LPS-triggered pro-inflammatory cytokine release *in vivo* is stefin B-dependent.** *A,* Kaplan-Meier plot showing the percentage of survival over time of age-matched wild type (*WT*) ($n = 13$) and StB KO mice ($n = 11$). *, $p < 0.05$ (log-rank (Mantel-Cox) test). Mice were injected intraperitoneally with 30 mg/kg LPS, and survival was monitored six times daily for a total of 4 days. *B,* for serum cytokine analysis, mice were injected intraperitoneally with 10 mg/kg LPS, and blood was taken 0, 2, 4, and 6 h after LPS administration. Levels of indicated cytokines in serum were quantified by bead-based multiplex for the flow cytometer. Statistical significance between WT and StB KO mice was determined in serum for IL-1β at 4 and 6 h, for IL-18 at 0, 2, 4, and 6 h, and for TNF-α at 2 h post-LPS injection. Data were obtained from three independent biological experiments performed in triplicate, and the results are presented as means ± S.D. *, $p < 0.05$; **, $p < 0.01$.

than in WT BMDMs (Fig. 2*A*). The expression of caspase-11 is regulated by NF-κB and STAT transcription factors (40). In reporter cell line RAW-blue overexpressing stefin B, we confirmed a decreased NF-κB activation upon TLR4 signaling (Fig. 2*B*). These findings therefore provide evidence that stefin B may be involved in the modulation of NF-κB activity and gene expression.

Because it has been shown that cathepsin L, an inhibitory target of stefin B, is translocated into the nucleus to process a transcriptional regulator CUX1 (41) and that the nuclear cathepsin L might affect gene expression by altering post-translational histone modifications (42, 43), we hypothesized that the effect of stefin B deficiency on gene expression could be mediated by deregulated cathepsin L. To test this hypothesis, we studied global distribution of histone H3 dimethylated at lysine 9 (H3K9me2) and histone H3 trimethylated at lysine 9 (H3K9me3), two repressive chromatin marks strongly affected by inhibition of nuclear cathepsin L by MENT (44) and by cathepsin L knock-out (43). Immunofluorescence experiments with chromosome spreads showed that global arrangement of H3K9me3 and H3K9me2 was not significantly changed in either WT or StB KO cells (data not shown). To precisely identify gene-specific distribution of H3K9me2, a repressive histone modification playing an important role in gene-specific silencing (45), we applied chromatin immunoprecipitation followed by sequencing (Chip-seq). We were particularly interested in the caspase-11 gene (*Casp4*), as it was highly up-regulated in StB KO BMDMs. As expected, we observed a decreased level of H3K9me2 at the promoter of caspase-11 in StB KO BMDMs (Fig. 2*C*). Moreover, there were essentially no differences in the distribution of the H3K4me2 variant at promoter regions in the IL-1β gene of WT and StB KO BMDMs (Fig. 2*C*). We concluded that the lack of the H3K9me2 mark at the caspase-11 promoter could contribute to the increased caspase-11 expression.

Downloaded from http://www.jbc.org/ at Jozef Stefan Institut on January 20, 2015

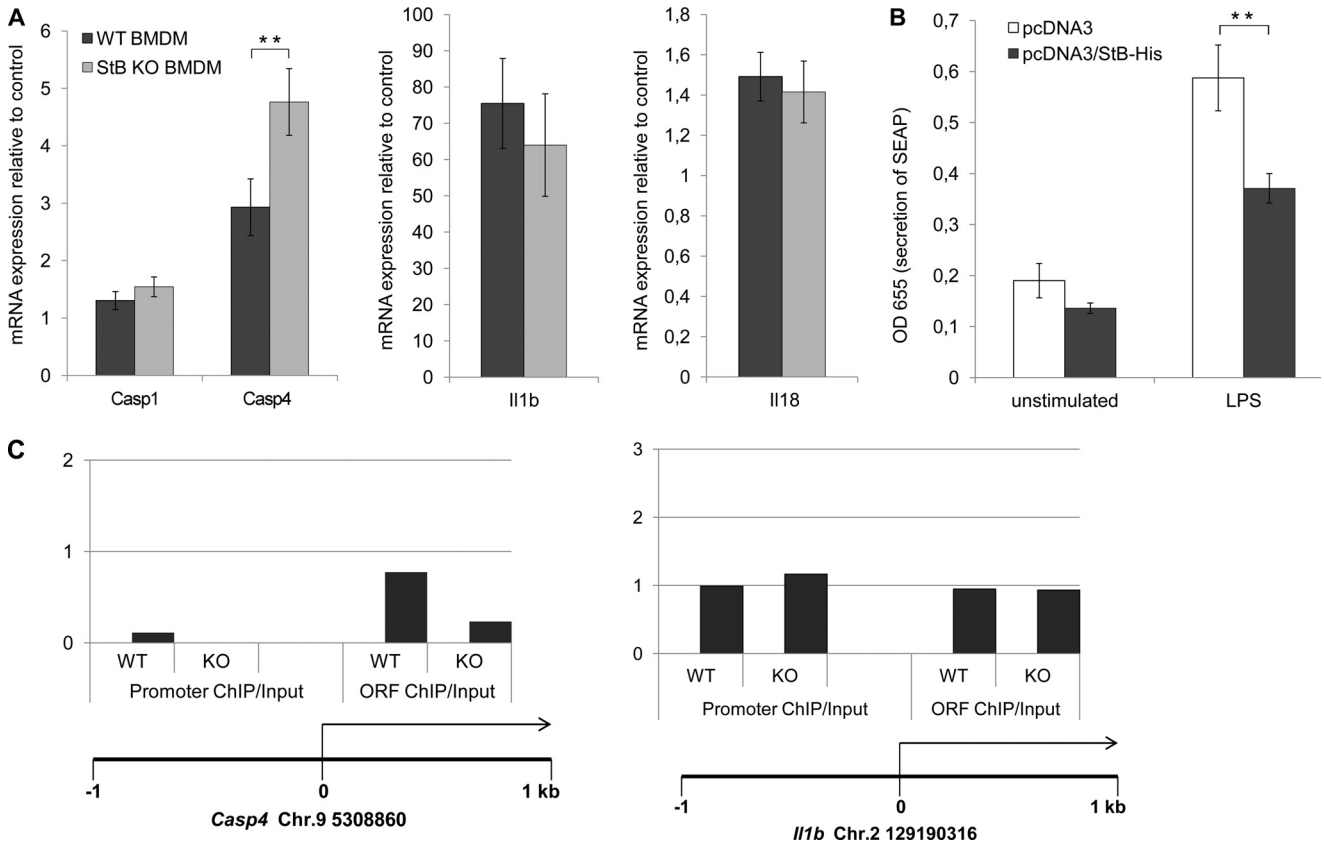

FIGURE 2. **Transcription of caspase-11 is up-regulated in LPS-stimulated StB KO BMDMs.** *A,* BMDMs were stimulated with LPS and total RNA was isolated 4 h post-stimulation. Relative mRNA expression was determined. RNA expression was normalized to reference genes *Gapdh* and *B2m* and presented as fold increase. Data were obtained from three independent experiments performed in triplicate, and the results are presented as means ± S.D. **, $p < 0.01$. *B,* increased expression of stefin B diminished NF-κB activation. RAW-blue cells (InvivoGen) were transfected with empty (control) pcDNA3 vector or pcDNA3/Stefin B-HisTag to induce stefin B overexpression. SEAP activity was assessed by reading the OD at 655 nm. *C,* fold enrichment (*ChIP/Input*) of H3K9me2 immunoprecipitated nucleosomes at the promoter and the open reading frame (*ORF*) downstream of the transcriptional start of the mouse caspase-11 gene (*Casp4*) IL-1β (*IL-1β*) gene.

Increased Expression of Caspase 11 Is Not Because of Activation of TRIF Pathway and Type I IFN Signaling—Rathinam *et al.* (13) reported that TLR4-TRIF-IFN-β signaling pathway is essential for caspase-11 activation. To assess the role of IFN-β in increased caspase-11 expression in StB KO BMDMs, we pretreated BMDMs with interferon α/β receptor (IFNAR1)-blocking antibody prior to LPS stimulation. Anti-IFNAR1 antibody treatment did not diminish caspase-11 expression in StB KO BMDMs (Fig. 3*A*). Next, we examined the relative mRNA expression levels of IFN-β 2 h after LPS stimulation in the BMDMs derived from StB KO and WT mice, and we determined that relative IFN-β mRNA expression was lower in StB KO than in WT BMDMs (Fig. 3*B*). Fang *et al.* (46) showed that epigenetic mark H3K9me2 is a suppressor of IFN and IFN-inducible antiviral gene expression. We applied Chip-seq and determined increased levels of H3K9me2 at the promoter of IFN-β in StB KO BMDMs in comparison with WT BMDMs in normalized samples (Fig. 3*D*). This result suggested that the increased H3K9me2 mark at the IFN-β promoter could contribute to the lower IFN-β expression. The biological effects of IFN-β are mediated largely through activation of STAT1 and STAT2. We show that IFN-β-induced phosphorylation of STAT1 was significantly augmented in the absence of stefin B (Fig. 3*E*). Because IFN-β expression and signaling are decreased in StB KO BMDMs, we reasoned that that TRIF signaling is not essential for the increased caspase-11 expression determined in StB KO BMDMs.

Caspase-11 and Caspase-1 Activation Is Enhanced in StB KO BMDMs—Because the levels of IL-1β and IL-18 were highly up-regulated in the serum of LPS-injected mice, we examined the effects of stefin B deficiency on the activation of the Nlrp3 inflammasome in the BMDMs derived from StB KO and wild type mice. Pro-inflammatory caspase-11 is essential for caspase-1-independent macrophage death and caspase-1-dependent IL-1β and IL-18 production in response to inflammasome activators (15). Upon LPS priming and ATP stimulation, the formation of the p26 subunit of caspase-11 and the p10 subunit of caspase-1 was more prominent in StB KO BMDMs, suggesting a more efficient pro-inflammatory caspase proteolytic activation in StB KO BMDMs (Fig. 4). Pro-IL-1β in control samples was found at undetectable levels, which increased significantly at 4 h after LPS priming (Fig. 4), which correlates well with the inducible IL-1β gene expression (Fig. 2*A*). A high extracellular ATP concentration provides the second signal for the NLRP3 inflammasome assembly and the caspase-1-mediated processing of pro-inflammatory cytokines. The levels of IL-1β and IL-18 pro-form decreased in both genotypes upon addition of ATP; however, the drop was more evident in StB KO samples that is in line with a higher caspase-1 activation (Fig. 3). IL-1β and IL-18 mature forms were determined by Western

Downloaded from http://www.jbc.org/ at Jozef Stefan Institut on January 20, 2015

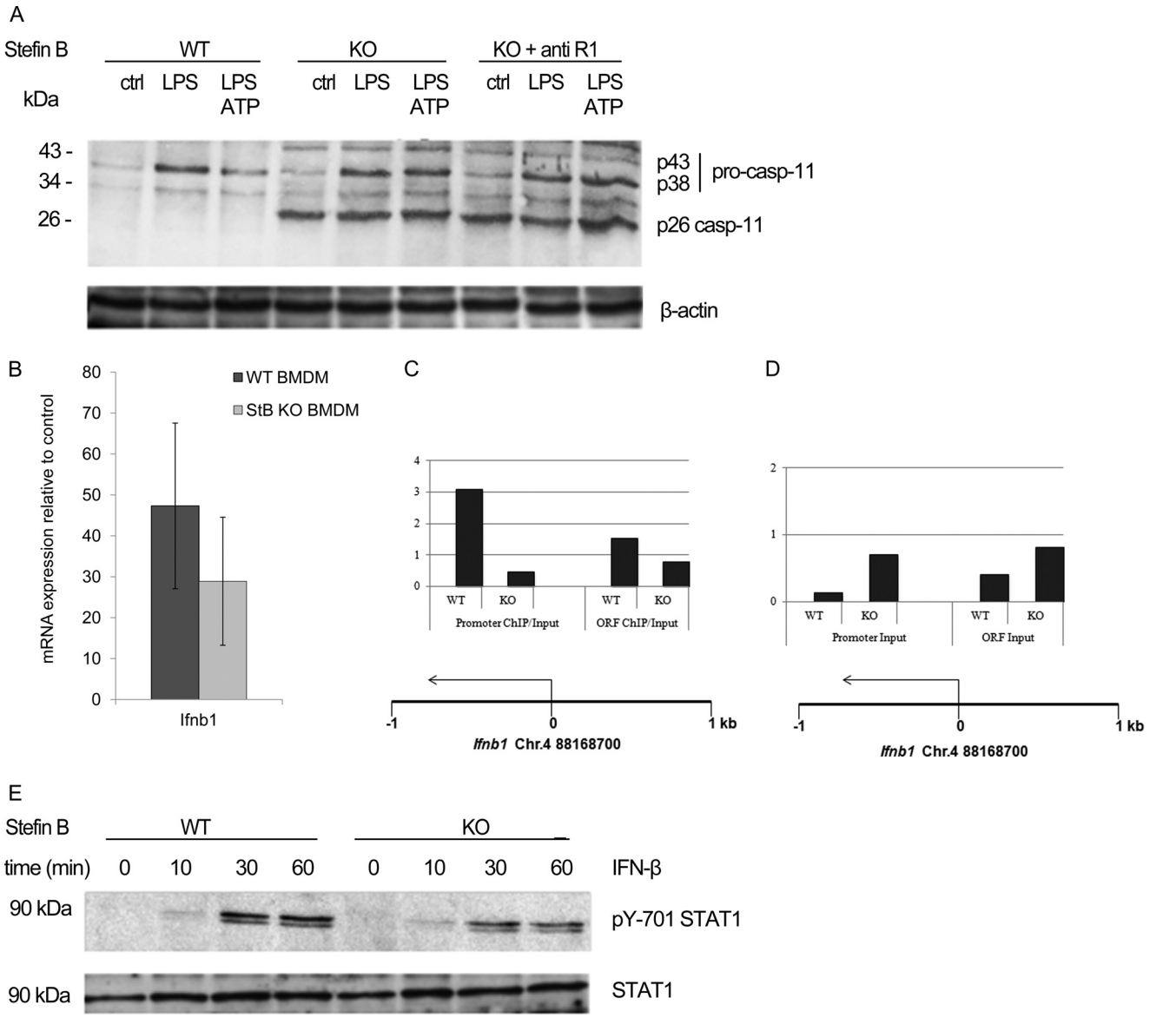

FIGURE 3. **Decreased IFN-β expression and signaling in StB KO BMDMs.** *A,* BMDMs from WT and StB KO mice were treated with inhibitory anti IFNAR1 antibody and stimulated for 4 h with LPS (100 ng/ml). Cell lysates were immunoblotted with anti-caspase-11 antibodies recognizing pro-caspase (*casp*)-11 (inactive zymogen) and subunits generated by proteolytic cleavages. Lysates were probed with anti-β-actin antibody as a loading control. Data shown are representative of three independent experiments. *B,* BMDMs were stimulated with LPS, and total RNA was isolated 2 h post-stimulation. Relative mRNA expression was determined. RNA expression was normalized to reference gene *B2m* and presented as fold increase. Data were obtained from three independent experiments performed in triplicate. *C,* fold enrichment (*ChIP/Input*) of H3K9me2-immunoprecipitated nucleosomes at the promoter and the open reading frame (*ORF*) downstream of the transcriptional start of the mouse IFN-β (*IFN-β*). *D,* input DNA normalized to genome average. *E,* immunoblotting of p-STAT1 (*pY-701*) and total STAT1 in WT and StB KO BMDM at the indicated times following stimulation with IFN-β. Data shown are representative of three independent experiments.

blots of cell culture supernatants (Fig. 3), additionally secreted IL-1β was quantified in media by a flow cytometer (Fig. 4*D*). In line with better processing of pro-form, we determined significantly increased levels of mature IL-1β in StB KO BMDM's media (Fig. 4*D*).

Inhibition of Lysosomal Cathepsin Activity Has No Effect on Nlrp3 Inflammasome Activation in StB KO BMDMs—Because it was reported that endolysosomal cathepsins participate in the NLRP3 inflammasome activation and IL-1β release (9, 10, 47), we hypothesized that the increased cathepsin activity, determined in the cells of EPM1 patients (48), is responsible for the Nlrp3 inflammasome activation in our model. A previous study showed that the loss of the lysosomal integrity resulted in the increase of cysteine cathepsin activity in the cytosol (37). First, we tested whether lysosomes get destabilized upon LPS and ATP stimulation. Lysosomal membrane integrity was determined with LysoTracker Green. LPS evoked slight attenuation in the green fluorescence, but addition of ATP increased lysosomal destabilization (Fig. 5*A*). However, stefin B deficiency had no effect on the lysosomal integrity (Fig. 5*A*). To quantify the extent of the lysosomal destabilization, we determined the cytosolic cathepsin activity by the fluorogenic broad cathepsin substrates Z-FR-AMC and Z-RR-AMC that are preferentially cleaved by cathepsin L and B (Fig. 5*B*). Cells were lysed with the 15 μg/ml digitonin extraction buffer under experimental conditions that did not disrupt lysosomes and

Downloaded from http://www.jbc.org/ at Jozef Stefan Institut on January 20, 2015

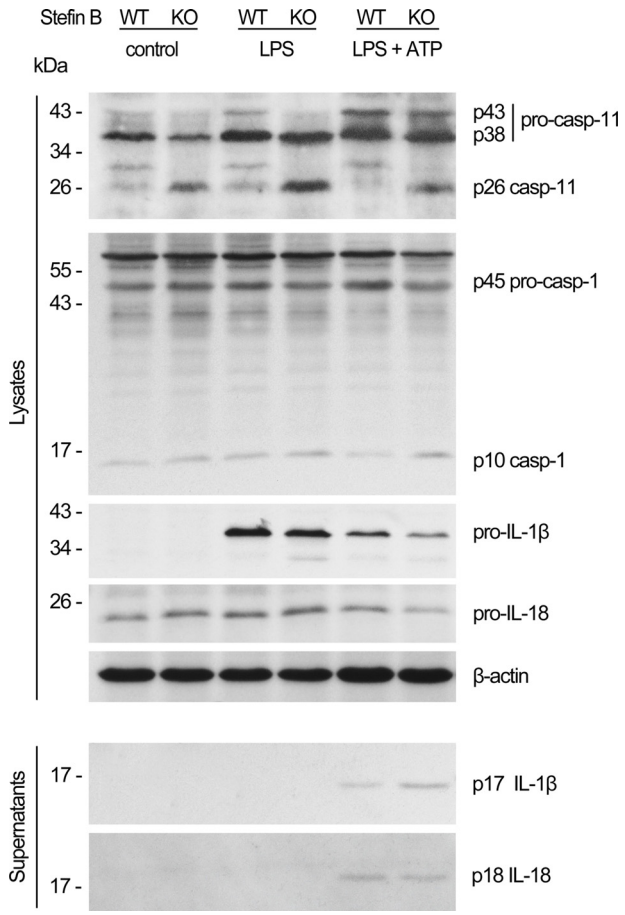

FIGURE 4. **Enhanced processing and secretion of IL-1β and IL-18 in stefin B-deficient BMDMs is caspase-1-dependent.** BMDMs from WT and StB KO mice were primed for 4 h with LPS (100 ng/ml), washed, and stimulated with ATP for 20 min (5 mM) to activate the Nlrp3 inflammasome. Cell lysates and culture supernatants were immunoblotted with the indicated antibodies. Anti-caspase-1 and anti-caspase-11 antibodies recognized pro-caspase (inactive zymogen) and subunits generated by proteolytic cleavages. Anti-IL-1β and anti-IL-18 antibodies recognized inactive pro-form in cell extracts and mature secreted cytokines in cell supernatants. Lysates were immunoblotted with anti-β-actin as a loading control. Data shown are representative of three independent experiments.

then incubated with the substrates. We determined the highest levels of cathepsin activity in ATP and LPS/ATP-stimulated StB KO BMDMs, whereas LPS itself had no effect on the cathepsin lysosomal release and activation in the cytosol (Fig. 5*B*). This finding is in line with recent studies showing that ATP-mediated lysosomal breakdown and cathepsin release were LPS-independent (49). Contrary to the hypothesis concerning the cathepsin involvement in the inflammasome activation, we found that preincubation of BMDMs with the membrane-permeable broad spectrum cathepsin inhibitor E-64d before the Nlrp3 inflammasome activation did not alter activation of pro-inflammatory caspases-1 and caspase-11 (Fig. 5*C*), and consequently, it had no effect on IL-1β release (Fig. 4*D*).

Besides IL-1β maturation and secretion, activation of caspase-1 can result in caspase-1-dependent inflammatory cell death termed pyroptosis (50). To investigate whether pro-inflammatory cytokines and cathepsins are released due to the cytolysis, we quantified the release of the cytolytic marker LDH in media (Fig. 5*E*). The difference in cell death between StB KO and WT BMDMs was not statistically significant. In addition, the levels of LDH in media were quite low (<15%), suggesting that the cell death was not the cause of cathepsin release.

LPS Induced Translocation of Stefin B into Mitochondria Where It Prevented Excessive Superoxide Generation—Recently, several studies examined the involvement of the mitochondrion-derived reactive oxygen species (mtROS) and mitochondrial DNA (mtDNA) in the inflammasome activation; however, the precise mechanism of how cellular stress induces mitochondria breakdown and ROS release is still unknown (11, 51, 52). Because we determined that the lysosomal leakage was not essential for the Nlrp3 inflammasome activation, we next investigated whether mtROS are implicated in an increased IL-1β secretion in the mice lacking stefin B. To demonstrate the intracellular localization of stefin B upon inflammasome activation, WT BMDMs were probed with the MitoTracker Red. Unstimulated cells showed no co-localization between stefin B and the MitoTracker probe, whereas in the LPS-treated WT BMDMs we determined co-localized regions (Fig. 6). Furthermore, we monitored the loss of mitochondrial membrane potential ($\Delta\Psi$m) by flow cytometry. As the mitochondrial membrane potential collapses, the MitoTracker Red CMXRos probe decreases its fluorescence. Unlike lysosomal integrity that was comparable between the WT and StB KO BMDMs (Fig. 4*A*), we detected a larger degree of damaged mitochondria in the LPS and LPS/ATP-stimulated StB KO BMDMs, suggesting a potentially protective role of stefin B in preserving the mitochondrial membrane integrity (Fig. 7*A*). Dysfunctional mitochondria are a key source of mtROS generation, and paralleled with the detected breakdown of $\Delta\Psi$m, LPS and LPS/ATP stimulations highly increased superoxide generation in StB KO and to a lesser extent in WT BMDMs (Fig. 6*B*). The above results show that in the mitochondria stefin B protects against the loss of $\Delta\Psi$m and prevents the production of mtROS.

DISCUSSION

In our study, we show that the StB KO mice are significantly more sensitive to the LPS-induced sepsis (Fig. 1*A*), suggesting an important role of stefin B during inflammatory responses. We have determined significantly increased caspase-11 mRNA expression in the LPS-stimulated StB KO BMDMs, although the differences in caspase-1, IL-1β, or IL-18 mRNA expression between StB KO and WT BMDMs were not significant (Fig. 2*A*). Kayagaki *et al.* (15) showed that the loss of caspase-11 rather than caspase-1 protected the mice from a lethal dose of LPS, and we propose that the increased lethality upon LPS challenge could be attributed to the increased caspase-11 expression in StB KO BMDMs.

The cathepsin L deficiency and cathepsin L inhibition by a nuclear protease inhibitor, MENT, were shown to cause a global rearrangement of specifically modified histones H3K9me3 and H3K9me2 from euchromatin to heterochromatin (43, 44). However, our observation that the global distribution of methylated histone 3 (H3K9me2 and H3K9me3) was not dramatically changed between stefin B-deficient and WT BMDMs suggests that the increased caspase-11 expression is unlikely to result from a global epigenetic rearrangement, but could be due

Downloaded from http://www.jbc.org/ at Jozef Stefan Institut on January 20, 2015

to some gene-specific mechanism. Stefin B was shown to interact with cathepsin L and histones H3, H2B, and H2A.Z in the nucleus (24). The cathepsin L deficiency and cathepsin L inhibition by the nuclear protease inhibitor MENT were shown to cause a global rearrangement of specifically modified histones H3K9me3 and H3K9me2 from euchromatin to heterochromatin (43, 44). The decreased level of histone variant H3K9me2 at the promoter of caspase-11 (*Casp4*) but not *Il1b* in StB KO BMDMs (Fig. 2*C*) is in accordance with the increased expression of caspase-11 in those cells. Furthermore, increased expression of stefin B in the nucleus delayed cell cycle progression, due to decreased cleavage of CUX1 transcription factor by cathepsin L (24), suggesting that the processing of CUX1 or some other gene-specific mechanism could be responsible for the up-regulation of caspase-11. Recently, it was reported that caspase-11 expression upon LPS-induced TLR4 signaling is

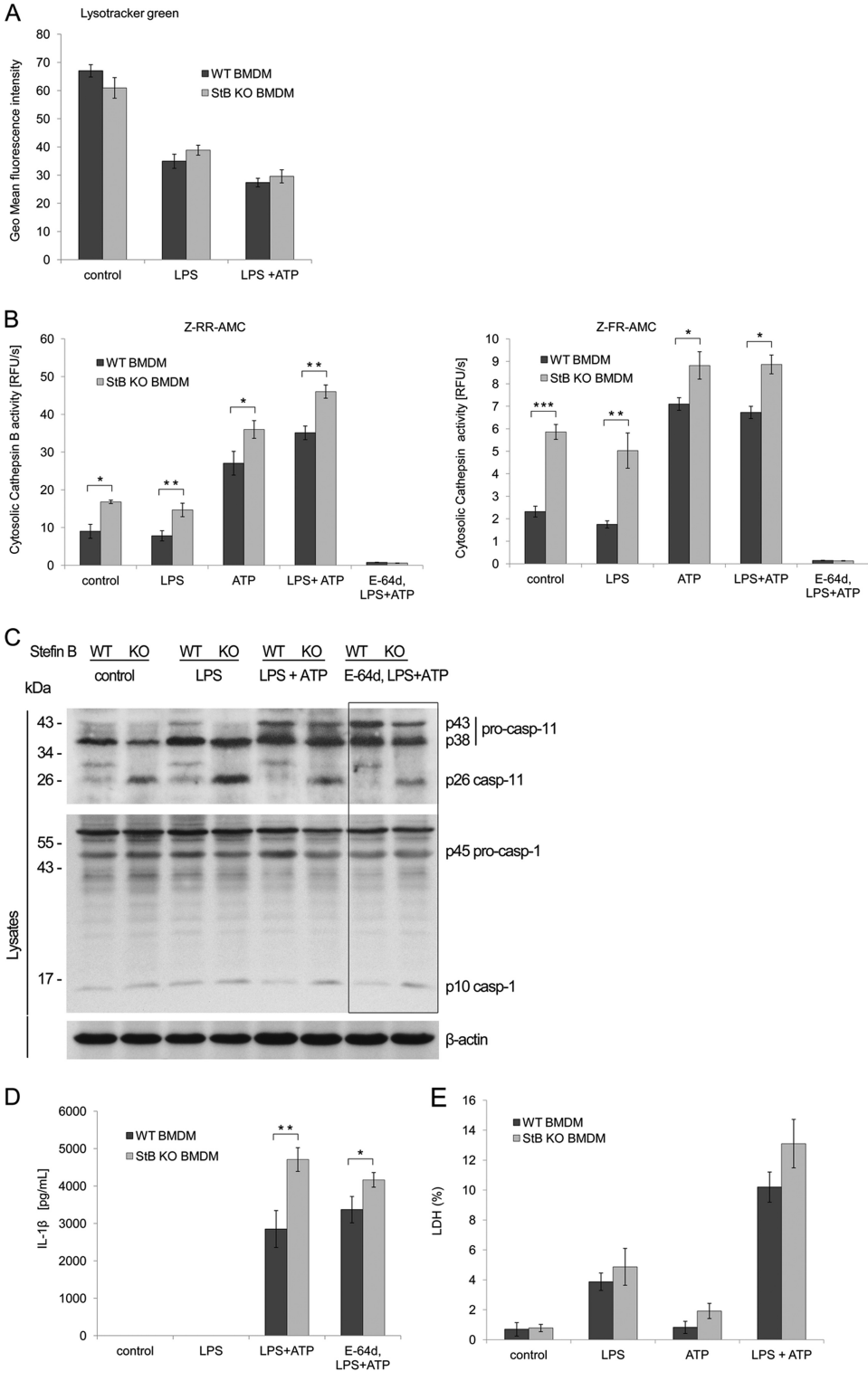

Downloaded from http://www.jbc.org/ at Jozef Stefan Institut on January 20, 2015

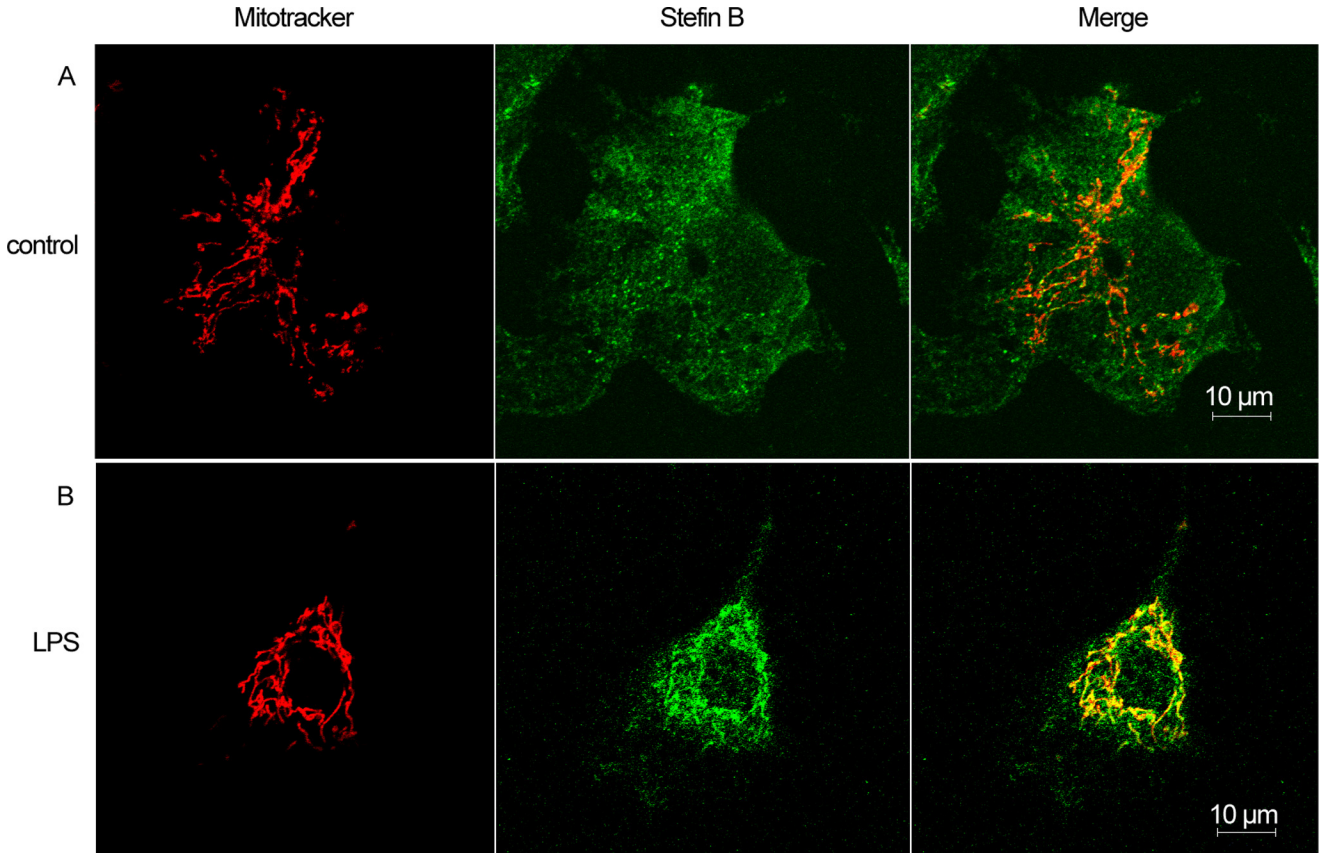

FIGURE 6. **Stefin B is localized into mitochondria upon LPS stimulation.** WT BMDMs were left untreated (*A*) or LPS (100 ng/ml)-primed (*B*). The localization of stefin B was determined by immunofluorescence. The images were merged to visualize co-localization of stefin B and mitochondria. *Scale bar,* 10 μm.

dependent on MyD88-dependent and TRIF-dependent pathways that both lead to the activation of NF-κB (16).

The activation of TRIF pathway leads to type-I interferon expression (13). Engagement of IFNAR1 then stimulates STAT1 and IRF9 signaling pathways that also contribute to the up-regulation of caspase-11 expression (13, 14). In our work, we showed that blocking of IFNAR1 with inhibitory antibody did not prevent caspase-11 up-regulation in StB KO BMDMs. In addition, we determined decreased IFN-β expression, as well STAT1 activation in StB KO BMDMs in comparison with WT BMDMs. Previous studies reported that stefin B interacted with the STAT-1 in monocyte-derived and placental macrophages (53). However, the recent study from the same group could not confirm the direct interaction of stefin B with STAT1 (54). They reported that stefin B interacted with several different proteins in HIV-1-infected macrophages; among others the two proteins were involved in JAK/STAT signaling pathway (54). In our recent work, we showed significantly lower STAT3 signaling in LPS-stimulated StB KO BMDMs, which resulted in decreased IL-10 expression (55). Therefore, we propose that stefin B interferes with the signaling pathway upstream of STAT1 and STAT3. The precise mechanism by which stefin B influences JAK/STAT signaling has yet to be elucidated.

Because stefin B overexpression was found to down-regulate the NF-κB signaling (Fig. 2*B*), we propose that stefin B could modulate the caspase-11 gene expression in an NF-κB-dependent manner. Stefin B deficiency resulted in significantly higher serum levels of IL-1β and IL-18 (Fig. 1*B*), as well as in higher levels of IL-1β (Fig. 4*D*) in BMDM media compared with the WT controls. The maturation and release of the pro-inflamma-

FIGURE 5. **Increased inflammasome activation in StB KO BMDMs is independent of lysosomal cysteine cathepsins.** *A,* biosynthesis and integrity of lysosomes were studied by LysoTracker Green probe, as described under "Experimental Procedures." The lysosomal fluorescence intensity was quantified upon LPS and ATP stimulations. Lysosomal destabilization was increased by ATP addition and was comparable between genotypes. Data were obtained from three independent biological experiments performed in triplicate, and the results are presented as means of geometric mean fluorescence intensity ± S.D. *B,* release of cathepsins into the cytosol and their activity were measured after indicated stimulations using fluorogenic substrates specific for cathepsins. Incubation of BMDMs with E-64d completely prevented cathepsin activity. *C,* BMDMs from WT and StB KO mice were primed for 4 h with LPS (100 ng/ml), washed, and stimulated with ATP for 20 min (5 mM) or primed with broad spectrum cysteine cathepsin inhibitor E-64d for 1 h (15 μM), followed by LPS and ATP stimulation. Cell lysates were immunoblotted with indicated antibodies. Lysates were immunoblotted with anti-β-actin as a loading control. Incubation of BMDMs with E-64d did not affect the processing of caspase-1 and pro-inflammatory cytokine release. Data shown are representative of three independent experiments. *D,* BMDMs were seeded into 96-well plates and stimulated as above. IL-1β release was quantified in the media by FlowCytomix™. StB KO BMDMs secreted higher amounts of IL-1β into the media compared with the WT; however, priming with E-64d did not affect IL-1β release (*n.s.,* nonsignificant difference). Data were obtained from four independent experiments performed in triplicate, and the results are presented as means ± S.D. *, $p < 0.05$; **, $p < 0.01$. *E,* viability of BMDMs was assessed by LDH release into the cell culture media upon inflammasome activation. The cytotoxicity was expressed as the percent of the total LDH release. Data were obtained from three independent experiments performed in triplicate, and the results are presented as means ± S.D. *, $p < 0.05$; **, $p < 0.01$; ***, $p < 0.001$.

Downloaded from http://www.jbc.org/ at Jozef Stefan Institut on January 20, 2015

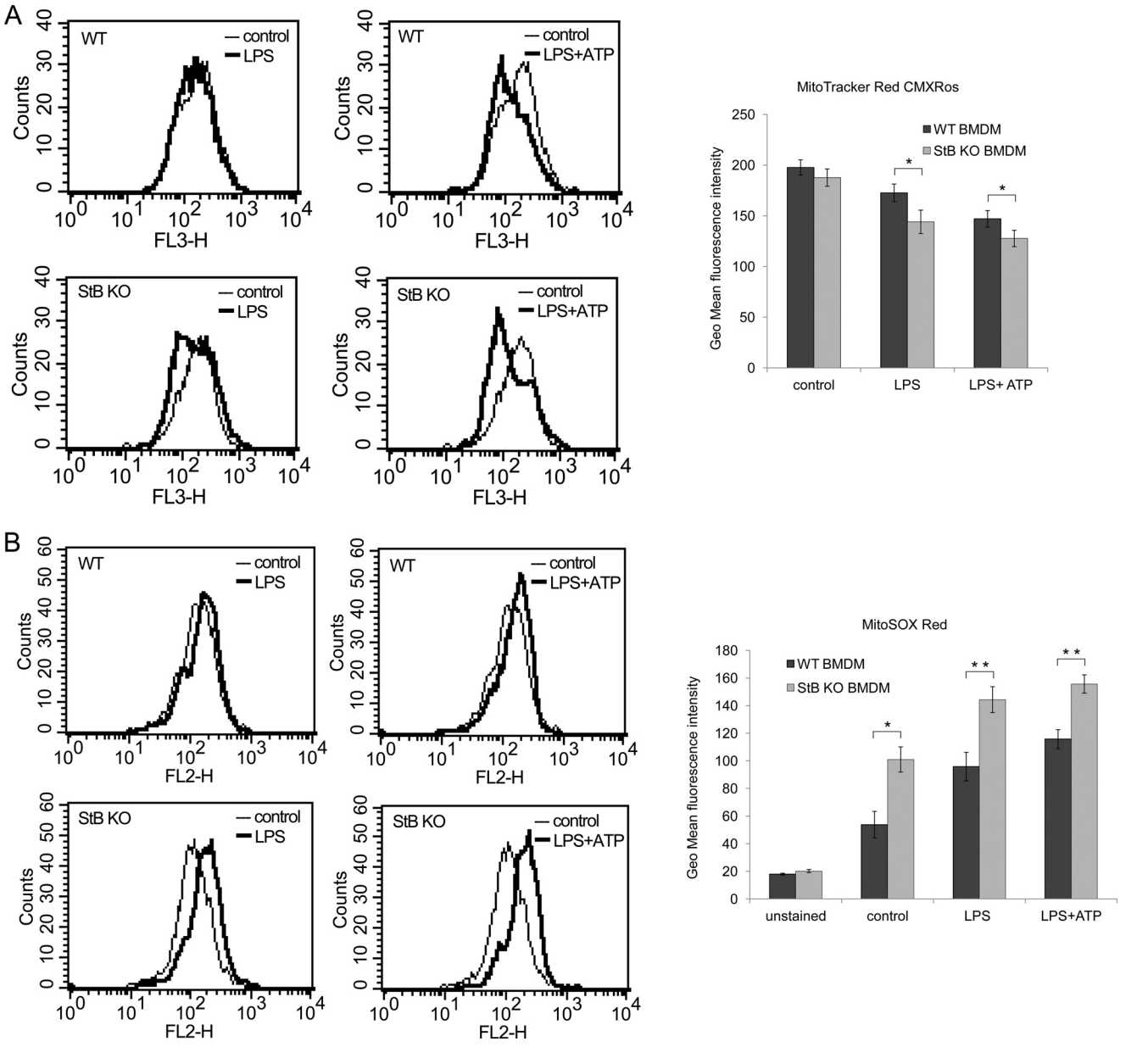

FIGURE 7. **Mitochondrial disruption resulted in increased superoxide generation in StB KO BMDMs.** *A,* MitoTracker Red CMXRos uptake was quantified by flow cytometry. The decrease in red fluorescence correlates with the loss of mitochondrial membrane potential. Mitochondria of StB KO BMDMs turned to be more susceptible to LPS and ATP stimulation. Results are representative of three independent experiments performed in duplicate and presented as histogram plots and as columns of geometric mean fluorescence intensity of three independent experiments performed in duplicate and presented as means ± S.D. *, $p < 0.05$. *B,* BMDMs were stimulated and probed with 5 μM MitoSOX Red fluorogenic dye as indicated under "Experimental Procedures." Red fluorescence was measured by flow cytometry. LPS and LPS/ATP stimulations induced significant increase in superoxide (mtROS) generation in StB KO compared with WT BMDMs. Results are representative of three independent experiments performed in duplicate and presented as histogram plots and as columns of geometric mean fluorescence intensity of three independent experiments performed in duplicate and presented as means ± S.D. *, $p < 0.05$; **, $p < 0.01$.

tory cytokines IL-1β and IL-18 are dependent on the caspase-1 activation on inflammasome (56). In noncanonical inflammasome activation, triggered by some of the bacteria, caspase-11 can interact with caspase-1 and forms a heterodimeric complex (15, 57). Both pro-caspase-11 p43 and its cleaved p26 subunit interacted with caspase-1 in the BMDMs, when exposed to cholera toxin B and *E. coli*; however, a much weaker interaction was detected upon canonical LPS/ATP stimulation (15). The differences in caspase-1 activation (Fig. 3) that we observed in StB KO and WT BMDMs upon canonical inflammasome activation with LPS/ATP could be at least partially attributed to the increased caspase-11 expression and activation. Because stefin B is essentially a cathepsin inhibitor, our first hypothesis was that the increased cathepsin activity reported before in the lymphocytes of EPM1 patients (48) and confirmed in our experiments in BMDMs (Fig. 4*B*) is responsible for the increased Nlrp3 inflammasome activation. We have shown that under our experimental conditions lysosomes get destabilized, and the released cathepsins are more active in StB KO BMDMs. However, the addition of broad spectrum inhibitor E-64d did not alter caspase-1 and -11 processing. Although the cathepsin activity was higher in StB KO BMDMs, the effect of stefin B deficiency

Downloaded from http://www.jbc.org/ at Jozef Stefan Institut on January 20, 2015

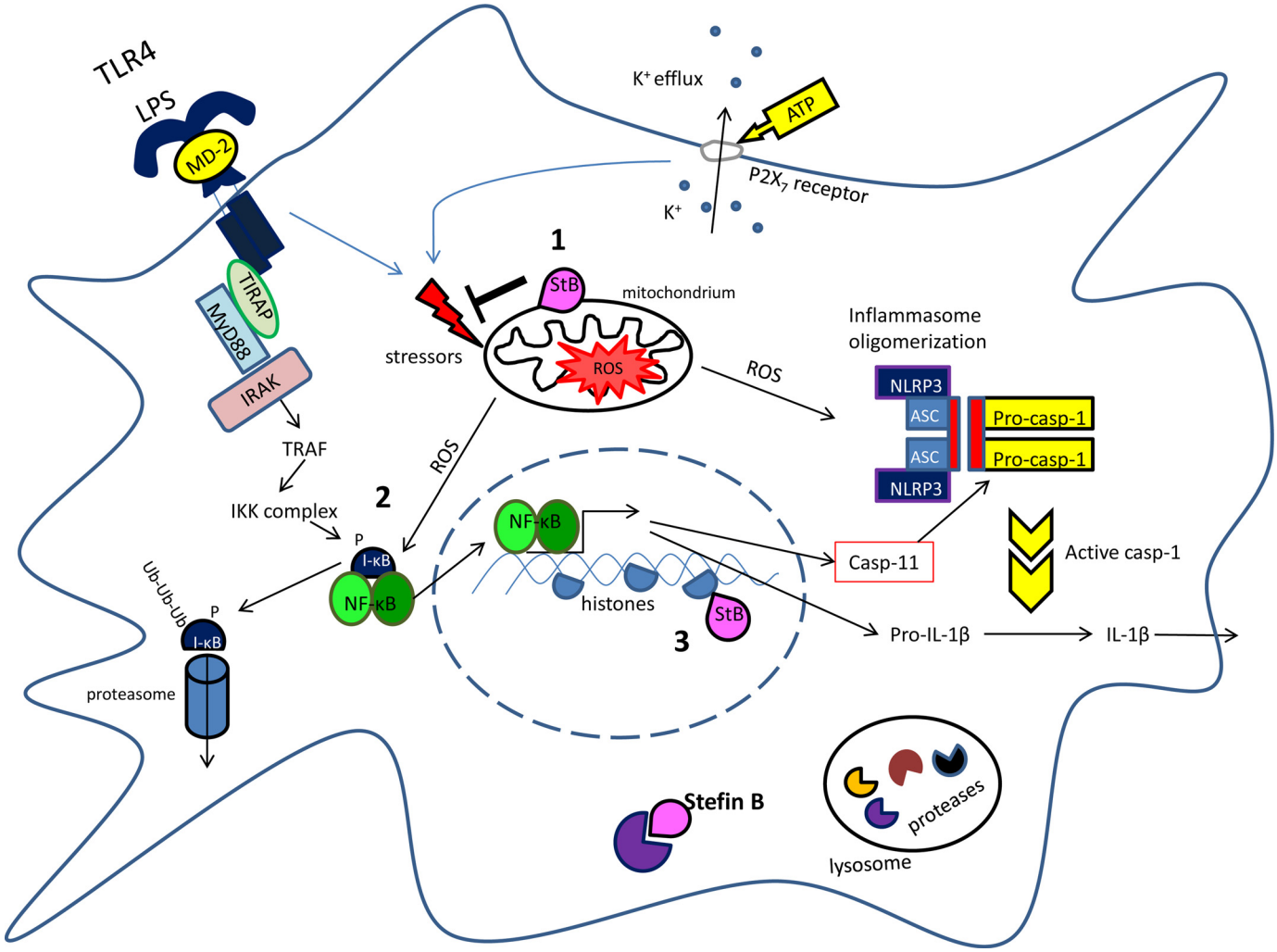

FIGURE 8. **Schematic of proposed model for the role of stefin B in Nlrp3 inflammasome activation.** *Step 1,* upon LPS stimulation stefin B translocates into mitochondria and protects mitochondrial integrity. *Step 2,* mitochondrial ROS up-regulate NF-κB activation. *Step 3,* in the nucleus, stefin B deficiency resulted in a decreased level of H3K9me2-repressive histone variant at caspase-11 promoter and increased level of caspase-11 mRNA expression.

on ATP-mediated caspase-1 activation and consequently on IL-1β processing was not reversed by the addition of the cathepsin inhibitor E-64d, a result showing that the cysteine proteinase activity is not essential for the differences in inflammasome activation in StB KO and WT BMDMs. The above results are in line with other studies, showing that ATP-induced IL-1β release was unaltered in the presence of cathepsin inhibitors (9, 49). The generation of ROS is another evolutionarily well conserved mechanism, triggered in response to infection or injury, and emerging studies strongly support the ROS pathway in the inflammasome activation (11, 58). Recent studies have shown that the mitochondrial dysfunction and relocation of the Nlrp3 complex to the mitochondrion-associated endoplasmic reticulum membranes is essential for the inflammasome activation (11, 59). Furthermore, Nakahira *et al.* (12) reported that depletion of the autophagy proteins beclin-1 or LC3B in macrophages leads to the activation of caspase-1 and the release of IL-1β and IL-18 by promoting the accumulation of dysfunctional mitochondria. These data suggested that the mitochondrial dysfunction represents an endogenous stimulus for inflammasome activation. Our findings revealed that stefin B is localized in the mitochondria upon LPS stimulation (Fig. 5), and with flow cytometry experiments, we confirmed its role in the protection of mitochondrial membrane integrity (Fig. 6*A*). Recently two independent studies demonstrated that mtROS and oxidized mtDNA released into the cytosol are key players in the Nlrp3 inflammasome activation (12, 51). Our results show that the lack of stefin B in BMDMs resulted in increased mtROS production (Fig. 6*B*). Interestingly, Lehtinen *et al.* (60) showed that stefin B protects cerebellar granule neurons from the oxidative stress, and the stefin B deficiency resulted in the increased apoptosis in the cerebellum. In addition, Butinar *et al.* (61) reported that stefin B-deficient tumor cells were significantly more sensitive to cell death upon the increased oxidative stress. Furthermore, Shimada *et al.* (51) showed that staurosporin (STS), a pro-apoptotic protein kinase inhibitor, was sufficient to act as a second signal for the NLRP3 inflammasome activation. In our previous study, we showed that STS-treated StB KO thymocytes were more sensitive to STS-induced apoptosis (33). Although we did not measure ROS in that study, other studies reported the disruption of electron transport, loss of $\Delta\psi$m, and the production of ROS in the STS-induced apoptosis (62).

Downloaded from http://www.jbc.org/ at Jozef Stefan Institut on January 20, 2015

Based on these results, the following model is proposed for the protective role of stefin B in inflammation (Fig. 8). Upon LPS stimulation, stefin B is translocated into mitochondria and protects mitochondrial integrity. Stefin B deficiency resulted in the breakdown of mitochondrial membrane potential and increased mtROS generation. It was reported that NF-κB could act as a sensor for oxidative stress (63). ROS were shown to activate NF-κB directly (64) or indirectly by other stimuli such as TNF-α and IL-1β (65). The increased mtROS detected in StB KO BMDMs upon LPS/ATP stimulation could therefore lead to the increased NF-κB activation and consequently caspase-11 expression. In the nucleus, stefin B deficiency resulted in a decreased level of H3K9me2 repressive histone variant at the caspase-11 promoter, and this could contribute to the increased level of caspase-11 mRNA expression.

Halle *et al.* (9) reported NLRP3 inflammasome activation by amyloid-β in microglia in the case of Alzheimer disease resulted in the maturation and secretion of IL-1β. Because in StB KO mice early microglial activation preceded neuronal loss in the brain (66), it is tempting to speculate that Nlrp3 inflammasome activation is an important stage of the disease progression. In addition, Penacchio *et al.* (28) reported that StB KO mice develop corneal lesions as they age. TLR and NLRP3 expression was reported also in corneal tissue (67, 68). This might suggest that the increased incidence of the corneal inflammation in StB KO mice is a consequence of the increased inflammasome activation in the cornea.

In conclusion, in this study we report for the first time the mitochondrial localization of stefin B and the increased mtROS formation in StB KO BMDMs. The increased mortality of StB KO mice upon LPS challenge could be a consequence of an increased mtROS formation that leads to an increased NF-κB activation and expression of NF-κB target genes. Our *in vivo* data indicate that stefin B may be the critical effector of deleterious inflammatory responses. Therefore, elucidating the precise mechanism by which stefin B up-regulates caspase-11 (caspase-4 in humans) expression may be essential for the treatment of sepsis.

Acknowledgments—We thank Janja Završnik for help with mouse experiments and discussions and Mojca Trstenjak-Prebanda and Loulou Kroon-Žitko for expert technical assistance. We are grateful to R. M. Myers (Stanford University, Stanford, CA) for kindly providing StB KO mice. Confocal images were taken at the Carl Zeiss Reference Center for Confocal Microscopy (LN-MCP, Institute of Pathophysiology, School of Medicine, Ljubljana, Slovenia). We thank Phillip I. Bird (Monash University, Australia) and Roman Jerala (National Institute of Chemistry, Slovenia) for the critical reading of the manuscript and Marko Kreft for advice in confocal microscopy.

REFERENCES

1. Cohen, J. (2002) The immunopathogenesis of sepsis. *Nature* **420,** 885–891
2. Kawai, T., and Akira, S. (2010) The role of pattern-recognition receptors in innate immunity: update on Toll-like receptors. *Nat. Immunol.* **11,** 373–384
3. Medzhitov, R. (2007) Recognition of microorganisms and activation of the immune response. *Nature* **449,** 819–826
4. Martinon, F., and Tschopp, J. (2007) Inflammatory caspases and inflammasomes: master switches of inflammation. *Cell Death Differ.* **14,** 10–22
5. Latz, E., Xiao, T. S., and Stutz, A. (2013) Activation and regulation of the inflammasomes. *Nat. Rev. Immunol.* **13,** 397–411
6. Bauernfeind, F. G., Horvath, G., Stutz, A., Alnemri, E. S., MacDonald, K., Speert, D., Fernandes-Alnemri, T., Wu, J., Monks, B. G., Fitzgerald, K. A., Hornung, V., and Latz, E. (2009) Cutting edge: NF-κB activating pattern recognition and cytokine receptors license NLRP3 inflammasome activation by regulating NLRP3 expression. *J. Immunol.* **183,** 787–791
7. Rathinam, V. A., Vanaja, S. K., and Fitzgerald, K. A. (2012) Regulation of inflammasome signaling. *Nat. Immunol.* **13,** 333–342
8. Kahlenberg, J. M., and Dubyak, G. R. (2004) Mechanisms of caspase-1 activation by P2X7 receptor-mediated K^+ release. *Am. J. Physiol. Cell Physiol.* **286,** C1100–C1108
9. Halle, A., Hornung, V., Petzold, G. C., Stewart, C. R., Monks, B. G., Reinheckel, T., Fitzgerald, K. A., Latz, E., Moore, K. J., and Golenbock, D. T. (2008) The NALP3 inflammasome is involved in the innate immune response to amyloid-β. *Nat. Immunol.* **9,** 857–865
10. Hornung, V., Bauernfeind, F., Halle, A., Samstad, E. O., Kono, H., Rock, K. L., Fitzgerald, K. A., and Latz, E. (2008) Silica crystals and aluminum salts activate the NALP3 inflammasome through phagosomal destabilization. *Nat. Immunol.* **9,** 847–856
11. Zhou, R., Yazdi, A. S., Menu, P., and Tschopp, J. (2011) A role for mitochondria in NLRP3 inflammasome activation. *Nature* **469,** 221–225
12. Nakahira, K., Haspel, J. A., Rathinam, V. A., Lee, S. J., Dolinay, T., Lam, H. C., Englert, J. A., Rabinovitch, M., Cernadas, M., Kim, H. P., Fitzgerald, K. A., Ryter, S. W., and Choi, A. M. (2011) Autophagy proteins regulate innate immune responses by inhibiting the release of mitochondrial DNA mediated by the NALP3 inflammasome. *Nat. Immunol.* **12,** 222–230
13. Rathinam, V. A., Vanaja, S. K., Waggoner, L., Sokolovska, A., Becker, C., Stuart, L. M., Leong, J. M., and Fitzgerald, K. A. (2012) TRIF licenses caspase-11-dependent NLRP3 inflammasome activation by Gram-negative bacteria. *Cell* **150,** 606–619
14. Broz, P., and Monack, D. M. (2013) Noncanonical inflammasomes: caspase-11 activation and effector mechanisms. *PLoS Pathog.* **9,** e1003144
15. Kayagaki, N., Warming, S., Lamkanfi, M., Vande Walle, L., Louie, S., Dong, J., Newton, K., Qu, Y., Liu, J., Heldens, S., Zhang, J., Lee, W. P., Roose-Girma, M., and Dixit, V. M. (2011) Non-canonical inflammasome activation targets caspase-11. *Nature* **479,** 117–121
16. Broz, P., Ruby, T., Belhocine, K., Bouley, D. M., Kayagaki, N., Dixit, V. M., and Monack, D. M. (2012) Caspase-11 increases susceptibility to *Salmonella* infection in the absence of caspase-1. *Nature* **490,** 288–291
17. Wang, S., Miura, M., Jung Yk, Zhu, H., Gagliardini, V., Shi, L., Greenberg, A. H., and Yuan, J. (1996) Identification and characterization of Ich-3, a member of the interleukin-1β converting enzyme (ICE)/Ced-3 family and an upstream regulator of ICE. *J. Biol. Chem.* **271,** 20580–20587
18. Turk, V., Stoka, V., Vasiljeva, O., Renko, M., Sun, T., Turk, B., and Turk, D. (2012) Cysteine cathepsins: from structure, function and regulation to new frontiers. *Biochim. Biophys. Acta* **1824,** 68–88
19. Bird, P. I., Trapani, J. A., and Villadangos, J. A. (2009) Endolysosomal proteases and their inhibitors in immunity. *Nat. Rev. Immunol.* **9,** 871–882
20. Kopitar-Jerala, N. (2006) The role of cystatins in cells of the immune system. *FEBS Lett.* **580,** 6295–6301
21. Lenarcic, B., and Bevec, T. (1998) Thyropins–new structurally related proteinase inhibitors. *Biol. Chem.* **379,** 105–111
22. Turk, V., Stoka, V., and Turk, D. (2008) Cystatins: biochemical and structural properties, and medical relevance. *Front. Biosci.* **13,** 5406–5420
23. Turk, B., Turk, D., and Salvesen, G. S. (2002) Regulating cysteine protease activity: essential role of protease inhibitors as guardians and regulators. *Curr. Pharm. Des.* **8,** 1623–1637
24. Ceru, S., Konjar, S., Maher, K., Repnik, U., Krizaj, I., Bencina, M., Renko, M., Nepveu, A., Zerovnik, E., Turk, B., and Kopitar-Jerala, N. (2010) Stefin B interacts with histones and cathepsin L in the nucleus. *J. Biol. Chem.* **285,** 10078–10086
25. Pennacchio, L. A., Lehesjoki, A. E., Stone, N. E., Willour, V. L., Virtaneva, K., Miao, J., D'Amato, E., Ramirez, L., Faham, M., Koskiniemi, M., Warrington, J. A., Norio, R., de la Chapelle, A., Cox, D. R., and Myers, R. M. (1996) Mutations in the gene encoding cystatin B in progressive myoclo-

Downloaded from http://www.jbc.org/ at Jozef Stefan Institut on January 20, 2015

nus epilepsy (EPM1). *Science* **271,** 1731–1734
26. Lalioti, M. D., Mirotsou, M., Buresi, C., Peitsch, M. C., Rossier, C., Ouazzani, R., Baldy-Moulinier, M., Bottani, A., Malafosse, A., and Antonarakis, S. E. (1997) Identification of mutations in cystatin B, the gene responsible for the Unverricht-Lundborg type of progressive myoclonus epilepsy (EPM1). *Am. J. Hum. Genet.* **60,** 342–351
27. Joensuu, T., Lehesjoki, A. E., and Kopra, O. (2008) Molecular background of EPM1-Unverricht-Lundborg disease. *Epilepsia* **49,** 557–563
28. Pennacchio, L. A., Bouley, D. M., Higgins, K. M., Scott, M. P., Noebels, J. L., and Myers, R. M. (1998) Progressive ataxia, myoclonic epilepsy, and cerebellar apoptosis in cystatin B-deficient mice. *Nat. Genet.* **20,** 251–258
29. Houseweart, M. K., Pennacchio, L. A., Vilaythong, A., Peters, C., Noebels, J. L., and Myers, R. M. (2003) Cathepsin B but not cathepsins L or S contributes to the pathogenesis of Unverricht-Lundborg progressive myoclonus epilepsy (EPM1). *J. Neurobiol.* **56,** 315–327
30. Di Giaimo, R., Riccio, M., Santi, S., Galeotti, C., Ambrosetti, D. C., and Melli, M. (2002) New insights into the molecular basis of progressive myoclonus epilepsy: a multiprotein complex with cystatin B. *Hum. Mol. Genet.* **11,** 2941–2950
31. Lew, W., Oppenheim, J. J., and Matsushima, K. (1988) Analysis of the suppression of IL-1α and IL-1β production in human peripheral blood mononuclear adherent cells by a glucocorticoid hormone. *J. Immunol.* **140,** 1895–1902
32. Weischenfeldt, J., and Porse, B. (2008) Bone marrow-derived macrophages (BMM): isolation and applications. *CSH Protoc.* 10.1101/pdb.prot5080
33. Kopitar-Jerala, N., Schweiger, A., Myers, R. M., Turk, V., and Turk, B. (2005) Sensitization of stefin B-deficient thymocytes towards staurosporin-induced apoptosis is independent of cysteine cathepsins. *FEBS Lett.* **579,** 2149–2155
34. Zhang, H., Zhong, C., Shi, L., Guo, Y., and Fan, Z. (2009) Granulysin induces cathepsin B release from lysosomes of target tumor cells to attack mitochondria through processing of bid leading to necroptosis. *J. Immunol.* **182,** 6993–7000
35. Nekrasov, M., Amrichova, J., Parker, B. J., Soboleva, T. A., Jack, C., Williams, R., Huttley, G. A., and Tremethick, D. J. (2012) Histone H2A.Z inheritance during the cell cycle and its impact on promoter organization and dynamics. *Nat. Struct. Mol. Biol.* **19,** 1076–1083
36. Popova, E. Y., Xu, X., DeWan, A. T., Salzberg, A. C., Berg, A., Hoh, J., Zhang, S. S., and Barnstable, C. J. (2012) Stage- and gene-specific signatures defined by histones H3K4me2 and H3K27me3 accompany mammalian retina maturation *in vivo*. *PLoS One* **7,** e46867
37. Špes, A., Sobotic, B., Turk, V., and Turk, B. (2012) Cysteine cathepsins are not critical for TRAIL- and CD95-induced apoptosis in several human cancer cell lines. *Biol. Chem.* **393,** 1417–1431
38. Morrison, D. C., and Ryan, J. L. (1987) Endotoxins and disease mechanisms. *Annu. Rev. Med.* **38,** 417–432
39. Puren, A. J., Fantuzzi, G., and Dinarello, C. A. (1999) Gene expression, synthesis, and secretion of interleukin 18 and interleukin 1β are differentially regulated in human blood mononuclear cells and mouse spleen cells. *Proc. Natl. Acad. Sci. U.S.A.* **96,** 2256–2261
40. Schauvliege, R., Vanrobaeys, J., Schotte, P., and Beyaert, R. (2002) Caspase-11 gene expression in response to lipopolysaccharide and interferon-gamma requires nuclear factor-κB and signal transducer and activator of transcription (STAT) 1. *J. Biol. Chem.* **277,** 41624–41630
41. Goulet, B., Baruch, A., Moon, N. S., Poirier, M., Sansregret, L. L., Erickson, A., Bogyo, M., and Nepveu, A. (2004) A cathepsin L isoform that is devoid of a signal peptide localizes to the nucleus in S phase and processes the CDP/Cux transcription factor. *Mol. Cell* **14,** 207–219
42. Duncan, E. M., Muratore-Schroeder, T. L., Cook, R. G., Garcia, B. A., Shabanowitz, J., Hunt, D. F., and Allis, C. D. (2008) Cathepsin L proteolytically processes histone H3 during mouse embryonic stem cell differentiation. *Cell* **135,** 284–294
43. Bulynko, Y. A., Hsing, L. C., Mason, R. W., Tremethick, D. J., and Grigoryev, S. A. (2006) Cathepsin L stabilizes the histone modification landscape on the Y chromosome and pericentromeric heterochromatin. *Mol. Cell. Biol.* **26,** 4172–4184
44. Istomina, N. E., Shushanov, S. S., Springhetti, E. M., Karpov, V. L., Krasheninnikov, I. A., Stevens, K., Zaret, K. S., Singh, P. B., and Grigoryev, S. A. (2003) Insulation of the chicken β-globin chromosomal domain from a chromatin-condensing protein, MENT. *Mol. Cell. Biol.* **23,** 6455–6468
45. Shinkai, Y., and Tachibana, M. (2011) H3K9 methyltransferase G9a and the related molecule GLP. *Genes Dev.* **25,** 781–788
46. Fang, T. C., Schaefer, U., Mecklenbrauker, I., Stienen, A., Dewell, S., Chen, M. S., Rioja, I., Parravicini, V., Prinjha, R. K., Chandwani, R., MacDonald, M. R., Lee, K., Rice, C. M., and Tarakhovsky, A. (2012) Histone H3 lysine 9 di-methylation as an epigenetic signature of the interferon response. *J. Exp. Med.* **209,** 661–669
47. Hoegen, T., Tremel, N., Klein, M., Angele, B., Wagner, H., Kirschning, C., Pfister, H. W., Fontana, A., Hammerschmidt, S., and Koedel, U. (2011) The NLRP3 inflammasome contributes to brain injury in pneumococcal meningitis and is activated through ATP-dependent lysosomal cathepsin B release. *J. Immunol.* **187,** 5440–5451
48. Rinne, R., Saukko, P., Järvinen, M., and Lehesjoki, A. E. (2002) Reduced cystatin B activity correlates with enhanced cathepsin activity in progressive myoclonus epilepsy. *Ann. Med.* **34,** 380–385
49. Lopez-Castejon, G., Theaker, J., Pelegrin, P., Clifton, A. D., Braddock, M., and Surprenant, A. (2010) P2X(7) receptor-mediated release of cathepsins from macrophages is a cytokine-independent mechanism potentially involved in joint diseases. *J. Immunol.* **185,** 2611–2619
50. Bergsbaken, T., Fink, S. L., and Cookson, B. T. (2009) Pyroptosis: host cell death and inflammation. *Nat. Rev. Microbiol.* **7,** 99–109
51. Shimada, K., Crother, T. R., Karlin, J., Dagvadorj, J., Chiba, N., Chen, S., Ramanujan, V. K., Wolf, A. J., Vergnes, L., Ojcius, D. M., Rentsendorj, A., Vargas, M., Guerrero, C., Wang, Y., Fitzgerald, K. A., Underhill, D. M., Town, T., and Arditi, M. (2012) Oxidized mitochondrial DNA activates the NLRP3 inflammasome during apoptosis. *Immunity* **36,** 401–414
52. Murakami, T., Ockinger, J., Yu, J., Byles, V., McColl, A., Hofer, A. M., and Horng, T. (2012) Critical role for calcium mobilization in activation of the NLRP3 inflammasome. *Proc. Natl. Acad. Sci. U.S.A.* **109,** 11282–11287
53. Luciano-Montalvo, C., and Meléndez, L. M. (2009) Cystatin B associates with signal transducer and activator of transcription 1 in monocyte-derived and placental macrophages. *Placenta* **30,** 464–467
54. Rivera-Rivera, L., Perez-Laspiur, J., Colón, K., and Meléndez, L. M. (2012) Inhibition of interferon response by cystatin B: implication in HIV replication of macrophage reservoirs. *J. Neurovirol.* **18,** 20–29
55. Maher, K., Završnik, J., Jerič-Kokelj, B., Vasiljeva, O., Turk, B., and Kopitar-Jerala, N. (2014) Decreased IL-10 expression in stefin B-deficient macrophages is regulated by the MAP kinase and STAT-3 signaling pathways. *FEBS Lett.* **588,** 720–726
56. Schroder, K., and Tschopp, J. (2010) The inflammasomes. *Cell* **140,** 821–832
57. Wang, S., Miura, M., Jung, Y. K., Zhu, H., Li, E., and Yuan, J. (1998) Murine caspase-11, an ICE-interacting protease, is essential for the activation of ICE. *Cell* **92,** 501–509
58. Jabaut, J., Ather, J. L., Taracanova, A., Poynter, M. E., and Ckless, K. (2013) Mitochondria-targeted drugs enhance Nlrp3 inflammasome-dependent IL-1β secretion in association with alterations in cellular redox and energy status. *Free Radic. Biol. Med.* **60,** 233–245
59. Tschopp, J. (2011) Mitochondria: Sovereign of inflammation? *Eur. J. Immunol.* **41,** 1196–1202
60. Lehtinen, M. K., Tegelberg, S., Schipper, H., Su, H., Zukor, H., Manninen, O., Kopra, O., Joensuu, T., Hakala, P., Bonni, A., and Lehesjoki, A. E. (2009) Cystatin B deficiency sensitizes neurons to oxidative stress in progressive myoclonus epilepsy, EPM1. *J. Neurosci.* **29,** 5910–5915
61. Butinar, M., Prebanda, M. T., Rajkovič, J., Jerič, B., Stoka, V., Peters, C., Reinheckel, T., Krüger, A., Turk, V., Turk, B., and Vasiljeva, O. (2014) Stefin B deficiency reduces tumor growth via sensitization of tumor cells to oxidative stress in a breast cancer model. *Oncogene* **33,** 3392–3400
62. Ricci, J. E., Muñoz-Pinedo, C., Fitzgerald, P., Bailly-Maitre, B., Perkins, G. A., Yadava, N., Scheffler, I. E., Ellisman, M. H., and Green, D. R. (2004) Disruption of mitochondrial function during apoptosis is mediated by caspase cleavage of the p75 subunit of complex I of the electron transport chain. *Cell* **117,** 773–786
63. Li, N., and Karin, M. (1999) Is NF-κB the sensor of oxidative stress? *FASEB J.* **13,** 1137–1143

Downloaded from http://www.jbc.org/ at Jozef Stefan Institut on January 20, 2015

64. Schreck, R., Rieber, P., and Baeuerle, P. A. (1991) Reactive oxygen intermediates as apparently widely used messengers in the activation of the NF-κB transcription factor and HIV-1. *EMBO J.* **10,** 2247–2258
65. Schreck, R., Grassmann, R., Fleckenstein, B., and Baeuerle, P. A. (1992) Antioxidants selectively suppress activation of NF-κB by human T-cell leukemia virus type I Tax protein. *J. Virol.* **66,** 6288–6293
66. Tegelberg, S., Kopra, O., Joensuu, T., Cooper, J. D., and Lehesjoki, A. E. (2012) Early microglial activation precedes neuronal loss in the brain of the $Cstb^{-/-}$ mouse model of progressive myoclonus epilepsy, EPM1. *J. Neuropathol. Exp. Neurol.* **71,** 40–53
67. Karthikeyan, R. S., Leal, S. M., Jr., Prajna, N. V., Dharmalingam, K., Geiser, D. M., Pearlman, E., and Lalitha, P. (2011) Expression of innate and adaptive immune mediators in human corneal tissue infected with *Aspergillus* or *Fusarium*. *J. Infect. Dis.* **204,** 942–950
68. Wu, X. Y., Gao, J. L., and Ren, M. Y. (2007) Expression profiles and function of Toll-like receptors in human corneal epithelia. *Chin. Med. J.* **120,** 893–897

Downloaded from http://www.jbc.org/ at Jozef Stefan Institut on January 20, 2015